

POLITECNICO DI MILANO



DEPARTMENT OF ENVIRONMENTAL AND CIVIL ENGINEERING
DOCTORAL PROGRAMME IN
Structural, Earthquake and Geotechnical Engineering

SELF-HEALING CAPACITY OF CEMENTITIOUS COMPOSITES

Supervisor:
Prof. Liberato Ferrara

Doctoral Dissertation by:
Visar Krelani

Co-Supervisor
Prof. Romildo D. Toledo Filho

Chair of the Doctoral Program:
Prof. Roberto Paolucci

March 2015

Visar Krelani
Self-Healing Capacity of Cementitious Composites
© March 2015
email:
visar.krelani@polimi.it
Department of Civil and Environmental Engineering

SELF HEALING CAPACITY OF CEMENTITIOUS COMPOSITES

A THESIS
PRESENTED TO
THE ACCADEMIC FACULTY

by

Visar Krelani

In Partial Fulfillment
of the Requirements of the Degree
Doctor of Philosophy
in
Structural, Earthquake and Geotechnical Engineering

March 2015

page intentionally left blank

Doctoral School in Structural, Earthquake and Geotechnical Engineering
Department of Environmental and Civil Engineering
Politecnico di Milano

XXVI cycle

Faculty Member

Prof. Roberto Paolucci (Co-ordinator)
Prof. Fabio Biondini
Prof.ssa Gabriella Bolzon
Prof.ssa Claudia Comi
Prof. Alberto Corigliano
Prof. Dario Coronelli
Prof. Claudio di Prisco
Prof. Marco di Prisco
Prof. Roberto Felicetti
Prof. Liberato Ferrara
Prof. Attilio Frangi
Prof.ssa Elsa Garavaglia
Prof.ssa Cristina Jommi
Prof. Pier Giorgio Malerba
Prof. Stefano Mariani
Prof. Umberto Perego
Prof. Federico Perotti
Prof.ssa Lorenza Petrini
Prof. Luigi Zanzi
Prof. Raffaele Ardito

page intentionally left blank

*To my mother Shqipe
and
To my father Rexhep
(who would have been so
happy to see this thesis)*

page intentionally left blank

ABSTRACT

The self-healing capacity of cementitious composites employed for either new or repairing applications opens challenging perspectives for the use of construction materials intrinsically able to recover its pristine durability levels, thus their guaranteeing a longer service life of the designed applications and a performance less sensitive to environmental induced degradation. One possibility of achieving the aforementioned self-healing capacity stands in the use of additives featuring a “delayed crystalline” activity. These additives are able, when in contact with water or atmosphere humidity, to form chemical compounds which are able to reseal the cracks thus guaranteeing the recovery of a pristine level of mechanical performance.

In order to approach the investigation, besides conventional concrete (with and without the aforementioned admixtures) the characterization of the self-healing capacity of High Performance Fiber Reinforced Cementitious Composites (HPFRCCs) with steel fibers and combination with the natural ones was also studied, i.e. their capacity to completely or partially re-seal cracks, as a function of the material composition, maximum crack opening and exposure conditions. This also implies a new structure concept and a wider worthiness of the sustainability of engineering applications which can be achieved thanks to the use of high performance cement based materials, which encompasses and overcomes the traditional one related to the use of by-products in mix-compositions, which can be effectively pursued also in this case

In order to quantify this self-healing ability and its effects on the recovery of mechanical properties a methodology has been developed and will be presented in this dissertation. It consisted in pre-cracking up to different crack opening levels (a three point bending scheme with COD measurement was employed) prismatic beam specimens, made with both concrete, with or without the aforementioned additive. On the other hand, for HPFRCCs, through this dissertation topic has been investigated including the effect of different flow-induced alignment of fibers, triggered through tailored casting, which can result into a material exhibiting either a strain hardening or softening behavior, whether stressed parallel or perpendicularly to the fibers. In all cases, specimens were initially pre-cracked, according to a 4-point bending scheme, and up to different values of crack openings. Specimens were then submitted to different “conditioning environment” (natural winter or summer

environment, water immersion, exposure to humid or dry air, wet-and-dry cycles, representative temperature and humidity cycles representative of winter and summer exposure) for different exposure times. After scheduled exposure duration the specimens were tested up to failure according to the same scheme employed for pre-cracking and results, in terms of load-crack opening curves were compared to those obtained from virgin specimens before any “treatment”.

Dedicated microscopic investigation completed the experimental program and allowed to have a deeper insight into the true nature of the crack healing products and hence of the self-healing mechanism. The significant amount of garnered experimental results also allowed suitable self-healing indices to be defined and quantified, as from the measured recovery of mechanical properties, including load bearing capacity, ductility and stiffness; which is a much needed approach in order to consistently consider the self-healing phenomenon into a durability based design.

Preface

Just like an old castle that is constructed, stone by stone, through the years, that is how I feel when I think of the "construction" of this thesis. The stones represent each and every one of you who helped me in such a professional and dedicated manner through this journey and set the foundations for my castle.

I would like to express a special acknowledgment to my supervisor, Prof. Dr. Liberato Ferrara, which from the beginning with his attention and his priceless supervision, made this research activity more challenging and interesting than I would ever imagine. You have been much more than a Supervisor to me!

A thankful and grateful recognition goes to my Co-Supervisor, Prof. Dr. Romildo D. Toledo Filho, from Universidade Federal do Rio de Janeiro, Brazil - which thanks to the European Project "ENCORE," gave me the opportunity to work with him and not just obtain precious ideas and results about my thesis but also giving me the possibility to be a part of COPPE/UFRJ, which was an unforgettable and unique experience.

Special thanks go to Ing. Marco Lamperti, for always being available to implement our ideas and find a solution when the precious "Instron" machine was "not responding". Likewise, to Prof. Roberto Felicetti and Dr. Patrick Bamonte for their precious advices during this experimental activity. Also, a big thank you to Tonino and Paolo for their continuous help in the laboratory. Thanks to Prof. Giovanni di Luzio for your kind patience with me on implementing such a problem on the numerical model.

Thank you Prof. Dr. Flavio de Andrade Sliva, from Pontifical Catholic University of Rio de Janeiro, Brazil, for the hours spent with me to discuss better ideas for experimental tests and to Saulo Rocha Ferreira, for his excellent and positive energy who helped me to implement these tests and to all the carioca technicians at the COPPE laboratories.

Looking back in time, I have to thank a really good friend of mine, Milot: thanks to whom I had the first possibility to "touch" the laboratories and life in Politecnico di Milano, which university with its power captured all my interests to start this research and to be where I am today.

This work would never be so extraordinary if it wasn't for extraordinary students such as Matteo, Raffaele, Irene, Valentina, Silvia, Marco, Gregorio, Alessandro, Enrico, Tamara and Karine.

A special thank goes to Emmanuela for her reminders about deadlines, to Simona and Cinzia for their awesome patience with me.

This journey would not be as interesting as it has been to me, if it wasn't for the 12:45 special lunch and the happy times at Poli with Manuel, Francesco, Elena, Juan, Bruno, Ramin, Giovanni, Mira, Grigor, Fabrizio and at UFRJ with Marco, Thiago, Fabricio...I will never forget these moments.

To Piero e Paolo ("Spazio 57") that made me understand how important is to work on my research activity, to Rafael ("TermoCop") that supported me in the last part of writing this thesis.

My special thanks goes to my family, to my Mother that was always agreeing and supporting my journey, with a positive "ok, son;" to Vegim, Enva and Veton that were dealing with bureaucratic parts of completing paperwork in order to make my stay here and for always being there; I would like to express my sincere thanks to two people who are not among us anymore but their presence and advice is ever present, my Father Rexhep and to my Grandfather Ahmet. I must thank Burim, Gjylsym, Neki, Edon and Blendi for their continuous support and assistance and for always reaching with their hands to help me.

I would like to thank Ligia, not just for taking care of some details on my thesis, designing its cover, etc. but for also supporting me through these years and giving me the energy to never stop.

Finally, in a particular and in an unusual way, I would like to give my thanks to the Italian Constitution (Third Article), which beside the scholarship gave me the possibility to develop my research activity and participate normally in the human activities of this country. It has given me the opportunity to invest all my energy in the development of my research activity while at the same time exchanging with the marvelous people of this country, to whom I will always be in debt!

A lot of people have been a part of this journey so please accept my sincere apologies if I may have forgotten any particular names but please be sure that without you, it would be impossible!

See you in future endeavors!

Visar Krelani

page intentionally left blank

Contents

Abstract	xvi
Preface	xviii
List of Figures	xxvii
List of Tables	xliii
1. Introduction	1
1.1. The engineering motivation	1
1.2. Objective and Structure of this Thesis	3
1.3. Manuscript Organization	5
2. State of the Art	9
2.1. Materials Performance in Time	9
2.2. Bio-Inspired Materials	13
2.3. Self-Healing Materials.....	14
2.4. Self-Healing Mechanisms	20
2.4.1. Crystallization of calcium carbonate.....	21
2.4.2. Further reaction of un-hydrate cement	23
2.4.3. Sedimentation of particles	26
2.4.4. Swelling of the cement matrix	28
2.5. Factors influencing self-healing.....	29
2.5.1. Mix constituents.....	30
2.5.2. Presence of water and water type	30
2.5.3. Water pressure, Water pH and Water temperature.....	31
2.5.4. Crack width.....	32
2.5.5. Stability of the crack and the stress along the crack	34

2.5.6. Mechanical properties of healed cracks	36
2.6. Concrete incorporating additions	38
2.6.1. Concrete incorporating fly ash, chemical admixtures, expansive agents and geo-materials	39
2.7. Bioconcrete	41
2.7.1. Degradation of urea	42
2.7.2. Calcium lactate-based bacteria	44
2.7.3. Effect of bacteria cells and walls on concrete strength	46
2.8. Fiber reinforced cementitious composites (FRCC).....	47
2.8.1. Self-healing capacity of FRCs.....	50
2.8.2. Self-healing capacity of ECCs	51
2.8.3. Natural fibers to enhance the performances and healing capacities of concrete.....	53
2.9. Concretes employing polymers.....	55
2.9.1. Sap-modified concrete.....	56
2.10. Concrete with capsules	58
2.10.1. Vascular systems: engineered healing systems	61
2.11. Self-Healing Capacity of Asphalt Concrete	64
2.12. Quantifying healing effectiveness	68
2.13. Modelling Self-Healing Ability in Cement Composites.....	74
2.14. Applications in Self-Healing Materials	78
2.14.1. Scratch Guard Coating	78
2.14.2. React-A-Seal - Ballistic Puncture Healing	79
2.14.3. Self-Healing Concrete Pavilion (Breda, The Netherland).....	80
2.14.4. Water Irrigation Canal with Self-Healing Concrete Containing Bacteria (Ecuador).....	81
2.14.5. Retaining walls using Concrete with Crystalline Additives, Shanghai Airport, Terminal 3, Shanghai, People's Republic of China	82
2.14.6. Self-Healing Porous Asphalt Constructed on A58 Highway, The Netherlands.....	83
3. Experimental Campaign.....	89

3.1. Introduction	89
3.2. Self-Healing Investigation on Conventional Concrete	91
3.2.1. Materials and Manufacturing	91
3.2.2. Curing and Exposure Conditioning	99
3.2.3. Post-Exposure Testing	101
3.3. Self-Healing Investigation on High Performance Reinforced Cementitious Composite (HPFRCC) with Steel Fibers	102
3.3.1. Introduction	102
3.3.2. Materials and Manufacturing	102
3.4. Self-Healing Investigation on High Performance Reinforced Cementitious Composite (HPFRCC) with Hybrid Fibers; Natural and Steel Fibers	112
3.4.1. Introduction	112
3.4.2. Materials and Manufacturing	113
4. Analysis and Discussion of Experimental Results	121
4.1. Introduction	121
4.2. Conventional Concrete	122
4.2.1. Normal Strength Concrete	122
4.2.2. Ultrasonic Pulse Velocity tests	123
4.2.3. Index of Damage Recovery as per UPV tests	127
4.2.4. Three-point bending tests (3PBT)	129
4.2.5. SEM analyses	146
4.3. Conclusions about Conventional Concrete	150
4.4. High Performance Fiber Reinforced Cementitious Composites (HPFRCCs)	152
4.4.1. Introduction	152
4.4.2. Four point bending test (4pbt)	152
4.4.3. Comparison Indices of Mechanical Properties Recovery and Index of Crack Healing	162
4.4.4. Damage evolution laws	180
4.4.5. Comparison Indices of Mechanical Properties Recovery and Index of Crack Healing	183

4.4.6. SEM analyses.....	186
4.4.7. Conclusion about HPFRCCs	189
4.5. High Performance Reinforced Cementitious Composites with Hybrid Fibers	191
4.5.1. Introduction	191
4.5.2. Four point bending test (4pbt)	191
4.5.3. Uniaxial Tensile Testing.....	195
4.5.4. SEM and Thermo-gravimetric analysis.....	197
5. Numerical simulation of self-healing capacity	207
5.1. Introduction.....	207
5.2. Solidification-Microprestress-Microplane (SMM) Model and Self- Healing Model	208
5.3. Multi-Physics Formulation	209
5.3.1. Mechanical Behavior.....	210
5.4. Heat Transfer and Moisture Diffusion	214
5.5. Cement Hydration	216
5.5.1. Self-healing.....	216
5.6. Aging Model	217
5.6.1. Stiffness and Creep	219
5.6.2. Strength and Fracture Energy.....	219
5.7. Numerical Results	221
5.8. Zero-Thickness Interface Formulation For Fracture Analysis For Self-Healing Concrete.....	224
5.8.1. Introduction	224
5.8.2. Zero-thickness interface model: general assumptions	224
5.8.3. Fracture and Porosity-Based Softening Rules	227
5.8.4. Tangent Stiffness Operator	229
5.8.5. Validation of the proposed interface model	230
5.8.6. Concluding remarks	233
6. Conclusions and future perspectives	235
6.1. Conclusions.....	235

6.2. Future Perspectives 237

List of Figures

Figure 1.1.	Lifecycle of conventional concrete (on the left) and concrete with recycled aggregates (in the right).....	2
Figure 1.2.	The natural process of self-healing on human body (a) blood clotting and (b) “restructuration” of the bone through the process called remodeling. Courtesy by Fratz et al. [3].....	3
Figure 1.3.	Actual situation on the self-healing materials in the world level (top) and due to the University level (bottom). Courtesy by Scopus	4
Figure 1.4.	Outline of the thesis	6
Figure 2.1.	Performance (on the left) and cost (on the right) as function of time for normal (A) and high quality (B) structures. Schematic example by Van Breugel [6]	10
Figure 2.2 .	Performance (on the left) and cost (on the right) with elapse of time for a structure made of self-healing concrete. Schematic example by Van Breugel [6].	10
Figure 2.3.	Computed service life (a) and life cycle cost (b) showing the effect of self-healing. The "construction cost" here, refers to mainly the initial material cost. Courtesy by Li et al [7]	12
Figure 2.4.	Quantitative backscattered electron image (qBEI) of a bone trabecula gray scales (left). Bone mineralization density distribution (BMDD), which describes the Ca content. Courtesy of Weinkamer et al [9].	13
Figure 2.5.	Detail of the sample self-healing of the crack by crystal filling (left); chemical composition of the filling crystal with a maximum of calcium content (right). Courtesy by Qian et al [11]	14
Figure 2.6.	Microscopic study of the cracked specimens and the healing after 28 days of water leakage. Courtesy by Want et al.	16
Figure 2.7.	Definition of self-healing/repairing concrete by JCI	18
Figure 2.8.	Definition of self-healing/repairing concrete by Mihashi and Nishiwaki [23].....	19
Figure 2.9.	Schematic presentation of self-healing in concrete.	19

List of Figures

Figure 2.10.	Self-Healing Mechanisms in Concrete: (a) formation of calcium carbonate or calcium hydroxide, (b) sedimentation of particles, (c) continued hydration, (d) swelling of the cement [25]	20
Figure 2.11.	Equilibrium concentrations of ions of Ca, CO ₃ e HCO ₃ as pH function (Edvardsen, 1999).....	22
Figure 2.12	a) Interfaces and reactions in CaCO ₃ - CO ₂ - H ₂ O system by Edvardsen [19] b) Precipitation of the calcium carbonate. 23	
Figure 2.13.	Degree of Hydration of the principal hydration components in cement by Shah et al.	24
Figure 2.14.	Permeability versus extent of hydration by Hearn and Morley [26]	25
Figure 2.15.	Cement paste (top) and un-hydrated particles after 1 year of hydration. Courtesy of He et al [32].....	25
Figure 2.16.	The hydration degree of cement and fly ash as a function of time. Courtesy of Termkhajornkit et al [46].....	26
Figure 2.17.	Glanville's permeability curves from Hearn and Morley: a) effect of reversal direction of flow in a sandstone specimen; b) effect of reversal flow direction in a concrete specimen. Courtesy of Glanville [28].....	27
Figure 2.18.	Schematic showing the mechanism so self-healing using SAP Van Tittelbom et al [17]	28
Figure 2.19.	Total healing of a 138- μ m crack a specimen in containing 1% SAP B after wet/dry cycles. Courtesy of Snoeck, De Belie, et al [33]	29
Figure 2.20.	Representantion of the dependency of the crack permeability K on crack width and temperature. Courtesy by Rehinardt and Jooss [38].....	32
Figure 2.21.	The evolution on the measurement of the crack width, from the most traditional to the most advanced as the digital microscope measurement [44][45].....	33
Figure 2.22.	Relationship between rate of self-healing and initial crack opening. Courtsy of Gagnè et al [49]	34
Figure 2.23.	Relationship between water flow and time for different crack width. Courtesy of Edvardsen [19].....	35
Figure 2.24.	Relationship between flow and time for active cracks by Edvardsen [19]	35
Figure 2.25.	Typical preloading and reloading tensile stress–strain curve for two cases of ECC with predetermined tensile deformation of (a) 0.3%, and (b) 3%, after different environmental conditioning regimes [48].....	37

List of Figures

- Figure 2.26. Average mechanical behaviour of reference specimens (stored without crack in water for 10 weeks, and then cracked and immediately reloaded) and of cracked specimens stored in water for 10 weeks before reloading. Courtesy of Granger et al. [58]38
- Figure 2.27. SEM Cross-section picture for concrete after self-healing: (a) normal cement concrete; (b) concrete specimen with 30% slag; (c) concrete specimen with 40% fly ash. Courtesy by Zhou et al. [62].....40
- Figure 2.28. Self-healed re-hydration products in crack by hydrogarnet phases C-A-H and calcite phases. Courtesy by Kishi and Ahn [63] 41
- Figure 2.29. Developing of calcite crystals at higher magnification. Rod-shaped objects, consistent with the dimensions of *Bacillus Pasteurii* are spread around the crystals. Courtesy by Siddique and Chahal [70]. 43
- Figure 2.30. Cement stone specimens with incorporating healing agent. (*B. Cohnii* spores plus calcium lactate), cracked after 7 (panels A: 250x and B: 1000x) and 28 days curing (panels C: 500x and D: 2000x). The large mineral precipitates visible on the surface of the younger specimens seem to be due to the conversion of calcium lactate by bacteria. The small precipitates on older specimen's surface resemble those produced by abiotic specimens. Courtesy by by Jonkers [72] 45
- Figure 2.31. Typical tensile strain softening and hardening behavior of FRC Courtesy by Namman and Reinhardt [77].48
- Figure 2.32. (a) Different Types of steel fibers ; (b) Expected comparison of pull-out load versus slip response of smooth, hooked and twisted steel fibers. Courtesy of Naaman [77] 49
- Figure 2.33. Morphology of crack within ECC specimen from ESEM: (a) Autogenous self-healing crystalline formations in ECC crack after permeability testing; (b) ECC crack before permeability testing. Courtesy by Yang et. al [90] 52
- Figure 2.34. At the left: partial crack healing in an ECC with PVA .The scale bar has a height of 20 μm ; at the right: bridging effect of PVA fibers. Courtesy by Antonopoulos [96] 53
- Figure 2.35. Polymer film in epoxy cement composite. Courtesy by Lukowski and Adamczewski [100].....56
- Figure 2.36. Schematic showing the mechanism of self-healing using SAP. Courtesy by Van Tittelbom et at [17]. 57

List of Figures

- Figure 2.37. (left) basic method of the microcapsule approach: (i) cracks form in the matrix; (ii) the cracks rupture the microcapsules, releasing the healing agent through capillary action; (iii) the healing agent contract the catalyst, triggering polymerization thus ensuring the closure of the nearby cracks and (right) ESEM image showing a ruptured microcapsule. Courtesy by Van Tittelboom and De Belie [17].....58
- Figure 2.38.(left) Hollow glass fibers and (right) damage visual enhancement in composite laminate by the bleeding action of a fluorescent dye from hollow glass fibers. Courtesy by Van Tittelboom and D Belie [103].....60
- Figure 2.39. Schematic illustration of the forces acting on an internally encapsulated healing agent. Courtesy of Huang and Ye et al [106]60
- Figure 2.40. Vascular based self-healing approaches. Leakage of the healing agent from the tank via the vascular into the crack due to gravitational and capillary forces and eventual (hydrostatic) pressure. One channel (A) and multiple channel vascular systems (B). Courtesy by Van Tittelbom et al [17]..... 62
- Figure 2.41. General concept proposed which make use of porous network concrete. Courtesy by Sangadji and Schlangen [111]..... 62
- Figure 2.42. Self-healing experimental arrangement on a schematic presentation and the specimens during experimental campaign. Courtesy by Gardner [112].....63
- Figure 2.43. Schematic illustration of activated repairing system. Courtesy by Nishiwaki and Mihashi 64
- Figure 2.44. a) Traditional pavement failure modes and b) fatigue cracking in asphalt pavements. Courtesy by Highway Agency, London [119]66
- Figure 2.45. a) Infrared images of a porous asphalt concrete sample under heating; b) Stress–strain curves for samples with 5.66% steel wool type 000 (related to the volume of bitumen) and sand-bitumen ratio 1.60. Courtesy by Liu et al [124]..... 67
- Figure 2.46. Techniques used to evaluate the healing efficiency. Courtesy of Van Tittelbom and De Belie at [128].....69
- Figure 2.47. Morphology of crack within ECC specimen from ESEM: Autogenous self-healing crystalline formations in ECC a) before and b) after permeability test. Courtesy by Yang et. al [90].....70

List of Figures

Figure 2.48. (a) ESEM image of ‘stone-like’ healing product and (b) its EDS spectrum. Courtesy by Kan, et al [129].....	70
Figure 2.49. Typical curves load (P)-crack opening displacement (δ) curves of the self-healing before and after healing.....	72
Figure 2.50. (Left) Representation of a half of the concrete cube containing the capsule and consisting of un-carbonated (below) and carbonated (above) parts. The computational domain for a two dimensional mathematical model. Courtesy by [136]	74
Figure 2.51. a) SIF module vs relative bridged zone length, $K_0 = \sigma_0 \pi l$; b) SIF module vs relative bond stiffness, $K_0 = \sigma_0 \pi l$. Curtesy by Perelmuter [137]	75
Figure 2.52. (up) Typical deformed mesh; (bottom) Stress contour plot. Courtesy by Schlangen et al. [138]	76
Figure 2.53. Flexural stress versus displacement for different simulations. Courtesy by Schlangen et al [138]	76
Figure 2.54. Single crack intersected with cement paste. Courtesy by He et al [139].....	77
Figure 2.55. Schematic diagram of modelling system (InP represents inner products, OutP represents un-hydrated cement particles) [139]	78
Figure 2.56. (left) Comparisons between conventional paint and the Scratch Shield; (right) Scratch Shield performance before self-repairing and after-repairing. [10].....	79
Figure 2.57. (left) To stage model for ballistic self-healing in EMMA films; (right) SEM of healed EMMA composite (projectile entrance side). Courtesy by Sugama et al [140]	79
Figure 2.58. (left) Self-healing concrete shell of 60 mm thick; (right) Self-Healing concrete Pavilion-Breda. Courtesy by TU delft [141] 80	80
Figure 2.59. (left) Schematic presentation of the cracks into the canal; (right) Part of the constructed canal in Ecuador. Courtesy by Jonkers et al [142].....	81
Figure 2.60. (left) The Shanghai Airport area, Singapore; (right) The underground structures on the Terminal 3. Courtesy by [143].....	82
Figure 2.61. (left) Close view of the sign of efflorescence accompanied with water marks were noted on wall 3; (right) some crystal grew in the crack due to core samples extracted on the leakage zone. Courtesy by Loh et al [143]	83

List of Figures

Figure 2.62.	(left) Porous asphalt specimen made of the same materials which constructed the road; (right) The construction of the layers by self-healing material. Courtesy by Schlangen et al [124]	84
Figure 3.1.	Schematic Presentation of the Experimental Campaign.....	90
Figure 3.2.	Schematic presentation for the proposed experimental methodology	91
Figure 3.3.	Observations on the crystalline additive; Visual observation on different scale of additive particles of in a scanning; (left) original visualization of the additive; (middle, right) scanning electron microscope in different magnifications	92
Figure 3.4.	Chemical characterization of the crystalline additive showed in (Figure 3.3) by the Energy dispersive spectroscopy (EDS) test.	92
Figure 3.5.	Distribution of the used aggregate and the proposal for the optimal distribution and the ideal one (Bolomey)	93
Figure 3.6.	Manufacturing of the specimens; (left) casted slab; (middle) reference cube specimens; (right) slabs under wet towels.	93
Figure 3.7.	(left) Slabs stored on a chamber room; (middle) cutting machine; (right) specimens like “beam” after cutting.....	94
Figure 3.8.	Code Identification of the specimen.....	94
Figure 3.9.	(left) Three point bending test set-up for pre-cracking procedure; (right) clip gauge used for measuring the crack opening mouth displacement	96
Figure 3.10.	Typical Load vs CMOD response from 3PBT; (left) pre-cracking CMOD until 150 μm ; (right) pre-cracking CMOD until 300 μm	96
Figure 3.11.	(up) Schematic presentation of the UPV measurement set-up [147]; (down) Set-Up For Ultrasonic Pulse Velocity Tests (Emitter-Receiver Distance = 90 Mm)	97
Figure 3.12.	(left) Oscilloscope used for the UPV; (right) Screen Program of (UPV-Generic)	98
Figure 3.13.	(left) Climatic chamber; (middle) Water immersion; (right) air exposure.....	99
Figure 3.14.	(left) Temperature and relative humidity simulated by the climate chamber; (right) T and RH recorded along the specimen exposure period.....	100
Figure 3.15.	Synopsis of experimental programme (n° of specimens per each test condition)	100

List of Figures

Figure 3.16. Typical Load vs CMOD response from 3PBT during pre-cracking and the same specimen response in post-conditioning stage.....	101
Figure 3.17. (Left) Straight Steel Fibers ($l_f = 13$ mm; $d_f = 0.16$ mm); (right) Granulometric curve for the used sand.....	103
Figure 3.18. (left) Simem mixer and (right) casting of the slabs.	105
Figure 3.19. (up) Schematic presentation for casted slabs and flow induced with fiber alignment; (left, middle) casted slab with lines to be cut; (right) cutting procedure in half slabs.	106
Figure 3.20. (up) Schematic presentation of the four point bending test; (left) four point bending test set-up; (right) the measurement detail by the linear variable differential transformer (LVDT transducers).....	107
Figure 3.21. Nominal stress σ_N vs. COD curves for specimens featuring: (left)unstable post-cracking localization and deflection softening behavior (fibers orthogonal to the bending axis) and (right) stable pre-peak multi-cracking and deflection hardening behavior (fibers parallel to the bending axis).	108
Figure 3.22. Digital microscope Dino-Lite	109
Figure 3.23. Mapping of the cracking in the intrados zone of the specimen	109
Figure 3.24. Microscope images of the cracks.....	110
Figure 3.25. Temperature and Relative Humidity (RH) recorded along the specimens exposure period	111
Figure 3.26. The comparison between the pre-cracking and post-conditioning behavior for (a) deflection softening and (b) deflection hardening.....	111
Figure 3.27. (left) Sisal fibers origin “Agave”; (middle) Production of fibers; (right) final production (long sisal fibers Courtesy by [158]).....	113
Figure 3.28. Sisal fiber morphology showing: (left) fiber composed of several fiber-cells linked by the middle lamellae; (middle) detail of middle lamellae (composed of lignin and hemicellulose) with its exterior layer; (left) hydrolysis of sisal. Courtesy by Silva et al [159]	114
Figure 3.29. Mass gain in time due to the water absorption of different natural fibers. Courtesy by Ferreira et al. [158].....	114
Figure 3.30. (left) Short Sisal fibers used in the mix design; (right) Fiber classification due to their tensile strength. Courtesy by Silva et al [159].....	115

List of Figures

- Figure 3.31. Monotonic response of steel HPFRCC (a) and steel + sisal HPFRCC (b) specimens for fibers parallel and orthogonal to the applied bending stress – COD pre-cracking thresholds are highlighted; c) multiple crack pattern due to the alignment of fibers and d) single crack due to orthogonal direction.116
- Figure 3.32. Uniaxial Tensile testing on HPFRCC with Steel and Steel + Sisal Fibers. 117
- Figure 3.33. Monotonic response under uniaxial tensile test for HPFRCC for steel and steel + sisal (top), induced single crack due to the notches in both sides of the specimen (bottom).118
- Figure 4.1. Strength development of concrete with and without crystalline additives vs. EC2 provisions 122
- Figure 4.2. Relative UPV vs. exposure time for water/air exposure (a-b); summer (c-d) and winter (e-f) chamber conditioning; pre-cracked (a, c, e) vs. un-cracked (b, d,f) specimens. 124
- Figure 4.3. IDR (from UPV tests) vs. exposure time for water/air exposure (a, b); summer (c, d) and winter (e, f) chamber conditioning; p re-cracked (a, c, e) vs. un-cracked (b, d, f) specimens. 126
- Figure 4.4. Example of load vs. COD curves for specimens submitted to pre-cracking and post-conditioning 3pb tests; definition of quantities for calculation of self-healing indices 129
- Figure 4.5. Index of Damage Recovery (as evaluated from 3pb test results) vs. exposure time for water immersion/air exposure (a); summer (b) and winter (c) chamber conditioning.131
- Figure 4.6. Comparison between Indices of Damage Recovery evaluated per UPV and 3pb test results. 132
- Figure 4.7. Fitted damage evolution laws for pre-cracked concrete specimens with (a,c,e,g,i,m) and without (b,d,f,h,l,n) crystalline additive and different exposure conditions: water immersion (a,b); air exposure (c,d); climate chamber conditioning in summer climate (e-h) for specimens pre-cracked at 100 μm (e,f) and 200 μm (g,h); climate chamber conditioning in winter climate (i-n) for specimens pre-cracked at 100 μm (i,l) and 200 μm (m,n). 136
- Figure 4.8. Graphical explanation of the procedure to estimate crack closure from damage evolution laws built as in Figure 4.7 (a-n).137
- Figure 4.9. Index of Crack Healing (as evaluated from damage evolution laws) vs. exposure time for water immersion/air exposure (a); summer (b) and winter (c) chamber conditioning. ... 138

List of Figures

- Figure 4.10. Healed cracks for specimens with (a) and without (b) crystalline additive after six months of immersion in water; specimens with (c) and without (d) crystalline additive after six months of exposure to open air. 139
- Figure 4.11. Healing cracks for specimens with crystalline additive before exposure (a, c) and after two (b) or four weeks (d) in climate chamber (summer cycles)..... 139
- Figure 4.12 Index of Load Recovery (as evaluated from 3pb test results) vs. exposure time for water immersion/air exposure (a); summer (b) and winter (c) chamber conditioning; un-cracked specimens on (d) summer and winter cycles and (e) water immersion/air exposure.....141
- Figure 4.13. Graphical explanation of the procedure to estimate crack closure from stress vs- Crack Opening Displacement curves. 143
- Figure 4.14. Index of Crack Healing (as evaluated from σ -COD curves) vs. exposure time for water immersion/air exposure (a); summer (b) and winter (c) chamber conditioning. 143
- Figure 4.15. Index of Damage Recovery as evaluated from 3pb (left) vs. Index of Crack Healing as estimated from fitted damage evolution laws as in Figure 4.8..... 144
- Figure 4.16. Index of Load Recovery vs. Index of Crack Healing as evaluated from stress vs. COD curves obtained from 3pb tests..... 144
- Figure 4.17. Index of crack healing evaluated from stress - COD curves vs. damage curves. 145
- Figure 4.18. Sample of concrete with crystallite additive and immersed in water for 3 months..... 146
- Figure 4.19. Different SEM images of crack surface from the sample on Figure 4.18..... 146
- Figure 4.20. EDS analysis of products shown in Figure 4.19. 147
- Figure 4.21. SEM image a) and EDS analysis b) of sample of Figure 4.18 along the surface orthogonal to the crack..... 147
- Figure 4.22. SEM image a) of sample of Figure 4.18 in correspondence of the area between the crack surface (denoted as B) and the one orthogonal to it (denoted as A); EDS analysis of zone 147
- Figure 4.23 Sample of concrete cast without crystalline additive and immersed in water for 3 months. Detail of the sample a) along the crack surface b). 148

List of Figures

Figure 4.24. SEM image a) and EDS analysis b) of sample of Figure 4.23 along the crack surface.....	148
Figure 4.25. SEM image a) and EDS analysis b) of sample along the crack surface in a zone different from that observed in Figure 4.24.....	149
Figure 4.26. σ_N vs. COD curves for deflection softening specimens for different exposure conditions and pre-cracked up to 0,5 mm: water immersion for different pre-crack ages (a) 11 months, (b) 2 months ; (c) air/external exposure; (d) wet/dry (water immersion and 50%RH with 20°C; (e) wet (high humidity with 90%RH and 20°C and (f) dry (50%RH with 20°C).	154
Figure 4.27. Schematic presentation for the Index of stress recovery for the deflection softening behavior (Equation 4.9).....	155
Figure 4.28. Index of Stress Recovery vs. conditioning time for deflection softening specimens (hollow markers refer to values of single tests, solid markers represent average values of nominally identical tests).	156
Figure 4.29. Healed cracks for specimens pre-cracked up to $\text{cod}_{\text{tot}}=0.5$ mm (a,c,e) and immersed in water for (b) 1 month; (d) 3 months and (e) after six months of water immersion.....	157
Figure 4.30. Healed cracks for specimens pre-cracked up to $\text{cod}_{\text{tot}}=0.5$ mm (a,c,e) and conditioned up to 1 month in; (b) natural environment; (d) high humidity and (e) wet/dry cycles. .	158
Figure 4.31. Schematic presentation for the used stiffnesses to calculate Index of Damage Recovery (Equation 4.11).....	159
Figure 4.32. Index of Damage Recovery vs. conditioning time for deflection softening specimens (hollow markers refer to values of single tests, solid markers represent average values of nominally identical tests).	160
Figure 4.33. Graphical explanation of the procedure to estimate crack closure from damage evolution laws.....	161
Figure 4.34. Index of Crack Healing vs. conditioning time for deflection softening specimens (hollow markers refer to values of single tests, solid markers represent average values of nominally identical tests).	161
Figure 4.35. Correlation between ISR and ICH for the softening deflection behaviour.	163
Figure 4.36. Correlation between IDaR and ICH.....	163
Figure 4.37. σ_N vs. COD for deflection hardening specimens for different exposure conditioning pre-cracked up to 1 mm: water	

List of Figures

- immersion for different pre-crack ages (a) 11 months; (b) 2 months (c) air/external exposure; (d) wet/dry (water immersion and 50%RH with 20°C; (e) wet (high humidity with 90%RH and 20°C and (f) dry (50%RH with 20°C). 165
- Figure 4.38. σ_N vs. COD for deflection hardening specimens for different exposure conditioning pre-cracked up to 2 mm: water immersion for different pre-crack ages (a) 11 months; (b) 2 months; (c) air/external exposure; (d) wet/dry (water immersion and 50%RH with 20°C; (e) wet (high humidity with 90%RH and 20°C and dry (50%RH with 20°C). 166
- Figure 4.39. σ_N vs. COD for deflection hardening specimens for different exposure conditioning pre-cracked up to 0,5 mm after the peak: water immersion for different pre-crack ages (a) 11 months; (b) 2 months; (c) air/external exposure; (d) wet/dry (water immersion and 50%RH with 20°C; (e) wet (high humidity with 90%RH and 20°C and dry. (50%RH with 20°C). 167
- Figure 4.40. Notation and significance of Index of stress recovery for deflection hardening specimens pre-cracked in the pre-peak regime..... 169
- Figure 4.41. Index of Stress Recovery vs. conditioning time for deflection hardening specimens pre-cracked up to 1 mm (hollow markers refer to values of single tests, solid markers represent average values of nominally identical tests). ... 170
- Figure 4.42. Index of Stress Recovery vs. conditioning time for deflection hardening specimens pre-cracked up to 2 mm (hollow markers refer to values of single tests, solid markers represent average values of nominally identical tests). ... 170
- Figure 4.43. Index of Stress Recovery vs. conditioning time for deflection hardening specimens pre-cracked up to 0.5 mm after the peak (hollow markers refer to values of single tests, solid markers represent average values of nominally identical tests). 171
- Figure 4.44. Healed cracks for specimens pre-cracked up to (a) $c_{odtot}=1\text{mm}$; (c) $c_{odtot}=2\text{mm}$ and (e) $c_{odtot}=0.5\text{mm}$ after the peak; (b,d,e) after one month of water immersion. ... 172
- Figure 4.45. Healed cracks for specimens pre-cracked up to (a) $c_{odtot}=1\text{mm}$; (c) $c_{odtot}=2\text{mm}$ and (e) $c_{odtot}=0.5\text{mm}$ after the peak; (b,d,e) after six months of water immersion.173
- Figure 4.46. Schematic presentation for the Index of ductility recovery for the deflection hardening specimens..... 174

List of Figures

- Figure 4.47. Index of Ductility Recovery vs. conditioning time for deflection hardening specimens pre-cracked up to 1 mm (hollow markers refer to values of single tests, solid markers represent average values of nominally identical tests).176
- Figure 4.48. Index of Ductility Recovery vs. conditioning time for deflection hardening specimens pre-cracked up to 2 mm (hollow markers refer to values of single tests, solid markers represent average values of nominally identical tests).176
- Figure 4.49. Index of Ductility Recovery vs. conditioning time for deflection hardening specimens pre-cracked up to 0.5 mm after the peak (hollow markers refer to values of single tests, solid markers represent average values of nominally identical tests).177
- Figure 4.50. Schematic presentation for the used stiffnesses to calculate Index of Damage Recovery (Equation 4.16) 178
- Figure 4.51. Index of Damage Recovery vs. conditioning time for deflection hardening specimens pre-cracked up to 1 mm. 178
- Figure 4.52. Index of Damage Recovery vs. conditioning time for deflection hardening specimens pre-cracked up to 2 mm (hollow markers refer to values of single tests, solid markers represent average values of nominally identical tests).179
- Figure 4.53. Index of Damage Recovery vs. conditioning time for deflection hardening specimens pre-cracked up to 0.5 mm after the peak (hollow markers refer to values of single tests, solid markers represent average values of nominally identical tests).179
- Figure 4.54. Fitted damage evolution laws for pre-cracked concrete specimens from water immersion (a, b) for specimen pre-cracked at 2 mm (a) and 0.5 mm after the peak (b) 180
- Figure 4.55. Graphical explanation of the procedure to estimate crack closure from damage evolution laws.181
- Figure 4.56. Index of Crack Healing vs. conditioning time for deflection hardening specimens pre-cracked up to 1 mm. 182
- Figure 4.57. Index of Crack Healing vs. conditioning time for deflection hardening specimens pre-cracked up to 2 mm (hollow markers refer to values of single tests, solid markers represent average values of nominally identical tests). ... 182
- Figure 4.58. Index of Crack Healing vs. conditioning time for deflection hardening specimens pre-cracked up to 0.5 mm after the peak (hollow markers refer to values of single tests, solid

List of Figures

	markers represent average values of nominally identical tests).....	183
Figure 4.59.	Correlation between Index of Stress Gain (ISR) and Index of Crack Healing (ICH) for the hardening specimens	184
Figure 4.60.	Correlation between Index of Damage Recovery (IDaR) and Index of Crack Healing (ICH) for the hardening specimens	184
Figure 4.61.	Correlation between Index of Damage Recovery (IDaR) and Index of Crack Healing (ICH) for the hardening specimens	185
Figure 4.62.	Correlation between Index of Ductility Recovery (IDuR) and Index of Stress Recovery (ISR) for the hardening specimens	185
Figure 4.63.	Sample of HPFRCCs immersed in the water	186
Figure 4.64.	Microscopic images due to different magnification, a) 100 μm and b) 500 μm	186
Figure 4.65.	Macroscopic pictures of the extracted concrete in the cracked surface	187
Figure 4.66.	Magnified images of samples taken from the crack (a), (b) and fracture surface (c), (d) at different magnifications. .	187
Figure 4.67.	SEM images and EDS analysis of the sample taken from near the crack: detail of fibers and cement matrix (a) and (b), EDS of the cement paste to the edge of the crack and fiber (c), (d).....	188
Figure 4.68.	SEM images and EDS analysis of the cement paste on the cracked surface: detail of fibers and cement matrix (a) and (d), EDS of the cement paste on the cracked surface (b), and the self-healing product through the aggregate (c).	188
Figure 4.69.	σN vs. COD curves for deflection softening (a,c) and deflection hardening (b,d) steel+sisal (a,b) and steel (c,d) specimens, for wet and dry cycles.	192
Figure 4.70.	Index of stress recovery for different analyzed specimens	193
Figure 4.71.	Index of of ductility recovery for different analyzed specimens.....	193
Figure 4.72.	Completely healed cracks in steel+sisal (a) FRC deflection softening specimens after 3 months cycling and of partially healed cracks in steel (b) FRC deflection softening specimens after 6 months cycling (0.5 mm pre-crack; different scales of magnification).....	194

List of Figures

Figure 4.73.	Completely healed cracks in steel + sisal and forming of new cracks after wet/dry cycles for about 3 months.....	195
Figure 4.74.	σ_N vs. COD response for uniaxial tensile test for double-edge-notched specimens for HPFRCC with steel and steel + sisal after 3 months conditioning water immersion (a) and (b) wet/dry cycles	196
Figure 4.75.	Healed cracks for; (a) steel + sisal HPFRCC after 3 months wet/dry cycling and healed cracks in steel (b) HPFRCC after 3 months wet/dry cycling.	196
Figure 4.76.	Macroscopic observation on the cracked surface after failure testing on uniaxial double-edge-notched prismatic specimens.....	198
Figure 4.77.	SEM investigations of the specimen showed in the Figure 4.76, for the dark and the grey zones.....	198
Figure 4.78.	SEM investigations of the specimen showed in the Figure 4.76, for the dark and the notched zone	199
Figure 4.79.	Investigated sample extracted from the healed specimen under wet/dry cycle for 3 months.....	199
Figure 4.80.	Thermo-gravimetric testing for different samples, for pre/post conditioning.....	200
Figure 4.81.	Polymorphic transformation of Calcium Carbonate (CaCO_3) 201	201
Figure 4.82.	SEM images of the steel fibers at the pre-cracking stage...	201
Figure 4.83.	Crystal formation under wet/dry cycles	202
Figure 4.84.	Crystal formation under wet/dry cycles	203
Figure 4.85.	SEM observations for the steel fiber bonding with the cement matrix after the conditioning (3 months wet/dry cycles)	204
Figure 4.86.	Comparison between SEM images obtained during the pre-cracking and after 3 months wet/dry cycles.	204
Figure 4.87.	SEM observations for the sisal fibers; (a) the absorbing and releasing of the water inside the matrix and (b) the concentration of the healing product around the sisal fiber 205	205
Figure 5.1.	Schematic representation of the constitutive model. Courtesy by Di Lazio, Cusatis.....	211
Figure 5.2.	Load-COD curve obtained with 3pb tests from the same specimen before and after the 'self-healing'	222
Figure 5.3.	Relative humidity evolution in the longitudinal mid-plane of the specimen the curing (31 days) and the treatment in water (28 days).	223

List of Figures

- Figure 5.4. Failure hyperbola by Carol et al. [14], Mohr-Coulomb surface, plastic potential and modified flow rule. 225
- Figure 5.5. Scaling function $S[\xi_{\#}]$ (where $\# = p_i$) considering different values of $\alpha 2\pi$228
- Figure 5.6. Porosity-based rule for the self-healing description $SH[\psi_{\#}]$ (with $\# = p_i$) against the effective porosity $_c$: as example the figure reports the case in which $\phi_0 = 0.8$ and $\phi_f = 0.2$ 229
- Figure 5.7. Specimen geometry according to experimental tests on 3PB 231
- Figure 5.8. Finite element mesh, interfaces and possible crack path of the three-point bending..... 231
- Figure 5.9. Load-deflection behavior on three-point beam: experimental results vs. numerical predictions.....232

List of the Tables

Table 3.1. Mix-design of the investigated mortar	92
Table 3.2. Identification of the specimen in front of the type material ...	94
Table 3.3. Identification of the specimen in front of the Conditioning type 94	
Table3.4. Identification of the specimen in front of duration of conditioning	95
Table 3.5. Exposure conditioning and the duration for each of them	99
Table 3.6. Mix-Design of HPFRCC with steel fibers	102
Table 3.7. Petrographic characterization of the sand	103
Table 3.8. Cement Composition.....	104
Table 3.9. Slag composition	104
Table 3.10. Mixing timetable.....	105
Table 3.11. Synopsis of the experimental program: number of specimens tested per each exposure condition and duration, age of pre- cracking, deflection hardening/softening behavior and pre- crack opening	112
Table 3.12. Mix-Design of HPFRCC with natural (sisal) fibers	115

page intentionally left blank

Key words:

self-healing, concrete durability, high performance fiber reinforced cementitious composites, deflection hardening, deflection softening, natural fibers

page intentionally left blank

*In life a human being needs a cup of science,
A bottle of attention, and an ocean of patience
Ismail Kadare*

1. Introduction

1.1. The engineering motivation

Sustainability concerns are becoming more and more relevant to any human activity, including civil engineering as also highlighted by the recent fib Model Code 2010. The sustainability of buildings and structures is strongly influenced by the choices made in design and construction, and it should be evaluated for the whole service life of the structure. Huge amount of energy is employed in the construction industry, e.g. for cement production, manufacturing, transporting, and casting procedure emitting an important quantity of carbon dioxide in the atmosphere.

In the present situation, the cement industry is estimated to contribute from 5 to 10% to the whole released dioxide carbon dioxide [1].

This, together with the estimated with the annual economic impact associated with maintaining, repairing or replacing deteriorating structures is ending up to 16 to 21 billion USD in the U.S. only (Vision 2006-2020), poses dramatic challenges.

The substitution of a certain amount of the cement with fly ashes (a land-filled material) or the replacement of natural aggregates with recycled aggregates from construction and demolition wastes, represent

viable solution to face the aforementioned challenges extending the lifecycle of conventional concrete (Figure 1.1), and thus reducing the overall environmental impact.

The use of self-healing materials undoubtedly represents an innovative and cutting edge issue for sustainable civil engineering industry. According to definitions given by design codes, the durability of a structures consists in the capacity of guaranteeing the requested performance, vs. anticipated design actions, all along the service live, without any unplanned maintenance or intervention. The use of self-healing materials able to repair by themselves and without any external intervention, may reduce the need for unforeseen maintenance and repair, thus resulting in longer maintenance-free periods and hence, despite the higher construction cost, thus representing an interesting asset for sustainable civil engineering.

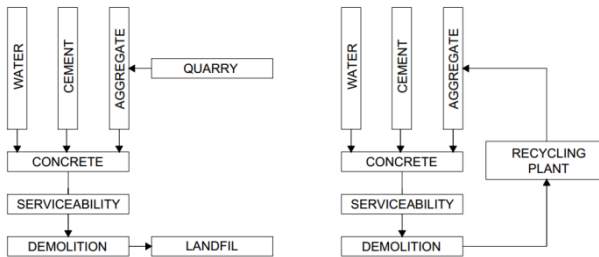


Figure 1.1. Lifecycle of conventional concrete (on the left) and concrete with recycled aggregates (in the right)

The “inspiration” to study the self-healing construction material as well as “embedding” self-healing concept into civil engineering practice has come from “processes” occurring - e.g. inside the human body, such as blood clotting or repairing of the fractured bones (Figure 1.2).

An attractive and interesting analogy can hence be established between the health of a human body – all along its life being governed by the self-healing capacity of its organs and tissues, and the health and safety of a structure, which all along its service life, will benefit from the healing capacity of its constituents material.

In the last years the research activity on self-healing materials has undergone a tremendous development (Figure 1.3). Nevertheless, In Italy and Brazil (the two countries in which the work reported in this

thesis has been done) it is still at its initial stage with the two research institution in which the thesis has been developed (Politecnico di Milano and Universidade Federal do Rio de Janeiro-UFRJ) leading the research field.

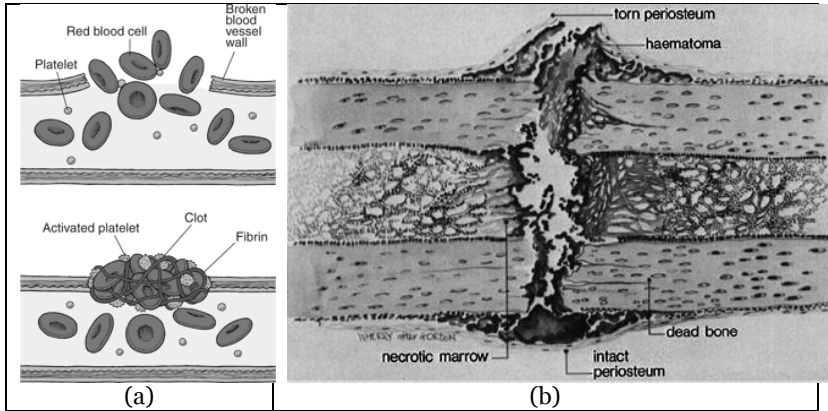


Figure 1.2 The natural process of self-healing on human body (a) blood clotting and (b) “restructuration” of the bone through the process called remodeling. Courtesy by Fratz et al. [3]

1.2. Objective and Structure of this Thesis

In the engineering framework explained above, the present work is aimed at studying the self-healing capacity of a conventional concrete and an advanced fiber reinforced cementitious material with steel micro fibers combined with natural ones.

The main objective of the whole work has consisted in proposing and validating a testing methodology through which the effect of self-healing – in the different kinds of investigated cement based materials – could be highlighted on the recovery of the mechanical properties such as strength, stiffness, deformation capacity, also as a function of new design variables, such as amount of damage, exposure conditions/durations etc.

This with the aim of defining and quantifying healing indices which could be employed in the framework of a durability based design.

State of the Art

The mechanism of self-healing as from the microscopic results when characterized is explained through a detailed microscopic investigation.

Finally a numerical modelling approach has been proposed and validated which would enable, through its predictive skills to include the “self-healing capacity” of a material into the variables governing the design process.

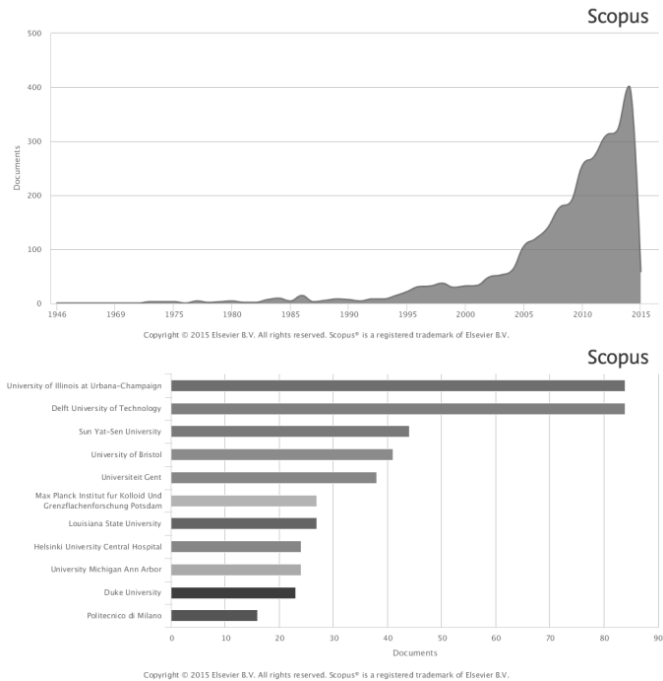


Figure 1.3. Actual situation on the self-healing materials in the world level (top) and due to the University level (bottom). Courtesy by Scopus

1.3. Manuscript Organization

The dissertation is organized into a total of six chapters, starting with this first introductory Chapter concerning the engineering motivations and the objectives of the research work.

Chapter Two presents the state of the art of the research field with particular reference to the influence of different factors on the self-healing capacity of cementitious composites and different self-healing engineered techniques.

Chapter Three deals with the choice and characterization of the tested materials in terms of the employed constituents and the manufacturing processes. Description of the sample preparation, for the different testing procedures, and their identification is given, as well as the different environmental conditions to investigate are described their healing capacity.

In Chapter Four The experimental results are presented and discussed with the aim addressed above. For the different investigated materials the effects of the healing of the recovery of the mechanical properties are analyzed and quantified and through the support of the microscopy studies, the fundamental mechanisms underlying them are identified and discussed.

In Chapter Five the proposed numerical modelling approach is presented and validated by means of comparison with selected experimental results.

Chapter Six summarizes the findings and conclusions of the research work and, finally, remarks for further developments are given.

State of the Art

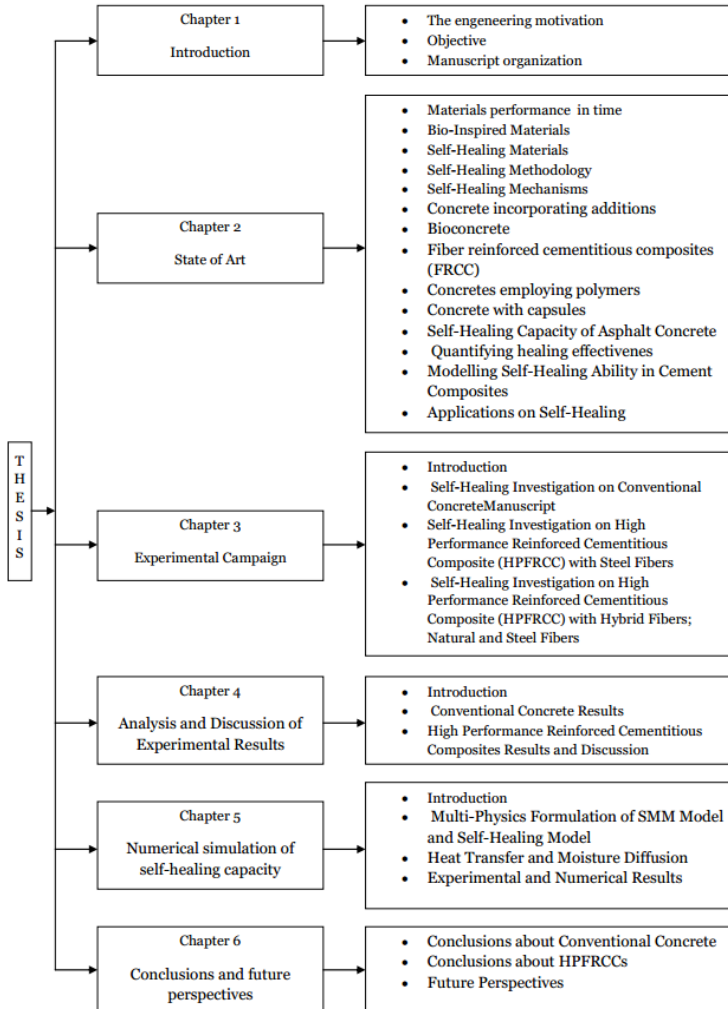


Figure 1.4. Outline of the thesis

*Overcoming is the learning with humility from the past,
Don't repeated it in the present and challenge the future.
Hugho Bethlehem*

2. State of the Art

2.1. Materials Performance in Time

The request that we (as human beings) have made to construction materials and products over the centuries has evolved from the simple basic need of being able to provide a shelter from outdoor environment to more “articulate” performance demands in terms of more complex concepts as safety, serviceability, durability etc.

From the traditional requests of the codes as serviceability and structural safety in different damage states [4], lately a new concept was introduced in the Model Code 2010 as sustainability, that is meant as the ability of the material, structure or structural members to fulfilment of the present needs of humankind with respect to nature, society and humans, without compromising the ability of the future generations to meet their needs in a similar manner [4]. These fundamentals requests have to be declined in a context which is characterized, at least in most of the countries, by the need of building faster, taller buildings, higher capacity infrastructures etc.

Over the life cycle of a structure materials are exposed to different kind of deteriorations, which also implies the concept of thinking in terms of lifecycle of the buildings [5]. In this respect the design

may choose to fulfil the required lifetime performance by using materials featuring different performance level but also different kinetics of decay of their performance in time. These design philosophies are presented in the Figure 2.1 and Figure 2.2 where Van Breugel [6] shows the variability of performance and cost of maintenance in time, based on the quality of materials that was decided to be used. The use of a lower performing material (A) will result in a lower construction cost but will also require an earlier maintenance because of the more rapid deterioration of the performance. These repairing operations lead to an increase of the cost represented by the steps in the graph on the right. It's matter of fact and experience that the employment of a more performing material (curve B) at the beginning of the process will require higher initial investments, but will result in a decrease of the life-cycle cost of the structure, due to the lower number of maintenance actions.

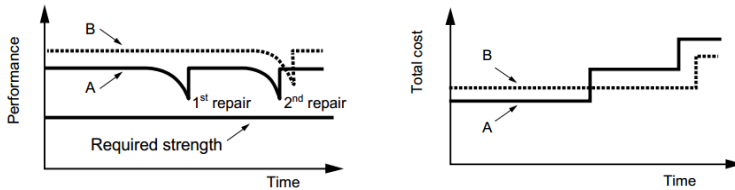


Figure 2.1. Performance (on the left) and cost (on the right) as function of time for normal (A) and high quality (B) structures. Schematic example by Van Breugel [6].

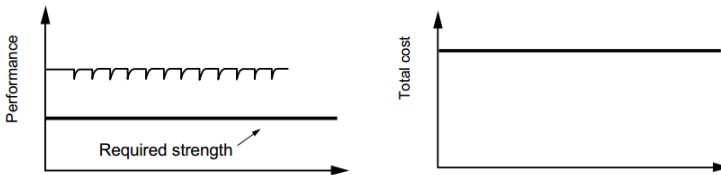


Figure 2.2 Performance (on the left) and cost (on the right) with elapse of time for a structure made of self-healing concrete. Schematic example by Van Breugel [6].

In the case of self-healing materials, the occurrence of a crack or a damage would always activate the automatic process of reparation of the

material itself, which will regain the initial level of performance. Use of this kind of materials would be justified since its costs, higher at the beginning, would be fixed and lower than the costs of other solutions, when projected on the life-cycle of the structure (Figure 2.2). Nevertheless, all these information still are not included in the most recent codes for the life-cycle and durability predictions and several research groups in academia together with the industry are investing on increasing the knowledge about the behavior of these materials.

A concrete example of application of the aforementioned concepts can be found in a study by Li et al. [7] who investigated the life-cycle of a reinforced concrete bridge deck subjected to chloride attack. The cost of construction and maintenance of the bridge deck was determined by parameters as employed materials (Engineered Cementitious Composites - ECC), the conditions of these materials (un-cracked RC and ECC, cracked RC, cracked ECC, ECC with self-healing and without self-healing) and the environment of the region where is built the exposed structure (in this case the region of Detroit, Michigan). The condition of the material as for ex. the crack pattern determines the service strain level of the material for the chosen level of the structural application.

The simulation results based on experimental studies performed by the same authors showed a life cycle cost of the best performing ECC significantly lower (about half) than the life cycle cost of a conventional solution employing reinforced concrete over an estimated service life of 100 years, vs. a three times higher initial cost. Self-healing could perform a further cost reduction of about 25% in comparison with the same material unable to self-heal (Figure 2.3).

As van Breugel [6] hypothesizes, owners might be interested in a product that does not show any decay. As matter of fact it is also evident that the balance between the increasing of the initial costs and the cost saving for the maintenance over time has to be optimized.

Actually today's knowledge of self-healing phenomena in concrete is not enough enhanced to develop structures presenting such a characteristic, but engineered approaches to self-healing already exist. These have followed essentially four ways: inclusion of bacteria, encapsulation of chemical agents, employment of mineral additions and stimulation of self-healing under self-controlled crack width. The possibility of developing many self-healing cement based materials (with controllable healable performance) has been hypothesized for long time but only in last decades a tremendous number of self-healing studies has been published. The obtained knowledge from this research activity and

its application will reduce the maintenance cost and increase life-cycle of the structure whereas the future expectations on using self-healing materials will be reality.

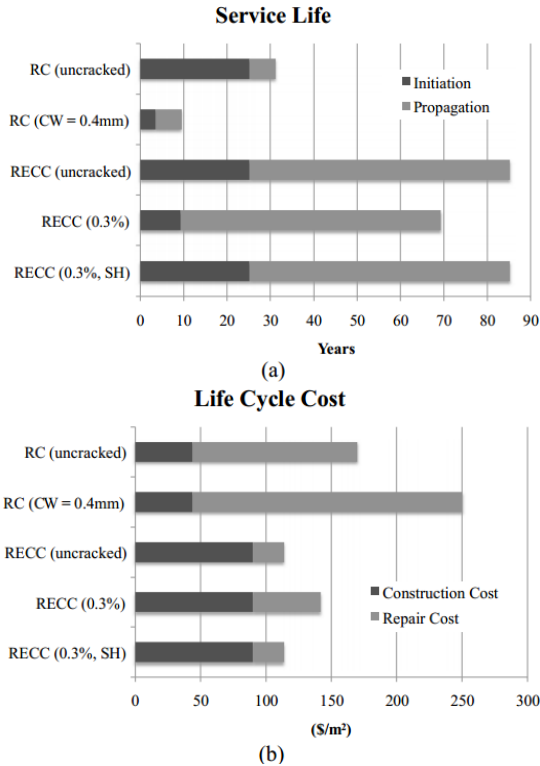


Figure 2.3. Computed service life (a) and life cycle cost (b) showing the effect of self-healing. The "construction cost" here, refers to mainly the initial material cost. Courtesy by Li et al [7]

2.2. Bio-Inspired Materials

The inspiration of self-healing “embedding” process in construction materials has come from a few natural processes as blood clotting or the repairing of fractured bones [8]. Many biological materials have the property to be responsive their environmental changing, to reacting with their ability to adapt the microstructural and mechanical properties on the new reality [9]. In fact, an increase of knowledge about “bio-inspired” way of thinking is incentivized in front of traditional building principles about artificial materials. An examples of a material that performs these abilities is represented by wood which have the ability of mechanical adaption whereas blood and bones perform the healing or recrystallizing of structure [3]. The damage recovery of the teeth and bones via remodeling, is performed by means of a natural process known as “bio-mineralization” [9].

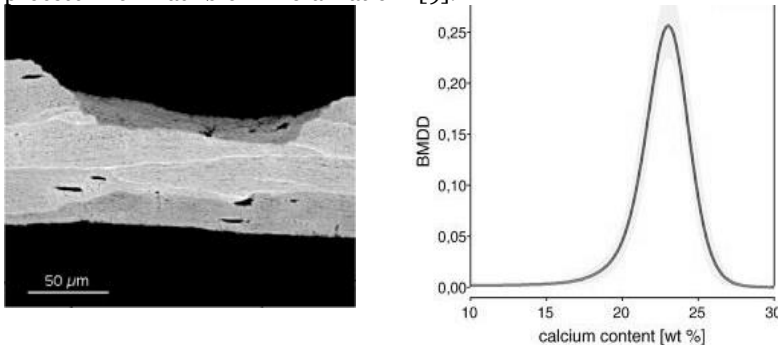


Figure 2.4. Quantitative backscattered electron image (qBEI) of a bone trabecula gray scales (left). Bone mineralization density distribution (BMDD), which describes the Ca content. Courtesy of Weinkamer et al [9].

Self-healing ability performed by natural materials is presented as an intrinsic property and the same way is expected to be performed by “artificial” materials. Constituents of the cement composites such as cement, mineral additives, micro-encapsulated agents, bacteria etc, are called to perform in the “artificial” materials a similar self-healing ability, when damage occur. Based on the aforementioned ability a similar chemical composition presented by the bone “remodeling” (Figure 2.5)

and the healing of a concrete crack (Figure 2.5) is found. The reactive mechanism to the damage can be performed as passive or active [10].

Self-healing process of the bones is a complicated process in front of the adaptive or remodeling process of the trees, whereas the artificial materials and their heterogeneity makes it even more complicated. Nevertheless, there are found important similarities between the bone mineralization and the “crystallization” of the closed cracks in the cement composites showed in Figure 2.5.

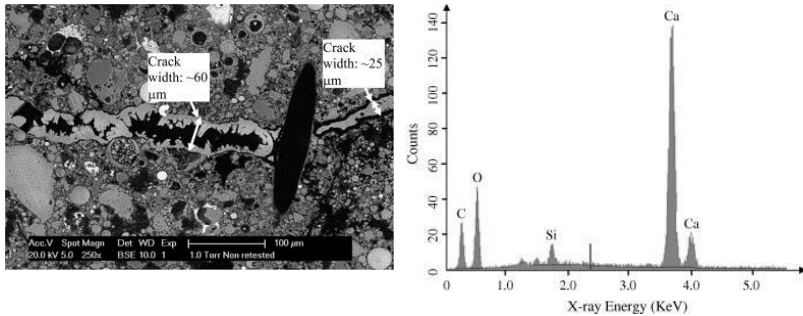


Figure 2.5. Detail of the sample self-healing of the crack by crystal filling (left); chemical composition of the filling crystal with a maximum of calcium content (right). Courtesy by Qian et al [11]

2.3. Self-Healing Materials

One of the first reports about self-healing ability, by the French Academy of Science, dates back to 1836: it was reported that the conversion of the calcium hydroxide leaching from the hydrated cement into calcium carbonate closes the cracks on atmospheric exposure.

Abrams, in 1913, was among the first researchers who explained the autogenous self-healing in concrete [12]. He suggested that the healed strength of concrete is caused by the retarded or the interrupted hydraulicity of the cement.

Gilkey in 1930 [13] studying a concrete about six months old, found that the recovered strength is inversely proportional to the age of concrete. In the same report Bogue concluded that the healing action is represented by the continued hydration, supplemented by physical

stresses, helping the formation of the precipitated bonds between severed grains.

Another idea was reported by Loving 1936, who found the cracks in the concrete tubes filled by the calcium carbonate.

Whitehurst (1951), in a soniscope testing of cracked concrete structures subjected to wet spring, following a freezing and thawing season reported an increasing of the dynamic modulus in the healed concrete [14].

An important study on the strength recovery and on the explanation of the possible healing mechanisms of the healed cracks surfaces was performed by Lauer and Slate [15]. They showed that the strength gain from autogenous healing in the water is not linear with time but follows of a parabolic trend with time whereas in a 95% relative humidity environment this healing activity is more nearly linear, though the recovery is slower but in a greater length in time.

Dhir et al. [16] performed an extended experimental campaign investigating the autogenous healing potential of nine different mortars, varying the aggregate/cement ratio and comparing virgin with fractured specimens. Investigation showed that all types of tested mortars had the ability to self-heal. This ability is highlighted in percentage of recovery due to higher content of cement in front of other mortars with the higher water/cement ratio that showed a higher initial tendency of healing but lower in time.

Several studies performed by Van Tittelbom et al. [17], Li et al. [18] and Edvardsen et al. [19] showed a reduction in water permeability of concretes between the un-cracked and cracked state, lead to the conclusions that this reduction was performed by the self-healing of the cracks.

Ludelli et al [20] on some old brick masonry structures constructed in 1873 showed a high level of precipitation of CaCO_3 which filled cracks up to 50-70 μm . Petrographic analysis showed the filling material to be essentially 100% calcium carbonate and calcium hydroxide crystals and no hydrated products where found [20].

As a matter of fact all the aforementioned studies showed that the products of healing reactions, deposition along the crack faces, may contribute not only to close or seal the crack but may also result into recovery of the mechanical performance of the material.

Whether the product is formed by delayed hydration of un-hydrated cement particles, coming into contact with water or atmosphere moisture upon cracking, or by carbonation it depends – as recognized by

Neville - on the age of concrete when the healing starts occurring as well as the mix composition [21] .

The former case is typical of young concrete, in which the cement has not yet completely reacted with water, or of cement with low (or very low) water to cement ratio, because of which a certain amount of the binder particles may remain un-hydrated.

The latter case on the other hand mainly occurs in the older concretes, the calcium hydroxide reacting with carbon dioxide produced by the cement hydration [22].

A typical case which visually shows a healed/sealed crack due to the water leaching is presented in the Figure 2.6

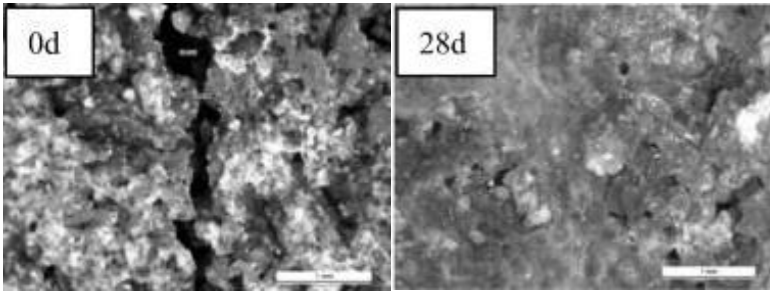


Figure 2.6. Microscopic study of the cracked specimens and the healing after 28 days of water leakage. Courtesy by Want et al.

2.3.1. Self-Healing Terminology

In the development of this research field during last decades different researchers were using different terminology to describe more or less the same phenomena or otherwise the same word for different phenomena. JCI (Japanese Concrete Institute) TC-075B first provided definitions of self-healing which were further taken as reference by RILEM (Reunion Internationale des Laboratoires et Experts des Materiaux, Systemes de Construction et Ouvrages) Ex221-SHC.

As Schlangen [23] reports in his book, a first classification was proposed as follows:

- **Autogenous Healing:** a natural process of filling and sealing cracks without any external operations and works;
- **Engineered Healing or repairing:** artificial and intentional methods for filling and sealing cracks. The healing materials or devices are introduced as a designed function into concrete in advance;
- **Self-Healing or repairing:** process of filling and sealing cracks that automatically takes place in situ without any practical works by workers; this point can be interpreted as the sum of the previous points: self-healing or repairing can automatically happen due to the autogeneous healing processes or the action of an engineered healing.
- **Natural healing:** natural phenomena of filling and sealing cracks that results from some chemical reactions, such as further hydration and carbonation, or mechanical blocking at crack faces (Figure 2.8).
- **Autonomic healing:** involuntary healing of cracks that is provided by admixtures. The admixtures such as fly ash and a specific expansive agent are intentionally incorporated into concrete in advance (Figure 2.8).
- **Activated repairing:** automatic repairing using some artificial devices, which usually consist of sensors and actuators. Repairing function is given by different substances from original constitutions of concrete. This may be considered as "intelligent materials" or "smart systems" (Figure 2.8).
- **Repairing:** general repairing which needs practical works and treatments in situ by workers.

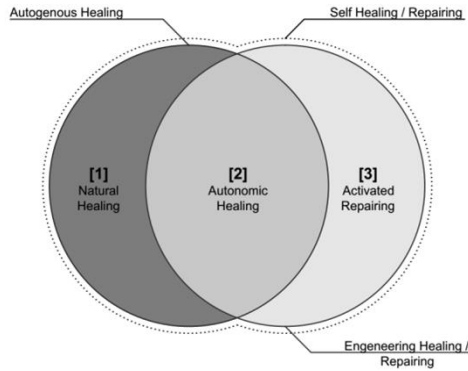


Figure 2.7. Definition of self-healing/repairing concrete by JCI

Mihashi [23] has reported that the following definitions were used by RILEM to further develop a classification of self-repairing:

- **Passive self-repairing:** repairing that occurs due to the reaction to external stimulus without the need of human intervention;
- **Active self-repairing:** repairing that occurs due to the reaction to external stimulus with the need of human intervention;

RILEM took the JCI subdivision between autogenous and autonomic self-healing (Figure 2.8), operating a further classification based on the repairing as a process in the following list:

- **Autogenic self-closing:** own generic material closes cracks;
- **Autogenic self-healing:** own generic materials restores properties;
- **Autonomic self-closing:** engineered additions close cracks;
- **Autonomic self-healing:** engineered additions restore properties.

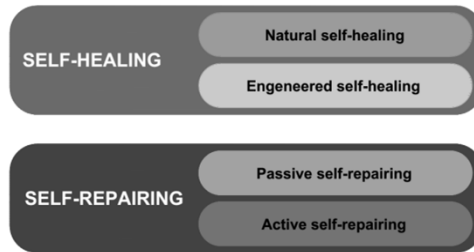


Figure 2.8. Definition of self-healing/repairing concrete by Mihashi and Nishiwaki [23]

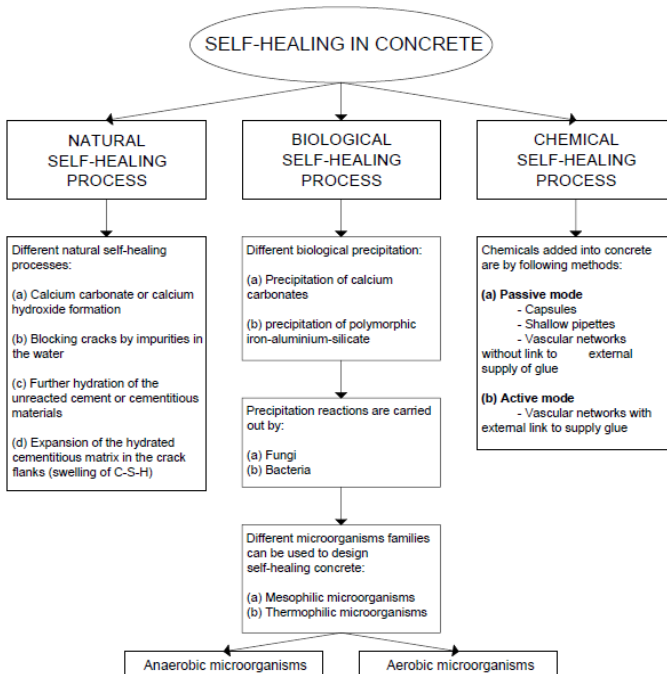


Figure 2.9. Schematic presentation of self-healing in concrete.

In Figure 2.9 a detailed scheme is shown, describing self-healing in concrete, including if the same comes from a natural or engineered modality.

In the following paragraphs the mechanisms of self-sealing/healing will be first of all presented and discussed and the different self-healing engineering techniques will critically reviewed.

2.4. Self-Healing Mechanisms

For a concrete structure to be serviceable, cracking must be controlled and deflections must not be excessive. The non-linear behavior that complicates serviceability in concrete structures is due to cracking, tension stiffening, creep, and shrinkage [31]. A variety of conditions are crucial for the type of mechanism that can generate sealing/healing of the cracks. As mentioned in the previous paragraph there are different even opposite ideas about “how” the cracks close and “which” activity is responsible for that. Organizing all these ideas in a list it is possible to recognize the different mechanism of self-healing as follow [25](Figure 2.10):

- chemical precipitation of calcium hydroxide and calcium carbonate;
- closing of the crack by solid matters during water flow;
- further reaction of anhydrate cement and
- expansion of the concrete in the crack flanks

Among them, only the first and the third are permanent and may determine the healing [25]. We will try to explain more in details every single mechanism and the conditions that favors and affect each of them.

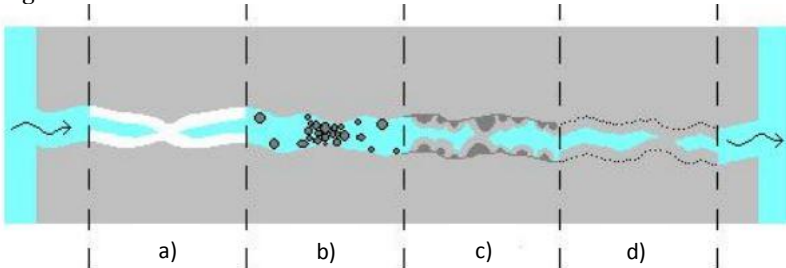
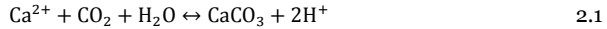


Figure 2.10. Self-Healing Mechanisms in Concrete: (a) formation of calcium carbonate or calcium hydroxide, (b) sedimentation of particles, (c) continued hydration, (d) swelling of the cement [25]

2.4.1. Crystallization of calcium carbonate

One of the most important mechanisms of self-healing is represented by calcium hydroxide reaction, which is one of the products of hydration in concrete, with carbon dioxide CO_2 (atmosphere or dissolved in water) to form calcium carbonate [24].

The reaction ($CaCO_3$) is the following:

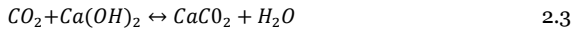


Where Ca^{2+} are the calcium ions, ($CO_2 + H_2O$) represent the external environment, entering in reaction and forming the calcium carbonate ($CaCO_3$).

Calcium hydroxide ($Ca(OH)_2$) in the area of the crack can dissolve in the water inside the crack and precipitate calcium ions at the crack surface.



On the crack surface of concrete some calcium carbonate will be formed due to the reaction of CO_2 present in the crack ingress water with Portlandite (calcium hydroxide) present in the concrete matrix according to the following reaction:



The amounts of calcium carbonate production depends on the presence and amount of CO_2 . Portlandite is a rather soluble mineral in fact most of it present on the crack surface will dissolve and diffuse out of the crack into the overlying water mass. Subsequently, as more CO_2 is present in the overlying water, dissolved Portlandite will as yet precipitate in the form of calcium carbonate but somewhat even away from the crack itself.

Apart from the temperature, pH and partial pressure of CO_2 , the formation of calcium carbonate in the slot depends mainly from the index saturation Ω and, with it, the ion concentration of Ca^{2+} and CO_3^{2-} present in the solution and the solubility product of calcite K_c .

Furthermore thermodynamic considerations have shown that the circumstances which favour the precipitation of CaCO_3 in a slit can be:

- raising the temperature of the water;
- increase of the pH value of the water;
- partial fall of CO_2 in water.

Figure 2.11 shows the equilibrium concentration of the ions Ca^{2+} , CO_3^{2-} and HCO_3^- as a function of the pH value of the solution.

Based on the graph, the curve of solubility of CaCO_3 has a minimum at a pH value of approximately 9.8, where it has a lower demand of Ca^{2+} necessary for the initiation of the precipitation of calcite primary. The minimum solubility of CaCO_3 occurs at a pH value intermediate between that of the hardened cement paste (pH = 13.5) and what is usually encountered in water (pH = 5.5 - 7.5). The water present in the slit reaches the minimum pH of solubility (equal to 9.8) and thus triggers the primary precipitation of CaCO_3 .

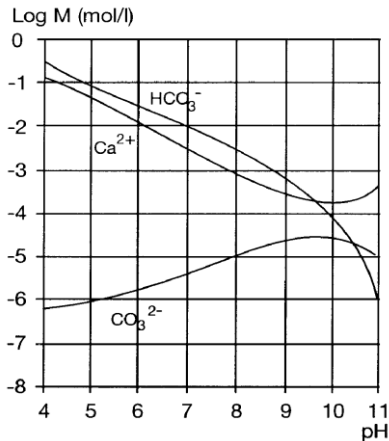


Figure 2.11. Equilibrium concentrations of ions of Ca, CO_3 e HCO_3 as pH function (Edwardsen, 1999).

As an example is presented a petrographic study that shows that the filling of the cracked zone by the calcium carbonate. As long as calcium hydroxide and water are present, carbon crystals precipitate on

the free surfaces of the crack and fill it. The kinetics of crystal growth is a surface-controlled process but later on changes to a diffusion-controlled crystal growth. A similar mechanism was suggested also in the earlier studies of the self-healing mentioned before by Lauer and Slate [15].

Studies conducted by Edvardsen [19] showed the formation of calcium carbonate as the sole cause of "self-repair." It was found that the growth rate of the crystals of CaCO_3 depends on the width of the slits and by the water pressure; while the composition of the cement (cement types used and the nature of the aggregates) and the water hardness does not have any influence on the self-healing mechanisms (Edvardsen, 1999).

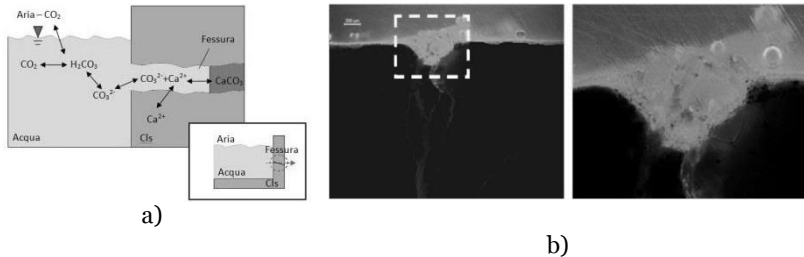


Figure 2.12 a) Interfaces and reactions in $\text{CaCO}_3 - \text{CO}_2 - \text{H}_2\text{O}$ system by Edvardsen [19] b) Precipitation of the calcium carbonate

2.4.2. Further reaction of un-hydrate cement

The hydration process, as known, mostly occurs during early ages of concrete (Figure 2.13). Depending on the different cement/binder and water (cement + binder) ratios the binder particles will continue the hydration process also in front of the environmental conditions, in particular in the presence of the water or moisture whereas. The presence of the cracks emphasize the continuation of cement hydration, because larger amounts of un-hydrated particles would be exposed to water or moisture and hence would continue to hydrate. From this point of view, continuing hydration of concrete is, with the formation of calcium carbonate, the main reaction conducting to the crack sealing/healing.

As early as in 1913 by Abrams [12], this phenomenon was recognised, but only in the last two decades, thanks to the progress in cracked concretes permeability studies, scientists have approached it considering its independence from the other self-sealing reactions.

Hearn [25], stated that continuing hydration and the other healing mechanisms occur under different boundary conditions. In fact, continuing hydration is also observed in systems where there's not any presence of CO_2 , where the carbonation can't occur.

The phenomenon is more evident during the early ages of specimens: Hearn and Morley [28] observed that 26 years old concretes didn't show un-hydrated portions of cement, because the hydration was already consumed by then. Furthermore, their experiments showed that the most important effect occurs in the first 100 hours of exposition to water.

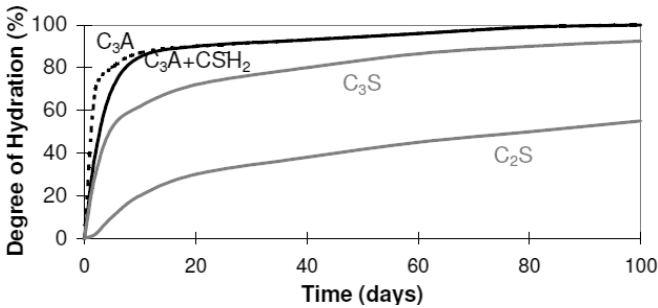


Figure 2.13. Degree of Hydration of the principal hydration components in cement by Shah et al.

As mentioned before, Neville [19] attributed importance to the continuing hydration only for concretes in their early ages, when autogenous healing can occur, whereas calcium carbonate crystallization can be more important in later ages.

With reference to the water/(cement + binder) ratio, this parameter governs the hydration degree and the time when the self-healing activity can develop: a lower ratio promotes the reaction due to the presence of more particles of un-hydrated cement, that react upon the water flowing inside the crack or the atmosphere moisture entering on it.

In Figure 2.15 a tentative is presented to simulate the quantity of the un-hydrated nucleus in time. The results show that a lower w/c ratio

promotes a higher possibility to self-heal thanks to the higher number of un-hydrated product still to be hydrated after one year, in this case.

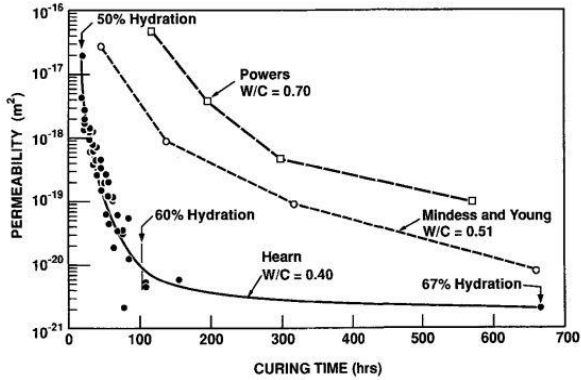


Figure 2.14. Permeability versus extent of hydration by Hearn and Morley [26]

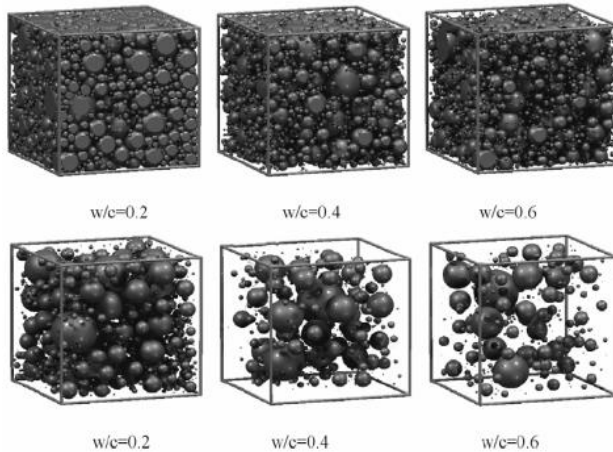


Figure 2.15. Cement paste (top) and un-hydrated particles after 1 year of hydration. Courtesy of He et al [32]

When pozzolanic components as fly-ash are introduced in the cementitious composites, the hydration process changes and gets slower. In an interesting study by Termkhajornkit et al [46], it is presented the amount of hydration in time for a conventional concrete and one with fly-ash. They calculated the ratio between the hydrated parts with the total hydration for different percentage of fly ash in compared to Portland cement paste (Figure 2.16). We can say that in this case, if the crack are always occur during the early days or even months the products of the normally occurring hydration reactions would fill and heal the cracks.

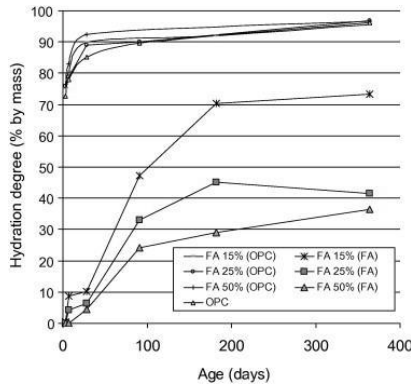


Figure 2.16. The hydration degree of cement and fly ash as a function of time. Courtesy of Termkhajornkit et al [46]

2.4.3. Sedimentation of particles

The cracks can be clogged by particles carried by any liquid or by cement particles lost by the surface, that ultimately can get stuck in the narrowest parts of the concrete fractures.

Hearn [25] wrote that physical clogging has been one of the most common explanation for self-sealing. Mc Millan and Lyse in 1930 would consider it to be the main cause of healing in cracked concrete.

Hearn and Morley [28] report that Glanville (Figure 2.17) demonstrated that sedimentation of particles was not responsible for self-sealing. He conducted flow-reversal tests in order to detect the increase of permeability that occurred after several flow cycles. Comparing the

results of concretes with the responses of sandstone specimens, Glanville observed that while the permeability of sandstone increased with every reversal, concrete exhibited a small increase only after the first reversal.

Glanville attributed the increase of flow in sandstone after every reversal to the opening of new passages, rather than to particle movement. On the other hand, concrete showed only a slight increase after reversing the flow, which means that physical clogging cannot be responsible of permanent self-healing of cracks.

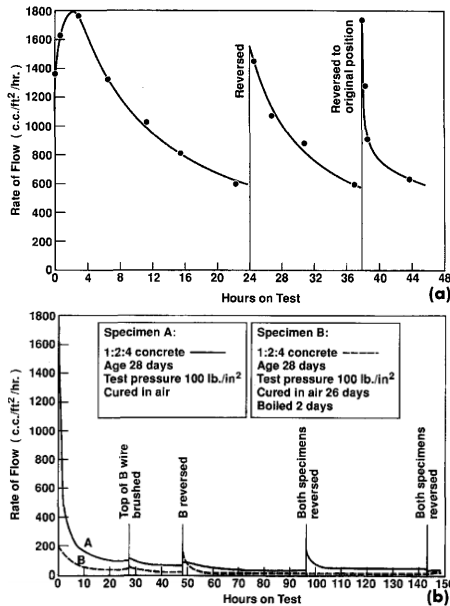


Figure 2.17. Glanville's permeability curves from Hearn and Morley: a) effect of reversal direction of flow in a sandstone specimen; b) effect of reversal flow direction in a concrete specimen. Courtesy of Glanville [28]

Le Roy et al. [29] performed a study promoting the closure of the crack by the particles produced in the event of physical failure or damage such as micro-granular particles. Recently it has been demonstrated that nanoparticles will segregate into the cracks and notches caused by the mechanical damage, and they will close the crack reducing the

permeability of the water and avoiding the passage of aggressive agents [33].

2.4.4. Swelling of the cement matrix

The movement of water into or out of a cement matrix causes respectively swelling or shrinkage [17]. During the hydration, the cement matrix features a loss of water and, in this case, shrinkage at early age induces strains of such a magnitude that are larger than the tensile strain capacity at the same age, thus resulting into cracking. Concrete shrinkage plays a major role in each of these aspects of the service behaviour of concrete structures [30], [31]. Shrinkage makes the flanks to move further away from each other and hence, the crack width increases.

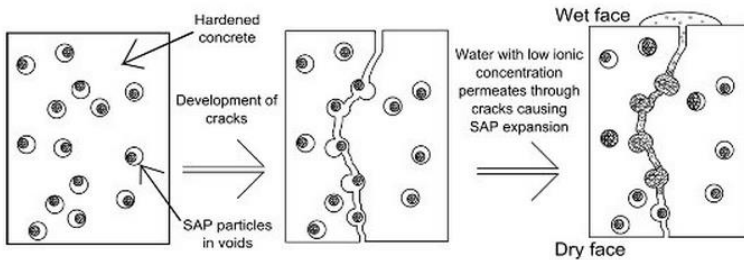


Figure 2.18. Schematic showing the mechanism so self-healing using SAP Van Tittelbom et al [17]

The significance of swelling phenomena was well demonstrated earlier by Hearn [25] with the propan-2-ol/water replacement method proposed by Feldman, which is a particular test to determine diffusion of chloride in concrete. The results showed that, when CSH was not saturated by water, its layer collapsed and the permeability appeared to be one order of magnitude bigger than that calculated for saturated specimens.

She also stated that self-sealing effect encompasses the autogenous healing and continued hydration. She designated the swelling of CSH as a "false Sel-Sealing-Effect-SSE", since it influences the permeability depending on the saturation conditions, without permanent effects. One of the solution to contrast this problem is the expansion of

matrix which consist in the closing of crack flanks moving their sides closer.

The swelling mechanism is the basic also of the functioning of SAP, a topic which, also with reference to the self-healing potential, has been receiving attention in the last years. [33]-[35].

Snoeck et al. [33] showed that in an environment with a relative humidity higher than 60%, only samples with superabsorbent polymers exhibited healing. Figure 2.19 shows the effect of the SAPs content on the healing of the crack when exposed to higher humidity environment.

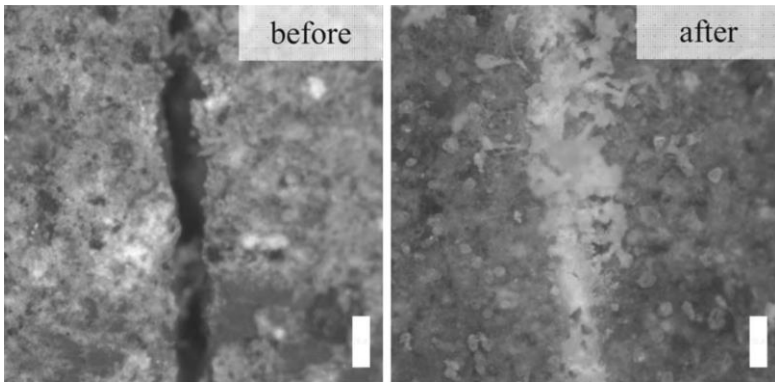


Figure 2.19. Total healing of a 138- μm crack a specimen in containing 1% SAP B after wet/dry cycles. Courtesy of Snoeck, De Belie, et al [33]

2.5. Factors influencing self-healing

The activation of one of the mechanisms discussed above will produce the expected result of self-healing, but the effectiveness of these mechanisms depends on several factors that affect the self-healing reactions such as:

- Mix constituents
- Presence of Water, water type, water pressure, water temperature, water pH;
- Environmental Conditions (Temperature and Humidity);

- Crack width, Stability of the crack and Degree of Damage in Concrete (The Roughness of the Cracked Zone, Stress across the Crack and Stability of the crack);
- Content of Self-Healing agent (if any).

It's not easy to describe the influence of each one of factors on the self-healing phenomena because of their mutual interaction, but in the following paragraphs a more detailed explanation will be provided.

2.5.1. Mix constituents

The typical and the simplest constituents of the concrete, as well-known, are water, cement, fine aggregates and coarse aggregates. The characteristics and the quantity of these constituents determine the mechanical characteristics of concrete. However, the variation of these components doesn't make the difference just in the mechanical behaviour, but also in the possibility to heal the cracks when they occur. Effect of mix design variations are mostly studied in the self-healing investigations [12], [15],[18],[28],[30], [39],[52], [56].

The presence of additions such as fly ash or silica fumes in the cement paste affects the pore structure and determines the level of early and later hydration of the binder phase. The pore size of the paste will compact and determine the formation or not of the cracks [11], [38]. Moreover, the quantity of additions and cement particles determine the reactivity of the material with its environment [30]. Also, an increase in cement amount will result in increasing of available particles for further hydration when the cracking occurs due to the higher quantity of possible unreacted particles. In this case, two different ratios become important: the cement/binder ratio and the water/(cement + binder) ratio, as better explained in the paragraph 2.3.2. Fly ash and silica fumes help in later stages inducing other hydration reactions that contribute to the formation of sealing/healing products.

2.5.2. Presence of water and water type

Water is essential for all the aforementioned self-healing mechanisms: when there is no presence of water or moisture from the atmosphere in the crack, the autogenous healing mechanisms do not activate [19].

Lauer and Slate [15] stated that, when the relative humidity is less than 95%, the extent of healing is much lower and the growth of the filling crystals is irregular. Furthermore, some author tried to give an explanation for this phenomenon: in a humid environment, carbon dioxide is present only on the surface of water films and carbonation becomes slow [25]. Thus, in order to promote the autogenous healing, the surfaces must be in contact with water. The type of water in terms of ion concentrations also affects the self-healing.

Edvardsen [19] has investigated the effect of the hardness of water on the sealing of cracks. Her experiments revealed that the concentration of CO_3^{2-} and HCO_3^- ions didn't limit the calcite precipitation, as not all of the ions were consumed by the reaction. This evidence might occur because the quantity of Ca^{2+} ions present in the exposed regions of the crack is smaller than the quantity of carbonate ions present in hard water in contact with the crack.

Fagerlund and Hassanzadeh [39] performed tests on pre-cracked specimens, exposing respectively to tap water, brackish water and sea water, under different modes of water exposure: permanent immersion, cyclic immersion and one-side capillary suction. They found out that the permanent immersion in sea water was the most effective curing method, followed by brackish and tap water respectively.

The effect of sea water on self-healing was furthermore investigated by Li [16] and few others [17, 18] in the field of ECC and SAPs-modified concretes. Their results will be presented in the next paragraphs.

2.5.3. Water pressure, Water pH and Water temperature

When the water flows too fast through the crack, self-healing is slower. Edvardsen [19] conducted some experiments in order to verify the water flow in different crack width, under different pressure conditions. She found that, after 7 weeks exposure for lower pressure of the water, the cracks were closed completely whereas the same one for higher pressure had just 25% of closure.

Fagerlund and Hassanzadeh [39] and Ramm, Biscopig [40] reported that the cracks exposed to pressure healed more effectively in a given time than stress-free cracks. The contrast among the results could be due to the influence of several factors, such as the different thickness

of the specimens and the length of the crack. These parameters indeed affect the coefficient of flow through concrete.

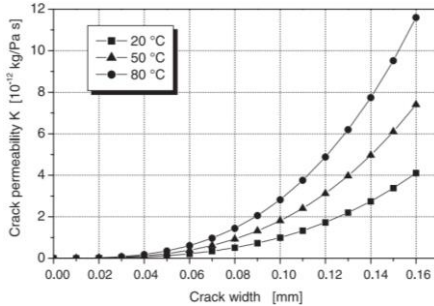


Figure 2.20. Representation of the dependency of the crack permeability K on crack width and temperature. Courtesy by Reinhardt and Jooss [38].

Reinhart and Jooss [38] made tests on specimens with different crack widths, keeping three different temperature levels: 20, 50 and 80 °C (Figure 2.20). The permeability tests showed that on increasing the temperature, self-healing became faster. This property was more evident when the width of the crack was smaller.

2.5.4. Crack width

The width of the crack is one of the most important parameters: it determines the volume to be filled by reactions products and the quantity of water that will flow through the fracture. The amount of water that flows through the crack is the parameter that characterises the durability, somehow being related to the amount of the aggressive agents that can flow inside the concrete affecting seriously its function.

With reference to their opening w , indicatively the cracks classified as follows:

- capillarity cracks with $0.0 < w < 0.2$ mm (not easily visible);
- small cracks with $0.2 < w < 0.4$ mm (visible but not clearly);
- large cracks with $0.4 < w < 0.8$ mm (clearly visible).

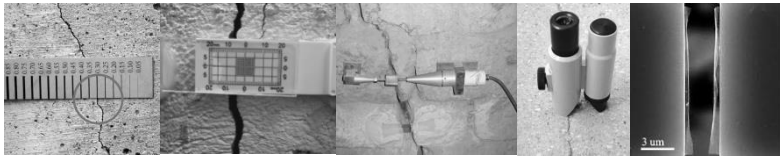


Figure 2.21. The evolution on the measurement of the crack width, from the most traditional to the most advanced as the digital microscope measurement [44][45].

As explained before, the last group of the cracks represents a serious static damage of the structure and they are not included in the design phase. The appearance of the cracks (Figure 2.21), even in the minimum size in order to be considered meaningful, depends on the exposure conditions during casting and curing [44]. Based on different studies and the numerous codes the admissible crack width can be:

- Indoors casting0.35 mm
- Outdoor environments casting 0.25 mm
- casting in particularly aggressive environments 0.15 mm

The research didn't arrive to the point of establishing exactly the maximum width that can be autogenously healed, because there are too many factors that can simultaneously affect this value e.g.. From the causes of cracking (bending moment, tension, shrinkage, etc.) depends even the shape of the crack, which is one of the parameters that affect the effectiveness of self-healing together with the exposure conditions during the curing period. Crack width and the effectiveness in various environment conditioning has been studied by some researchers, but not all of them have the same idea for the effect of crack width on self-healing [38]-[40] [49].

Generally, the volume of hydration products of cement is not sufficient to close large cracks. Li and Yang [47] had reported in their studies on ECC that 50 µm is the maximum crack width to achieve the full recovery of mechanical and transport properties in concrete. Between 50 and 200 µm in general only a partial recovery can be achieved.

Gagné et al. [49] stated that self-healing for finer cracks until 50 µm (Figure 2.22) is performed a healing rate of 15 µm/month, closing totally these cracks in five months of water immersion. On the other hand, for cracks up to 200 µm, there is a higher rate of healing by 15-30 µm/month because a larger crack is likely to expose to a higher amount of

un-hydrated—and hence—reactive particles to the outdoor environment. The only point about which the two author groups agree is that in larger cracks as wide as 300 μm , just 20% of healing was presented after 5 months in water.

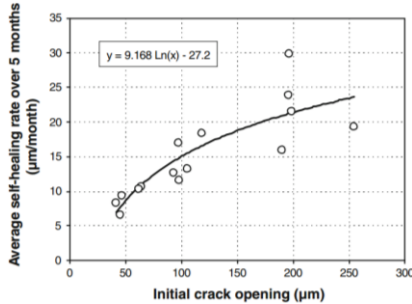


Figure 2.22. Relationship between rate of self-healing and initial crack opening. Courtesy of Gagnè et al [49]

Edwardsen [19] confirmed these numbers in her experiments on permeability of healed concretes, in terms of water flow through the specimen (Figure 2.23).

2.5.5. Stability of the crack and the stress along the crack

The crack should be prevented from growth and motion, to allow the healing products to fill the space between the crack flanks. The stability of the crack in fact depends on the stress in the structure that passes through the crack. When the crack is dynamic, the healed cracks ruin again. Anyway, an autogenous healing can also occur in active cracks. This healing is comparable to the one of dormant cracks only at the minimum crack width, as shown again in Edwardsen's [19] research work (Figure 2.24).

Very few researchers [53] performed a study on the healing capacity of cracked cementitious composites under sustained stresses.

As a matter of fact different response should be expected whether the through – cracks stress will be compressive or tensile and/or caused by force of bending moment.

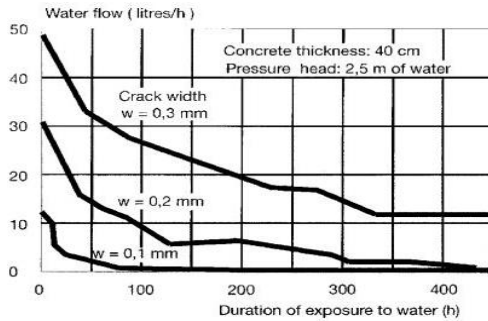


Figure 2.23. Relationship between water flow and time for different crack width. Courtesy of Edvardsen [19]

Very recent Albertini et al. [54] tested FRC specimens pre-cracked in bending up to 0.5mm CMOD and healing under wet/dry weekly cycles subjected to a uniform compression through crack. Stresses were set equal to half the residual flexural stress exhibited by the same materials upon the pre-cracking. As expected the applied stress greatly enhanced the healing capacity with respect to the stress – free case.

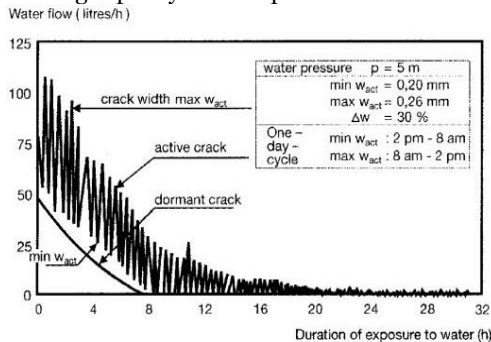


Figure 2.24. Relationship between flow and time for active cracks by Edvardsen [19]

This topic anyway still deserves a truly greater attention because of its representativeness of conditions truly occurring in structural elements when in service.

2.5.6. Mechanical properties of healed cracks

Most of the studies about autogenous healing capacity of concrete were focused on the permeability characteristics of healed specimens. Only a few researches concentrated on the recovery of mechanical properties.

Sahraman et al. [61] and Jacobsen et al. [55] investigated the recovery of compressive strength after the introduction of cracks marked by different cracking modes. In the first case, cracking is performed pre-loading specimens up to 90% of their compressive strength.

Sehramant et al. [61] showed that when pre-loaded up to 90% of their ultimate strength and after conditioning for 30 days of water curing, the strength reduction of pre-damaged specimens was only 7% with respect to virgin specimens at the same age, indicating a substantial healing.

In the second case Jacobsen et al. [55] deteriorated the specimens by rapid freeze/thaw tests. Once the conditioning was done, the specimens were stored in water at 20 °C. After three months, Jacobsen et al compared the mechanical properties of specimens after deterioration and after healing. They evaluated their frequency response as well. The experiments showed that the specimens regained most of the resonance frequency. However, only a 4-5% of the mechanical strength recovery was observed on an initial loss of 22-29%.

As Abdel Jawad [56] had already observed, resonance frequency does not, therefore, correlate with the recovery of strength of self-healed specimens.

Ter Haide [25] provided some results on the behaviour of cracked concrete at the early ages.

Li et al [47] and [57] also investigated effect of healing on the recovery of mechanical properties.

In his study, Abdel Jawad [56] cracked up to different widths cement specimens that were cured in moist or dry curing at room temperature (23°C) for 20, 24, 48 and 72 hours respectively. The effect of an applied compressive stress during healing was investigated after 7, 28, and 90 days, the samples were loaded up to failure to evaluate the effect of time on self-healing. Ultrasonic pulse velocity measurements were taken to evaluate the healing capacity of damaged specimens. The results revealed that compression was of great influence, since it allowed the specimens to heal and reach the strength of non-cracked concrete. On the

other hand, the specimens which were not under compression showed a total recovery of the stiffness with only a partial recovery of strength. As expected the better results were obtained when stored in moisture environment vs. dry conditioning to the room temperature.

Yang, Li et al [48] performed another type of test to study the mechanical properties of the healed cracks in ECCs. They performed uniaxial tension tests on specimens at early age of three days after casting and damaging at different levels, from 0,3%; 0,5%; 1%, 2% and 3% strain (Figure 2.25) . Specimens were conditioned in different environment such as water immersion, air exposure, wet/dry cycles. The better healing was promoted when in water immersion and longer time of exposure. Upon longer exposure higher strength and stiffness regain was obtained correlated with a higher amount of healing products observed. Moreover, less calcium carbonate was produced upon shorter exposure time because of short time allowed for its formation.

Granger et al. [58], in their study on ultra-high performance cementitious materials, compared the effect of the storage in air and water for cracked specimens, measuring the healing capacities at different ages.

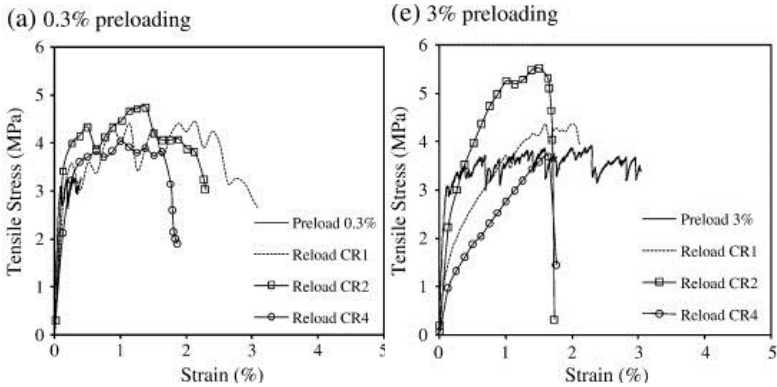


Figure 2.25. Typical preloading and reloading tensile stress–strain curve for two cases of ECC with predetermined tensile deformation of (a) 0.3%, and (b) 3%, after different environmental conditioning regimes [48].

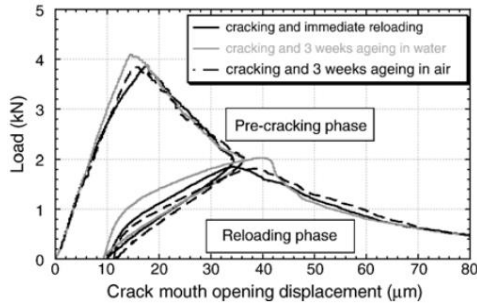


Figure 2.26. Average mechanical behaviour of reference specimens (stored without crack in water for 10 weeks, and then cracked and immediately reloaded) and of cracked specimens stored in water for 10 weeks before reloading. Courtesy of Granger et al. [58]

They observed that specimens aged in air had the same mechanical behaviour as that of samples reloaded just after cracking, while specimens stored in water showed an increase in stiffness and reloading peak that evolved with the time of conditioning (Figure 2.26).

However, these conclusions can be valid only for the materials employed in the surveyed studies, because of the strong influence of the specific composition of the mix.

2.6. Concrete incorporating additions

The use of admixtures in concrete during last decades became an important part of the cement composites industry, multiplying the use of concrete in aggressive environments achieving “ideal” resistance and workability. Consequently, the last few years, researchers have been conducting studies on the promotion of self-healing with the addition of agents that favors the deposition of crystals inside the crack.

According to the definitions of JCI and RILEM, these materials provide an *autonomic or engineered healing*.

Different methods and additives can concur to optimize the self-healing reactions. One way is to add fly ash or blast furnace slag, which, by reducing the porosity of material, let a portion of cement un-hydrated even at later ages because of the pozzolanic reaction that they produce. In

this case, autogenous healing of concrete is attributed to continuing hydration.

On the other hand, researchers have studied the self-healing capacities of mixes including expansive materials, crystallizing agents and geo-materials.

In this latter case, chemical agents such as carbonates can activate the expansive agents and lead to the precipitation of calcium carbonate crystals and the formation of hydration products: CSH, CASH (gehlenite hydrate $2\text{CaO}\cdot\text{Al}_2\text{O}_3\cdot\text{SiO}_2$), $\text{Ca}(\text{OH})_2$, AFt (minerals in which are present $t=$ three groups of anhydrite, such as the ettringite), AFm (minerals in which is present one anhydrite group).

Although the addition of geo-materials and expansive agents can result into healing, they always have to be accompanied by a superplasticizer, since they absorb a large quantity of water and decrease the workability. Furthermore, the mix must be done carefully, for the wrong quantity of chemical agents can cause undesired expansions and result in the consequent formation of cracks. Moreover, the compatibility between the different materials is not always verified.

2.6.1. Concrete incorporating fly ash, chemical admixtures, expansive agents and geo-materials

The use of fly ash has been seen not just as one of “promoters” of self-healing but it contributes directly to the retardation of the hydration process.

Firstly the use of fly ash has been seen as the reducer of the pores in concrete [59], [60]. Results indicates that the addition of fly ash even contributes at later curing age, reducing the critical pore size in front of reference sample. Sahmaran et al. [61] tested the self-healing capacity of specimens in which 35% or 55% of cement mass was respectively substituted by fly ash. The samples were pre-loaded up to 70% and 90% of their compressive strength to generate micro cracks and then stored in water. Even in this case the main application of fly ash is to improve the water tightness and to stop leakage in concrete structures. These experiments focused not only on the permeability properties but also on the mechanical properties. The results in terms of mechanical properties showed that the higher fly ash replacement in the specimens, the lower was the initial compressive strength. On the contrary, the specimens with

more fly ash were able to recover more strength than the others, especially after a long period (after 30 days).

Conversely, the UPV test, showed different results in front of the mechanical ones, independently of the percentage of fly ash. For both the tests before and after the curing period, the values for the 55% fly ash specimens were comparable to those of plain cement specimens, while the 35% fly ash specimens showed higher values.

Finally the permeability tests exhibited a decrease in water flow, depending on the quantity of fly ash. This trend was more evident when the curing period was longer, probably because of the slower hydration of fly ash.

A possible explanation of the previous results was given by Termkhajornkit *et al.* [46], who studied the physical effect of self-healing on the pore structure of concrete by performing various compressive and RCP (Rapid Chloride Permeability Test) tests along a period of one year on specimens presenting cracks due to autogeneous shrinkage. The evidence was that the specimens with more slag and fly ash (50%) had the best healing capacities, though they needed more time to develop the hydration products and improve their strength.

A study conducted by Zhou *et al.*[62], confirmed that after a 30 days curing period under different conditions, the specimens which showed the higher recovery of strength were the samples containing 20% to 30% of fly ash and in the Figure 2.27 it can be seen the increasing amount of the crystals due to the increasing of the percentage of the slag.

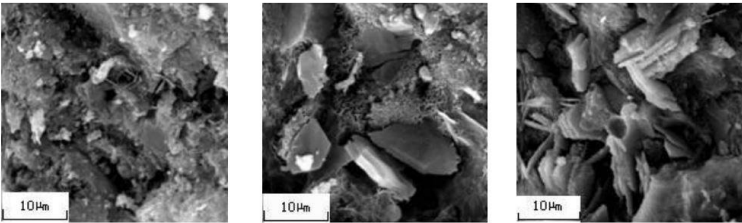


Figure 2.27. SEM Cross-section picture for concrete after self-healing: (a) normal cement concrete; (b) concrete specimen with 30% slag; (c) concrete specimen with 40% fly ash. Courtesy by Zhou et al. [62]

In another study, Kishi and Ahn [63] tested the addition of carbonates to different mixes. Their aim was to verify the effectiveness of these compounds in presence of expansive and superplasticizer agents, under water conditioning after cracking.

This research showed that all the carbonates led to the deposition of crystals on the cracks surfaces. However, crystal bridges were formed only in presence of C_4A_3S (hauyne). The best results were obtained only with the collaboration between the expansive and chemical agents (Figure 2.28).

Furthermore, the researchers investigated the chemical nature of crack fillers, which, in all the cases, were composed of CSH, CASH, $Ca(OH)_2$, AFt, AFm and calcium carbonate deposits, depending on the chemical agent employed.

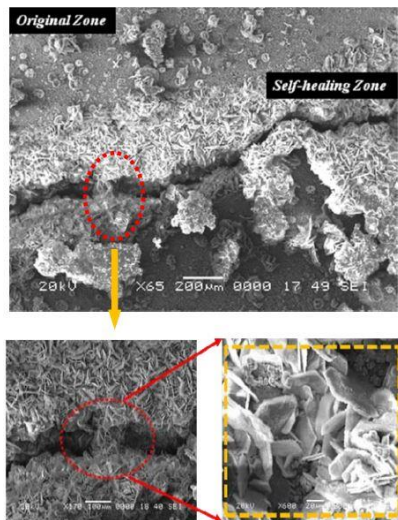


Figure 2.28. Self-healed re-hydration products in crack by hydrogarnet phases C-A-H and calcite phases. Courtesy by Kishi and Ahn [63]

2.7. Bioconcrete

One way to stimulate the production of calcium carbonate to fill cracks is the addition of mineral-producing bacteria to concrete.

Bacteria had already been employed in ecological engineering for the removal of chemical agents from waste [64], water and for bioremediation of contaminated soils [65].

As Mihashi [23] reports from Jonkers, in concrete environment there are several conditions to be satisfied to make the employment of bacteria possible: their lifetime should be at least as long as the lifetime of the structure; they must be enough resistant to survive the mixing process and the alkaline environment of concrete. Furthermore, bacteria shouldn't deteriorate properties like mechanical strength.

"Extremophilic bacteria" revealed themselves to respect all the above mentioned conditions. The name "extremophilic" was given to bacteria species that can live in extreme environments; they can be found in deserts, rocks and also in ultra-alkaline environments that are comparable to that of internal concrete.

Furthermore, extremophilic bacteria are in general characterized by the capacity to form endospores, which can metabolize calcium carbonate. The endospores have resistance against high chemical and mechanical stresses and their lifespan varies between 50 and 200 years. According to RILEM and JCI definitions, concrete containing bacteria can be defined as *engineered self-healing material*.

Schlangen [23] remarks that deposition of calcium carbonate is a chemical process governed mainly by four parameters: concentration of calcium, concentration of inorganic carbon, pH level and availability of nucleation sites.

In literature, different calcium carbonate-producing bacteria were investigated with different aims. Essentially two are the methods employed for repairing cracks in concrete by means of bacteria: the urea-based system and the calcium lactate-based system.

2.7.1. Degradation of urea

Ureolytic bacteria can precipitate CaCO_3 in their micro-environment by the conversion of urea into ammonium and carbonate.

Bacterial degradation of urea decreases the pH locally, thereby, favouring the formation of carbonates with calcium in calcium rich environments, thus, filling the cracks.

Bacteria precipitate CaCO_3 by means of the following chemical reactions of secretion of the enzyme urease which catalyses the conversion of urea into ammonium and carbonate.

Since the cell wall of bacteria is negatively charged, it attracts the Ca^{2+} ions to deposit on their surface, leading to reaction with CO_3^{2-} to form CaCO_3 . Hence, the bacteria surface serves as the nucleation site.



Gollapudi et al. [66] in 1994 foresaw the employment of a bacterium called *Bacillus Pasteurii* to test the possibility of plugging flow columns filled with sand. They found out that the microbial activity could enhance the production of $CaCO_3$. They remarked that the optimal pH to favour the deposition of mineral was 8.5; furthermore, the experiments showed that contaminants, such as benzene, nitrate and carbon tetrachloride, slowed the growth of bacteria.

Ramachandran *et al.* [67] provided concrete remediation by using *Bacillus Pasteurii* (Figure 2.29) and *Pseudomonas Aeruginosa*. They tested two types Portland cement mortar specimens; the first type has been mixed with micro-organisms and the others, were notched and filled with microbial solutions. The tests confirmed that micro-organisms, when added in a low quantity, could increase the compressive strength in concrete cubes and remediate cracks by producing calcite when PH was lower than 12.

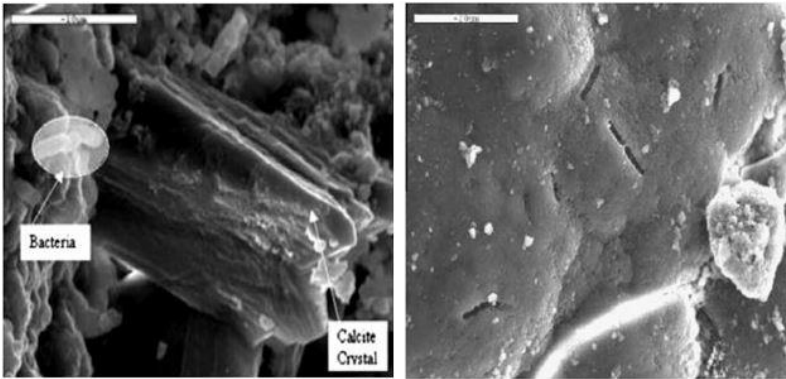


Figure 2.29. Developing of calcite crystals at higher magnification. Rod-shaped objects, consistent with the dimensions of *Bacillus Pasteurii* are spread around the crystals. Courtesy by Siddique and Chahal [70].

Van Tittleboom et al. [68] reported and studied about the importance on the protection of bacteria to enhance the production of calcium carbonate. They applied silica gel carrying *Bacillus Sphaericus* bacteria in concrete samples. They found that bacteria protected in silica

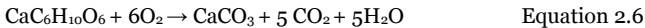
gel filled the cracks completely while pure bacteria could not. Based on their conclusions, this happened before the CaCO₃ precipitation started. Specimens were cured in a urea-calcium solution to provide food to bacteria.

In 2010 Wang et al. [69] studied the employment of both polyurethane and silica gel as capsules to embed and protect bacteria during the mixing storage. Their results remarked the better performances of polyurethane concerning the regain of strength and the diminution of water permeability.

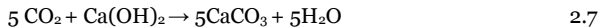
2.7.2. Calcium lactate-based bacteria

As per Schlangen et al. [71] reports, in order to guarantee the precipitation of calcium carbonate, bacteria cells need an organic substrate to convert metabolically into inorganic carbon, which can react with free calcium to precipitate calcium carbonate. Though cement matrix is rich of calcium ions due to dissolved portlandite, organic carbon is usually not present in the matrix. Many researchers tested the direct application of bacteria and their nutrients at the crack surfaces of bio concrete. In a real structure, the detection of cracks is a long and expensive work which would cost more than normal maintenance.

In 2010 Jonkers et al. [72] tested the direct integration of bacteria in concrete which could automatically act as internal self-healing agent. They proposed the employment of a two component healing agent constituted by bacteria from genus *Bacillus* (*Pseudofirmus* and *Chonii*, Figure 2.30) and calcium lactate directly added to the mix. The experiments showed that bacteria acted like a catalyst, transforming the lactate into calcium carbonate, as per the following reaction:



The quantity of calcium carbonate precipitate increased when the produced CO₂ reacted with the molecules of portlandite, as per the following carbonation reaction.



They observed (Figure 2.30) a large production of 20-80 μm sized particles in the first week, which precipitated on cracks surfaces. However, in 28 days long curing period, the study showed a decrease in particles production. This phenomenon was due to the loss of spores

following the restriction of pores in the matrix: the pore diameter got reduced from 0.1-1 μm to 0.01-0.1 μm with age, as a result of which 0.8-1 μm diameter spores could not be accommodated.

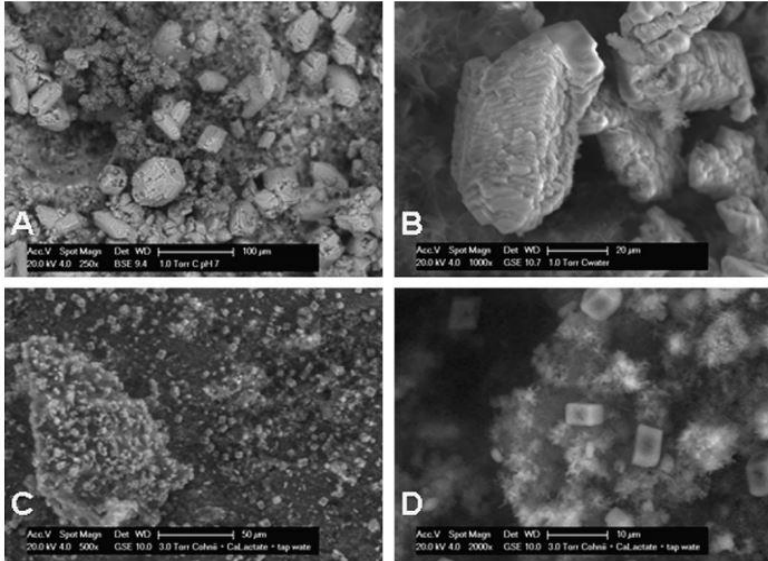


Figure 2.30. Cement stone specimens with incorporating healing agent. (*B. Cohnii* spores plus calcium lactate), cracked after 7 (panels A: 250x and B: 1000x) and 28 days curing (panels C: 500x and D: 2000x). The large mineral precipitates visible on the surface of the younger specimens seem to be due to the conversion of calcium lactate by bacteria. The small precipitates on older specimen's surface resemble those produced by abiotic specimens. Courtesy by Jonkers [72]

This process not only presents the advantage of being a human-independent self-healing method but also considers the health of concrete, contrary to urease-based system. In the latter, production of ammonium considerably increases the risk of reinforcement corrosion and degradation of concrete which gets further oxidized by bacteria to form nitric acid [73].

Wiktor and Jonkers [73] immobilized a two-component healing agent in porous clays particles, which constituted calcium lactate and

Bacillus Alkalinitrilicus. In this research, the authors tried to increase the service life of the spores, which in the above mentioned study had revealed a functional life of only 1-7 days, due to the effect of high alkalinity that generally decreased the viability and mineral-producing capacity of spores. Their research showed an increase of bacteria's life up to 100 days. Furthermore bacteria revealed to enhance the self-healing capacity by closing 0.46 mm width cracks, while normal concrete samples healed 0.18 mm width cracks only at maximum during the same curing conditions.

2.7.3. Effect of bacteria cells and walls on concrete strength

Many researchers drew conclusion that inclusion of different bacteria does have variable effects on compressive strength of concrete. Furthermore, different kinds of nutrients revealed themselves to have a negative effect on the tested specimens mechanical behavior.

Gosh et al.[10] Investigated the use of micro-organisms to improve the strength of cement mortar, by adding bacteria from genus *Shewanella* and *Escherichia Coli* to cement-sand mortars. They obtained an improvement of 25% in compressive strength after 28 days with the first bacterium when a cell concentration of 105 cells/ml of solution was used, while the latter wasn't able to improve mortar capacity. So far, they concluded that the increase of compressive strength is not a common property of bioconcrete.

Jonkers [72] in his study mentioned that the addiction of a high number of bacterial spores lead to a 10% decrease in the compressive strength of concrete measured at 3, 7 and 28 days.

Ramachandran et al. [67] tested mortar cubes in which *Bacillus Pasteurii* and *Bacillus Aeruginosa* were suspended with saline or phosphate buffer and compared the results with control specimens. Saline medium revealed a significant decrease in the compressive strength of concrete, probably due to the presence of chloride ions. Cubes prepared in phosphate solution showed otherwise a consistently higher strength. The results highlighted that an increase of compressive strength in cubes that contained all the form of biomasses. In particular, the 7-days-compressive test increased with the increase of cell concentration, regardless of their form. At 28 days, the compressive strength was enhanced by adding either live or dead cells of both the bacteria together,

whereas the admixtures composed only by *Bacillus Pasteurii* showed the opposite trend.

It can be concluded that the incorporation of bacteria in concrete makes it possible to repair wide cracks up to 460 μm after 100 days curing, by utilizing only the capacity of bacteria to produce calcium carbonate.

Bacteria can also yield other benefits: in dependence with the type of micro-organism embedded, concrete strength can increase and its pore structure become finer.

Though, the use of bacteria presents many difficulties. At first, bacteria must survive to the mixing process; one way to improve the strength of cells is to embed bacteria in synthetic capsules, but also this method can be not convenient due to the incompatibility that could occur between capsules and bacteria or due to the changing that capsules perform on the micro-environment.

Anyway, the idea to have bacteria, though inactive, in their own walls, might scare people and limited the use of this technology, which at the moment is anyway not ready to be employed on a real structure.

2.8. Fiber reinforced cementitious composites (FRCC)

Fiber reinforced cementitious composites, today are listed in the Model Code 2010 representing one of options as structural materials which can be used in each field and environment. From an historical point of view everything started with the simplest use of small fibres that permitted to “link” the matrix, as was used in the ancient times of Egypt e Babylonia. Later on, in the early sixties of last century, the aim of reducing the brittleness of concrete promoted the use of different types of fibers such as glass, carbon, synthetic and natural ones.

In the 1960s, Romualdi et al. [74] investigated the behavior of fiber reinforcing mechanisms in cementitious composites. Different studies performed later on investigated the absorption of energy and tensile strength [Shah et al., 1971, [75]. ACI committee [76] proposed some applications as slabs on grade, industrial floors, pavements, overlays, decks, shotcrete linings, as well as for enhancement of fire resistance, repairing and strengthening works. Naaman and Reinhardt 2006 [77] proposed a classification (Figure 2.31) depending on tensile response specifically either strain-hardening (multiple cracking occurs

before reaching the peak value of stress) or strain-softening behavior (deformations localize in one crack).

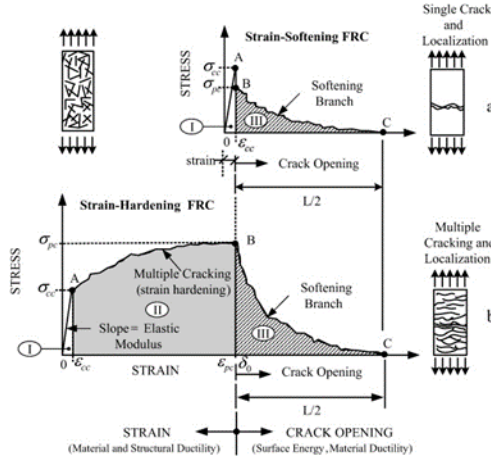


Figure 2.31. Typical tensile strain softening and hardening behavior of FRC Courtesy by Namman and Reinhardt [77].

From this classification it is possible to classify the materials that show hardening behavior in direct tension are classified as High Performance Fiber Reinforced Cementitious Composites (HPFRCC) if their compressive strength is below 200 N/mm², otherwise, if compressive strength is greater than 200 N/mm² they can be classified as Ultra High Performance Cementitious Composites (UHPRCC). ECC (Engineered Cementitious Composites) are a particular category of HPFRCC, originally developed at the University of Michigan, which has a moderate tensile strength (4-6 MPa) and a very high ductility (3-5 %).

Different studies performed by Di Prisco et al. and Ferrara et al. [80]-[89] clarified important aspects of HPFRCC as workability, dispersion of the fibers into the matrix and correlate it with the fresh state performance which can be controlled through the rheology and the casting process, and which affects the hardened state performance.

The shape of the fibers will be classified into three categories, depending on the cross sectional dimensions of the fibers:

- Microfibers - cross section diameter $\leq 100 \mu\text{m}$, size of the cement particles;

- Mesofibers - cross sectional $\leq 0.1 \leq$ diameter ≤ 0.3 mm;
- Macrofibers - larger than 0.3 mm

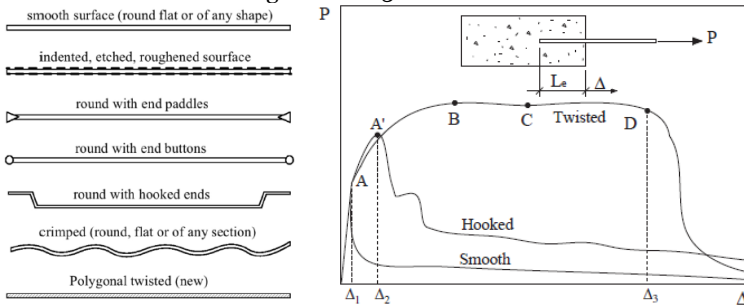


Figure 2.32. (a) Different Types of steel fibers ; (b) Expected comparison of pull-out load versus slip response of smooth, hooked and twisted steel fibers. Courtesy of Naaman [77]

The type of fiber affect the pull-out mechanisms of failure (Figure 2.32.a). These mechanisms generally develops along four stages (Figure 2.32b);

- o: Elastic Stage;
- A: Micro-cracking Stage (stable propagation);
- B: Macro-cracking Stage (basically unstable propagation);
- C: Bridging (stabilizing stage 2).

Micro-cracking is one of the fatal deteriorations generated in service which can bring to catastrophic failure of the composites ad significantly shorten the lifetimes of structures [79]. In fact cracks are inevitable [21]; micro cracks can be occurred during service life of concrete structures due to external loading, intrinsic volumetric instability or deteriorious from chemical reactions [23]; the main philosophy of using small fibers is the cracking pattern control of the cement composites.

The cracks on HPRCCs, even at ultimate load, doesn't increase their width, which remains in the range of 50 to 80 μm , aslso as a function of the fiber content. This reduce the possibility that aggressive agents affect the durability of the concrete [90].

2.8.1. Self-healing capacity of FRCs

The attention of researchers in the field of self-healing cementitious composites has been focused on ECCs, thanks to their intrinsic capacity of crack control and their ductility. However, a few researches also focused on the capacity of ordinary FRC to self-repair.

Hannant and Keer [91] studied the autogeneous healing of thin polypropylene-fibre reinforced mortar sheets, by investigating the recovery of tensile strength and stiffness of cracked specimens after a long period. After having induced multiple cracks (more than 20) in their polypropylene-reinforced specimens, specimens were divided in two groups, where one subjected to open air and the remaining inside a laboratory, to prevent them from exposure to weather changes.

They were retested after a period of 7 months to 2 years. After 7 months weathering the specimens healed completely; the tensile strength of the healed cracks after two years in natural weathering conditions was about 50% of the tensile strength of the un-cracked samples of same age. On the other hand, these specimens showed almost complete recovery of stiffness whereas no autogenous healing was observed in samples stocked indoor, and no stiffness recovery.

Gray [92] performed self-healing study performing pull-out tests on 7 and 28 days old specimens (before healing) which were then cured and tested again at 28 and 90 days respectively. An apparent bond strength increased by a factor of 3 for specimens healed between 7 and 28 days and by a factor of 1.7 for samples healed between 28 and 90 days. Recovery of the compressive strength was observed but never as in the virgin state.

Homma *et al.* [93] investigated self-healing of FRCC with different fiber reinforcements ratio. Samples containing polyethylene fibres (PE), steel cords (SC) and hybrid fibres composites containing both PE and SC were casted. Self-healing ability was studied after a curing period of 28 days immersion in the water by means of tensile strength and permeability tests. Microscope observation was conducted at 3, 7 and 28 days of curing. After 3 days, it was already possible to remark the formation of crystals in PE and PE plus SC samples due to the attachment both at the crack surface and at the PE fibres. But the specimens with steel cord didn't show attachment of crystals.

The authors concluded that this difference was due to the higher percentage in volume of fibres contained in PE samples, which

constituted a network that supported the formation and increase of crystals between the faces of cracks.

Mihashi [24] reported that Koda et al. carried out an experiments on FRC similar to the above mentioned study by Homma [93]. They employed PE and PVA fibres at 1.5% by volume and they investigated the self-healing of cracks on pre-loaded specimens. They concluded that the capacity to heal cracks thinner than 100 μm was about the same for both types of fibres, but for larger openings, the chemical polarity of PVA fibres increased the capacity of the samples to self-heal, because of the possibility to attract the healing products.

2.8.2. Self-healing capacity of ECCs

Different studies about the autogenic self-healing of ECC were performed by Li et al. [7], [57], [90], [94]. In one of them the self-healing capacity of ECCs was analysed under aggressive conditions, testing the specimens in a 3% NaCl solution, to simulate the sea-water. The author confirmed that in such an environment the specimens could self-control micro-cracks width during strain hardening, and even under large deformations it is possible to have an average crack width of about 50 μm and up to 100 μm . This study reveals the ability of ECCs to self-heal crack damage even in extreme environments as chloride concentration. Chemical analysis showed that the chloride ions interacted with the interface between matrix and fibres with the matrix, promoting the leaching of calcium hydroxide, which increased the porosity in the mix and sealed/healed firstly the small cracks and reduced larger ones.

Pre damaging the ECC samples and performing different wet/dry cycles was proposed by Yang et. al [90], to simulate the raining and un-cloudily days in different temperatures. Firstly, 6 months of wet/dry cycles were performed in both cases with 20 ± 1 °C. The second conditioning was about wet/hot dry, with water immersion at 20 ± 1 °C for 24h and then drying of the specimen in 55°C for about 2h. Resonance frequency measurements, permeability and uniaxial tensile strength tests were carried out. A complete recovery for cracks below 50 μm and partial recovery for cracks up to 150 μm (Figure 2.33).

When recovery occurs, the resonance frequency increases with the number of cycles, initially at a rapid rate but eventually after at least 4 or 5 cycles levels off. The full benefit of self-healing could be achieved: resonance frequency was totally recovered and the stiffness was actually enhanced. The second cycle showed worse performances on self-healing in terms of resonance frequency and stiffness.

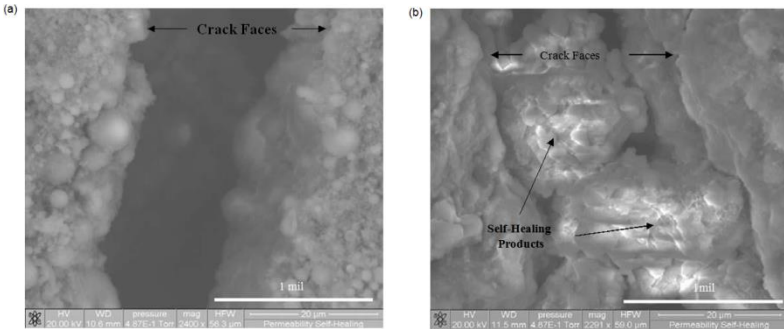


Figure 2.33. Morphology of crack within ECC specimen from ESEM: (a) Autogenous self-healing crystalline formations in ECC crack after permeability testing; (b) ECC crack before permeability testing. Courtesy by Yang et. al [90]

Tziviloglou [95] studied the self-healing capacity of PVA reinforced-ECC materials with low content of different micro-fibres and micro-particles. Prismatic specimens were tested under four point bending test. He found out that the flexural strength of all the healed specimens increased more than that of virgin specimens cured in the same conditions, especially in the samples cracked at a later age, which showed the best recovery capacity. However, the regain of stiffness never reached the original values.

Antonopoulos [96] worked on ECC in which high content of micro-fibres and SAP polymers were considered. She investigated five different mixes: the first contained 2% PVA fibres by volume, three mixes employed PVA at 2% along with steel fibres at 1, rockwool fibres at 1% and 8 grams of SAP polymers and the last one saw a reduction of the PVA fibres from 2 to 1% by volume and the addition of steel fibres at 2% (Figure 2.34).

She stated that a higher proportion of additives could negatively influence the recovery of mechanical capacity as for e.g. the mixture by Tziviloglou containing SAPs in a lower quantity attained 31% higher value in strength recovery and 18% in stiffness than a mixture that had higher SAP quantity.

Sahmaran et al. [53] conducted experiments on ECC beam specimens preloaded at different deformation levels and then exposed to chloride ponding. Immersion tests on cracked and un-cracked ECC and

steel reinforced mortar and immersion tests were conducted on ECC and mortar cylinders to determine the chloride penetration depth as a function of immersion time. They found out that ECC chloride penetration depth was lower than the depth in mortar specimens at all the ages. This is probably due to the capacity of ECC to maintain the width of crack below to 50 μm , while in mortar samples the failure comes with the formation of one big crack that constitutes a weak point in terms of permeability as well.

The capacity of ECC to control the width of crack (Figure 2.34) makes these materials ideal even to prevent the penetration of aggressive agents, such as chloride ions or wet/dry on hot air temperatures.

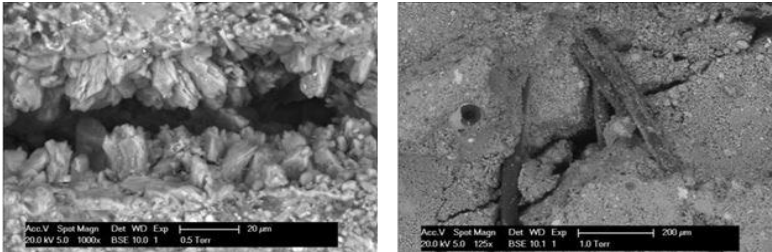


Figure 2.34. At the left: partial crack healing in an ECC with PVA .The scale bar has a height of 20 μm ; at the right: bridging effect of PVA fibers. Courtesy by Antonopoulos [96]

2.8.3. Natural fibers to enhance the performances and healing capacities of concrete

The idea of employing natural fibres to improve the self-healing properties of concrete is relatively new.

In 2009 De Rooij et al. [97] published a paper on their research at the DTU, in which they studied the physical and mechanical properties of different types of natural fibres in order to prepare future works on self-healing of concrete.

Basically, De Rooij recognized the possibility of using fibres extracted from different plants or leaves, (such as larch, pine, lianas, sisal and similar) as vectors for carrying some healing agent in concrete.

These fibres indeed, are present in a large variety of sizes, ranging in length from 30 to 150000 μm and diameters from 5 to 800 μm . Moreover, they're environmentally friendly and available in wide quantities all over the world.

The characteristics previously mentioned, combined with the pore structure of the fibres, that can store in their holes and cell walls up to 0.5mm³ of healing agent per millimetre fibre length, would be ideal to act as a vehicle system for healing agents as the glass hollow pipe systems on which it will be discussed in the next paragraphs.

Natural fibres have another fundamental characteristic that makes them suitable to employ in concrete: their tensile strength and capacity to bond with the cement paste. Ranging from 130 to 900 MPa, the strength of natural fibres is comparable to the strength of polymeric fibres, such as PP (770-780 MPa), or steel fibres (1200 MPa).

From the experience on ECC, and from other experiences that will be presented later on it's possible to state that natural fibres can be used in substitution of PVA fibres and other healing agents that presents a high cost, complicated procedure of casting, of activating and usually are not environmentally friendly.

The employment of natural fibres in concrete have been studied later, in the contest of the international cooperation project *EnCoRe*. Ferrara et al. [98] investigated the effect of natural reinforcements such as sisal fibres on self-healing of concrete.

In this study a combinations between sisal and steel fibres has been investigated. The steel fibres play a "structural role" maintaining a stronger bridge between the cracks where the natural fibres provide better ability to heal the cracks.

4 point bending test, were performed for the pre-cracking of the specimens. Immersion in water, exposure to open air, dry conditions with 50% of relative humidity, moist conditions with 90% of relative humidity and wet/dry cycles for periods of one, three and six months before reloading were performed. In order to quantify the healing, the same tests performed for the pre-cracking phase were performed after different conditioning.

Results of related investigation will form part of this thesis and will be presented further on.

2.9. Concretes employing polymers

Since 1990, the worldwide interest in polymer-concrete has become stronger, thanks to the research and development of high performance and multifunctional construction materials [99].

Concrete-polymer composites are made by replacing a part of the cement binder of conventional mortar or concrete with polymer. They can be classified into three categories:

- Polymer modified mortar (PMM) or concrete (PMC), which is a category of concrete-polymer composites made by partially replacing the cement hydrate binders of conventional cement mortar or concrete with polymers or polymeric admixtures.
- Polymer concrete (PC), which is formed by polymerizing a mixture of a monomer and aggregate, without other bonding materials;
- Polymer-impregnated concrete (PIC), which is produced by impregnating or infiltrating a hardened Portland cement concrete with a monomer and subsequent polymerizing the monomer in situ.

In the following paragraphs, the self-healing capacity of polymer-modified concretes will be considered.

According to JCI and RILEM definition, polymer-modified concrete can be included in the category of engineered self-healing materials.

Research on self-healing properties of polymer modified concretes is a relatively new topic. Not many types of PMC have been studied yet nor has been the interaction and behaviour of this polymeric film with the self-healing reactions.

Abd Elmoaty [100] studied the autogenous healing behaviour of concrete containing SBR latex and ACR (acrylic) with a solid content of about 52%. The dosage of SBR in different percentage was studied as the effect of cement content, the type and the age of deterioration were considered. UPV (Ultrasound Pulse Velocity) tests were conducted to determine the level of self-healing immediately after 28 days curing, and then again after 20, 40 and 60 days of conditioning.

UPV results increased in the first 20 days, whereas between 20 to 60 days the rate of healing process decreased evidently. The authors concluded with stating that 20 days of curing must be enough to convert most of un-hydrated particles to hydrated particles.

Probably this was due to the membrane of polymer formed around the un-hydrated particles, which prevented them from further hydration, thereby retarding this process. Moreover, the increasing of the age of damage decreased the self-healing capacity.

In another study Lukowski and Adamczewski [101] have investigated concretes modified with epoxy resins (EP) without hardener.

The observation of the microstructure (Figure 2.35) showed what has been stated before: that the introduction of polymers in the form of conventional liquid resins leads to the formation of a continuous film which coats the cement particles. Later, this has revealed to be the best way to enhance the self-healing in the samples.

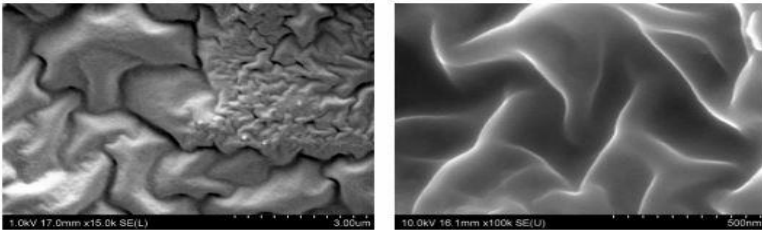


Figure 2.35. Polymer film in epoxy cement composite. Courtesy by Lukowski and Adamczewski [100]

Based on the showed results, self-healing ability combined with polymers, which forms a film inside the matrix, limits the hydration just in the first 10-20 days of their “life”, performing a limitation for the autogenic self-healing when the un-hydrated cement particles could be able to continuously hydrate. Nevertheless, for the dry conditioning - where the re-hydration hardly will take place - this can be a possible solution.

2.9.1. Sap-modified concrete

Another family of polymers which has been widely studied is the superabsorbent polymer one (SAP). SAPs are cross-linked polymers that absorb, swell and retain large quantity of liquid without dissolving, depending on the PH degree of liquid, its salinity and the presence of various types of ions. For example, the free swelling of SAPs can reach

values of 5000g/g in deionised water, whereas it can decrease to 10 g/g and less in concrete pore solution.

The cement hydration makes the SAPs to release water, thereby leaving its pores in the concrete paste, in sizes with range from ten to hundreds of microns. These pores can be seen as defects in the paste, being intercepted by the occurring cracks. Once in contact with the environment humidity, SAPs are free to swell again. The schematic performance of SAP has been presented before on the swelling cement matrix (Paragraph 2.3.4) and in Figure 2.36 a schematic mechanism of their action on self-healing is presented.

Kim and Schlangen [102] have investigated the self-healing in ECCs stimulated by SAPs under flexural cyclic loads. The exposure cycles wet/dry cycles, open air and water represented the curing condition of the samples after cracking. The improvement of their mechanical behaviour was observed during wet/dry cycles, right after the first two cycles. The author hypothesises was that the reaction of un-hydrated cement was consumed after the first two cycles.

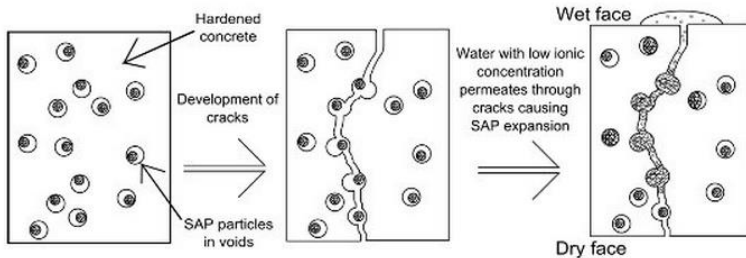


Figure 2.36. Schematic showing the mechanism of self-healing using SAP. Courtesy by Van Tittelbom et al [17]

Snoeck et al. [33] studied mortar mixtures with fibre reinforcements and varying amount of SAPs. Four-point bending and permeability tests were performed after various curing conditions. Better self-healing was achieved with water immersion when compared to high humidity conditions (RH90%) and wet/dry cycles.

The later results showed the nature of these materials, that are capable of absorbing water also from the moist and for this reason their application is interesting for dry environments, where normally autogeneous self-healing could not occur due to the absence of water in high concentrations. Moreover, the worsening of some mechanical

performances of concrete represents a limit for the possible employments of the material.

2.10. Concrete with capsules

Microencapsulation can be described as the process of enclosing different-sized particles of solids, liquids or gases in an inert shell, which isolates and protects them from undesirable reactions with the external environment.

According to the above described definitions of JCI and RILEM, the concretes containing capsules belong to the category of *smart or intelligent materials*. As reported by Mihashi [23], in fact the capsules are able to sense the crack (sensing function) and automatically release the healing agent (processing function), which fills the crack (actuating function)(Figure 2.37).

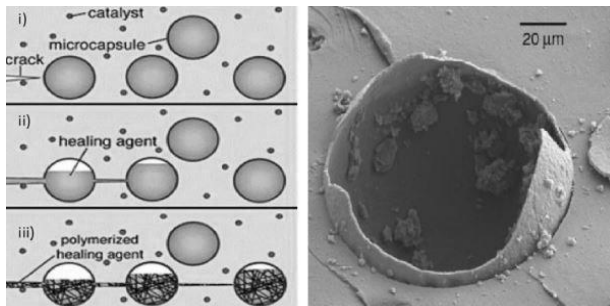


Figure 2.37. (left) basic method of the microcapsule approach: (i) cracks form in the matrix; (ii) the cracks rupture the microcapsules, releasing the healing agent through capillary action; (iii) the healing agent contract the catalyst, triggering polymerization thus ensuring the closure of the nearby cracks and (right) ESEM image showing a ruptured microcapsule. Courtesy by Van Tittelboom and De Belie [17].

However, micro-capsules are usually incorporated into concrete in advance, during the mix phase. Because of that, it is possible to operate a further classification, allocating these systems in the category of *autonomic healing systems*, in which *passive self-repairing* is

performed. In this way, the outright microencapsulation can be distinguished from other encapsulating systems, such as the vascular ones.

Fundamental steps to be considered when making functional the autonomic healing with capsules are presented in the following list, based on the report of Van Tittleboom [17]:

- Survival to the mixing process;
- Influence on mechanical properties and workability;
- Compatibility with the healing agent and the cement matrix;
- Probability and release efficiency of the capsules and healable crack volume.

One of the first promoters of this methodology was White in 2001 [104]. Firstly he introduced the healing agent in polymeric composites, using the polymeric matrix as a catalyst - the shape was typically spherical or cylindrical. The general idea is that the capsules are broken by the occurring cracks, then the healing agent is supposed to flow out and react in the region of the damage (Figure 2.37). The dimensional range of the capsules runs from 4.15 to 4000 μm for the spheres and 40 to 7000 μm for the cylinders with lengths that varies from 15 to 250 mm.

It is important not only that the capsules have to pass through the mixing process, but also the releasing of the healing agent depends from the ultimate strength of the capsules, which has to be broken when the crack pass through the capsule. Because of these reasons, generally brittle materials are employed and the capsule thickness is optimized.

Schlangen [23] reports, for example, that Thao *et al.* tested hollow glass and perspex tubes as encapsulating vehicles for epoxy resin. The higher ductility and strength of the perspex has delayed the rupture, so the glass was finally chosen.

Different ways were proposed to protect these capsules during the mixing process.

Dry [105] proposed the protection by a water soluble glue - or combine the proper shell with another layer - Xia studied the encapsulation of SAP polymers with a cement plus paraffin layer and Schlangen [23] described that Pang coiled them with a spiral steel wire, followed by a thin mortar layer, to prevent them from premature damage. The breaking of the capsules at premature damage may change even the mechanical properties of concrete.

In the case of hollow tubes (Figure 2.39) it has also to be considered that capillary forces may contract the release of the healing agent (Figure 2.39) thus its effect.

Huang and Ye [106], proposed a schematic illustration of how the healing agents would react. They performed flexural tests to study the effect of the healing agents and there was observed a decreasing of the flexural strength of 27% and maximum deflection of 50%, whereas in the second case polyurethane capsules sometimes have increased the final strength. It is also important to consider the variability on the workability when hollow fibres (Figure 2.39) were used, while spherical capsules have not affect it significantly.

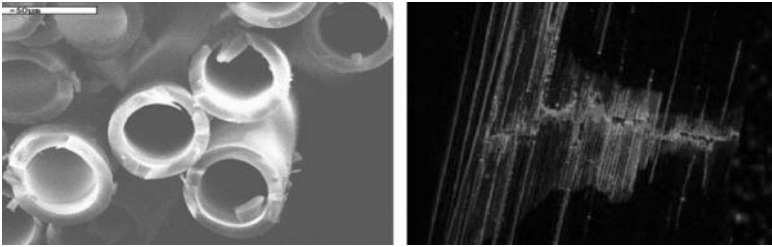


Figure 2.38. (left) Hollow glass fibers and (right) damage visual enhancement in composite laminate by the bleeding action of a fluorescent dye from hollow glass fibers. Courtesy by Van Tittelboom and D Belie [103]

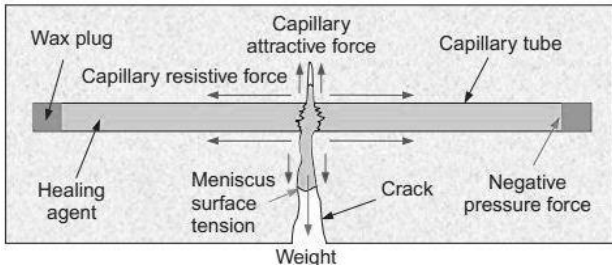


Figure 2.39. Schematic illustration of the forces acting on an internally encapsulated healing agent. Courtesy of Huang and Ye et al [106]

The compatibility of the capsules must be guaranteed with the strong alkali cement matrix and the healing agent. Generally inert materials, such as glass [107]-[108] or ceramics [103].

The probability that the occurring crack hits the embedded capsules is determined by many factors, which concern capsule size and distribution and crack size and length

Two statistical methods have been developed by Zemskov *et al.* [109] to calculate the optimum number of capsules and size to be applied in a self-healing material. The first case consists in the simplification of the model - which stands in considering the specimens as a layer structure with spheres randomly embedded - while in the second case a homogeneous structure is presented with casual embedding of sphere. In both of them probability is an explicit function of particle size, crack size and healing agent content ratio.

A Montecarlo method has been proposed by Huang and Ye [109] under the assumption that spherical shells always breaks in contact with crack.

2.10.1. Vascular systems: engineered healing systems

Another interesting healing way is represented by vascular systems (Figure 2.40) which consist of a network of hollow tubes that connect the internal part of the structure with external environment, where *reservoirs* - in which the healing agent is stored - can be placed.

Actually, these devices have been designed to solve the lack of the healing agent. In fact, it is it possible to maintain a constant level of the healing agent and provide new material in case of later cracking. The probability of crack passing through is almost a certain event, since these devices constitute weak lines inside concrete structures, acting as “crack risers”. Also, the problem of the compatibility with the cement matrix and the healing agent is automatically solved, because the cylinders are mostly made of glass, which is inert.

The dimensions of the tubes, such as the length and the diameter (at least 0.4 mm) suggest that a decreasing of mechanical properties can be expected. Furthermore, vascular systems cannot be normally added to the mixes, but they need to be implemented with care. Hence, they cannot be employed in normal concrete structures, but have been so far are confined in laboratories.

Vascular systems can be classified into singular and multiple channel systems (Figure 2.40).

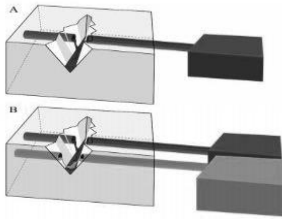


Figure 2.40. Vascular based self-healing approaches. Leakage of the healing agent from the tank via the vascular into the crack due to gravitational and capillary forces and eventual (hydrostatic) pressure. One channel (A) and multiple channel vascular systems (B). Courtesy by Van Tittelbom et al [17]

Sangadji and Schlangen [110] have simulated the "spongy bone" structure to create a porous network in their concrete specimens. The porous cores were covered with PVA films and put in the middle of a bigger mould. Self-compacting concrete cylinders were casted around them. During the tests, when cracks occurred, manual injection of healing agent was possible to fill up or seal voids.

Furthermore they [111] have implemented the system above with optic fibres as sensors of the damage state of the specimen and pumps as actuators for the supply of the healing agent and its diffusion from the pore core through the cracked specimen (Figure 2.41).

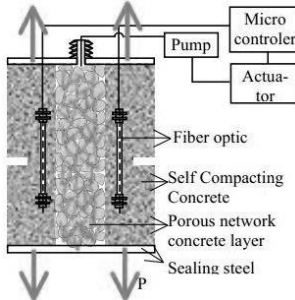


Figure 2.41. General concept proposed which make use of porous network concrete. Courtesy by Sangadji and Schlangen [111]

Gardner et al. [112] investigated the capability of the capillary rise model for a healing agent in a real crack on prismatic mortar beam specimens. Two loading cycles were performed, being the first loading cycle up to peak value. The test was then continued until the beam reached a CMOD of 0.3 mm.

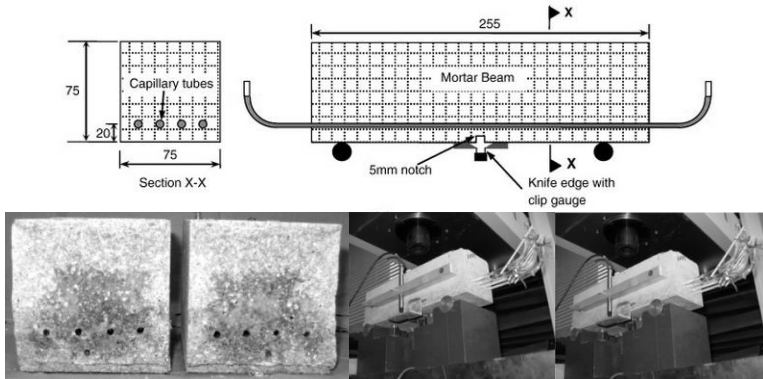


Figure 2.42. Self-healing experimental arrangement on a schematic presentation and the specimens during experimental campaign. Courtesy by Gardner [112]

The healing agent system presents four 3 mm inner diameter hollow capillary tubes (filled with cyanoacrylate), placed at 20 mm from the bottom of the beam and open to the atmosphere at both ends, as indicated in Figure 2.42. After a 24 hour period the beams were re-tested to failure. No change on the viscosity of the healing agent on time during its flow and slightly improvement of the flexural behaviour was observed .

Mihashi and Nishiwaki [24] employed a more complicated activated system connecting the couple sensor-actuator to a healing device consisting of copper plates. Once the crack was detected (Figure 2.43), the increase in electrical resistance promoted the heat transfer through the copper plates and melted the healing supplier pipes; the healing agent - epoxy resin - flowed out and sealed the crack.

In conclusion about the encapsulation of healing system it has been shown that different shapes of capsule can be produced, such as different dimensions can be chosen. Concrete strength is affected only when the dimension of the capsule is larger than the average dimension of the macro pores in the element. Designers can chose to embed macro

capsules to create weak points in the elements and stabilish a path to cracks; on the other hand they can embed a higher number of nano capsules and create a homogeneous material.

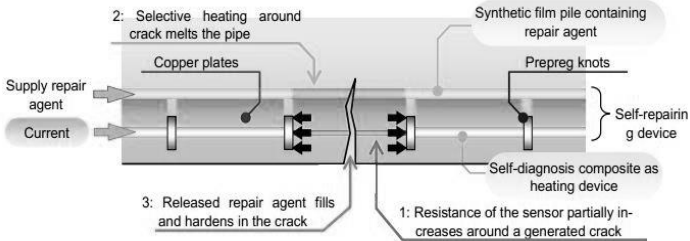


Figure 2.43. Schematic illustration of activated repairing system. Courtesy by Nishiwaki and Mihashi

Unfortunately, when big cracks are expected, as it happens in normal concrete structures, nano capsules do not contain enough healing agent to fill the fractures. An effective result can be achieved only by employing macro-capsules, affecting the concrete strength.

To guarantee a high quantity of healing agent and the possibility to refurbish, a vascular systems were also tested, but these solutions are too complicated to be integrated in buildings or normal structures, which moreover would be weakened.

At the state of the art, encapsulation does not seem really suitable for concrete structures, due to the actual difficulty in adapting capsules' parameters (such as dimension, shape, probability to be hit and quantity of carried healing agent) to the exigencies of strength of concrete. Also, cost to benefit should be investigated.

2.11. Self-Healing Capacity of Asphalt Concrete

Most of infrastructural pavements in the world are made by asphalt and similar products. An important environmental impact due to CO₂ emission is produced directly by the asphalt industry. Different methods are being used to reduce this emission by using recycled materials [112] or modernizing the producing machines. A possible of

self-healing ability on the asphalt materials would increase the life-cycle for several years before rehabilitation or reconstruction, consequently reducing the environmental impact throughout time.

Degradation of asphalt binder happens due to environmental factors, mostly the UV-radiation from the sun. Asphalt loses the ability to bind the surface particles together and this may result in cracks, which may allow damaging moisture into the lower pavement levels, creating surface roughness, pot holes, degradation and eventual structural failure [115].

Usually, sealant products are applied on the “visible” cracks in order to protect asphalt surfaces from environmental degradation and moisture penetration, or different chemical rejuvenators are employed, that can contribute to modify the chemical composition of bitumen when it is needed. Even helping to increase the lifetime of the roads, the aforementioned products have the disadvantages of only working in the first centimeters of the surface and reducing sliding resistance.

However, it must be clear that the self-healing systems should not only be effective under laboratory conditions. This implies that any self-healing technique to be applied in practice should survive the harsh conditions which prevail during mixing, laying and compaction as well as those during the service life when the pavement is used by traffic [116]. It is well known that the roads are subjected to different environmental conditions such as rain and dry conditioning, which probably would emphasize the healing mechanisms, since the presence of moisture increases the healing ability [11].

Asphalt roads can actually heal by themselves, but it is a slow process at ambient temperature, and it may only work if there is no traffic circulation on the road. As reported by Qiu et al. [117], different types of testing such as two point, three point and four point bending as well as push-pull and indirect tensile fatigue tests have been used to investigate the healing capacity of asphalt mixtures (Van Dijk et al., [120]; Castro et al.[121]; Carpenter et al. [122]; Grant [123]). In these investigations healing ability was defined by means of the higher number of load repetitions that could be applied on the specimens due to rest periods.

It is known that the amount of healing increases when the material is subjected to a higher temperature during the rest period (Bonnaure et al. 1982 [118]). In Figure 2.44 are shown traditional failure on the road pavements and the cracking due to fatigue.

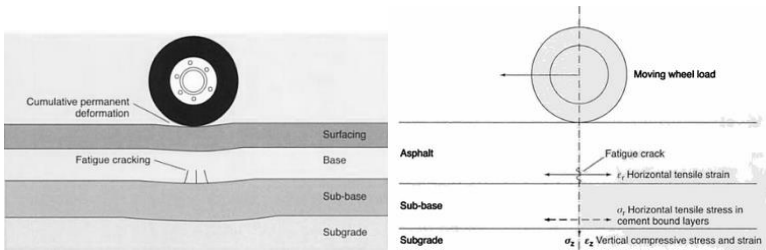


Figure 2.44. a) Traditional pavement failure modes and b) fatigue cracking in asphalt pavements. Courtesy by Highway Agency, London [119]

Another problematic issue of the road pavements is due to ravelling, which is defined as the loss of aggregate particles from the road surface [123].

Garcia et al. 2009 [123] proposed two different solutions to perform healing of the cracks: Induction heating of asphalt concrete and microcapsules filled with a healing agent. The first one proposes the use of microencapsulation, presenting the same expectations and problems described in paragraph 2.9. Capsules will break when the cracks appear, melted and damaged bitumen will be mixed creating contact with the bitumen around the closing cracks. Instead, the second proposed methodology works by generating the heating through the energy lost, when eddy currents (circular electric currents induced within conductors by a changing magnetic field in the conductor) meet with the resistance of the material and, finally, bitumen is melted and the crack is closed.

The heating methodology has been investigated by Liu et al. [124], damaging the prismatic porous asphalt concrete specimens containing steel wool by fatigue cyclic loading, and then heating them via induction energy. Healing ability is calculated as the difference between the mechanical resistance before and after heating. The heating (Figure 2.45.a)/damage (Figure 2.45.b) process was repeated until the accumulated damage in the material was too high to continue the healing process. The strength recovery (Figure 2.45) of the samples after the first healing is about 85% of the original value, becoming stable at about 70% of the original value. Finally, it decreased sharply after the sixth healing.

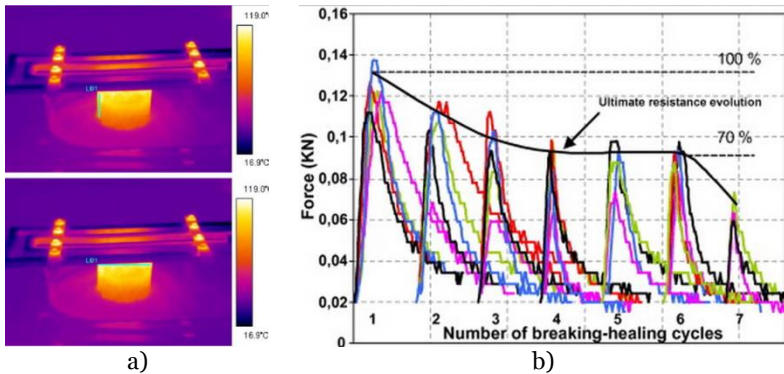


Figure 2.45. a) Infrared images of a porous asphalt concrete sample under heating; b) Stress-strain curves for samples with 5.66% steel wool type 000 (related to the volume of bitumen) and sand-bitumen ratio 1.60. Courtesy by Liu et al [124]

The authors concluded that porous asphalt concrete can restore its strength and stiffness by induction heating, extending its fatigue life and thus leading to a decrease in CO₂ emission and energy consumption for paving pavement.

Santagata et al. [126] investigated three different bituminous binders, including two neat bitumen (A and B) and one polymer modified binder (C). The investigation was performed by the application, in a stress controlled mode, of a continuous sinusoidal torque, with an intermediate rest period introduced between the first (loading) and the second (reloading) oscillation phase. One of the key aspects, which ensures a satisfactory reliability to the proposed approach, is the choice of single rest periods. They concluded that the cumulated damage of binders is composed by a reversible and a non-reversible part and self-healing depends on imposed damage, binder source and polymer modification.

Due to the mentioned benefits that self-healing could offer on asphalt materials, this topic is attracting important research investigations. Nevertheless, a lot still has to be done to improve the knowledge about self-healing ability of asphalt materials. This research activity is producing an important and promising outcome, and on a later stage the obtained data should be compiled on a guideline for possible practical use.

2.12. Quantifying healing effectiveness

One of the biggest challenges in the self-healing research is to quantify the healing efficiency of cement composites. The challenge is about the meaning of the parameters that would provide an engineering way to understand the both situations of the same material, when cracked, and later on, if healed.

Kessler in his report [127] states that the increased healing efficiency can be obtained either by increasing the healed material property or by the reduction of the virgin properties. Quantifying self-healing ability depends, first of all, on the investigation technique that is performed. Consequently the outcome information will be part of the “challenge” of being transformed on healing parameters.

In Figure 2.46 are shown some of the applied techniques in different experimental investigations that have been discussed in earlier paragraphs. On the right side some of the properties are shown that can be used to express the healing capacity.

The visualization techniques represent one of the most cleared way to show the cracking of the material (Figure 2.47, a) and then, the sealing (Figure 2.47, b) of the same cracks, if this occurs. If the sealing occurs, it should be the first parameter which motivate further definition of other possible parameters that would be used to quantify the healing ability.

By observing Figure 2.47, it can be concluded that the crack was mostly sealed, nevertheless more information can still be obtained to quantify the healing ability. It is highly recommended to measure the crack width at the “damaging” stage, and if the sealing occur, the difference between the sealed and the damaged state will provide the first parameter to quantify the healing ability . A possible index that would quantify sealing ability is shown in the following equation:

$$\Delta W = 1 - \frac{W^{\text{sealed}}}{W^{\text{cracked}}} \quad 2.8$$

Where ΔW , is the width difference of cracking width or the sealing index and the W^{sealed} is the sealed crack Width and the W^{cracked} is the crack Width in initial cracked state.

State of the Art

	Technique	Possibilities	
visualization and determination	Optical microscopy + image analysis	Visualization crystal deposition + determination healing rate	
	Scanning electron microscopy	Visualization crystal deposition	
	Environmental scanning electron microscopy	Visualization breakage of partially embedded capsule	
	Thin section analysis	Visualization crystal deposition inside crack	
	X-ray radiography	Visualization release encapsulated agent from embedded capsule	
	X-ray tomography	Visualization release encapsulated agent from embedded capsule in 3D	
	Digital image correlation	Visualization of crack closure upon heat treatment of SMA	
	X-ray diffraction analysis	Determination of crystalline materials	
	Ramann spectroscopy	Determination chemical composition	
	Infrared analysis	Determination of precipitated products	
regain tightness	Water permeability low pressure	Water flow through (healed) crack	
	Water permeability high pressure	Water flow through (healed) crack	
	Air permeability	Air flow through (healed) crack	
	Capillary water uptake	Capillary water uptake by (healed) crack	
	Neutron radiography	Visualize capillary water uptake by (healed) crack	
	Corrosion test	Resistance against corrosion	
	Frost salt scaling	Resistance against frost salt scaling	
	Chloride diffusion	Resistance against chloride ingress	
	Osmotic pressure	Resistance against ion ingress	
	Ultrasonic transmission measurements	Continuity of material	
regain mechanical properties	Compression test	Regain in strength, stiffness and/or energy obtained when reloading healed specimen	
	Tensile test		
	3-point bending test		
	4-point bending test		
	Horizontal deformation column/frame	Formation of new cracks <i>versus</i> reopening of old cracks	
	Impact loading slab		
	Acoustic emission analysis		Regain in energy/Notice capsule breakage
	Resonance frequency analysis		Regain in stiffness

Figure 2.46. Techniques used to evaluate the healing efficiency. Courtesy of Van Tittelbom and De Belie at [128]

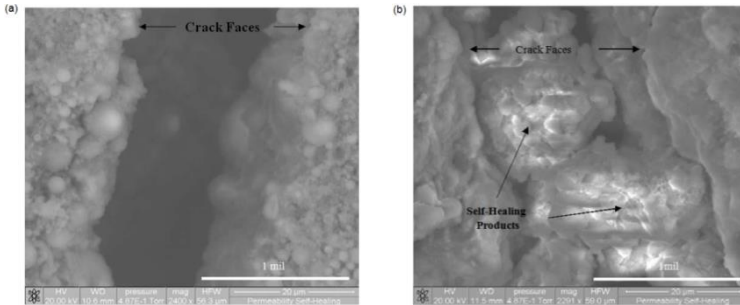


Figure 2.47. Morphology of crack within ECC specimen from ESEM: Autogenous self-healing crystalline formations in ECC a) before and b) after permeability test. Courtesy by Yang et. al [90]

By means of other technique, called by Van Tittelbom and De Belie [128] as “tightness regain”, it is possible to investigate by the variation in water/air permeability, chloride diffusion or ultrasound pulse velocity.

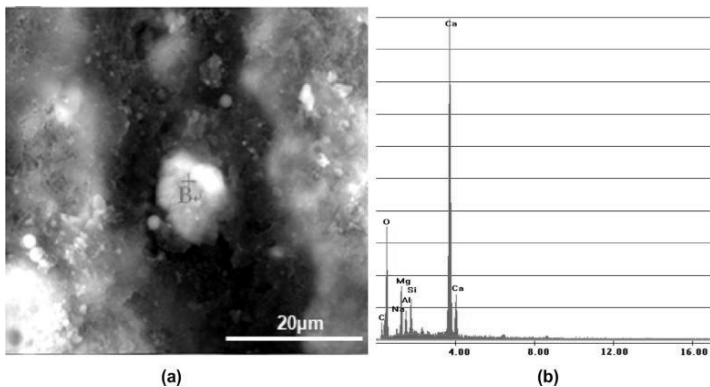


Figure 2.48. (a) ESEM image of ‘stone-like’ healing product and (b) its EDS spectrum. Courtesy by Kan, et al [129]

By observing a microscopic image (Figure 2.47) obtained by SEM (Scanning Electron Microscope), it would be possible to recognize even the type of formed crystals and provide a preliminary explanation about the fundamental mechanism that sealed the crack. If not, other techniques such as x-ray tomography/radiography or EDS (Energy Dispersive X-Ray Spectroscopy) can be used for the chemical characterization of the analyzed sample. The correlation between the ESEM and EDS techniques is shown in the Figure 2.48, and the chemical composition shows the properties of healing products.

Different healing indexes have been proposed when comparing the permeability of the specimens due to air pressure or water penetration, before/after cracking and after the conditioning. For ex. Yang, Li et al [90] used the permeability coefficient k , of the specimens wich represent the amount of the permeability that passes from the falling head to the head test. This is possible to be calculated by the following equations:

$$k = \frac{aL}{A t_f} \left(\frac{h_o}{h_f} \right) \quad 2.9$$

$$k = \frac{V L}{A h_o t_f} \quad 2.10$$

Where a is the cross sectional area of the standpipe, L is the specimen thickness in the direction of the flow, A is the cross sectional area subjected to flow, t_f is the test duration, h_o is the initial hydraulic head, h_f the final hydraulic head, and V is the volume of liquid passed through the specimen during the test. This technique allowed Yang, Li et al to evaluate the self-healing ability, making a comparison between the permeability in different type and periods of conditioning.

The last technique showed is useful when the study of transport properties is needed, but when it is about the mechanical properties, “regain of mechanical properties” has to be evaluated.

Depending on the type of performed mechanical test, such as tensile, compression three/four bending test. In the literature a ratio has been used between a healed material property and there of the undamaged material, to quantify this “intelligent” ability of cementitious composites.

Wool and O’Conner [131] defined crack healing efficiency (η) for fracture mode I of as:

$$\eta = \frac{K_{Ic}^{healed}}{K_{Ic}^{virgin}} \times 100\% \quad 2.11$$

Where: K_{IC}^{healed} is the mode one fracture toughness of a healed fracture specimen and K_{IC}^{virgin} is the mode one fracture toughness of a virgin specimen. For these kinds of specimen, toughness depends only on applied loads and not on crack length.

Comparing fractured energy it is possible to quantify self-healing;

$$\eta = \frac{G_{IC}^{healed}}{G_{IC}^{virgin}} \times 100\% \quad 2.12$$

Where G_{IC}^{healed} and G_{IC}^{virgin} represent the respective energy of fracture for the healed and virgin specimen.

White [104] adopted a definition of healing efficiency for appropriate height-tapered double cantilever beam (TDCD) comparing the following parameters:

$$\eta = \frac{P_C^{healed}}{P_C^{virgin}} \times 100\% \quad 2.13$$

Where P_C^{healed} and P_C^{virgin} are the critical loads loads at fracture for the healed and virgin specimen respectively, showed in the Figure 2.49.

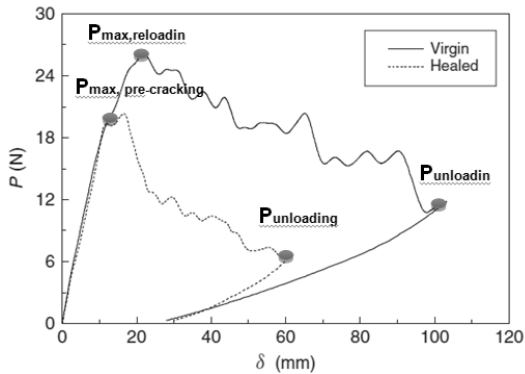


Figure 2.49. Typical curves load (P)-crack opening displacement (δ) curves of the self-healing before and after healing.

Bond [132] tried to give another explanation of self-healing ability using the flexural capacity of specimens. The residual flexural strength after damage and healing was compared with undamaged flexural strength, expressed as follow:

$$\eta_{flexural} = \frac{\sigma_{Cflexural}^{healed} - \sigma_{Cflexural}^{damaged}}{\sigma_{Cflexural}^{virgin} - \sigma_{Cflexural}^{damaged}} \times 100\% \quad 2.14$$

Where $\sigma_{Cflexural}^{healed}$ is the residual flexural strength of the material after that has been damaged and allowed to heal, $\sigma_{Cflexural}^{damaged}$ is the residual flexural strength of the material after it has been damaged but not allowed to heal, and $\sigma_{Cflexural}^{virgin}$ is the flexural strength of the undamaged material.

For structures, such as road pavements, fatigue testing will be a representative for a possible healing evaluation. The self-fatigue-healing efficiency can be calculated as proposed by Brown et al [133] :

$$\lambda = \frac{N_{healed} - N_{control}}{N_{control}} \quad 2.15$$

Where N_{healed} is the total number of cycles until failure for the healed sample and $N_{control}$ is the total number of cycles to failure for a similar sample without healing.

Based on the ideas presented here, quantifying self-healing ability depends firstly on the issue of interest, such as transport property or mechanical recovery. In the first case, if the transport properties are to be studied, the dependence on crack width is crucial, when self-sealing occurs. When is the mechanical recover, it is needed the mechanical parameters such as strength, fracture energy and more. Nevertheless, these properties still have to be related by the physical properties.

The “translation” of the improvement capacity into different indexes, which provide a quantitative assessment of the healing ability of different types of cement composites, represents one of the most important parts of this research activity.

2.13. Modelling Self-Healing Ability in Cement Composites

The research on the self-healing capacity of cementitious composites is still a relatively new topic. Most of the studies published so far deal with experimental investigations but modelling of self-healing phenomena is still quite limited [134]. Any predictive modelling approach has to take into account that still a lot of work has to be performed to confirm the experimental results, mainly with reference to the duration of the healing ability over extended time. Moreover the variety of healing engineering techniques may complicate the formulation of any model.

It has anyway to be remembered that the formulation of the prediction which must reflect the healing mechanism, which has to be confirmed and quantified by means of microstructural investigations.

M. Zhang et al. [135] proposed a model to predict the efficiency of microencapsulation system. The obtained output data will help on further practical implementation of this simulated healing system. The model has as the advantage of simulating different types of encapsulation systems, reducing the time/cost when compared to an experimental campaign. In this way, it may be possible to obtain an “ideal” encapsulation system to be further experimentally validated.

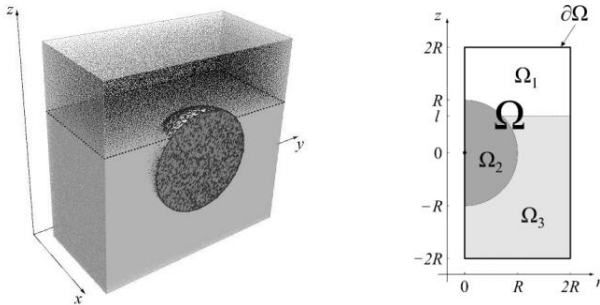


Figure 2.50. (Left) Representation of a half of the concrete cube containing the capsule and consisting of un-carbonated (below) and carbonated (above) parts. The computational domain for a two dimensional mathematical model. Courtesy by [136]

In another study Zemskov et al. [136] present an interactive mathematical model of self-healing in carbonated cementitious materials. The basic assumption is that the changing in time of carbonation, the rate of diffusion of sodium monofluorophosphate (Na-MFP) into the carbonated cement matrix and the reaction rates of the free phosphate and fluorophosphates with the components of the cement are comparable to the speed of the carbonation front.

With reference to a representative volume element of which only half was analyzed because of the symmetry (Figure 2.50.). Simulations showed that the healing process proceeds under accelerated carbonation conditions. The movement of the carbonation front influences the process of diffusion of Na-MFP and, hence, formation of the reaction products. Due to these results, it can be concluded that is necessary the right concentration of Na-MFP in the capsule and the number of capsules per unit volume of cement to form the desired reaction.

Perelmuter et al [137] proposed a bridged crack approach to model self-healing materials. In their study the bond properties define the stresses at the crack bridged zone, its size and, hence, the fracture toughness of the material, in which the stress intensity factor (SIF) represents the main factor for the self-healing quantification. Numerical calculations were performed for plane strain conditions on Cu-epoxy polymer specimens. Observing the Figure 2.51 it can be stated that for relative stiffness ratio of about higher than 10, the healing efficiency reaches the saturation if the crack has been filled with bonds for more than the half of its length

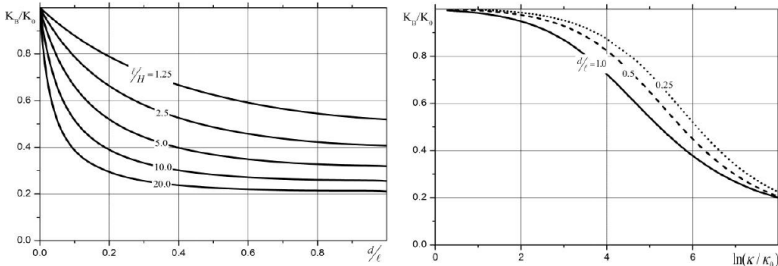


Figure 2.51. a) SIF module vs relative bridged zone length, $K_0 = \sigma_0 \sqrt{\pi l}$; b) SIF module vs relative bond stiffness, $K_0 = \sigma_0 \sqrt{\pi l}$. Courtesy by Perelmuter [137]

The evolution of the healing process as the dependence of SIF module versus relative bond stiffness (in logarithmic scale) is shown in Figure 2.51b and it can be seen that the saturation of the healing effect is obtained for bonds with rather higher stiffness.

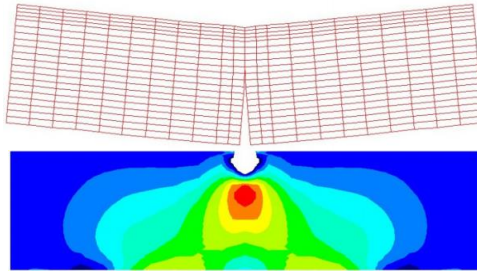


Figure 2.52. (up) Typical deformed mesh; (bottom) Stress contour plot. Courtesy by Schlangen et al. [138]

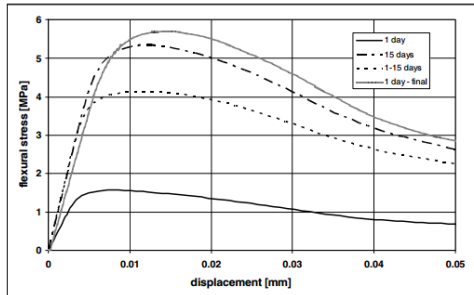


Figure 2.53. Flexural stress versus displacement for different simulations. Courtesy by Schlangen et al [138]

Schlangen et al [138] simulated an autogenic self-healing for concrete at early ages. They used a finite element model, which is based on the state parameters such as maturity, degree of hydration, temperature or moisture potential. The simulations with this model to simulate the results from experimental investigations on ongoing hydration of the cement. Typical 3-point bending test was simulated in 2D using plane stress conditions (Figure 2.52b). As in the experimental

investigations, there was simulated a discrete crack, created in the mesh using an interface element with a stress-crack opening relation (Figure 2.52a).

The pre-cracking was performed at the age of 15 days and crack opening was set at $w=0,44\text{mm}$. The specimen was then stored in water immersion about 14 days. Due to this crack opening, it is supposed that there will be enough water in contact with the un-hydrated particles along the crack faces.

From the Figure 2.53 it can be observed that the flexural stress, as well as the stiffness, in the specimen tested at 1 day is lower than the specimen tested at 15 days. The specimen pre-cracked at age of 1 day and tested after 14 days of healing (1-15 days) has the same stiffness as the un-cracked specimen tested at 15 days. The strength of this specimen is about 77% of the un-cracked specimen.

A hydration model with expanding cement particles was used by He et al.[139] to investigate the possibility of crack closure by continuing of hydration (Figure 2.54). This model depends in different parameters such as degree of hydration, the fineness of the cement and the crack width. The applied theories in this simulation are based on the water transport theory, ion diffusion theory and thermodynamics theory. Based on the simulated results, the amount of extra water can be optimized aiming at the highest self-healing efficiency (Figure 2.55).

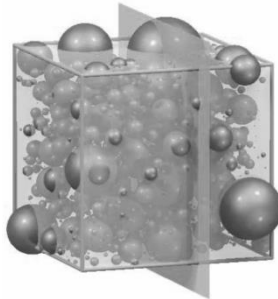


Figure 2.54. Single crack intersected with cement paste. Courtesy by He et al [139]

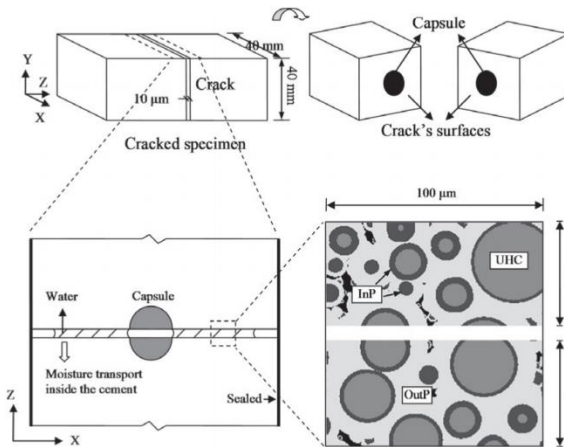


Figure 2.55. Schematic diagram of modelling system (InP represents inner products, OutP represents un-hydrated cement particles) [139]

2.14. Applications in Self-Healing Materials

The state of art presented in the earlier paragraphs tented to show the level of self-healing research activity during years. As it was emphasized, the research activity on this topic is quite new. Even collections of papers were published in some books, just few applications have been performed and using a restrict variety of materials, such as polymers, asphalt or cement based materials.

2.14.1. Scratch Guard Coating

Nissan announced in 2005 the “Scratch Guard Coat” painting system, which is a reflow-healing protective coating, in process of commercialization. It contains a newly developed high-elastic resin providing reflow in artificial scratches [10]. The new coating system is effective for about three years and it is five times more resistant to the abrasion caused by a car-washing machine when compared with a conventional clear paint (Figure 2.56).

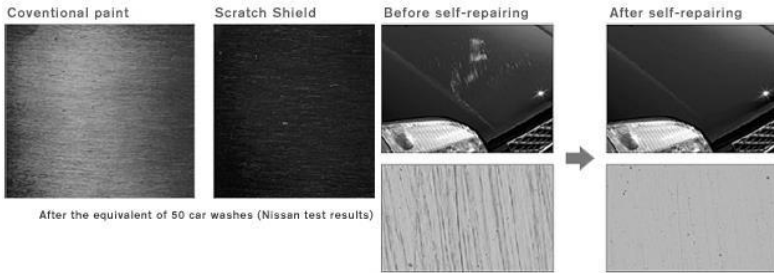


Figure 2.56. (left) Comparisons between conventional paint and the Scratch Shield; (right) Scratch Shield performance before self-repairing and after-repairing. [10]

2.14.2. React-A-Seal - Ballistic Puncture Healing

An interesting application was produced by Reactive Target Systems, Inc., named “React-A-Seal”. This is an ionomer product patented by DuPont Surlyn 8940 and marketed for multiple ballistic impact. The early history of the discovery of ballistic healing in ionomers is not well documented in the literature [140].

The discovery of a repair response beyond the one of ballistic puncture healing would yield an increase potential for use in these and other applications (Figure 2.57).

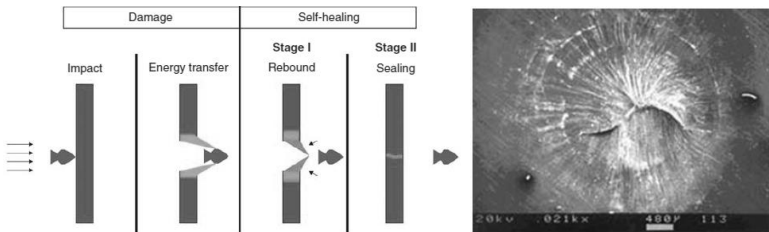


Figure 2.57. (left) To stage model for ballistic self-healing in EMMA films; (right) SEM of healed EMMA composite (projectile entrance side). Courtesy by Sugama et al [140]

These few applications presented here are not a part of the topic investigated in this dissertation, but have an important stimulation to study a solution for an application with cement based composites.

2.14.3. Self-Healing Concrete Pavilion (Breda, The Netherland)

The idea to construct a self-healing building is applied by "Innergy", designed by Marcus architects and Department of Self-Healing Materials at Delft University, Holland [141]. This pavilion accommodates the first aid and response & rescue unit, located on the lakeside, near the city of Breda (Figure 2.58). The pavilion, besides its functional content, is characterized by sustainability and "vandal proof" targets. The façade and gable are, made of 60 mm thick concrete a shell.

These bacteria are harmless, to both human and animal life. They are responsible for the development of limestone, promoting cracks repair without any additional or external assistance.



Figure 2.58. (left) Self-healing concrete shell of 60 mm thick; (right) Self-Healing concrete Pavilion-Breda. Courtesy by TU delft [141]

In this way, the need for maintenance is eliminated. The closure of the cracks will maintain the reinforcement unaffected by the aggressive agents and the concrete will have thus a longer life. In which the next two years it will be examined by TU Delft in circumstances the bacteria remain alive and how exactly the restoration of the concrete proceeds.

2.14.4. Water Irrigation Canal with Self-Healing Concrete Containing Bacteria (Ecuador)

Another interesting project has been applied in Andean Mountains in Ecuador [142]: an irrigation canal about 500 meters long has been constructed.

A collaboration between researchers from TU Delft and Universidad Catolica de Santiago de Guayaquil in Ecuador has applied concrete self-healing techniques to prevent irrigation canals from cracking, thus preventing expensive repair operations and seriously diminishing the chance of crop failure. Because of the high altitude and temperature variation, the material in the canal always experiences high stress, as which may induce cracks in concrete (Figure 2.59,left). As a result, the canal's durability is affected and the leakage of the canal results in malfunctioning. Replacing or repairing cracked parts of the canal is time consuming and very expensive.



Figure 2.59. (left) Schematic presentation of the cracks into the canal; (right) Part of the constructed canal in Ecuador. Courtesy by Jonkers et al [142]

A research group, headed by Jonkers and Wiktor, decided to use natural fibers together with a healing agent to improve the concrete performance, control the crack widths and guarantee the crack healing. The chosen fibers were Abaca, indigenous to Ecuador.

2.14.5. Retaining walls using Concrete with Crystalline Additives, Shanghai Airport, Terminal 3, Shanghai, People's Republic of China

The Shanghai Airport - Terminal 3 is situated in an area (*Figure 2.60, left*) with high presence of underground salt water flows. Due to this purpose, it was proposed the use of crystalline additives, whose effect will perform the waterproofing of all underground structures of Terminal 3 (*Figure 2.60, right* – There are 7, including 3 underground levels with the presence of ground water marina, 28 gates and 1,800 parking spaces). The proposed basement was constructed with three walls with thickness of about 600 mm. The casting of these structures was performed in year 2001.

In these applications, since cracks and the water leakage were expected, a monitoring study was performed a year later, in 2002. Water leakage was found along the crack line and tie pin after backfill. However this leakage, as it can clearly be seen from the pictures, had been stopped (*Figure 2.61, left*). For a deeper study, it was decided to extract three core samples drilled to a depth of 400mm.



Figure 2.60. (left) The Shanghai Airport area, Singapore; (right) The underground structures on the Terminal 3. Courtesy by [143]

With microscopic analyses performed on the cracked zone, the presence of crystals was observed. They were then studied with SEM and x-ray analysis (*Figure 2.61.right*), through which it was found that crystals consist of mainly Calcium (Ca), Silica reaction (Si), Oxygen (O), Sulfur (S) and Aluminum (Al). The CaCO_3 crystals were present as laminated texture in the samples.

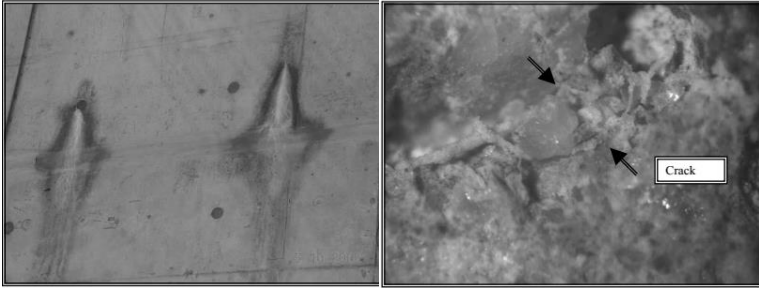


Figure 2.61. (left) Close view of the sign of efflorescence accompanied with water marks were noted on wall 3; (right) some crystal grew in the crack due to core samples extracted on the leakage zone. Courtesy by *Loh et al* [143]

2.14.6. Self-Healing Porous Asphalt Constructed on A58 Highway, The Netherlands

One of the most important issues when it comes to self-healing is its performance in asphalt or asphalt concrete. Due to different problems such as raveling – which has been previously explained - it was possible to construct a 400 m of highway with a porous asphalt. The project is carried out by the Microlab group of the Delft University of Technology, in collaboration with the group Road Engineering and has already been led to a real application [124]. A test track has been made on Highway A58 near Vlissingen in the Netherlands. Two different systems were constructed: the recently introduced two-layer porous asphalt and the traditionally used single layer porous asphalt. During these periods the testing performance of testing is ongoing on specimens (Figure 2.62, left) made with the same porous asphalt used to the real application (Figure 2.62, right).

The healing process is induced using an induction machine to heat up the steel-wool fibers that are placed inside the material. So, it should be “healed” the road regularly when needed and monitored for a long time. Today the mean lifetime of two-layer porous asphalt surfacing is about 7 years. The primary goal of the project is to build in a self-healing mechanism in which the asphalt constantly repairs itself and the lifetime of the two-layer porous asphalt increases to 12 years. For the

traditionally used single layer porous asphalt, the intention is to obtain an increasing of the average lifetime from 10 to 14 years.



Figure 2.62. (left) Porous asphalt specimen made of the same materials which constructed the road; (right) The construction of the layers by self-healing material. Courtesy by Schlangen et al [124]

*We are what we repeatedly do.
Excellence, then, is not an act, but a habit.
Aristoteles*

3. Experimental Campaign

1.1. Introduction

In this PhD work a “tailored” methodology has been proposed and thoroughly validated to study the self-healing capacity of a broad category of cement based materials ranging from conventional concrete to high performance cementitious composites with different types of fibers (Figure 3.1.)

The proposed methodology encompasses physical and mechanical testing and microstructural investigation in order to assess the self-healing effectiveness as a function of different variables, including the mix constituents, the exposure conditions and the level of damage (crack opening). In (Figure 3.2) a schematic of the experimental methodology is presented, as common to the different types of the investigated cementitious composites.

As it can be observed, the methodology consist of three stages. In the first one, specimens, after a preliminary non-destructive assessment in their undamaged state, are pre-cracked in 3 or 4 point bending or on direct tension as a function of the investigated material. The cracks produced as above are hence microscopically visualized and measured, while

consequently the second stage starts. This consist in environmentally conditioning the specimens exposing them to different conditions and for different durations

At the end of this stage the post-conditioning phase starts in which the specimens, after a microscope study of the (in case) healed cracks and a new non-destructive assessment of their healed post-conditioning state, are re-tested according to the same methodology employed for the Pre-cracking and the recovery of the mechanical performance can thus be evaluated.

Finally SEM (Scanning Electron Microscope) and EDS (Energy-dispersive X-ray spectroscopy) investigation on the healed cracks, complete the investigation.

Three different materials were investigated in three different experimental campaigns. Firstly, autogenic and engineered self-healing of ordinary concrete was studied, with and without a crystalline additive. As a part of the second stage, self-healing capacity of High Performance Fiber Reinforced Cementitious Composites (HPFRCC), with steel fibers was investigated. To complete the experimental campaign, in order to enhance the kinetics of self-healing, natural fibers were introduced on HPFRCC-s.

In this chapter the investigated materials, casting and manufacturing process and the experimental methodology employed in the investigation will be presented.

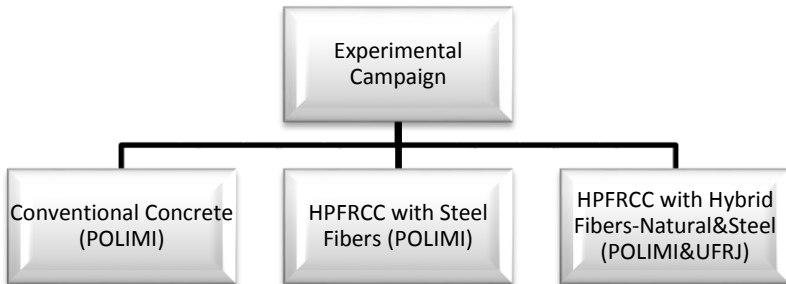


Figure 3.1. Schematic Presentation of the Experimental Campaign

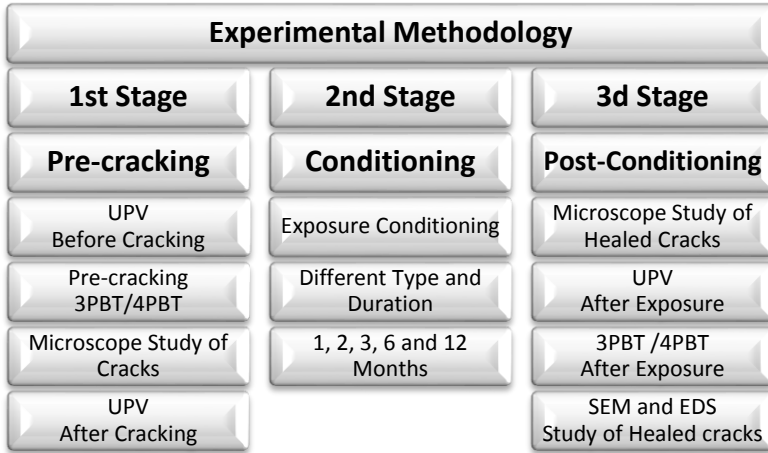


Figure 3.2. Schematic presentation for the proposed experimental methodology

3.2. Self-Healing Investigation on Conventional Concrete

3.2.1. Materials and Manufacturing

In this part, reference is made to a normal strength normal weight conventional vibrated concrete. The mix composition, detailed in Table 3.1, has been designed for a target cube compressive strength at 28 days equal to 30 MPa [145]. Because of the interest to evaluate the effects of crystalline additives on the self-healing capacity of concrete, a companion mix has been also produced with a 1% additive addition, by weight of cement. Mix compositions are detailed in Table 3.1.

The additive was dry mixed with the raw aggregates at the very beginning of the mixing sequence, which was then followed by the addition of cement and, upon further mixing, by the incorporation of water and superplasticizer.

Experimental Campaign

Constituent (kg/m ³)	Without Additive	With Additive
Cement type II-42.5 R	300	300
Water	190	190
Superplasticizier (lt/m ³)	3	3
Fine Aggregate 0-4mm	1078	180
Coarse Aggregate 4-16mm	880	880
Crystalline Additive	-	3

Table 3.1. Mix-design of the investigated mortar

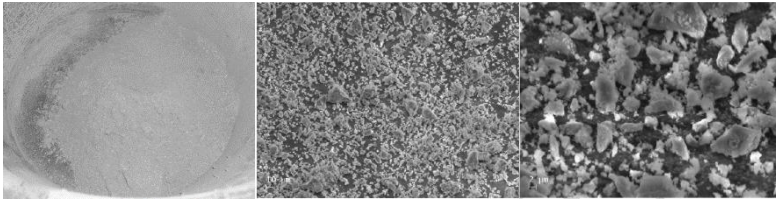


Figure 3.3. Observations on the crystalline additive; Visual observation on different scale of additive particles of in a scanning; (left) original visualization of the additive; (middle, right) scanning electron microscope in different magnifications

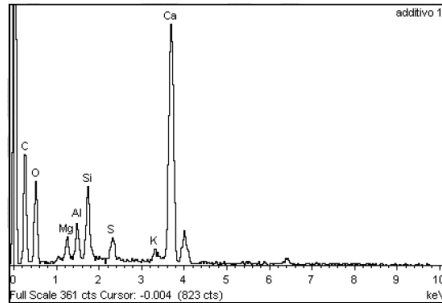


Figure 3.4. Chemical characterization of the crystalline additive showed in (Figure 3.3) by the Energy dispersive spectroscopy (EDS) test.

In Figure 3.3 it is possible to observe the particles of the crystalline admixture. They have irregular shape and size in the range of about 1-20 μm (Figure 3.3, middle-right); their morphology is similar to that of cement grains; as a matter of fact, also according to the manufacturer, cement is present in the admixture and this is confirmed by the presence of calcium, oxygen, silicon, magnesium, aluminum and potassium in the EDS microanalysis shown in Figure 3.4. This spectrum is comparable with that of

an Ordinary Portland Cement (OPC), except for the peak of sulphur which is slightly higher.

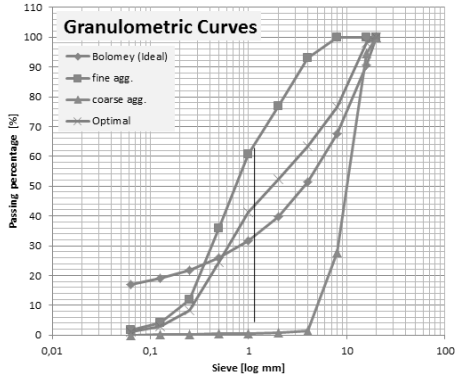


Figure 3.5. Distribution of the used aggregate and the proposal for the optimal distribution and the ideal one (Bolomey)

Aggregates were proportioned following the Bolomey curve approach (Figure 3.5).



Figure 3.6. Manufacturing of the specimens; (left) casted slab; (middle) reference cube specimens; (right) slabs under wet towels.

Slabs 1m long x 0.5 m wide and 50 mm thick were casted (Figure 3.7, left) with both mixes; after three days curing in lab environment under wet towels (Figure 3.7, right). Slabs were cut into prismatic “beam-like” specimens, each 500 mm long and about 100 mm wide (Figure 3.7) and cured in a moist room.

Comparison cube specimens (Figure 3.7, middle) were also cast for compressive strength measurements.



Figure 3.7. (left) Slabs stored on a chamber room; (middle) cutting machine; (right) specimens like “beam” after cutting

3.2.1.1. Specimen Identification

Specimens were identified with a code as follows (Figure 3.8) and the type of the material (Table 3.2), with different type of conditioning (Table 3.3) in different duration (Table 3.4).

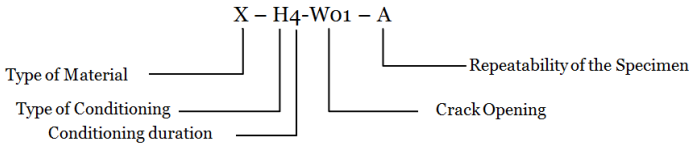


Figure 3.8. Code Identification of the specimen

Code	Type of the Material
X	Without Additive
P	With Additive

Table 3.2. Identification of the specimen in front of the type material

Code	Type of the Conditioning
H	H ₂ O – Water Immersion
C	Climatic Chamber
D	Dry – Natural air exposure
W/D	Wet/Dry – (Water immersion)/ Dry-20°C, 50% RH)
Dry	Climate Chamber –20°C, 50% RH
Humid	Hugh Humidity Climate Chamber – 20°C, 90% RH

Table 3.3. Identification of the specimen in front of the Conditioning type

Code	Duration of the Conditioning
1, 2, 3, 6, 12	months
C1,C2 and C4	weeks

Table 3.4. Identification of the specimen in front of duration of conditioning

3.2.1.2. Pre-cracking by three point bending test

According to the methodology proposed, in this study aims to evaluate the self-healing capacity of concrete and its effects on the recovery of mechanical properties. At the end of the curing period detailed above, the beam specimens were pre-cracked up to different levels of crack opening, equal to 150 and 300 μm . Un-notched specimens were pre-cracked employing the three-point bending (3pb) test set-up shown in Figure 3.9, where the clip-gauge measuring the Crack Opening Displacement (COD) at mid-span (used as test control variable) is also shown. Some specimens were kept un-cracked for reference as well. An electro-hydraulic machine type "Instron 8562", by maximum load of 200 kN, was used. The Instron machine performs testing procedure in two different ways, due to the Strain or Position control. The movement of the loading parts represent the displacement control, while the Strain mode control the crack opening by the clip gage. Firstly, the speed is set to 0.25 $\mu\text{m/s}$, until the loading becomes constant then it increased slowly until is 0.3 $\mu\text{m/s}$, speed that permits to pass to Strain control of the test. Note that the speed, due to the testing procedure, affects irretrievably the state of the specimen.

In order to avoid the sudden failure of the specimen, a load limitation equal to 500 N was set in the first stage. As described before, two different crack openings were, 150 and 300 μm .

When reached the set value of the CMOD the machine unloads automatically the specimen, obtaining the desired final crack opening (Figure 3.10). After total unloading the specimen is moved to the exposure conditioning, waiting for the post-conditioning test.

When a CMOD=300 μm is planned, an instantaneous loading/unloading cycles at a CMOD of 100 μm is anyway performed. After unloading at 100 μm , consequently the reloading until CMOD=300 μm is performed.

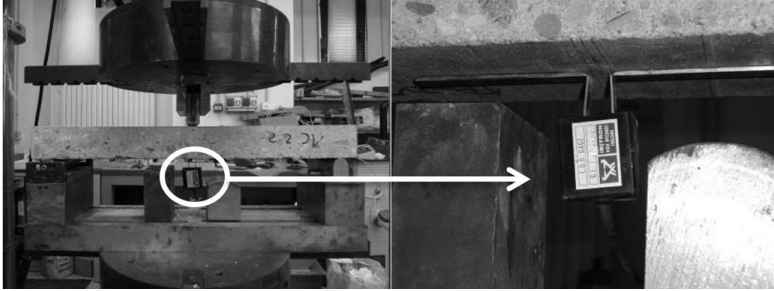


Figure 3.9. (left) Three point bending test set-up for pre-cracking procedure; (right) clip gauge used for measuring the crack opening mouth displacement

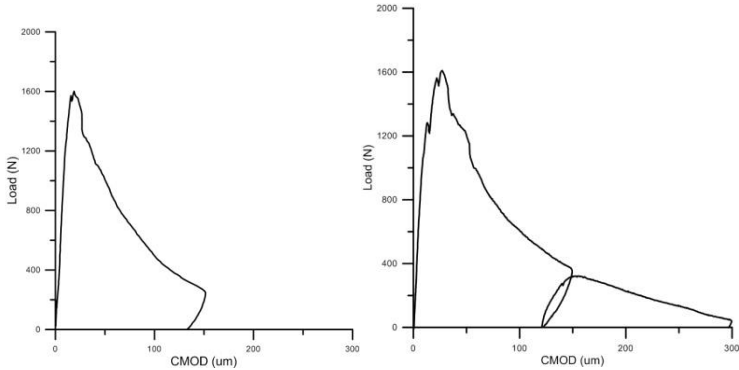


Figure 3.10. Typical Load vs CMOD response from 3PBT; (left) pre-cracking CMOD until 150 μm ; (right) pre-cracking CMOD until 300 μm

3.2.1.3. Ultrasonic Pulse Velocity (UPV)

Ultrasonic Pulse Velocity (UPV) tests were also performed on the same specimens employing the set-up shown in (Figure 3.11) along the pre-cracking/conditioning/final testing procedure described above:

- On truly virgin specimen, i.e. immediately before pre-cracking (initial stage)-BC;
- After the pre-cracking and immediately before the onset of the exposure/environmental conditioning (intermediate stage)-AC;

- After scheduled exposure/conditioning durations, immediately before final testing of the specimens to failure (final stage)- AT.

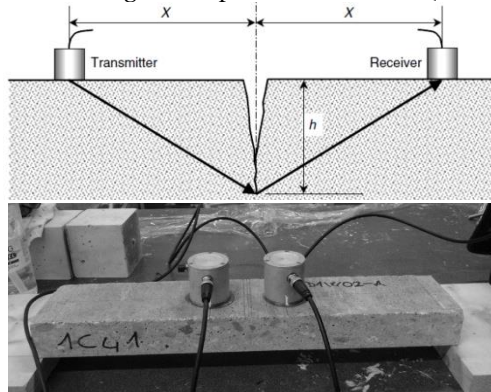


Figure 3.11. (up) Schematic presentation of the UPV measurement set-up [147]; (down) Set-Up For Ultrasonic Pulse Velocity Tests (Emitter-Receiver Distance = 90 Mm)

The cross comparison between results obtained from UPV tests, in terms of dynamic modulus of elasticity (obtained through the classical formula which correlates the wave speed through a solid medium to its stiffness and density), and those obtained from 3pb tests, in terms of beam flexural stiffness, allowed the reliability of the proposed test methodology to be further assessed.

The “raw” signal is then processed by aid of a program (proposed by Felicetti) (Figure 3.12, right) in which the algorithms are implemented for the identification of the arrival time was used: the fixed threshold method and AIC-Maeda [148].

It is possible to record the signal, which is nothing but a continuous function of time, or an analogy signal. To store this information in a computer is necessary to transform the analogy signal (voltage supply V) into a digital signal (a series of numbers). To perform this operation using an analogy digital converter that can be integrated into a digital oscilloscope (Figure 3.12, left).

There are three types of waves generated by a pulse applied to a solid mass:

- Surface waves, which are very slow and characterized by a particular elliptical movement of the particles;

- Transversal waves, with perpendicular displacement of the particles due to the direction of propagation;
- Longitudinal waves, also known as compression waves, which have a parallel displacement of the particles due to the direction of propagation; they are faster than the other types of waves providing more information.

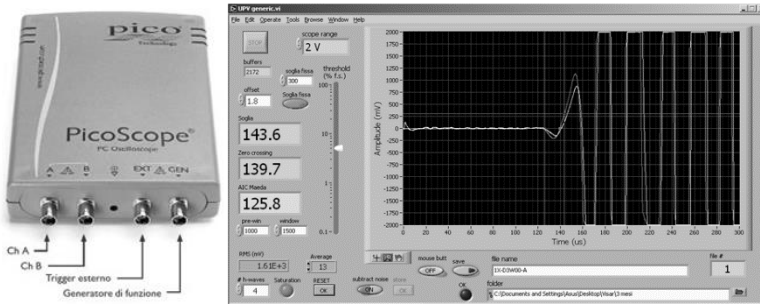


Figure 3.12. (left) Oscilloscope used for the UPV; (right) Screen Program of (UPV- Generic)

The electro-acoustic transducers used in our case mainly produce waves of this latter type; the other waves produce interference because of their reduced speed. The wave propagation speed [149]-[151] in a homogeneous material depends on the material density ρ (kg/m³), from the dynamic elastic modulus E_d (in N/mm²) and the Poisson's ratio ν , as shown in the formulas:

$$V = \sqrt{\frac{K \cdot E_d}{\rho}} \quad \left[\frac{\text{km}}{\text{s}} \right] \quad 3.1$$

$$K = \frac{(1-\nu)}{(1+\nu) \cdot (1-2\nu)} \quad 3.2$$

From a reasonable estimation of the Poisson's ratio, $\nu=0.2$ so the coefficient K is evaluated (Equation 3.1) and then the dynamic elastic modulus can be calculated

Due to the effect of the voids or cracks actually the elastic waves path can be longer than the distance between transmitter and receiver.

3.2.2. Curing and Exposure Conditioning

After the pre-cracking, UPV testing and microscopic study of the cracked zone, all the specimens (pre-cracked and reference) were exposed to different conditioning environments (Figure 3.13, Table 3.5). Immersion in water and exposure to open air in the lab courtyard; - in both cases up to 1 year-were considered as reference exposure conditions.

In Figure 3.14, left the recorded trends are shown of minimum and maximum temperatures and of relative humidity all along the exposure period.

Besides these “natural” exposure conditioning, accelerated conditioning in a climate chamber, also to assess the reliability of accelerated haling procedures, were performed. The performed cycles, each lasting 6 hours and meant as representative of exposure to either a winter or summer Northern Italy climate, are shown in Figure 3.14, right. Exposure up to 1,2 and 4 weeks in climate chamber for both types of accelerated cycles was performed.

Type of the Conditioning	Duration of the Conditioning
H – Water Immersion	1, 2, 3, 6, 12 months
D – (Dry) Natural air exposure	1, 2, 3, 6, 12 months
HD – Wet/Dry	1, 3 months
C – Climatic Chamber	1, 2, 4 weeks

Table 3.5. Exposure conditioning and the duration for each of them



Figure 3.13. (left) Climatic chamber; (middle) Water immersion; (right) air exposure

Experimental Campaign

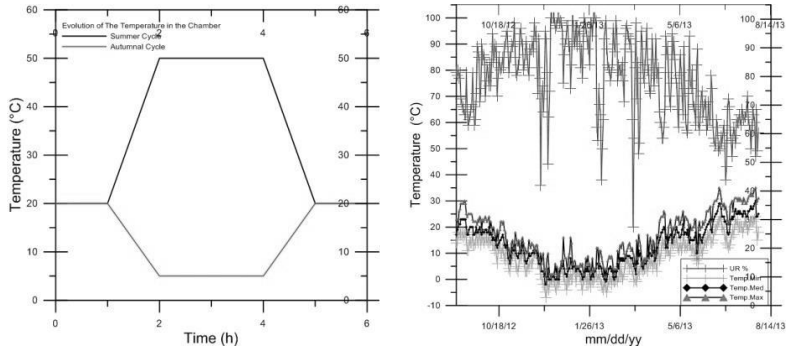


Figure 3.14. (left) Temperature and relative humidity simulated by the climate chamber; (right) T and RH recorded along the specimen exposure period.

At the end of the scheduled exposure times, the specimens were first of all analysed with an optical microscope to visually check the presence of the healing products in the cracks.

Then the specimens were tested up to failure according to the same set-up employed for the pre-cracking.

A typical response, in terms load vs COD in the case of healing, is shown in the (Figure 4.13) corresponds with the response exhibited by the same specimen in the pre-cracking stage.

	Exposure condition and duration															
	Water immersion				Open air exposure				Climate chamber							
	1m	2m	3m	6m	12m	1m	2m	3m	6m	12m	winter		summer			
	w/out additive															
Un-cracked	1	2	2	2	2	1	2	2	2	2	2	2	2	3	3	3
Pre-cracked 100 µm											2	2	3	3	3	3
Pre-cracked 200 µm	1	2	2	2	2	1	2	2	2	2	3	3	3	3	3	3
	with additive															
Un-cracked	1	2	2	2	2	1	2	2	2	2	2	2	2	6	6	6
Pre-cracked 100 µm											2	2	3	6	6	6
Pre-cracked 200 µm	1	2	2	2	2	1	2	2	2	2	3	3	3	6	6	6

m = months

w = weeks

Figure 3.15. Synopsis of experimental programme (n° of specimens per each test condition)

A synopsis of the experimental campaign in the normal strength concrete (NSC) is given in details in Figure 3.15.

3.2.3. Post-Exposure Testing

At the end of scheduled exposure periods, specimens were tested up to failure according to the same scheme employed for the pre-cracking.

A typical response (pre-cracking and post-conditioning for the same specimen) is shown in and highlights recovery of both bearing capacity and stiffness. Results will be analyzed in details in next chapter (Figure 3.16).

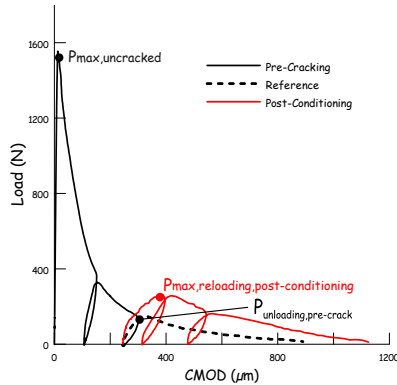


Figure 3.16. Typical Load vs CMOD response from 3PBT during pre-cracking and the same specimen response in post-conditioning stage.

The evident recovery of load bearing capacity (and the stiffness) was attributed (also by means of comparison with the behaviour of un-cracked specimens undergoing the same conditioning) to the healing of the cracks and it will be employed as it will be detailed in the fourth coming chapter of this thesis, for the quantification of the occurred healing

3.3. Self-Healing Investigation on High Performance Reinforced Cementitious Composite (HPFRCC) with Steel Fibers

3.3.1. Introduction

From a general point of view the composition of HPFRCCs is characterized by a high content of cement and binder (featuring either a pozzolanic or a cementitious activity) and a low water/binder ratio, both requirements aiming at a high compactness of the matrix.

The addition of fibres, tempering the inherent brittleness of the same matrix, also helps in controlling the opening of each single cracks. The synergy between mix composition – which is likely to “leave” a lot of unhydrated binder particles only upon cracking can come in contact with water/moisture and undergo delayed hydration and the crack opening control provided by the fibres, which keep the same opening below a certain “fillability threshold” is highly conducive to self-healing.

This makes the self-healing capacity of HPFRCCs worth being investigated to provide a further sustainability value to structures made of or retrofitted with this category of advanced cementitious composites.

3.3.2. Materials and Manufacturing

In this study reference has been made to a HPFRCCs (Table 3.6), extensively studied at Politecnico di Milano [82]-[88]:

Constituent (kg/m ³)	Dosage (kg/m ³)
Cement CEM I / 52.5 R	600
Water	200
Superplasticizer (lt/m ³)	33
Sand 0-2 mm	982
Slag	500
Straight Steel Fibers (l _f = 13 mm; d _f = 0.16 mm)	100
Water/cement	0.33
Water/binder	0.18
Fiber percentage in volume	1.28%

Table 3.6. Mix-Design of HPFRCC with steel fibers

Constituent	Percentage
Quartz	47.7 (35.9 monocrystalline) (11.8 polycrystalline)
Gneiss	15.5
Feldspar	9.5
Micas and micaschist	6.4
Granitoids rocks	5.1
Microcrystalline silica	2.7
Amphibolis	2.7
Carbonate rocks	2.4
Siltstone	2.4
Serpentinites	1.4
Garnet and iron oxides	0.7

Table 3.7. Petrographic characterization of the sand

Figure 3.17, left shows the fibers used in the mix

The used sand was sieved up to 2 mm (Figure 3.17, right) and its petrographic analysis is shown in the Table 3.7. The sand used can be defined as mixed quartz sand.

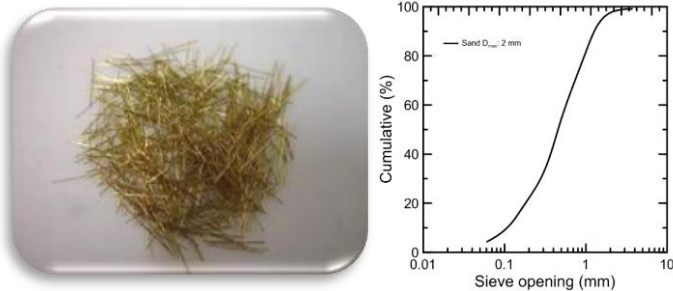


Figure 3.17. (Left) Straight Steel Fibers ($l_f = 13$ mm; $d_f = 0.16$ mm); (right) Granulometric curve for the used sand.

The composition of the Portland cement Type I, 52.5 R, containing 95% of clinker and 5% of gypsum is presented the in (Table 3.8) also its composition.

Constituents	Percentage (%)
C ₃ S	65%
C ₂ S	11%
C ₃ A	9%

Table 3.8. Cement Composition

The high amount of granulated blast furnace slag used in this case, as described previously, presents different advantages and one of the most important is cement substitution. The chemical analysis of the slag is shown in the Table 3.9, as from the XRF spectrometry test. The mixing procedure is crucial for obtaining the expected composite. The high performance fiber composites were prepared by means of a Simem mixer (Figure 3.18, left) according to the mixing protocol shown in Table 3.10.

Constituents	Percentage (%)
SiO ₂	39.0 %
Al ₂ O ₃	11.0 %
Fe ₂ O ₃	0.70 %
TiO ₂	0.55 %
CaO	37.50 %
MgO	8.30 %
K ₂ O	0.30 %
Na ₂ O	0.20 %
MnO	0.80 %
C	0.20 %
S	1.00 %

Table 3.9. Slag composition

Slabs 1m long x 0.5 m wide and 25 mm thick were casted; after two days curing in lab environment they were shifted to a humid climate chamber on a temperature 20°C and 95% RH for different periods – as it will be explained with more details in the next paragraph.



Figure 3.18. (left) Simem mixer and (right) casting of the slabs.

The same mix composition as recalled above, which also features significant amounts of superplasticizer to compensate for the low water/binder ratio, is conducive to a superior performance in the fresh state. As it can be seen from (Figure 3.18, right) the mix is self-compacting and thus the slabs were cast allowing the fluid materials to flow along the long direction up to complete mold filling.

Stage	Activity	Mixing Velocity	Duration (minutes)
Stage 1	Cement and slag was mixed in dry	Minimum	2:00
	Increasing of the velocity	Increased	0:30
	Mixing	Maximum	2:00
Stage 2	Adding of water and superplasticizer	Null	-
Stage 3	Mixing consenting the activation of the superplasticizer	Maximum	20:00
Stage 4	Adding of the fibers	Maximum	1:00
Stage 5	Mixing	Fast	5:00

Table 3.10. Mixing timetable.

Through this casting technique it is possible (as shown by several studies [80]-[89]) to align the fibers in the direction of the casting flow. This flow induced alignment of the fibers was duly taken into account when obtaining beam – like specimens from the casted slabs for the further self-healing investigations.

As a matter of fact the beam specimens were cut, as shown in the Figure 3.19 with their axis either parallel or orthogonal to the casting flow direction, and hence to the most probable alignment of the fibers.

This will result in fiber alignment parallel or orthogonal to the applied bending stress and hence in a deflection hardening or softening behavior respectively, which will be coherently considered in the whole testing procedure as hereafter detailed.

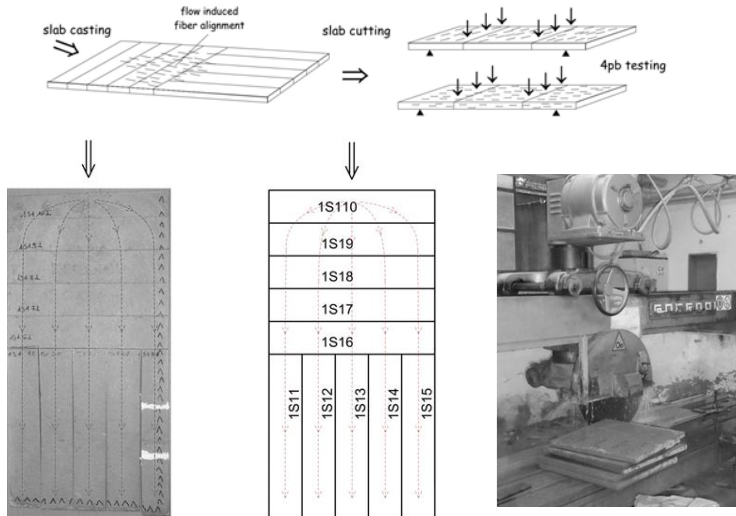


Figure 3.19. (up) Schematic presentation for casted slabs and flow induced with fiber alignment; (left, middle) casted slab with lines to be cut; (right) cutting procedure in half slabs.

3.3.2.1. Pre-cracking by four point bending test(4PBT)

For the experimental methodology employed to study the self-healing capacity of HPRCCs follows the same concept discussed above as for ordinary concrete.

The only difference stands in the type/scheme of the bending test employed in the pre-cracking and post-conditioning stage. As a matter of fact, because of the likely deflection hardening behavior, and also according

to the prescription of the Italian guidelines CNR2004 [155] and of fib Model Code 2010 [4] set-up, shown in Figure 3.20 was employed

With the adopted set-up it was effectively possible to discriminate the difference between a deflection softening behavior and deflection hardening behavior as caused by an alignment of the fibers respectively parallel or orthogonal to the applied bending stress.

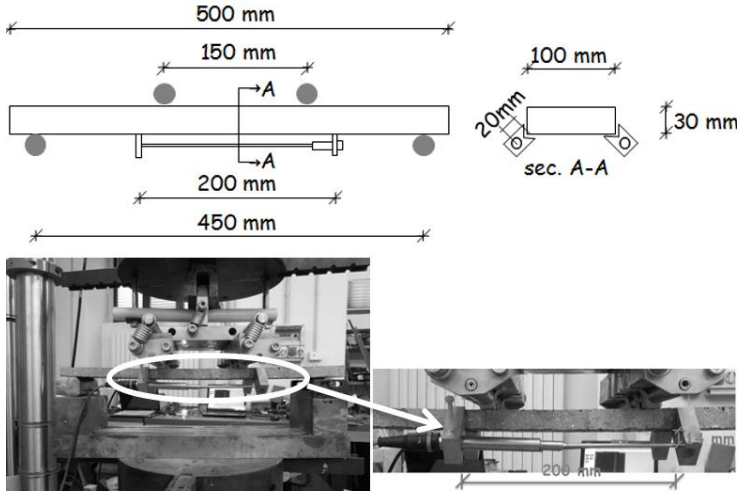


Figure 3.20. (up) Schematic presentation of the four point bending test; (left) four point bending test set-up; (right) the measurement detail by the linear variable differential transformer (LVDT transducers)

An example of the aforementioned behavior as from monotonic tests on reference specimens, is shown in Figure 3.21 together with the associated crack patterns: it can be interestingly observed that a single crack is obtained in the case of deflection softening behavior whereas multiple cracks are formed in the central (constant bending moment with a crack spacing close to the fiber length) region.

Because of the different behavior different pre-crack opening were selected:

- For deflection softening specimens where pre-cracked up to 0.5 mm;
- For deflection hardening specimens two COD values in the pre-peak regime were chosen (namely 1 mm and 2 mm) and one in the post peak regime (equal to $COD_{peak} + 0.5$ mm).

When applicable, at COD instantaneous un-loading/reloading cycles were performed to monitor also in the pre-cracking stage the evolution of stiffness. This was anyway done also as reference specimens tested up to failure according to the scheme in Figure 3.20.

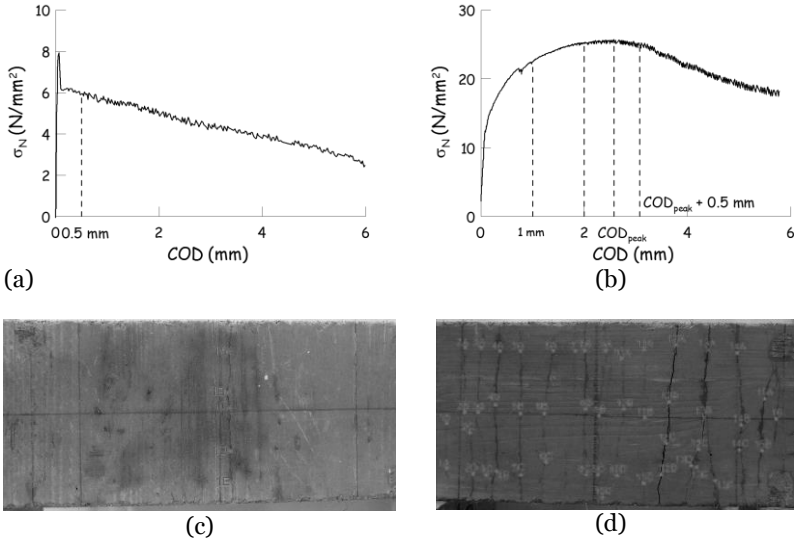


Figure 3.21. Nominal stress σ_N vs. COD curves for specimens featuring: (left) unstable post-cracking localization and deflection softening behavior (fibers orthogonal to the bending axis) and (right) stable pre-peak multi-cracking and deflection hardening behavior (fibers parallel to the bending axis).

The Crack Opening Displacement was measured by the LVDTs attached at the bottom edge of the specimen over a gage length of 200 mm (Figure 3.20). The measure in the case of a deflection hardening behavior characterized by multiple cracking is hence the sum of all openings of each single crack plus the elastic deformation, which any way remains small.

electron microscopy Zeiss Evo 50P equipped with oxford Inca Energy 200EDS having a ultra-thin window detector from 133 eV.

After pre-cracking and related investigations specimens were exposed to different curing environments and for different durations as in Table 3.4. With reference to open air exposure in Figure 3.25 the recorded trends of the temperatures and humidity along the exposure period are shown.

At the end of the schedules exposure periods the specimens were re-tested according to the same set-up employed for pre-cracking.

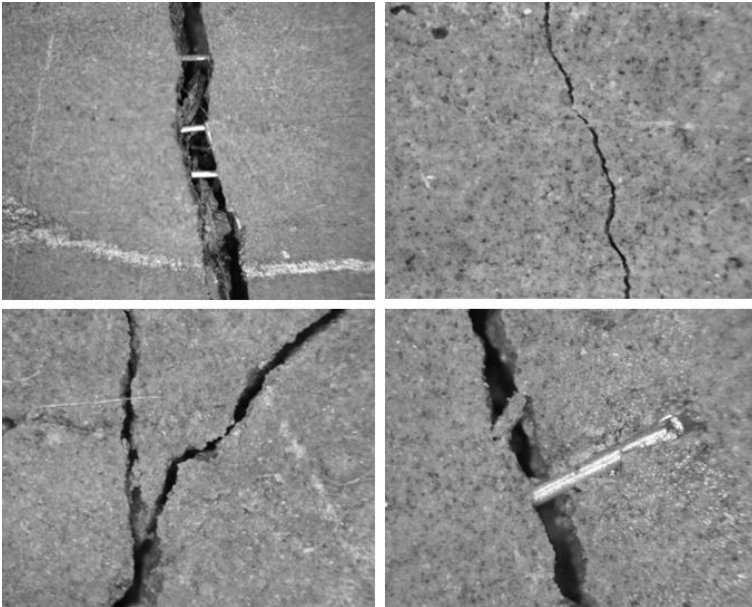


Figure 3.24. Microscope images of the cracks

In general, as from example results shown in the Figure 4.11, a regain of load bearing capacity, initial stiffness and, in case, ductility was observed, as a function of a new pre-cracking opening and age, such as exposure conditioning and durations.

By comparison with the behavior exhibited by undamaged specimens the strength, stiffness and ductility gain was attributed to hereby

observed by new opening of the crack as from the scheme in the Figure 3.24 through the optical microscope.

It is also worth remarking that in the post-conditioning stage during the tests up to failure a several instantaneous unloading/reloading cycles was performed to assess the evolution of the stiffness.

Self-healing, as it will be attributed in the forthcoming chapter, will be quantified through the strength, stiffness and ductility gain.

At the end of the tests healing products of the fractured surface were analyzed by an environmentally electron microscope.

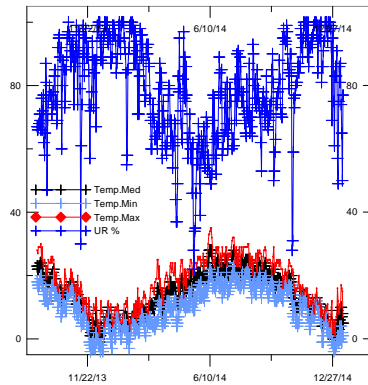


Figure 3.25. Temperature and Relative Humidity (RH) recorded along the specimens exposure period

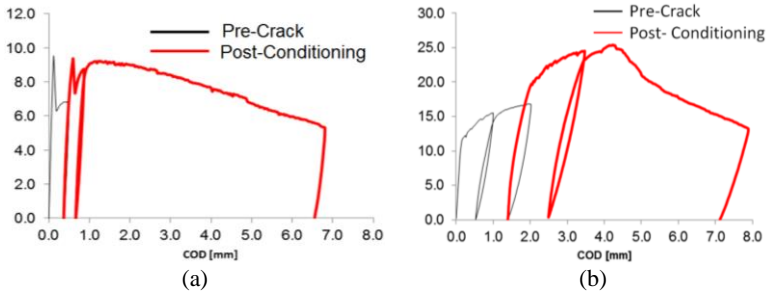


Figure 3.26. The comparison between the pre-cracking and post-conditioning behavior for (a) deflection softening and (b) deflection hardening.

Pre-crack opening		Deflection behavior											
		softening						hardening					
		0.5 mm		1 mm		2 mm		COD _{peak} + 0.5 mm		COD _{peak} + 0.5 mm		COD _{peak} + 0.5 mm	
Exposure Conditions	Age of Pre-crack	Exposure duration (months)											
		1	6	12	1	6	12	1	6	12	1	6	12
Water immersion	2 m	1	1	1	1	1	1	2	1	1	2	2	2
	11 m ¹	3	2	3	1	1	=	1	1	1	1	1	1
Air exposure	2 m	1	2	1	1	1	1	2	1	1	1	2	1
20°C – RH = 95%	2 m	1	2	1	1	1	1	2	1	1	2	2	2
20°C – RH = 50%	2 m	1	2	2	1	1	1	2	2	2	2	2	2
Wet and dry	2 m	1	2	2	1	1	1	2	2	2	2	2	2

Table 3.11. Synopsis of the experimental program: number of specimens tested per each exposure condition and duration, age of pre-cracking, deflection hardening/softening behavior and pre-crack opening

3.4. Self-Healing Investigation on High Performance Reinforced Cementitious Composite (HPFRCC) with Hybrid Fibers; Natural and Steel Fibers

3.4.1. Introduction

When presenting the state of art about self-healing capacity of cementitious composites in the second chapter, different techniques were described to engineer the self-healing capacity. The introduction in the mix of natural fibers, is one of them and in this thesis a collaboration was developed between Politecnico di Milano and Universidad Federal do Rio de Janeiro, Brazil.

In these experimental activities the effect of natural fibers on the self-healing capacity of cementitious composites has been studied. Reference has been herein made to a High Performance Cementitious Composite reinforced either with steel fibers only or with a hybrid mix of steel and sisal fibers. In this framework, the use of natural fibers in HPFRCCs is likely to be characterized by a twofold value. On the one hand they can contribute to the multiple cracking behavior, which, together with a peculiar mix composition, is an essential requisite for conductivity to autogeneous healing, as remarked

¹ For specimens pre-cracked at 11 months age the exposure durations were respectively 1 3 and 6 months

above. On the other hand because of their highly hydrophilic nature and porous microstructures, natural fibers, either even simply during the mixing process or through dedicated pre-saturation, can absorb water. Natural fibers, through their porous micro-structure, can create a large number of moisture paths, through which moisture, absorbed by the same fibers, can be released “on demand” and activate delayed hydration processes which contribute to the healing processes of damage and cracks.

3.4.2. Materials and Manufacturing

The high performance fiber reinforced cementitious composite (HPFRCC) used in this research activity is the same used on the one presented on Paragraph 3.3.2. The difference consists in the use of natural fibers which would emphasize and enhance the kinetics reactions of the self-healing mechanism.

Sisal fibers were used which originate from the “Agava” (botanical name) plant, native from Mexico but cultivated and naturalized in various countries. Sisal fibers used in this campaign were obtained from sisal plants cultivated in farms located in the Bahia state, Brazil. They were extracted from the sisal plant leaves in the form of long fiber bundles. The fibre extraction from the leaf was done by semi-automatic crushers. A sisal plant produces from 200 to 250 leaves before flowering. Each of them contains approximately 700-1400 fibre bundles, 0.5 to 1 m long. From 10 kg of sisal leaves about 1.35 kg extractable fibers could be obtained (Figure 3.27).



Figure 3.27. (left) Sisal fibers origin “Agave”; (middle) Production of fibers; (right) final production (long sisal fibers Courtesy by [158])

Their Chemical composition is represented from about 54-66% of cellulose; 12-17% hemicellulose; 7-14% lignine; 1% pectine and 1-7% ashes. From geometrical and morphological point of view, every technical fiber contains numerous (between 100 and 200) elongated individual fibre cells which are about 1.8 mm in length and 6-30 μm in diameter. Cell wall

thickness of a few microns have been reported, the remaining part of each fibre cell being occupied by the lumen. Cross section areas of individual technical fibre in the range 0.02-0.05 mm² have been reported (Figure 3.28).

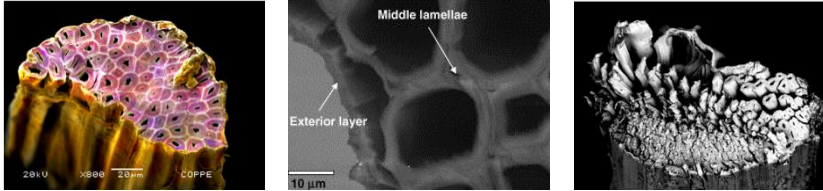


Figure 3.28. Sisal fiber morphology showing: (left) fiber composed of several fiber-cells linked by the middle lamellae; (middle) detail of middle lamellae (composed of lignin and hemicellulose) with its exterior layer; (left) hydrolysis of sisal. Courtesy by Silva et al [159]

Different uses are well known such as rope and twine, including papers, clothes wall coverings, carpets and dartboards. Their use in civil industries is encouraged due to their availability (Figure 3.27, left); low power consumption due to manufacturing (Figure 3.27, middle, right), lower environmental impact; high engineering properties due to their high tensile strain (Figure 3.30). Due to their hydrophilic nature and porous microstructures they increase their section when absorb the water and reduce it, when released (Figure 3.29).

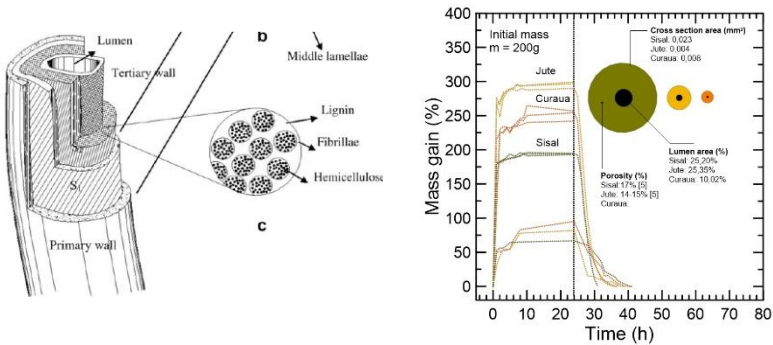


Figure 3.29. Mass gain in time due to the water absorption of different natural fibers. Courtesy by Ferreira et al. [158]

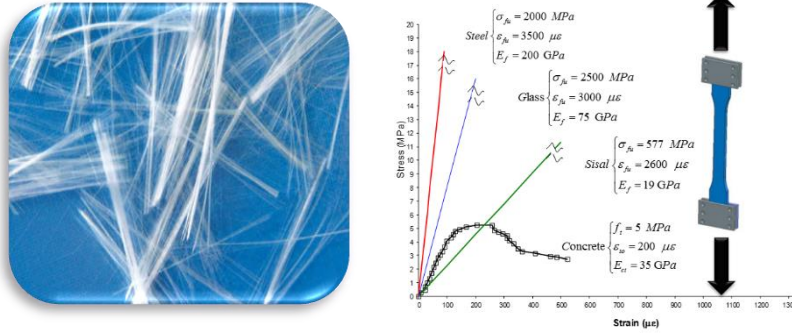


Figure 3.30. (left) Short Sisal fibers used in the mix design; (right) Fiber classification due to their tensile strength. Courtesy by Silva et al [159]

The mechanical properties of sisal fibers represented from such a tensile strength, shows values from 350 to about 600 MPa with Young modulus from 8-9 to 19 GPa (with lower variation if corrected for compliance). Their failure strain is about 2.5 to 5 % (Figure 3.30).

The mix composition of the hybrid sisal + steel HPRCCs, employed in this stud is shown in Table 3.12. Same mixing and specimens casting procedure from as for the steel only HPRCC were followed. Typical deflection hardening and softening response of steel+sisal hybrid HPRCC as compared with the steel only HPRCC are shown in the Figure 3.31

Constituent (kg/m ³)	Dosage (kg/m ³)
Cement CEM I / 52.5 R	600
Water	200
Superplasticizier (lt/m ³)	35
Sand 0-2 mm	982
Slag	500
Straight Steel Fibers	50
Sisal Fibers	7
Water/cement	0.33
Water/binder	0.18
Fiber percentage in volume	1.28%

Table 3.12. Mix-Design of HPRCC with natural (sisal) fibers

Despite the lower value of the load bearing capacity the influence of the flow induced alignment of fibers is confirmed and the ability, in the case of a favorable orientation, of involving a multiple cracking.

The testing procedure was the same as discussed above with the following differences:

In the case of deflection hardening specimens pre-crack opening was equal only to $COD_{peak} + 0.5$ mm;

Only wet and dry exposure conditioning were performed up to six months.

This condition is believed to emphasize the role of the natural fibers since they absorb water in the wet stage and release it during the drying stage disperse and diffuse it throughout the matrix also for far from the cracks because of their tubular structure, thus emphasizing the healing reactions.

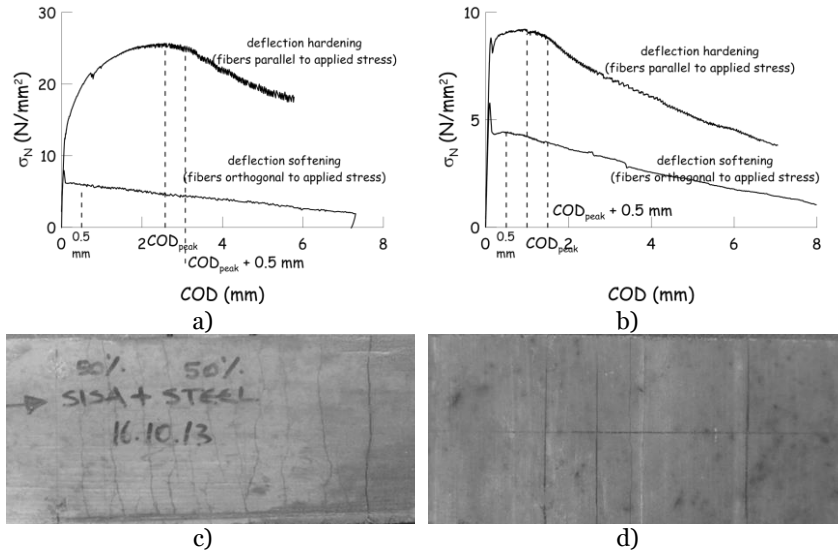


Figure 3.31. Monotonic response of steel HPRCC (a) and steel + sisal HPRCC (b) specimens for fibers parallel and orthogonal to the applied bending stress – COD pre-cracking thresholds are highlighted; c) multiple crack pattern due to the alignment of fibers and d) single crack due to orthogonal direction.

3.4.2.1. Direct Tensile Testing

HPFRCC with both steel and hybrid fibers (steel and sisal) used in the previous experimental campaign (Table 3.12), was also employed to cast specimens for direct tension tests. The fiber alignment was taken into account, casting slabs by 1 m long and 0.5 m wide. Prismatic specimens 300 mm long, 60 wide and 30 mm thick, notched laterally for about 1 cm each side, were cut in such a way to have fibers parallel to the direction of the tensile stress to be applied (Figure 3.32)

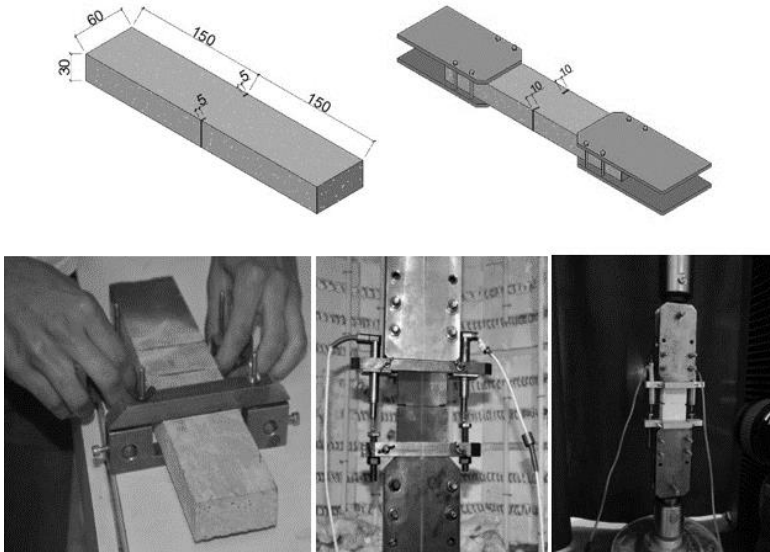


Figure 3.32. Uniaxial Tensile testing on HPFRCC with Steel and Steel + Sisal Fibers.

Based on the monotonic response of the direct uniaxial tensile test, shown in the Figure 3.33 it has been decided:

- to perform a pre-cracking test for a single crack equal to COD = 0.15 mm;
- two different conditioning such as water immersion and wet/dry cycles were performed up to three months.

Proposed tests were performed in a closed loop servohydraulic testing machine with a capacity of 500 kN (Figure 3.32). The tests were

controlled by the cross-head displacement at a rate of 0.1 mm/min. Two lateral lvd-t-s were used to measure the COD in the central zone.

The notches were created to concentrate the crack in the central zone, avoiding a possible multiple crack pattern. An interesting study of the crack will be done expecting a uniform crack opening through the section.

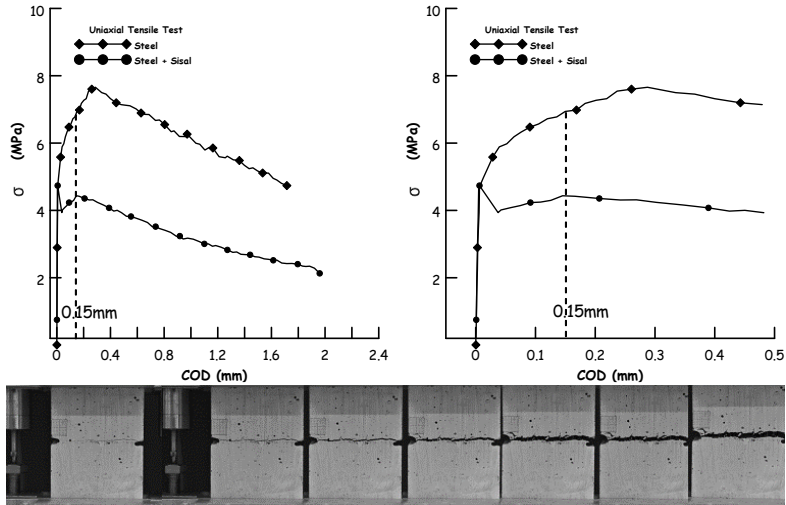


Figure 3.33. Monotonic response under uniaxial tensile test for HPRCC for steel and steel + sisal (top), induced single crack due to the notches in both sides of the specimen (bottom).

At the end of the conditioning period the direct tension tests were re-performed to evaluate effects of healing on the recovery of the mechanical performance.

The important thing is never stop questioning.

Albert Einstein

4. Analysis and Discussion of Experimental Results

4.1. Introduction

In this chapter the results of the experimental campaign presented in chapter 3 will be presented and analyzed with the aim of validating the proposed experimental methodology and assess the effectiveness of crack healing on the recovery of the mechanical performance of the investigated categories of concretes and cementitious composites.

In detail, the comparison between the nominal bending stress vs. COD response exhibited by the same specimen in its virgin state, i.e. when undergoing the pre-cracking stage test, and at the end of the prescribed exposure condition and duration in the cracked state, has allowed, as it will be detailed in the forthcoming sections of this dissertation, to assess the recovery, if any, of stiffness, load bearing capacity and accumulation of damage and irreversible deformations, as attributable to crack healing phenomena. This has been also instrumental at defining and quantifying suitable self-healing indices for the different analyzed mechanical properties, as it will be detailed in forthcoming section.

When applied cross comparison between results obtained from UPV tests, in terms of dynamic modulus of elasticity (obtained through the classical formula which correlates the wave speed through a solid medium to its stiffness and density), and those obtained from 3pb/4pb tests, in terms of beam flexural stiffness, allowed the reliability of the proposed test methodology to be further assessed.

The visual microscopic observation of the healed cracks and their detailed microstructural investigation will complement the analysis discussed above providing valuable information to understand and explain the observed “macro-mechanical” features of crack healing phenomena in cementitious composites.

4.2. Conventional Concrete

4.2.1. Normal Strength Concrete

The two investigated concretes, with and without the crystalline admixture, were first of all characterized by meaning the development of their compressive strength all along the 28 days curing period before the pre-cracking.

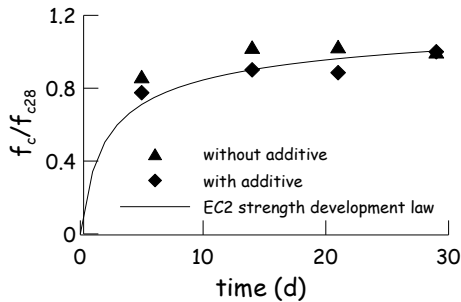


Figure 4.1 Strength development of concrete with and without crystalline additives vs. EC2 provisions

Based on the EC2, cubic specimens were tested (as described in the previous chapter). First of all the comparison between the concrete with and without admixture was performed, to evaluate the effect of admixture in the strength development of concrete. Then, EC2 predictive law has been plotted

on the same graph and compared with the strength development of both concretes.

By observing the graph on the Figure 4.1 it can be stated that:

- The crystalline admixture alone, in a sound concrete specimen, does not affect the strength of the material nor its development within time.

4.2.2. Ultrasonic Pulse Velocity tests

Characterization of healing started with Ultrasonic Pulse Velocity (UPV) tests, performed on the beam specimens employing the set-up shown in Figure 3.11, along the pre-cracking/conditioning/final testing procedure described in the previous chapter and at the following “steps”:

- On the truly virgin specimen, i.e. immediately before pre-cracking (initial stage);
- After the pre-cracking and immediately before the onset of the exposure/environmental conditioning (intermediate stage);
- After scheduled exposure/conditioning durations, immediately before final testing of the specimens to failure (final stage).

Wave speed was calculated (Paragraph 3.2.1.3) from measured transit time between the emitter and receiver units of the UPV test apparatus, with reference to the distance between the units (90 mm, as indicated in the caption of Figure 3.11). The velocity, as calculated for each specimen in its virgin state (see above), was assumed as a reference, and denoted as (UPV)₀. The values of the velocities calculated from measured transit times either after pre-cracking or after scheduled exposure/conditioning durations, dimensionless to the aforementioned reference value (UPV)₀, have been plotted as a function of the exposure time in Figure 4.2a-f, respectively for air exposure and water immersion (Figure 4.2a,b) as well as for accelerated conditioning in climate chamber representative of either summer (Figure 4.2c,d) or winter climate (Figure 4.2e,f). Results for concrete both without and with the crystalline admixture have been reported.

It is worth remarking that specimens were, in case, wiped and kept in lab environment for a few hours for stabilizing in a homogenous manner their moisture conditions – before performing the tests

The effectiveness of the crack repairing phenomena, either autogenic or catalyzed by the presence of the crystalline additive, clearly appears from the trend of the plotted relative ultrasonic pulse velocity for pre-cracked specimens.

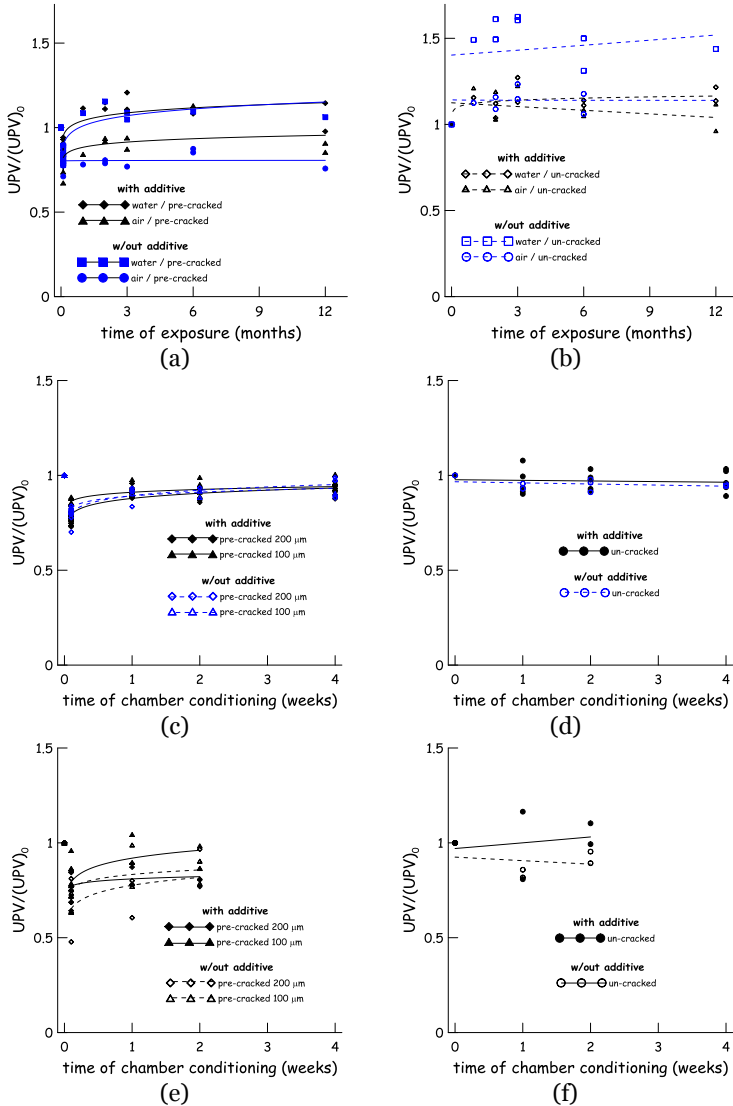


Figure 4.2. Relative UPV vs. exposure time for water/air exposure (a-b); summer (c-d) and winter (e-f) chamber conditioning; pre-cracked (a, c, e) vs. un-cracked (b, d,f) specimens.

The higher effectiveness of a continuous water immersion is also evident: specimens in water, after only one month, are able not only to recover their pristine features but even show an improvement with respect to the values of ultrasonic pulse velocity measured before any cracking and conditioning process. Concrete containing the crystalline additive performs, in its early age, slightly better than concrete without it.

On the other hand, specimens exposed to air, exhibit a slower recovery of their pristine level of performance. It has furthermore to be noted that only for specimens containing the crystalline additive, after longer exposure to natural weather conditions, i.e. from six to twelve months, a value of the ultrasonic pulse velocity almost comparable to that measured on the virgin specimens was gained back. Specimens made with concrete not containing any additive showed, all along the exposure time, an almost constant performance, stable on the level which characterized their “pre-cracked” behavior (Figure 4.2a). Un-cracked specimens (Figure 4.2b), on their hand, either immersed in water or exposed to air, did not exhibit any significant change in their behavior. Specimens not containing the crystalline additive and immersed in water stand as the only visible exception to that statement, since for them values of UPV even 50% higher than the reference one were measured as soon as after one month immersion; after then the values held almost constant. This may be explained considering very low absolute values of the UPV measured for virgin specimens made with concrete not containing the crystalline additive, as low as 3.5 km/s, compared to average velocity values of 4 km/s measured for specimens made with the concrete with it. Specimens without the additive, even if cured under moist towels before de-moulding, experienced significant plastic shrinkage, which also resulted in an observed diffused surface cracking, which could justify the aforementioned discrepancy. The delayed hydration of concrete promoted by water immersion, could have healed the plastic shrinkage cracking, thus explaining the measured recovery of performance. On the other hand, the crystalline admixture, with its action, could have been effective also in counteracting this phenomenon, healing the plastic shrinkage cracks even at early ages, and thus explaining the fact that no significant modification was measured for specimens containing the additive.

With reference to climate chamber conditioning (Figure 4.2c-f), the measured trend showed a tendency towards an almost complete recovery of pristine level of performance, as measured for virgin specimens. This was observed only at the end of the conditioning period for summer cycles (Figure 4.2c), whereas, in the case of winter cycles, it appears that, at least for specimens made with concrete containing the crystalline additive, two weeks were enough for the tighter crack opening (100 μm), which are likely to be healed faster and better than wider ones (200 μm) (Figure 4.2e).

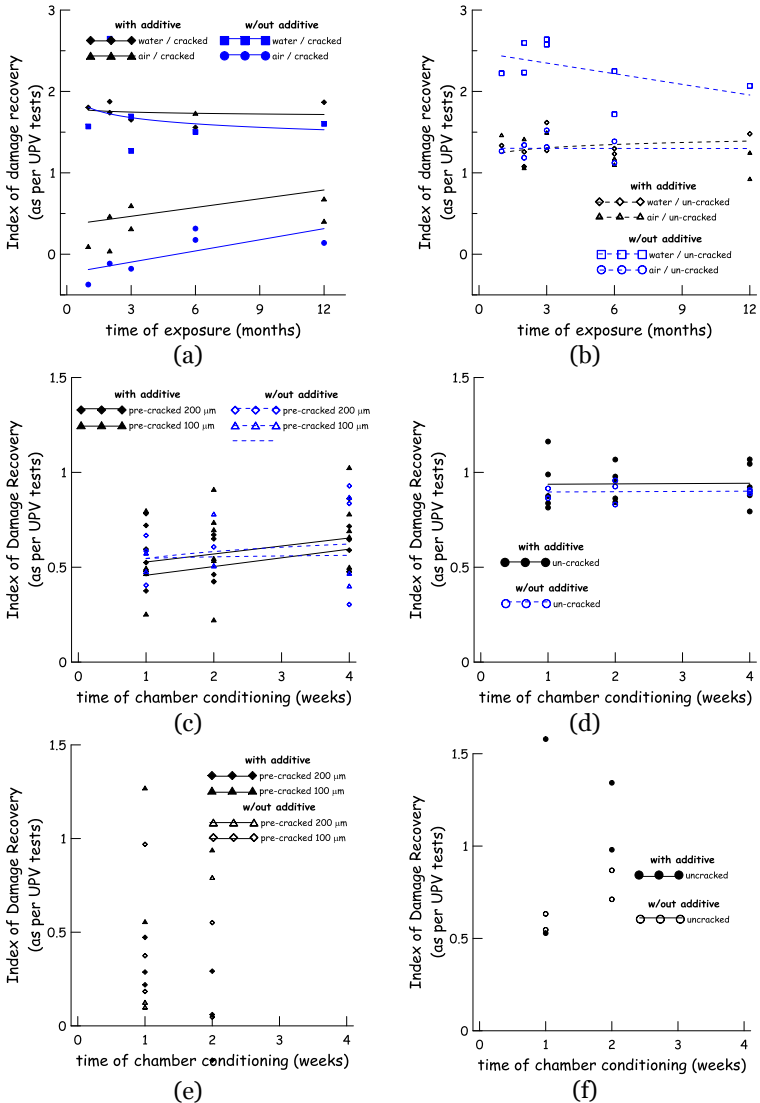


Figure 4.3. IDR (from UPV tests) vs. exposure time for water/air exposure (a, b); summer (c, d) and winter (e, f) chamber conditioning; p re-cracked (a, c, e) vs. un-cracked (b, d, f) specimens.

It is furthermore evident that, whereas in conditioning meant as representative of autumn/winter exposure, the performance of concrete containing the crystalline additive was significantly better than for concrete without it, differences were less evident, if almost scant, in the case of conditioning representative of spring/summer exposure. This could be attributed to the effect of the higher temperatures attained, together with the repetition of the warming/cooling cycles. Anyway, for both winter and summer temperature cycles, similarly to what happened for “natural” exposure conditions discussed in the previous paragraph, un-cracked specimens did not exhibit any significant variation of the measured properties (Figure 4.2d, f).

This evidence strongly supports the assumption that the measured recovery, in terms of ultrasonic pulse velocity, has to be attributed not to a bulky continuing hydration but rightly to a self-healing, either autogenic or engineered by the addition of the crystalline additive, of the cracks, due to the reaction with water or atmospheric humidity of potentially reactive material exposed upon cracking, being it un-hydrated cement or ready to react hydrophilic admixture particles.

From the formula which relates wave speed in a medium to its stiffness and density, Young modulus of concrete in tested specimens was evaluated and its values before cracking (reference value E_0), after cracking and after environmental conditioning analyzed similarly to what has been above presented with reference to UPV values. Plots in Figure 4.2g-l confirm the aforementioned statements with reference to the influence of exposure conditions and crystalline admixture on the effectiveness and “kinetics” of self-healing mechanisms.

4.2.3. Index of Damage Recovery as per UPV tests

From the values of Young moduli computed as explained in the previous paragraph, an Index of Damage Recovery (as per UPV test results) was evaluated as follows, for pre-cracked and un-cracked specimens:

$$DR(UPV), \text{cracked} = \frac{E_{\text{post-conditioning}} - E_{\text{pre-cracking}}}{E_0 - E_{\text{post-conditioning}}} = \frac{D_{\text{post-conditioning}} - D_{\text{pre-cracking}}}{D_{\text{pre-cracking}}} \quad 4.1$$

$$IDR(UPV), \text{un-cracked} = \frac{E_{\text{after-conditioning}} - E_0}{E_0} \quad 4.2$$

where E_0 represents the material stiffness, evaluated from UPV measured on the specimen in the virgin state; $E_{\text{after-cracking}}$ and $E_{\text{after-conditioning}}$ are the material Young moduli calculated from UPV results as obtained from

specimens after the pre-cracking and after the conditioning period respectively; $D_{\text{post-conditioning}}$ and $D_{\text{pre-cracking}}$ are the values of the damage variable, meant as an index of stiffness degradation, from the computed stiffness evaluated respectively in the post-conditioning and in the pre-cracking stage. It is worth here remarking that all the Young modulus values appearing in Eq. (4.1-4.2) have to be measured on the same specimen, as it has been done in this paper.

From the definition above, and from the concept of a “damage variable” as an index of stiffness degradation, the Index of Damage Recovery in Eq.(4.1) computes the ratio, to the damage accumulated upon pre-cracking, of the difference between the damage characterizing the response of the specimen in the post-conditioning stage and the one accumulated upon pre-cracking. It hence plainly follows that a value of the IDR equal to or larger than 1 corresponds to a complete recovery of the original level of performance, as far as UPV measurements are concerned.

From the graphs shown in Figure 4.3 the following statements can be drawn, which further support what has already been discussed with reference to plots shown in Figure 4.2,a:

- Pre-cracked specimens immersed in water show, since from the beginning of conditioning period, a significant stiffness recovery, which slightly changes upon prolonged immersion; specimens containing the crystalline admixture performed slightly better than specimens without it. The computed values of the IDR higher than one could be most likely attributed to some “bulk” continued hydration (Figure 4.3);
- Pre-cracked specimens exposed to air initially exhibited a significant loss of stiffness, and, for concrete without the crystalline additive, even with reference to the “post-cracking” stage (IDR negative). A gradual and slow recovery of stiffness has been then observed for specimens without the additive up to a slightly better stage than the pre-cracking one (IDR slightly larger than zero); specimens containing the crystalline additive featured a faster recovery, able to guarantee, after longer exposure, the attainment of a performance slightly lower than, but comparable to, the virgin one (Figure 4.3a);
- For un-cracked specimens the IDR held almost constant all along the exposure period; un-cracked specimens made of “not-admixed” concrete stand as a visible exception, since some worsening of the performance was measured with prolonged exposure (Figure 4.3b);
- Pre-cracked specimens conditioned in climate chamber (summer cycles – Figure 4.3c) exhibited a highly scattered and quite slight recovery of stiffness, which was not affected by the duration of the conditioning for specimens without the crystalline additive and

moderately increased with in the case of specimens containing the additive.

- Un-cracked specimens, mostly without the additive, conditioned in climate chamber (summer cycles–Figure 4.3d) featured almost constant behavior along the exposure period;
- The trend of the IDR for specimens conditioned in climate chamber (winter cycles – Figure 4.3e,f) appears to be much more scattered than for other cases (due to some inconsistencies in the experimental measurements); this makes the search of a trend fitting really scarcely significant, for which reason it was not reported in the graphs

4.2.4. Three-point bending tests (3PBT)

The same set-up employed for pre-cracking specimens up to selected crack-opening values (Figure 3.9), was employed to test the same specimens up to failure after scheduled times of exposure to the different investigated environment conditions, as highlighted in previous section.

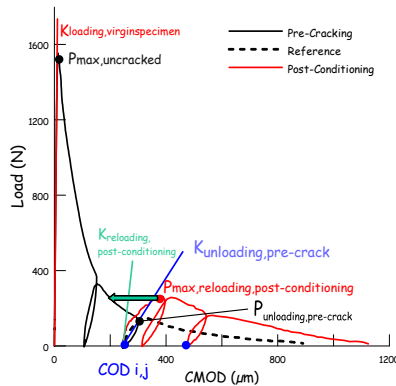


Figure 4.4. Example of load vs. COD curves for specimens submitted to pre-cracking and post-conditioning 3pb tests; definition of quantities for calculation of self-healing indices

In Figure 4.4 the results of a typical test, in terms of load vs. COD curves, are shown: it is worth remarking that the graphs are built up in a way that the curves pertaining respectively to the pre-cracking test and to the post-conditioning up-to-failure test for the same specimens are compared.

The analysis of the data garnered through the wide test program, allows the following remarks to be highlighted:

In general, specimens featured a recovery of the stiffness when tested after environmental conditioning, with respect to the unloading stiffness measured upon pre-cracking;

A recovery of the load bearing capacity has been also observed, but only for selected exposure conditions (e.g. water immersion, winter climate chamber) and/or prolonged exposure times (e.g. specimens immersed in water after three to six months or summer climate chamber after four weeks); recovery of load bearing capacity is evaluated by comparing the maximum load in the post-conditioning 3pb test with reference to the load attained in correspondence of the unloading during the pre-cracking 3pb test.

Data were analyzed in order to define and calculate self-healing indices as detailed hereafter:

4.2.4.1. Index of Damage Recovery as per 3pb tests

Based on the unloading/reloading cycles performed both during the pre-cracking and post-conditioning on 3 point bending test (Figure 4.4) an Index of Damage Recovery (Equation 4.3):

$$\text{IDR}(3\text{pb}) = \frac{K_{\text{reloading,post-conditioning}} - K_{\text{unloadingpre-crack}}}{K_{\text{loading, virgin specimen}} - K_{\text{unloadingpre-crack}}} \quad 4.3$$

The IDR can be defined as the ratio of the stiffness difference between the post-conditioning stage in front of the pre-cracking stage. In detail, the difference between the stiffness on the first loading stage (post-conditioning - $K_{\text{reloading,post-conditioning}}$) and the stiffness on the last unloading stage - obtained before treatment (pre-cracking stage - $K_{\text{unloading, pre-crack}}$) compared to the stiffness of the initial loading of the specimen (linear stage - $K_{\text{loading, virgin specimen}}$) (Figure 4.4).

Figure 4.5(a-c) show the trend of the Index of Damage Recovery, computed as above, vs. the exposure time for different exposure conditions. The following remarks hold:

- Specimens immersed in water (diamonds in Figure 4.5, a) and made with concrete containing the crystalline additive exhibited an almost immediate and quite significant recovery, which even upon prolonged exposure, e.g. after six and up to twelve months, showed continuing improvement of the recovered performance; on the other

hand specimens made with plain concrete and immersed in water (squares Figure 4.5,a) showed a more gradual recovery, which anyway, even after six months, barely attained half the level achieved by concrete with the crystalline additive. This does not match with the constant trend, after initial steep recovery, detected through UPV tests for specimens immersed in water, both with and without the crystalline additive. The influence of a bulk delayed hydration which can hinder the healing concentrated in the main crack could be called as an explanation.

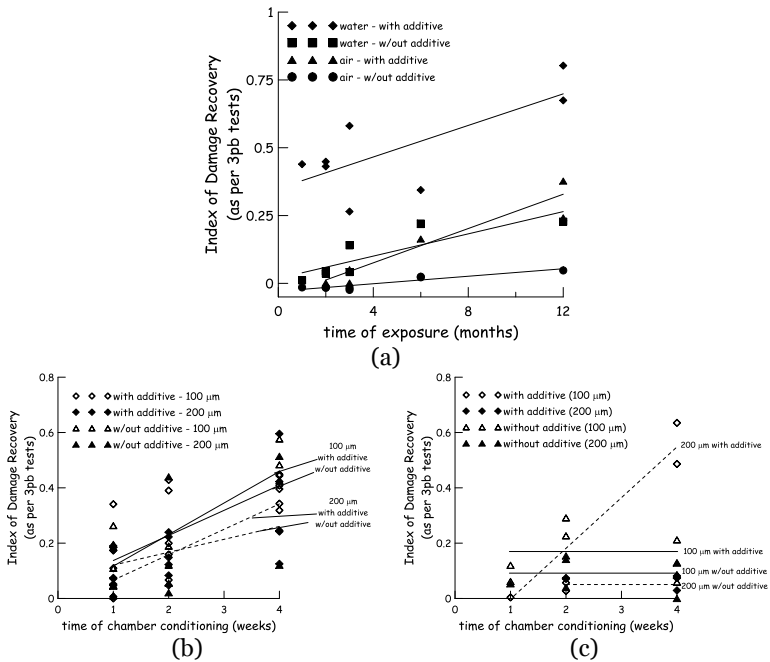


Figure 4.5. Index of Damage Recovery (as evaluated from 3pb test results) vs. exposure time for water immersion/air exposure (a); summer (b) and winter (c) chamber conditioning.

- Specimens exposed to open air and made with concrete containing the crystalline additive (triangles in Figure 4.5,a) showed a gradual recovery capacity, as high as the one exhibited by plain concrete specimens immersed in water; on the contrary a scant recovery

capacity at all was exhibited by specimens without the additive (maximum 5% after twelve months – circles in Figure 4.5a);

- Climate chamber conditioning, representative of both summer (Figure 4.5,b) and winter (Figure 4.5,c) climates, induced, in most cases gradual recovery of stiffness; the catalyst role of the crystalline additive in promoting self-healing reactions is confirmed.

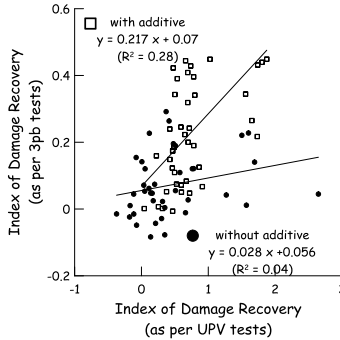


Figure 4.6. Comparison between Indices of Damage Recovery evaluated per UPV and 3pb test results.

Interestingly, the Indices of Damage Recovery as evaluated per both UPV and 3pb tests have been compared in Figure 4.6 (results refer only to cracked specimens). The results are quite scattered, and a higher scatter is detected for specimens without crystalline admixture. Despite that, it clearly appears that:

- Recovery of flexural stiffness is always lower than the recovery of “bulk” stiffness as evaluated through UPV tests. It can be in fact reasonably understood that whereas the stiffness measured through 3pb tests, mainly on pre-cracked specimens, is strictly dependent on the stiffness of the likely healed crack, the measure which can be garnered through UPV tests is also sensitive to the conditions of the whole volume of material between the emitter and receiver units and may also be affected by some healing of surface micro-cracks induced by plastic shrinkage and by some bulk continuing hydration;
- For the same level of damage recovery as measured per UPV tests, specimens containing the crystalline additive show a higher recovery of mechanical stiffness, quantified through the Index of Damage Recovery as per 3pb test results. This could reliably be

attributed to the crystalline additive, which promotes self-healing reactions and triggers the formation of crystalline compounds which, in addition to products of delayed cement hydration, which are likely to be formed in all the investigated mixes, contribute to additional strengthening of the healed cracks.

4.2.4.2. Damage evolution laws

As shown by the example nominal stress σ_N vs. COD curve in Figure 4.4, all along the 3pb test loading path, both in the pre-cracking and post-conditioning stages, a series of unloading-reloading steps were performed. This allowed secant unloading stiffnesses, $K_{unl,j}$, to be evaluated in correspondence of different values of the Crack Opening Displacement, COD_j , through which corresponding damage values could be calculated as:

$$D(COD_j) = 1 - \frac{K_{unl,j}}{K_{loading, virginspecimen}} \quad 4.4$$

With notation once again explained in Figure 4.4.

It was thus possible to build up the evolution laws of the damage variable vs. COD, through an exponential fitting of the data as:

$$D(COD) = \exp [-A/COD] \quad 4.5$$

Where **A** is a fitting constant, correlated to the speed of damage accumulation with progressive crack opening. The higher the **A**, the slower the damage growth.

Damage evolution laws built as above are shown in Figure 4.7, a to n for all the investigated cases. The following statements hold:

- specimens with the additive immersed in water (,a) exhibited the largest effects in terms of “slowering” of the damage evolution law as a function of the exposure time;
- for specimens without the additive immersed in water (Figure 4.7, b) an almost constant trend in the diminution of the damage evolution law has been observed as a result of the healing phenomena due to continued hydration; anyway these effects appear only after two months exposure, unlikely than in the

previous case; as a whole the recovery of the performance is lower than in the case with the additive;

- effects of healing in specimens containing the additive and exposed to air (Figure 4.7,c) are initially slow, as witnessed by the closeness of the damage curves for conditioned specimens to that calibrated on the virgin ones; Only after six months exposure a not negligible recovery appears, which anyway does not seem to proceed further upon prolonged exposure;
- Specimens not containing the additive and exposed to air (Figure 4.7 d) show the slowest recovery all along the investigated exposure period, which can only be appreciated after one year exposure;
- Specimens exposed to environmental summer climate chamber conditioning (Figure 4.7,e-h) show a gradual recovery of performance both in the case with (Figure 4.7 ,e,g) and without the additive (Figure 4.7 f,h); recovery is faster, as expectable, in the former case and also in the case of specimens with larger crack opening (Figure 4.7 g,h), because of larger crack surfaces exposed to moisture, as also recalled above;
- Specimens exposed to environmental winter climate chamber conditioning (Figure 4.7, i-n) show the same trend as for summer cycles, with damage evolution laws, in the case of specimens with the additive, which exhibit a faster “slowing” than if not containing it.

4.2.4.3. Estimation of crack closure from damage evolution laws

From the damage vs. COD evolution laws an estimation of the crack closure likely due to the self-healing phenomena could be provided, as graphically explained in Figure 4.8. The proposed methodology consists first of all in identifying the points representative of damage-COD, as evaluated upon reloading the specimen after environmental conditioning, assuming the initial crack opening coincided with the value measured at unloading during the pre-cracking stage. The points, identified as above, are then “shifted backward” along the COD axis until the fitted damage-COD evolution curve of the virgin specimen is met: the amount of this backward shifting can be assumed as an indicator of the crack closure effect produced by the self-healing phenomena.

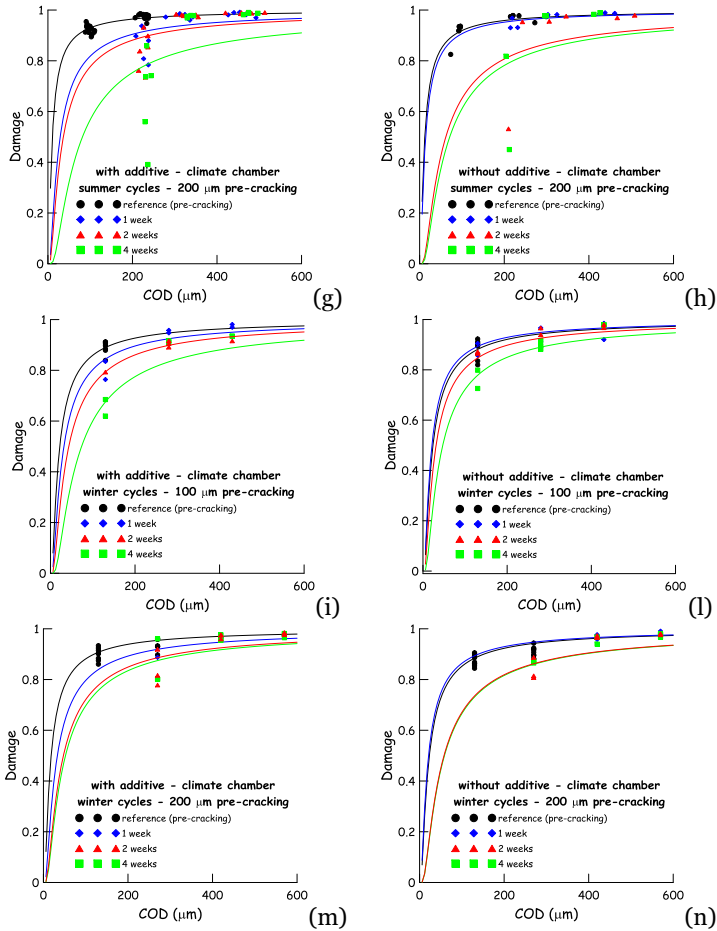


Figure 4.7. Fitted damage evolution laws for pre-cracked concrete specimens with (a,c,e,g,i,m) and without (b,d,f,h,l,n) crystalline additive and different exposure conditions: water immersion (a,b); air exposure (c,d); climate chamber conditioning in summer climate (e,h) for specimens pre-cracked at $100 \mu\text{m}$ (e,f) and $200 \mu\text{m}$ (g,h); climate chamber conditioning in winter climate (i-n) for specimens pre-cracked at $100 \mu\text{m}$ (i,l) and $200 \mu\text{m}$ (m,n).

An index of crack healing could hence be defined as follows:

$$ICH_{\text{damage evolution}} = \frac{COD_{\text{pre-cracking}} - COD_{\text{post-conditioning}}}{COD_{\text{pre-cracking}}} \quad 4.6$$

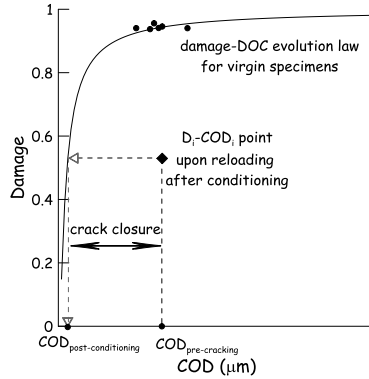


Figure 4.8. Graphical explanation of the procedure to estimate crack closure from damage evolution laws built as in Figure 4.7 (a-n).

The plots of the ICH calculated as above are shown in Figure 4.9 a-c. The following statements hold:

- A remarkable crack closure is estimated to occur, since from the beginning of the surveyed exposure times, for specimens containing the crystalline additive and immersed in water; the same specimens, when exposed to air, show a slower recovery capacity, which starts being evident after longer exposure, from there onward remaining almost constant;
- Immersion in water triggers the self-healing also for specimens without any additive, but at a much slower pace: only after 2 to 3 months effects start being visible and after 6 months a performance comparable to specimens with the additive was achieved; specimens without any additive exposed to air hardly show any recovery and only after prolonged exposure a moderate crack closure starts appearing;
- Pictures obtained by stereo-microscope in Figure 4.10 confirm the aforementioned statements;

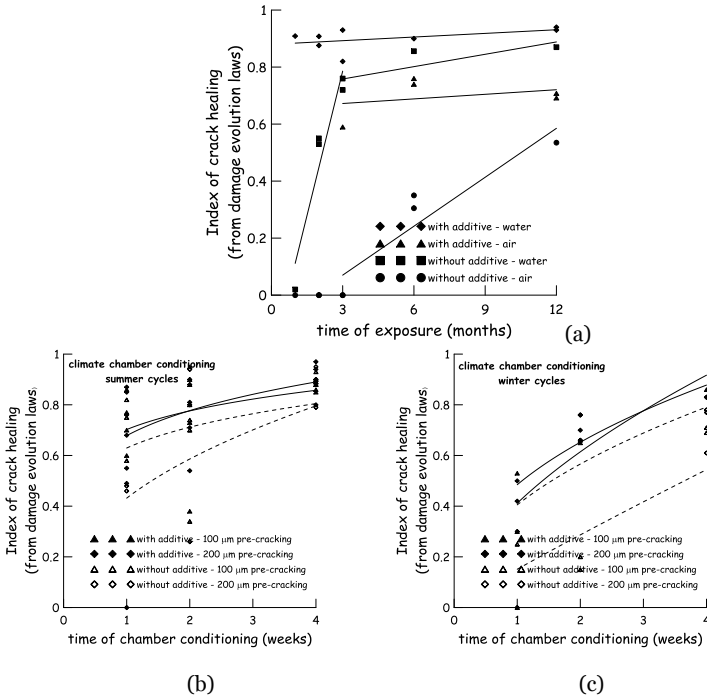


Figure 4.9. Index of Crack Healing (as evaluated from damage evolution laws) vs. exposure time for water immersion/air exposure (a); summer (b) and winter (c) chamber conditioning.

- In the case of climate chamber conditioning, for both the summer and winter cases, specimens with the additive show a faster recovery, almost independent of the pre-crack opening: this may be explained considering that, even if a large crack has to be healed, a larger crack surface is exposed to environment moisture and larger “clusters” of additive crystals are potentially active. In the case of specimens without the additive the estimated crack closure is evidently lower than in the previous case and, furthermore, a stronger influence of the pre-cracking damage appears, specimens with larger crack openings performing worse. The effect of unhydrated cement particles alone is not sufficient to cope with the larger crack to be healed (see Figure 4.10, a-d).

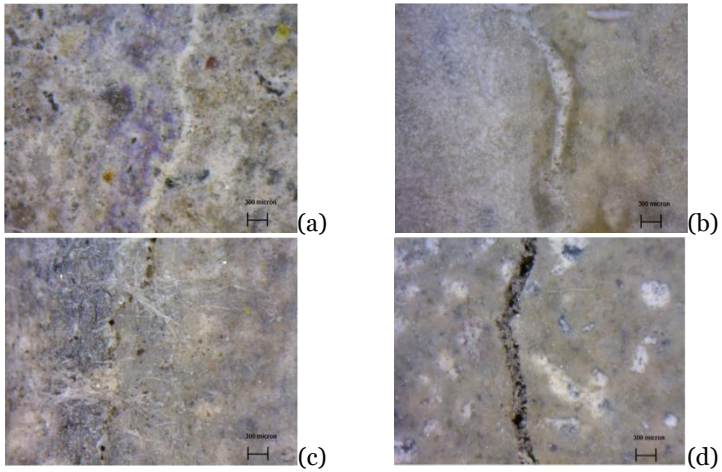


Figure 4.10. Healed cracks for specimens with (a) and without (b) crystalline additive after six months of immersion in water; specimens with (c) and without (d) crystalline additive after six months of exposure to open air.

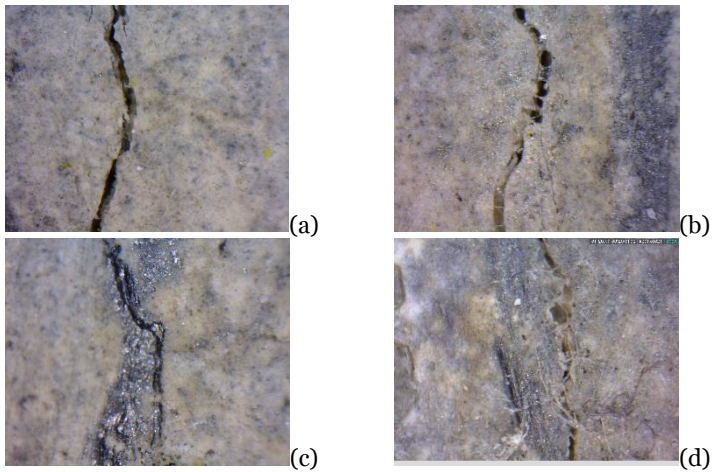


Figure 4.11. Healing cracks for specimens with crystalline additive before exposure (a, c) and after two (b) or four weeks (d) in climate chamber (summer cycles).

4.2.4.4. Index of load recovery

From the values of nominal flexural strengths/stresses as denoted in Figure 4.4 an Index of Load Recovery, as from 3pb test results, can be defined as:

$$ILR = \frac{\sigma_{N,max \text{ reloading, post-conditioning}} - \sigma_{unloading \text{ pre-crack}}}{f_{cf} - \sigma_{unloading \text{ pre-crack}}} \quad 4.7$$

Figure 4.12 a-c show the trend of the ILR, and the Figure 4.12 d-e shows the trend of un-cracked specimens due to the same conditioning and is computed as above, versus the exposure time.

- The observed recovery of load bearing capacity, with respect to the loss of load bearing capacity (softening) experienced upon cracking, as also affected by presence/absence of crystalline additive and different exposure conditions, is absolutely coherent with observed trends of recovery of other mechanical properties, measured and identified from stress-crack opening flexural response and in front of un-cracked specimens, as commented in the previous sections.

In detail:

- On one hand, with reference to natural exposure conditions (Figure 4.12a), i.e. immersion in water and exposure to open air, the same trends as previously discussed with reference to the index of damage recovery are confirmed; as a matter of fact, whereas an almost complete recovery of stiffness could be observed in the most favorable examined cases (specimens with the additive immersed in water), the recovery of load bearing capacity is much lower, slightly exceeding 20% only in the aforementioned most favorable situation and un-cracked specimens showed a stabled strength in time of exposure;
- On the other hand, with reference to climate chamber conditioning, results appear much more dispersed: it is evident that a lower recovery is achieved, with respect to water immersion, of the load bearing capacity for both winter and summer climates. Influence of temperature cycles on the strength development of self-healing reaction products could be also called to explain the highlighted results. Anyway, from a quantitative point of view, also in the case of accelerated climate chamber conditioning, recovery of load bearing capacity is always limited to about 20% of the one lost in the softening which accompanies the crack propagation stage.

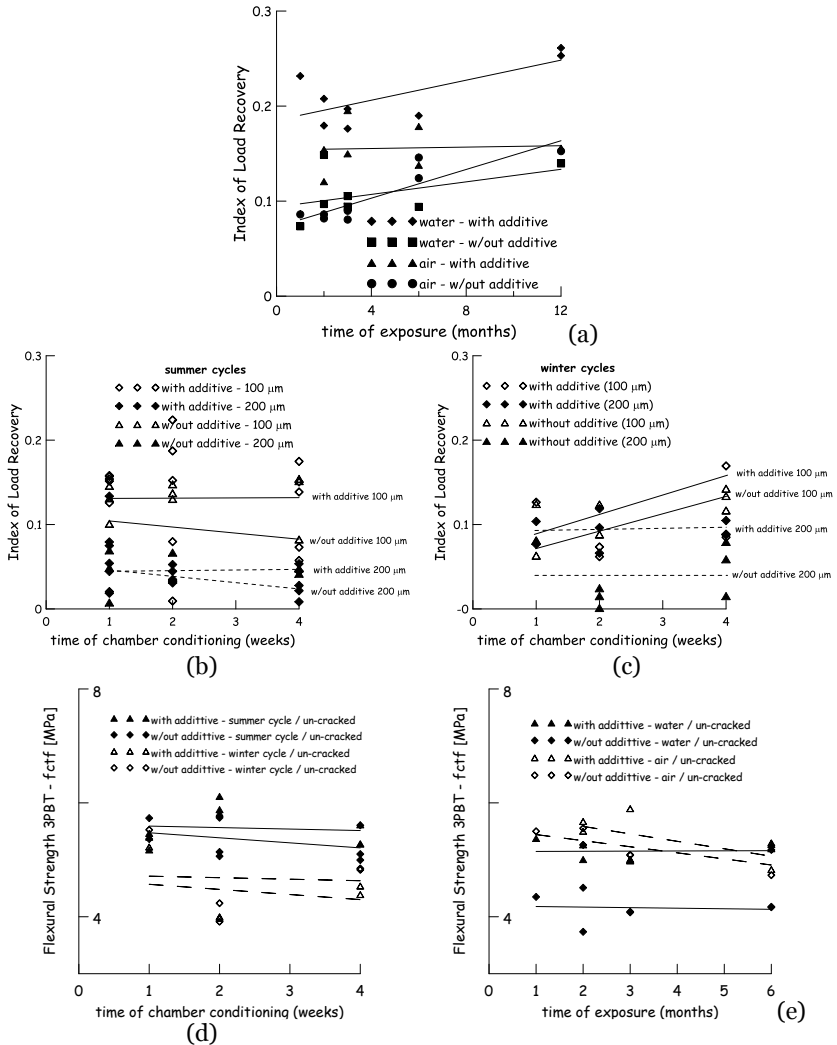


Figure 4.12 Index of Load Recovery (as evaluated from 3pb test results) vs. exposure time for water immersion/air exposure (a); summer (b) and winter (c) chamber conditioning; un-cracked specimens on (d) summer and winter cycles and (e) water immersion/air exposure.

4.2.4.5. Estimation of crack closure from load - COD curves

From the nominal bending stress σ_N vs. COD evolution laws, an estimation of the crack closure due to the self-healing can be provided, as graphically explained in Figure 4.13. The proposed methodology consists in operating a “backward” shifting along the COD axis, of the stress-COD curve representative of the behavior of each pre-cracked specimen after environment conditioning, until the stress-COD curve of the same specimen, as measured during the pre-cracking test on the virgin undamaged sample is met. The new value of the “origin” COD can be estimated by drawing, from the aforementioned point on the curve of the virgin sample, an unloading branch with a slope equal to that of the closest unloading previously measured on the virgin sample itself. This allows to quantify an indicator of the crack closure effect produced by the self-healing phenomena and an index of crack healing to be defined as:

$$ICH_{\text{stress-crackopening}} = \frac{\text{COD}_{\text{pre-cracking}} - \text{COD}_{\text{post-conditioning}}}{\text{COD}_{\text{pre-cracking}}} \quad 4.8$$

The plots of the ICH calculated as above are shown in Figure 4.14 a-c. Though evaluated by means of a different method and from different mechanical properties, and provided quantitatively lower than those shown in Figure 4.9, the estimated amounts of crack closures do exhibit coherent trends with previously shown elaborated results. This further confirm the influence of different investigated exposure conditions and of the addition of crystalline additives into the concrete mix on the effectiveness of self-healing capacity of the material.

4.2.4.6. Comparison between different “healing” indices

The comparison between different healing indices, calculated from 3-point bending tests, allows an insightful synopsis to be provided about the investigated phenomena as well as a preliminary methodological quantification to be attempted of the effects of the crack healing on the ability of the material to recover some of its distinctive mechanical properties:

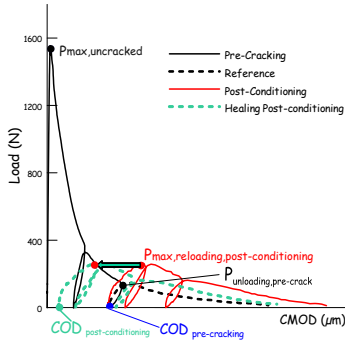


Figure 4.13. Graphical explanation of the procedure to estimate crack closure from stress vs- Crack Opening Displacement curves.

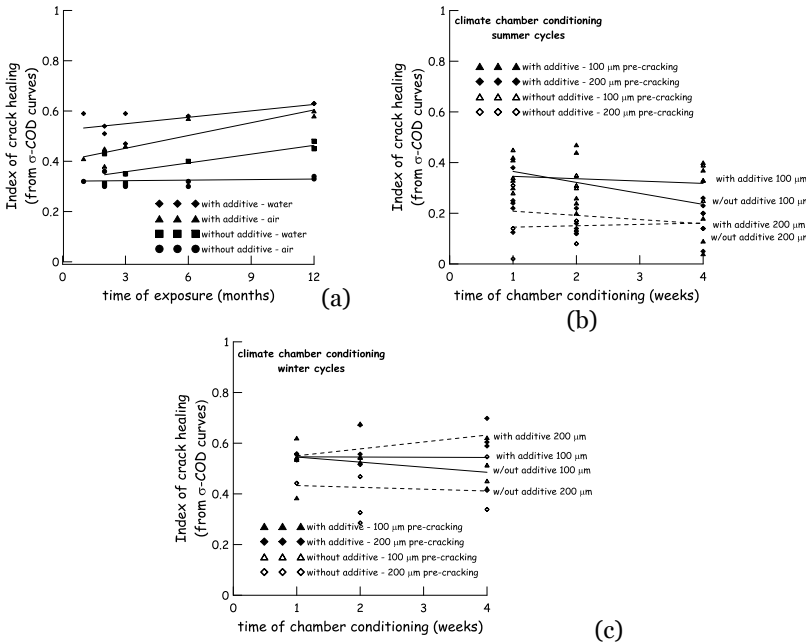


Figure 4.14. Index of Crack Healing (as evaluated from σ -COD curves) vs. exposure time for water immersion/air exposure (a); summer (b) and winter (c) chamber conditioning.

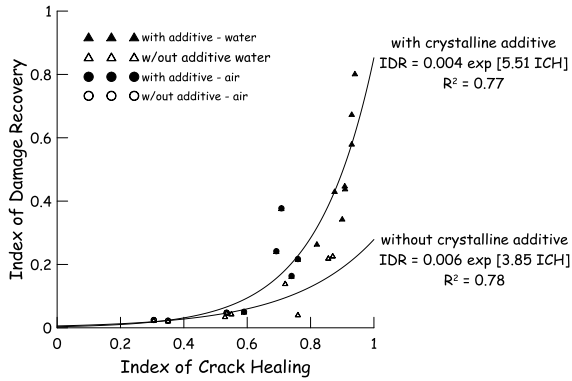


Figure 4.15. Index of Damage Recovery as evaluated from 3pb (left) vs. Index of Crack Healing as estimated from fitted damage evolution laws as in Figure 4.8.

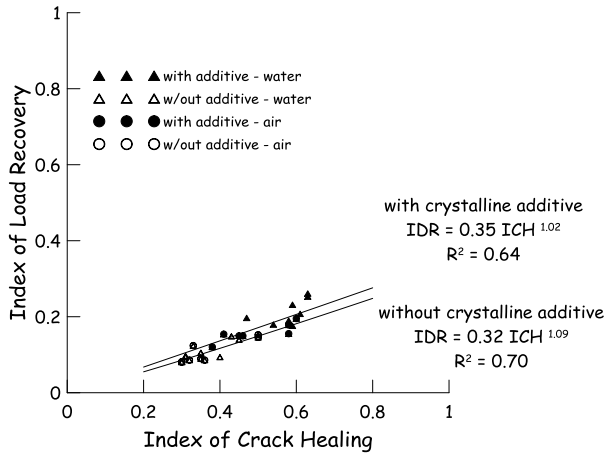


Figure 4.16. Index of Load Recovery vs. Index of Crack Healing as evaluated from stress vs. COD curves obtained from 3pb tests.

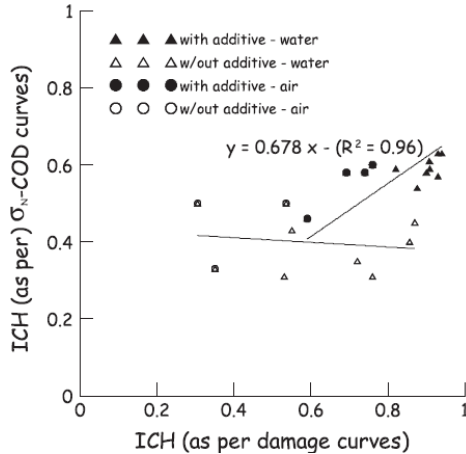


Figure 4.17 Index of crack healing evaluated from stress - COD curves vs. damage curves.

- The trend of damage recovery vs. crack healing, estimated from damage evolution laws (Figure 4.15) is coherent with the damage evolution model assumptions; it significantly appears that a remarkable crack healing is needed in order to start garnering a recovery of the specimen stiffness; effects of crystalline additive in the concrete mix is also evident, from the higher levels of recovery of stiffness for equal healing of the cracks;
- The plot of damage recovery estimated from UPV test results (Figure 4.15, right) vs. the same index of crack healing as above, estimated from 3pb test data processing, shows a more dispersed trend, also casting some doubt about the reliability of an UPV test based technique to assess the crack healing and its effects;
- Load recovery versus estimated crack healing (Figure 4.16) shows that some load bearing capacity appears to be recovered since for very low values of estimated crack healing. The modelled trend is anyway slower than what has been detected with reference to stiffness and hardly more than 20% of the stress decay experienced upon cracking could be garnered because of the crack healing
- A correlation (Figure 4.17) between both load recovery index based on 3 point bending test (Figure 4.4) and the same index calculated from the damage law (Figure 4.8) shows a better coherence in their trends for the concrete without additive than with the one with. A dedicated analysis of the strength development of self-healing

products, as also affected by exposure times and conditions, could be instrumental to a better understanding of the detected trends, which has been anyway regarded as out of the scope of this work.

4.2.5. SEM analyses

Observation on fracture surfaces of selected specimens were finally performed by using an environmental scanning electron microscopy ZeissEvo 50P equipped with oxford Inca Energy 200EDS having a ultra-thin window detector from 133 eV.

The same SEM analyses that were carried out on the crystalline admixture (Figure 3.4) added to the mixtures studied, has been performed even on fragments collected from crack surfaces of concrete specimens after conditioning exposure and testing to failure.

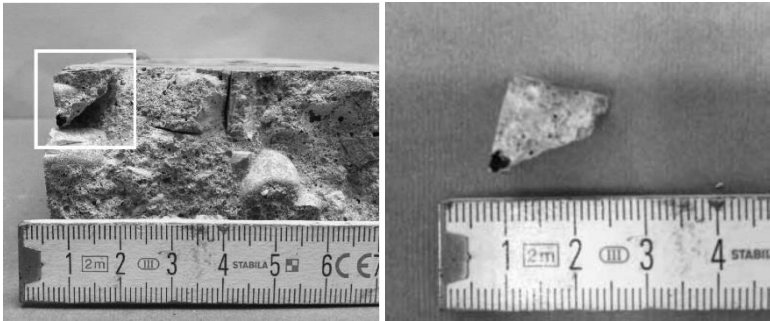


Figure 4.18. Sample of concrete with crystallite additive and immersed in water for 3 months.

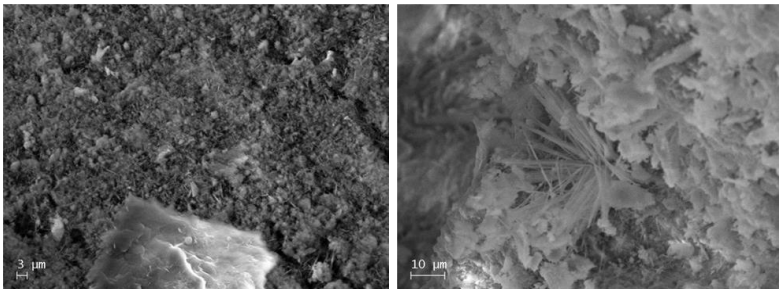


Figure 4.19. Different SEM images of crack surface from the sample on Figure 4.18

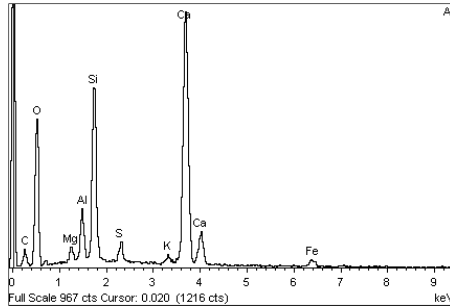


Figure 4.20. EDS analysis of products shown in Figure 4.19.

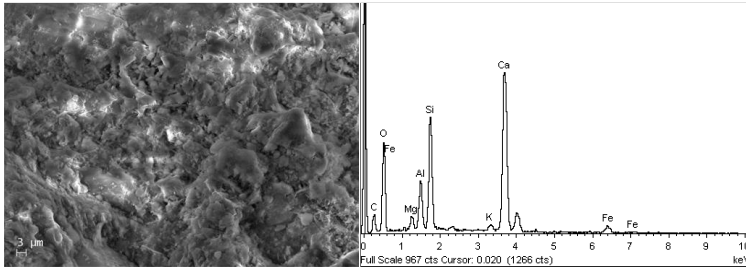


Figure 4.21. SEM image a) and EDS analysis b) of sample of Figure 4.18 along the surface orthogonal to the crack.

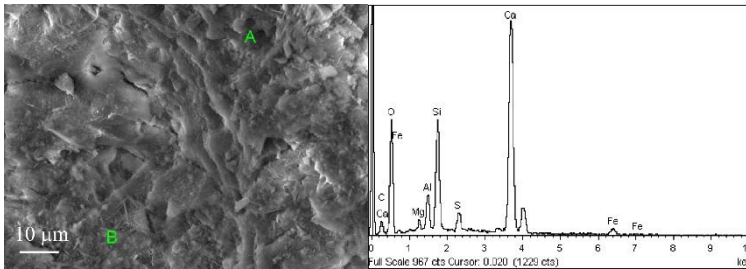


Figure 4.22. SEM image a) of sample of Figure 4.18 in correspondence of the area between the crack surface (denoted as B) and the one orthogonal to it (denoted as A); EDS analysis of zone

Figure 4.18 shows a sample collected from a concrete specimen, casted with crystalline admixture, after 3 months of immersion in water. Before the conditioning period in water the beam specimen was pre-cracked to a crack opening of 200 μm . The SEM observations were carried out at the end of conditioning period on the pre-crack surface and on a fresh fracture surface.

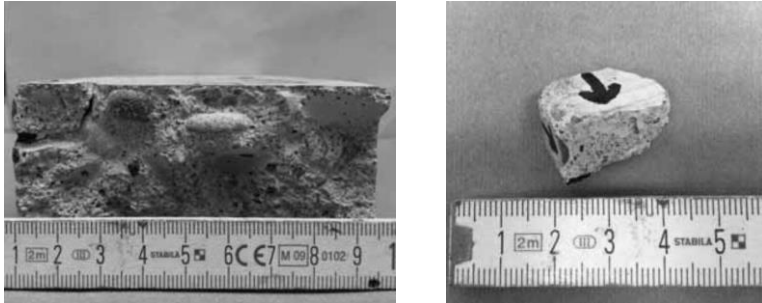


Figure 4.23 Sample of concrete cast without crystalline additive and immersed in water for 3 months. Detail of the sample a) along the crack surface b).

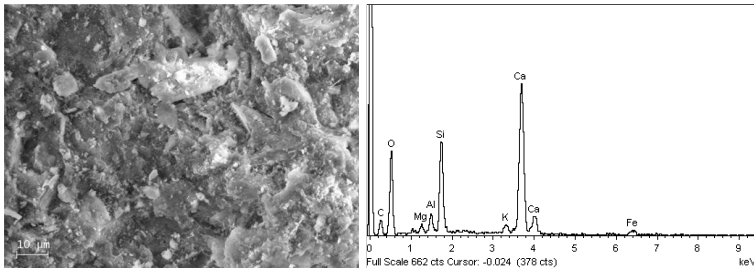


Figure 4.24. SEM image a) and EDS analysis b) of sample of Figure 4.23 along the crack surface

The cement matrix of the crack surface (dark gray zone in Figure 4.19, left) is covered with very fine fibrous products, as can be also seen in a different observed zone of the same crack surface (Figure 4.19, right). The morphology of these products is compatible with the crystalline structure of typical self-healing products; several authors have documented similar fibrous products [49] which were identified as very common microstructures found in self-healed samples. EDS analysis (Figure 4.20) of the products in Figure 4.19 shows mainly the typical elements of hydration products of

cement (calcium, oxygen and silicon in major amounts, in addition to magnesium, aluminium and potassium); a high peak of sulphur is also present.

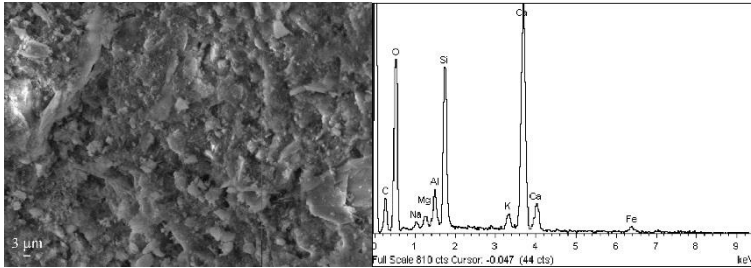


Figure 4.25. SEM image a) and EDS analysis b) of sample along the crack surface in a zone different from that observed in Figure 4.24.

The EDS analysis of the surface shows different fibrous products in spite of the different morphology of cement paste, the reaction products on crack surface are the result of the growth of same type of fibrous products within the crack. This observation is also in agreement with the macroscopic images of Figure 4.10, b which show the filling of the crack after the self-healing process. The growth of the fibrous products cannot be attributed to the carbonation reaction because of the saturated conditions of slab samples; in fact, diffusion of carbon dioxide is negligible through concrete pores filled with water.

Conversely the reaction products should be attributed to hydration reactions involving the crystalline admixture, which were promoted by the water saturated conditions. These reaction products were not present in the bulk of the concrete which was observed on a fresh fracture surface of the same sample. At the same magnification, it can be observed that the surface orthogonal to the crack (Figure 4.21a) shows a different morphology; furthermore, the corresponding EDS analysis (Figure 4.21b) differs from that of crack surface (Figure 4.20) because of the absence of the peak of sulphur.

The same sample has been observed in correspondence of the area (Figure 4.23a) between the crack surface (indicated with the letter B) and the one orthogonal to it (indicated with the letter A); the difference between the area A and B is not morphologically visible but the EDS analysis (Figure 4.21b), having made on both zones, confirms the presence of sulphur.

Figure 4.24 - show the SEM observations made on a sample collected from a specimen made of concrete without the crystallite additive, after 3 months of immersion in water.

Figure 4.24a-Figure 4.25a show different zones of the crack surface; it can be observed that the morphology of hydration products is similar to that typical of an ordinary concrete and to the one shown in Figure 4.21a (i.e., on the bulk concrete, where the reaction products of the crystalline admixture were not detected). Also EDS analysis carried out on the zone highlighted in Figure 4.24a-Figure 4.25a, confirms the absence of the sulphur peak (Figure 4.24b-4.22b).

4.3. Conclusions about Conventional Concrete

From the analyzed results, the following concluding remarks can be drawn:

- under water immersion even a normal strength concrete inherently possesses some autogenic self-healing capacity, as witnessed by visual observation (cracks were effectively closed) as well as by the measured recovery of UPV and dynamic stiffness, which, after about 3 months exposure, was able to get back to the pristine levels of a virgin undamaged material; the presence of crystalline additive in this case was effective in accelerating this recovery but had no effect on its final entity; -on the other hand, for air exposure, even if in quite humid climates, the presence of crystalline additives in the mix design was effective in engineering the self-healing and the recovery of dynamic Young modulus, as measured through UPV tests, which proceeded quite slower than in the case of water immersed specimens, though almost attaining, in the end, i.e. after one year exposure, the levels of virgin undamaged material. In the absence of any self-healing engineering catalyst, air exposure was not enough to induce any recovery neither of material continuity nor of its mechanical behavior;
- the same trends detected for UPV have been measured also for mechanical stiffness and load bearing capacity, as evaluated through three-point bending tests; the ratio of recovery of specimen bending stiffness was always quite lower than that quantified through UPV tests, most likely because of the nature of self-healing products, which may result in a weaker and softer behavior than that of a bulk hardened cement paste;

- similarly, recovery of load bearing capacity was always limited to maximum 20% of the flexural tensile strength of the virgin undamaged material;
- accelerated exposure conditions, under constant high relative humidity and cycling temperature, may be able to yield results comparable to those obtained under likely favorable natural exposure conditions; caution has to be anyway exerted in carefully checking artifacts which may be induced by accelerated temperature cycling, which could counteract and hinder positive effects due to healing phenomena;
- a methodology has been proposed to estimate the ratio of crack closure from damage evolution curves, as built from quantification of index of stiffness/damage recovery, quantified from three point bending stress results; a similar procedure was proposed also through the quantification of an index of load recovery, still calculated from the results of three point bending tests;
- evolution trends and correlation of the aforementioned stiffness and load recovery vs. crack healing indices showed, despite some scattering, showed that a crack closure above 70-80%, is necessary in order to start having an appreciable recovery of stiffness (i.e. larger than 20%); similarly it did occur for load recovery;
- SEM observations and EDS analyses confirmed the presence of reaction products on the cracked (and thus healed) surfaces. These products were clearly due to the delayed hydration reactions involving the crystalline admixture;

4.4. High Performance Fiber Reinforced Cementitious Composites (HPFRCCs)

4.4.1. Introduction

As described in previous chapters, the same experimental and analysis methodology as for normal strength concrete, has been applied also to investigate the self-healing capacity of HPFRCCs with suitable differences, as it will be furthermore explained, due to the peculiar behavior of these materials. The purpose of this part of the investigation has mainly been the validation of the proposed interpretation methodology of self-healing tests with reference to HPFRCCs.

The coherence of the data, and the related information, has to be evaluated in the framework of the reliability of the methodology (rather than with reference to single “numerical” values which in some cases can be affected by experimental scattering) with reference to the influence of the governing parameters such as crack opening and exposure conditions.

The experimental results processed as above will be first of all qualitatively analyzed to capture, if any, the trends of the healing on the mechanical performance of the material. In a further step, by comparing for each and all the specimens, the curves in the pre-cracking and in the post-conditioning regime for the same specimen, suitable indices will be defined to quantify the effects of healing on the recovery of the load bearing capacity, ductility, stiffness and damage accumulation.

A methodology will be finally proposed to estimate the amount of crack closure, to which the values of the aforementioned healing indices will also be correlated.

4.4.2. Four point bending test (4pbt)

4.4.2.1. Introduction

In this section, the results of the four point bending test, performed according to the methodology discussed in Chapter 3, will be analyzed. By comparing nominal bending stress σ_N vs. crack opening displacement COD curves – referring to the same specimen in the pre-cracking and in the post – conditioning stages – the effect of self-healing will be evaluated on the recovery of different mechanical properties which can be inferred from the same curves (load bearing capacity, ductility, stiffness and damage cumulating).

In the following, the case of the deflection softening behavior will be separately analyzed from the hardening, starting from the former, for the sake of closer affinity with the case of conventional plain concrete analyzed before.

4.4.2.2. Deflection softening specimens

In Figure 4.26 a to h, the nominal stress σ_N vs. Crack Opening Displacement COD curves are shown for the different investigated cases, i.e. for specimens pre-cracked at 1 to 2 month age and subjected to different exposure conditions (up to six months) and specimens pre-cracked at 11 months age and immersed in water up to six months.

It is worth here remarking that all the specimens undergoing the same exposure conditioning were obtained from the same slab (Figure 3.19) which also “reference” specimens were obtained which were tested monotonically to failure before the conditioning period started.

In general it can be observed that, in most cases specimens, when tested after conditioning exhibited a recovery of the load bearing capacity, with respect to the residual strength that each of them exhibited when unloaded upon pre-cracking.

As matter of fact un-cracked specimens which underwent the same curing and then conditioning as the pre-cracking and then conditioning as the pre-cracking ones did not show any significant difference neither as a function of the exposure nor as a function of the elapsed time.

The effects of age of pre-cracking and immersion time on the entity of this residual strength recovery capacity can also be appreciated. Whereas specimens pre - cracked at 9 or 11 months (Figure 4.26,a) obviously exhibited a far lower self-healing capacity than those pre-cracked at 2 months (Figure 4.26,b), prolonged exposure time was anyway, even for older specimens, instrumental at achieving a significant healing (Figure 4.26c) of the quite large crack (0.5 mm). This is clearly witnessed by the new “cracking peak” detected in post-immersion tests, followed by steep softening and then by a more gradual release of the stress, which can be evidently attributed to a quite strong re-establishment of “mechanical connections” between the two faces of the crack, due to the delayed hydration of anhydrous binder particles and the consequent formation of new hydration products which are likely to feature a high compatibility with the old material.

Analysis and Discussion of Experimental Results

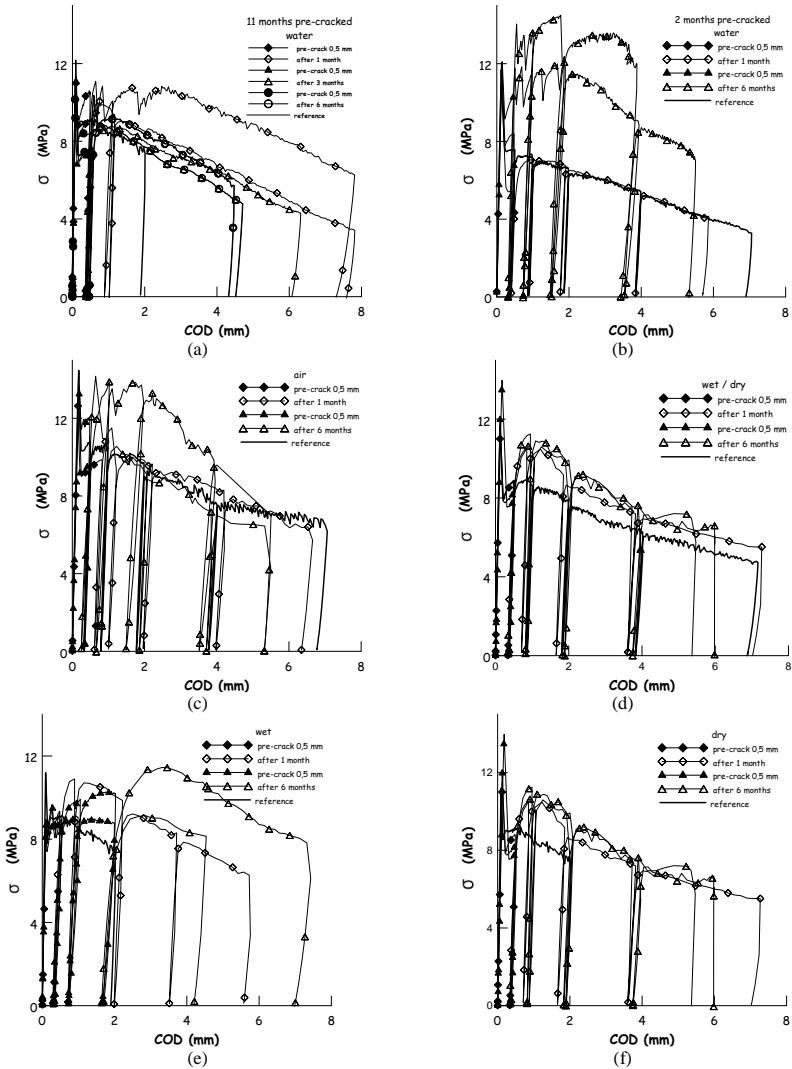


Figure 4.26. σ_N vs. COD curves for deflection softening specimens for different exposure conditions and pre-cracked up to 0.5 mm: water immersion for different pre-crack ages (a) 11 months, (b) 2 months ; (c) air/external exposure; (d) wet/dry (water immersion and 50%RH with 20°C); (e) wet (high humidity with 90%RH and 20°C and (f) dry (50%RH with 20°C).

4.4.2.3. Index of stress Recovery

As a matter of fact the “stress gain” due to self-healing was evaluated by comparing the difference between the post-treatment peak strength f_{peak} , after-conditioning and the unloading stress $\sigma_{N,unloading}$, dimensionless to the difference between first cracking strength $f_{peak, pre-crack}$ and the same unloading stress (Equation 4.9, Figure 4.27).

$$\text{Index of stress recovery ISR} = \frac{f_{peak,after-conditioning} - \sigma_{N,unloading}}{f_{t,pre-cracking} - \sigma_{N,unloading}} \quad 4.9$$

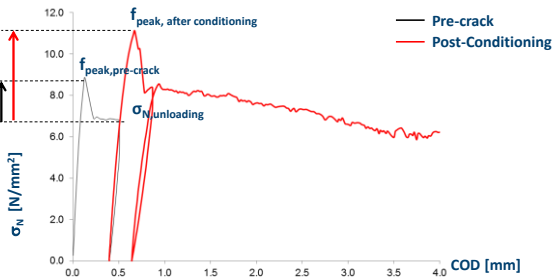


Figure 4.27. Schematic presentation for the Index of stress recovery for the deflection softening behavior (Equation 4.9)

The computed values and related trends of the ISR have been plotted in Figure 4.28. It can be evidently observed that:

- specimens immersed in water together with those exposed to natural environment (in a quite humid climate, like the Northern Italy one), featured, in average, the highest, and a quite similar actually, recovery trend, gaining, in the post-conditioning stage a strength even higher than the cracking strength of the virgin specimen;
- significantly, specimens pre-cracked at 11 months and immersed in water, even continued to show some moderate healing capacity, at a moderately increasing trend with prolonged immersion;
- specimens conditioned in a wet chamber (90%RH) featured an appreciable healing rate since from earlier immersion times, but which did not show any significant improvement with prolonged exposure time;

- as expectable specimens exposed to a dry environment featured an almost negligible healing, even if somewhat increasing with prolonged exposure time;
- quite poor, and again as coherently expectable, intermediate between the one of specimens in dry environment, was the performance exhibited by the specimens subjected to the wet and dry cycles.
- a visual confirmation, thought optical microscopic shows the healed cracks in the Figure 4.29 and Figure 4.30.

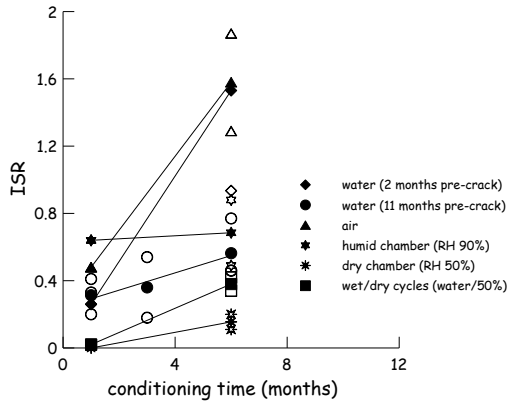
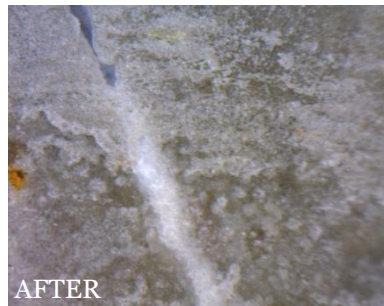


Figure 4.28. Index of Stress Recovery vs. conditioning time for deflection softening specimens (hollow markers refer to values of single tests, solid markers represent average values of nominally identical tests).



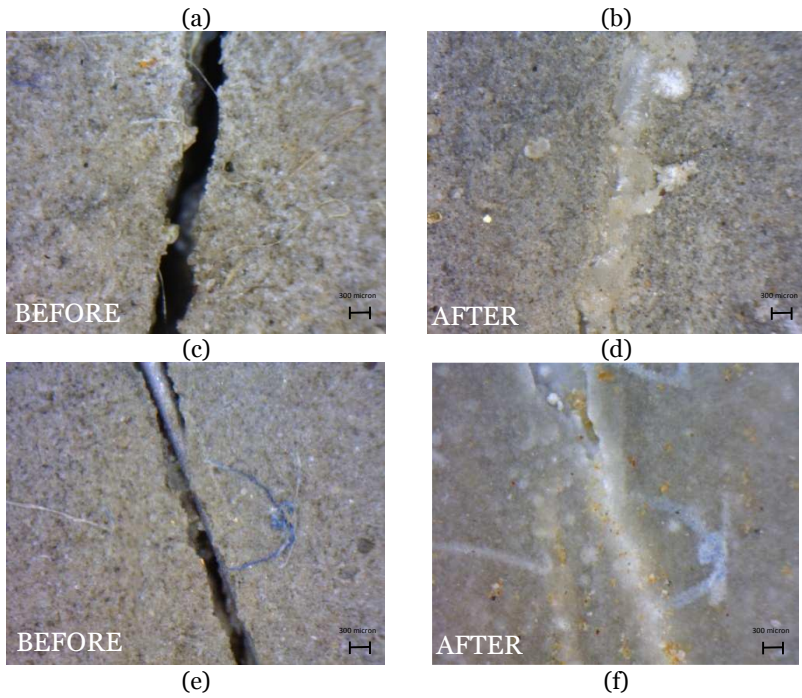


Figure 4.29. Healed cracks for specimens pre-cracked up to $cod_{tot}=0.5$ mm (a,c,e) and immersed in water for (b) 1 month; (d) 3 months and (e) after six months of water immersion.

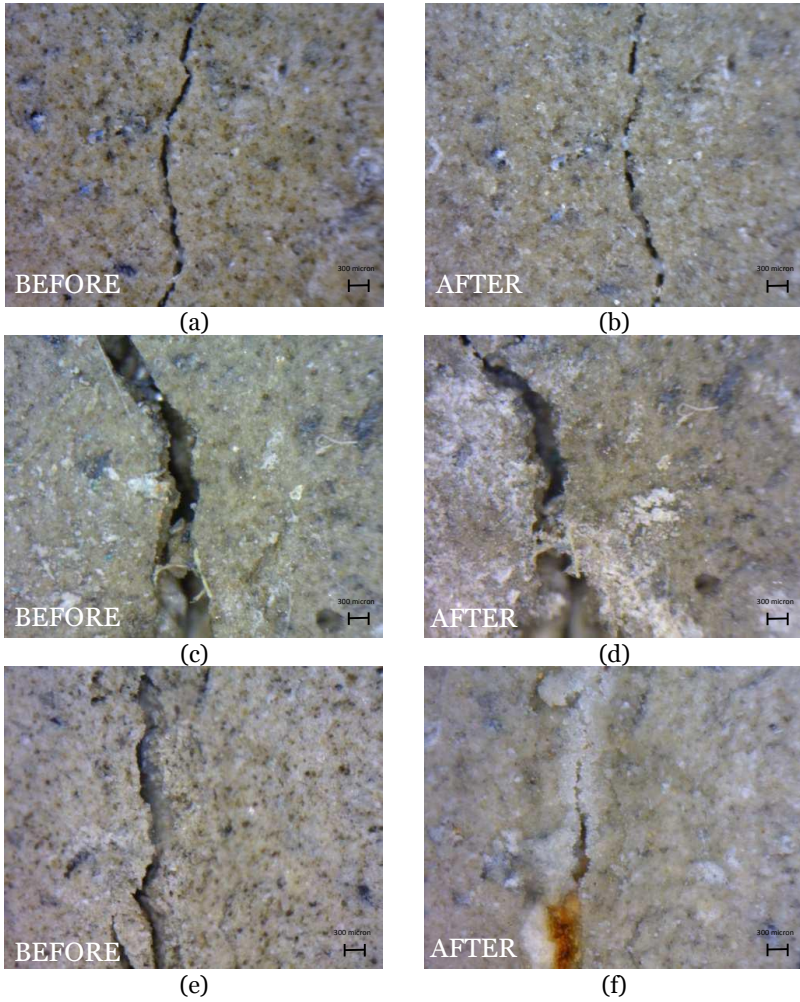


Figure 4.30. Healed cracks for specimens pre-cracked up to $cod_{tot}=0.5$ mm (a,c,e) and conditioned up to 1 month in; (b) natural environment; (d) high humidity and (e) wet/dry cycles.

4.4.2.4. Index of Damage Recovery

Thanks to unloading-reloading cycles performed both during pre-cracking and post-conditioning tests, the values of secant unloading and tangent reloading stiffness, respectively denoted as $K_{unl,j}$ and K_{j} , at different levels “j” of crack opening were evaluated. From them, an index of damage recovery was calculated as (Equation 4.11):

Index of Damage Recovery =IDaR

$$IDaR = \frac{K_{reloading,post\ conditioning} - K_{unloading,pre-cracking}}{K_{loading,pre-cracking}} \quad 4.10$$

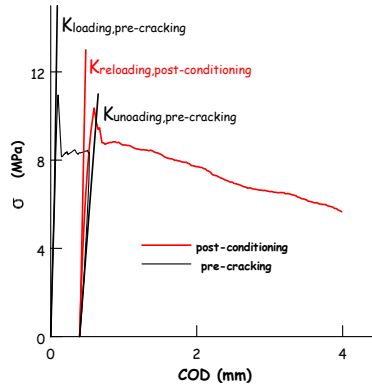


Figure 4.31. Schematic presentation for the used stiffnesses to calculate Index of Damage Recovery (Equation 4.11)

The results have been plotted in the Figure 4.32 appear to be coherent with the previously discussed trends with reference to the Index of Stress Recovery.

A moderate stiffness recovery (Figure 4.32) was always measured with some improvement over time, except for exposure to dry environment or air even if the un-cracked specimen stiffness was never completely got back.

In detail:

- the specimens immersed in water and pre-cracked at 1-2 months, exhibited an almost immediate significant recovery after the first month of exposure, which continued more slowly upon prolonged exposure;

- specimens immersed in water and pre-cracked at 11 months initially did not exhibit any recovery but showed an improving trend upon prolonged exposure similar it did occur for specimens conditioned in wet chamber or through wet and dry cycles;
- specimens exposed to air and to dry chamber show a decrease of the performance over time , most likely because of some drying effect.

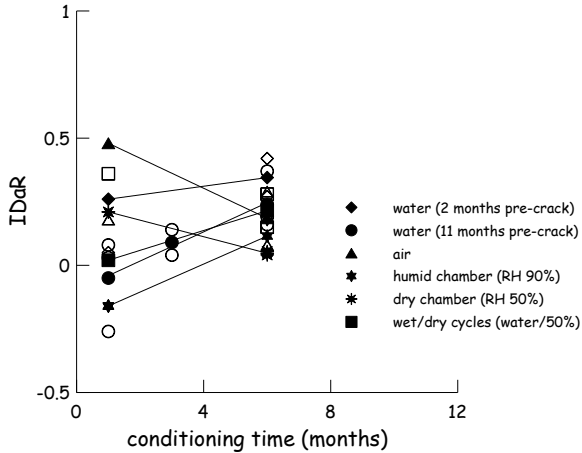


Figure 4.32. Index of Damage Recovery vs. conditioning time for deflection softening specimens (hollow markers refer to values of single tests, solid markers represent average values of nominally identical tests).

4.4.2.5. Index of Crack Healing

The influence of the different exposure conditions on the slowing of damage accumulation is coherent with previously analyzed recovery of strength and stiffness damage evolution laws were built for the different cases as for NSC. From the comparison between the fitted trend of the damage variable evolution in the pre-cracking and in the post-conditioning stages the crack closure due to self-healing could be estimated, as graphically explained in Figure 4.33 and an index of crack healing was defined as:

$$\text{Index of Crack Healing ICH} = 1 - \frac{\text{COD}_{\text{post-conditioning}}}{\text{COD}_{\text{pre-cracking}}}$$

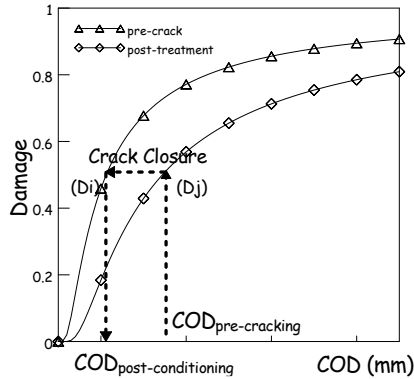


Figure 4.33. Graphical explanation of the procedure to estimate crack closure from damage evolution laws.

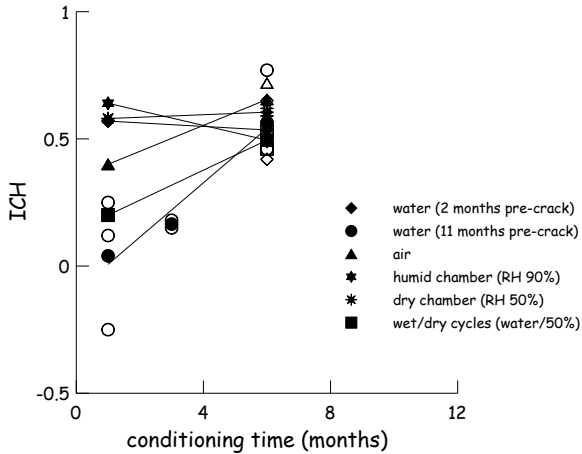


Figure 4.34. Index of Crack Healing vs. conditioning time for deflection softening specimens (hollow markers refer to values of single tests, solid markers represent average values of nominally identical tests).

Results (Figure 4.34) provide a further confirmation to the statements exposed above with reference to other indices. The coherence of the whole set of results garnered so far through the definition of different self-healing indices, may also stand as a proof of the reliability of the proposed methodology for the evaluation of effects of self-healing on the recovery of mechanical performance of HPFRCCs

In detail with reference to the plots of the ICH following the statements hold:

- a remarkable crack closure is estimated to occur, since from the beginning of the surveyed exposure times for specimens immersed in water; holding always for longer exposure;
- the effects of age of pre-cracking and immersion time on the crack closure can also be appreciated; here as specimens pre - cracked at 9 or 11 months obviously exhibited a far lower self-healing capacity than those pre-cracked at 2 months;
- The same occurs for specimens conditioned in wet chamber.
- The trend of crack healing for specimens pre-cracked at 11 months is coherent with what previously said, i.e. initially negligible by progresses over time;
- Specimens conditioned in open air and – to a lower extent – subjected to wet/dry cycles – show some crack healing prospering over time;
- The computed initial high value for ICH could probably be explained by some carbonation occurring upon exposure to air whose concentrated by the opposite effect of drying.

4.4.3. Comparison Indices of Mechanical Properties Recovery and Index of Crack Healing

A comparison between the Index of recovery of mechanic properties and the Index of Crack Healing has been plotted in Figure 4.35 and Figure 4.36.

With reference to Index of the Stress Recovery, despite some unavoidable scattering due to the different ages of the pre-cracking and exposure conditions, a common trend can be clearly captured, coherent with the logical expectations.

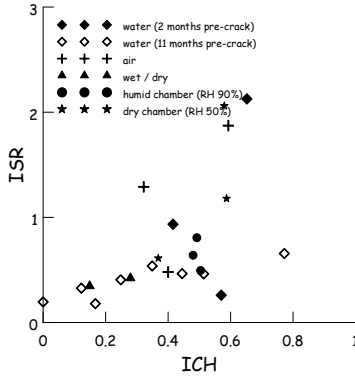


Figure 4.35. Correlation between ISR and ICH for the softening deflection behaviour.

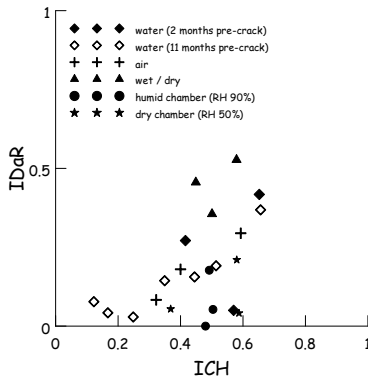


Figure 4.36. correlation between IDaR and ICH.

Anyway, it can be observed that even moderate crack closure can provide a recovery of the load bearing capacity (other than in the case of NSC) as a synergy between the effect of new composition and the presence of the fissures.

The scattering for Index of damage Recovery is even higher, most likely also because of some large uncertainties in the definition of the stiffness.

Anyway a trend can be captured which coherently highlight the effect and importance of different exposure conditions

4.4.3.1. Deflection hardening specimens

Results of bending test on deflection hardening specimens performed in the pre-cracking and post-conditioning stages are shown in Figure 4.37 to Figure 4.39.

It is worth here remarking that – as adopted in Paragraph 3.3.2.1, for deflection hardening specimens, pre-cracking was performed up to three different crack opening levels, two in the pre-peak stage (1 mm and 2 mm respectively) and one in the post-peak stage (up to 0.5mm after the peak)

The same pre-cracking ages and exposure conditioning as for the deflection softening specimens have been investigated.

In general a recovery of the mechanical performance has been observed, obviously as a function of the testing variables, i.e. pre-cracking opening and age of exposure conditions and duration.

A deeper investigation will hence be got through the deflection hardening and correlation of self-healing indices a previously done for deflection softening specimens. For the same conditions few un-cracked specimens cured and conditioned up to – previously on also shown in the in Figure 4.37 to Figure 4.39. The indices of the measured performance – quite independently of time – stands as a confirmation that any recovery can likely be obtained to healing of cracks due to the delayed hydration or un-hydrated binder particles. The last occur, because of the crack opening and water penetration inside the matrix. In un-cracked specimens, the un-hydrated particles are “protected” by the outer hard and quite impervious hydrated skin.

Analysis and Discussion of Experimental Results

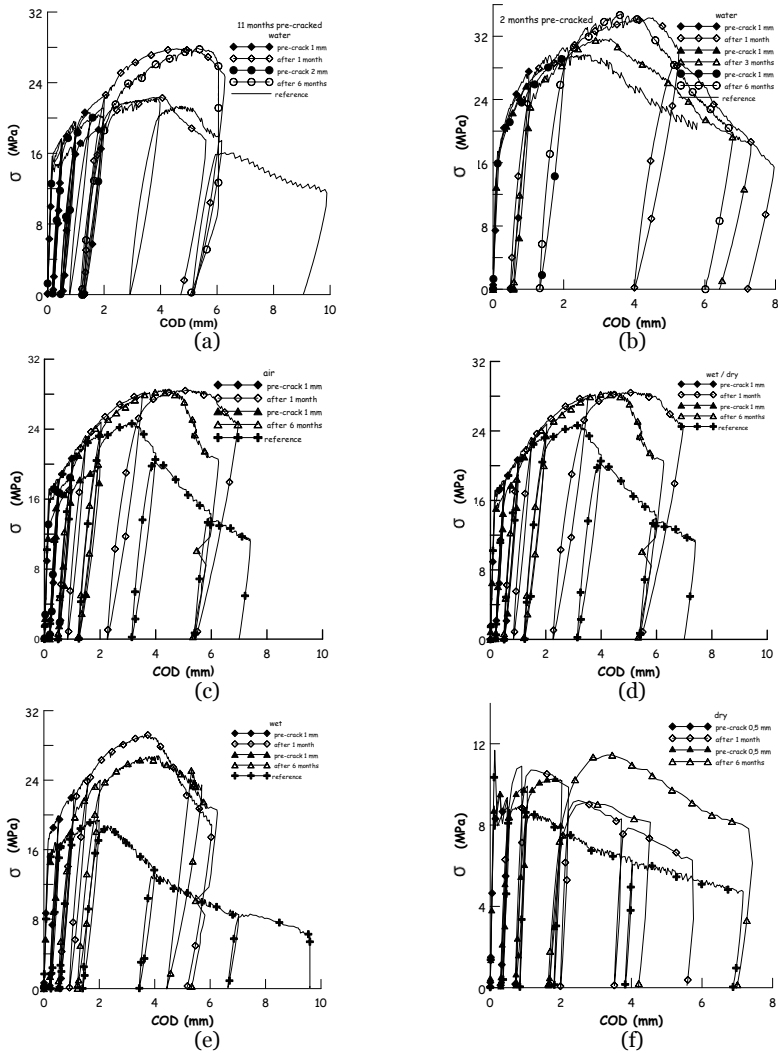


Figure 4.37. σ_N vs. COD for deflection hardening specimens for different exposure conditioning pre-cracked up to 1 mm: water immersion for different pre-crack ages (a) 11 months; (b) 2 months (c) air/external exposure; (d) wet/dry (water immersion and 50%RH with 20°C; (e) wet (high humidity with 90%RH and 20°C and (f) dry (50%RH with 20°C).

Analysis and Discussion of Experimental Results

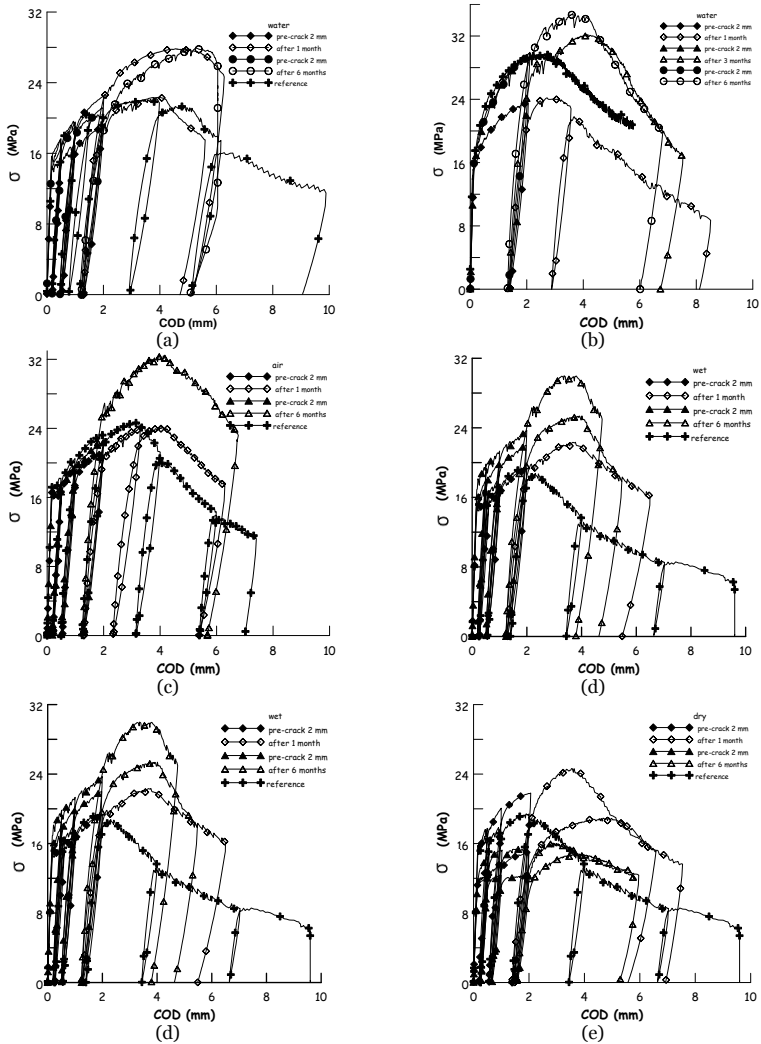


Figure 4.38. σ_N vs. COD for deflection hardening specimens for different exposure conditioning pre-cracked up to 2 mm: water immersion for different pre-crack ages (a) 11 months; (b) 2 months; (c) air/external exposure; (d) wet/dry (water immersion and 50%RH with 20°C); (e) wet (high humidity with 90%RH and 20°C and dry (50%RH with 20°C).

Analysis and Discussion of Experimental Results

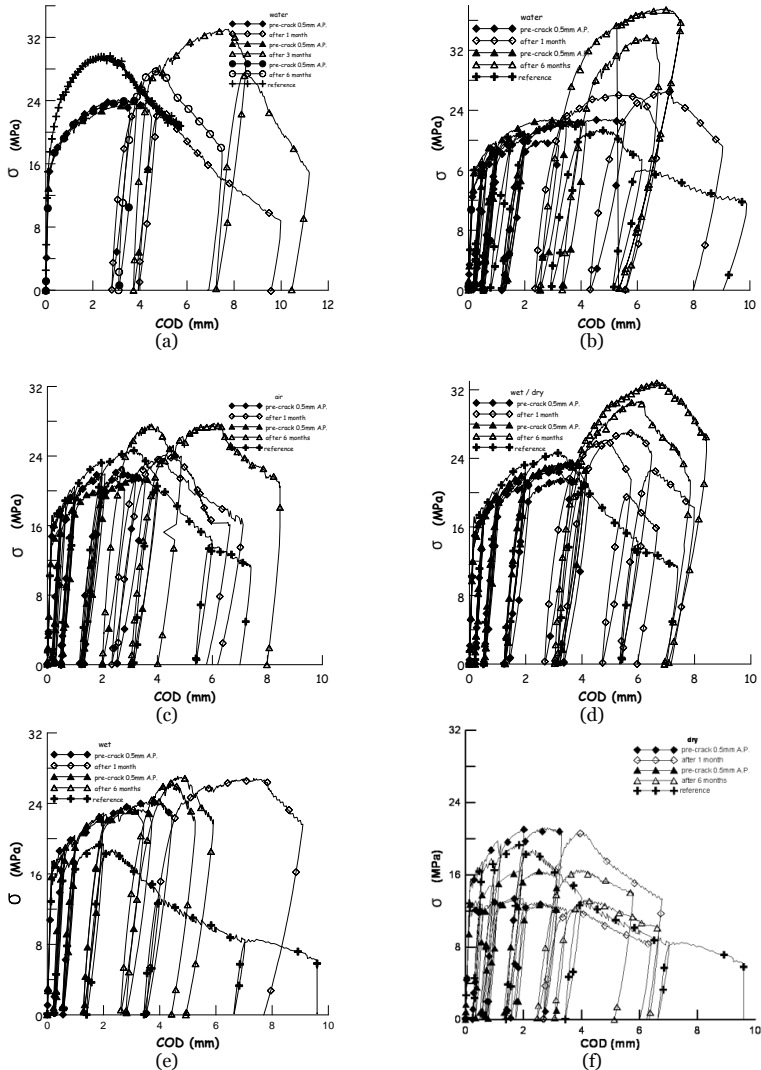


Figure 4.39. σ_N vs. COD for deflection hardening specimens for different exposure conditioning pre-cracked up to 0,5 mm after the peak: water immersion for different pre-crack ages (a) 11 months; (b) 2 months; (c) air/external exposure; (d) wet/dry (water immersion and 50%RH with 20°C); (e) wet (high humidity with 90%RH and 20°C and dry. (50%RH with 20°C).

4.4.3.2. Index of stress Recovery

The strength gain measured after the conditioning has to be suitably cleansed of the aforementioned deflection hardening capacity that specimens do inherently possess.

In the case of deflection hardening specimens pre-cracked in the pre-peak regime, i.e. at a COD value equal to either 1 mm or 2 mm and, the amount of stress bearing capacity recovered due to healing has to be carefully evaluated. As a matter of fact, since the pre-cracking threshold was set before the specimen could attain its peak and enter into the stage of unstable propagation of the localized crack (softening), a deflection hardening (wrongly interpretable as strength gain) would have anyway occurred even in instantaneous tests.

For deflection hardening specimens pre-cracked in the pre-peak regime, the formulation of the self-healing stress gain index (Equation 4.13, Figure 4.40) defined above has to be slightly modified as follows:

$$\begin{aligned}
 & \frac{\left(f_{peak,post-conditioning} - \sigma_{N,unloadingpre-crack} \right) - \frac{f_{f_{peak,virgin}} - \sigma_{N,unloadingvirgin}}{\sigma_{N,unloadingvirgin}} \sigma_{N,unloadingpre-crack}}{\left(f_{f_{peak,virgin}} - \sigma_{N,unloadingvirgin} \right) \frac{\sigma_{N,unloadingpre-crack}}{\sigma_{N,unloadingvirgin}}} \\
 = & \frac{\left(f_{peak,post-conditioning} - \sigma_{N,unloadingpre-crack} \right) \sigma_{N,unloadingvirgin}}{\left(f_{f_{peak,virgin}} - \sigma_{N,unloadingvirgin} \right) \sigma_{N,unloadingpre-crack}} - 1 \qquad 4.12
 \end{aligned}$$

The term $\frac{f_{f_{peak,virgin}} - \sigma_{N,unloadingvirgin}}{\sigma_{N,unloadingvirgin}} \sigma_{N,unloadingpre-crack}$ represents the amount of load bearing capacity that the specimen, due to its deflection hardening behavior, would have anyway gained after the pre-cracking test.

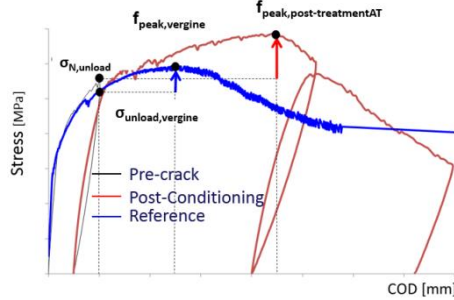


Figure 4.40. Notation and significance of Index of stress recovery for deflection hardening specimens pre-cracked in the pre-peak regime.

In the case of deflection hardening specimens pre-cracked up to 0.5 mm (Figure 4.39) after the attainment of the peak stress, the ISR is calculated as in Equation (4.12) for deflection softening specimens since, similarly to what happened for deflection softening specimens, the pre-cracking brought already the specimen into the stage of the unstable localized crack propagation. It has to be anyway remarked that whereas in the case of deflection softening specimens, in which only one crack formed, the ISR does really represent what is due to the healing of that same single crack, in the case of deflection hardening specimens pre-cracked after the peak, the value of the ISR computed as above will incorporate the effects of healing both the single localized cracks and also all the other micro-cracks which have been formed up to the peak.

The trends of ISR for deflection hardening specimens for the different pre-crack opening cases herein investigated are shown in Figure 4.41 to Figure 4.43 (respectively for pre-cracking up to 1 mm, 2 mm and 0.5 mm after the peak stress). With some exceptions, which can be hardly justified and can be reasonably attributed to some random experimental scattering, the trends and influence of exposure conditions, as discussed in detail for deflection softening specimens, are likely to be confirmed. It can be furthermore significantly observed that the ongoing healing of cracks was also instrumental to overcome the damage that, in some cases (see e.g. specimens pre-cracked up to 0.5 mm after the peak) was caused by some non-favorable exposure conditions (dry environment, or even for older specimens immersion in water).

Moreover, in this last case, the post-conditioning behavior looks much less sensitive to prolonged immersion, as if all the “residual” inborn self-healing capacity would be exhausted during earlier exposure

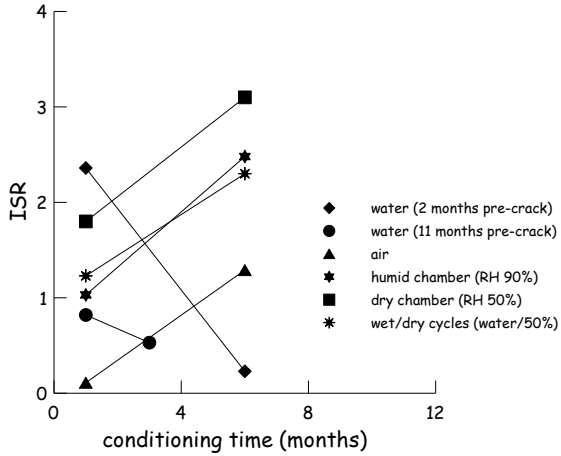


Figure 4.41. Index of Stress Recovery vs. conditioning time for deflection hardening specimens pre-cracked up to 1 mm (hollow markers refer to values of single tests, solid markers represent average values of nominally identical tests).

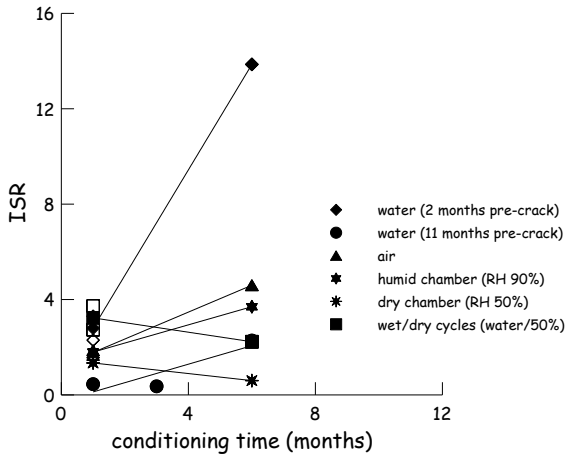


Figure 4.42. Index of Stress Recovery vs. conditioning time for deflection hardening specimens pre-cracked up to 2 mm (hollow markers refer to values of single tests, solid markers represent average values of nominally identical tests).

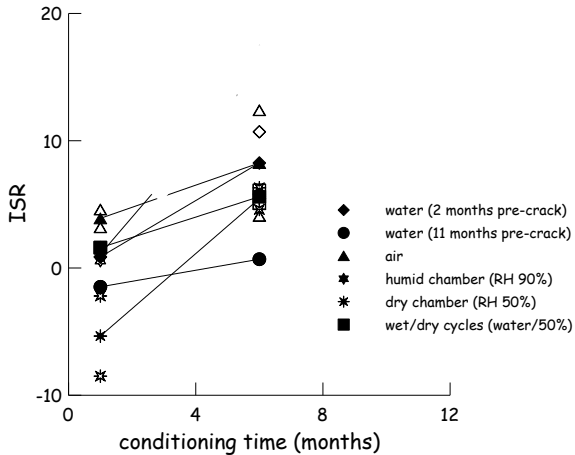


Figure 4.43. Index of Stress Recovery vs. conditioning time for deflection hardening specimens pre-cracked up to 0.5 mm after the peak (hollow markers refer to values of single tests, solid markers represent average values of nominally identical tests).

In most cases the absolute values of the index of Stress Recovery computed as above may appear quite high and unrealistically high, mainly for the specimen pre-cracked up to 2 mm and 0.5 mm beyond the peak. This can be understood by looking at the σ_N vs. COD at reference specimens which featured a quite wide and stable range around the peak, in which the stress held constant. (Figure 4.41 to Figure 4.43).

The pre-cracking COD values of 2 mm and 0.5 mm after the peak fall in this range, which makes – for reference specimens, the stress increases from 2 mm to COD_{peak} or/and the stress decrease from COD_{peak} up to 0.5mm beyond quite small. Any load bearing capacity recovery to the smaller values as above and is hence likely to turn out, in relative terms, quite higher even if limited to a few MPa in absolute ones.

Anyway, even in the so- defined relative terms – the fitted trends – confirming the expected effect of exposure conditions and also lead to hypothesize that in the investigated range – wider cracks (and hence deeper penetrating) may be more favorable to healing because there are likely to expose larger cluster of un-hydrated binder particles to the conditioning environment.

In Figure 4.44 and Figure 4.45 healed cracks due to different times and conditions of exposure can be observed.

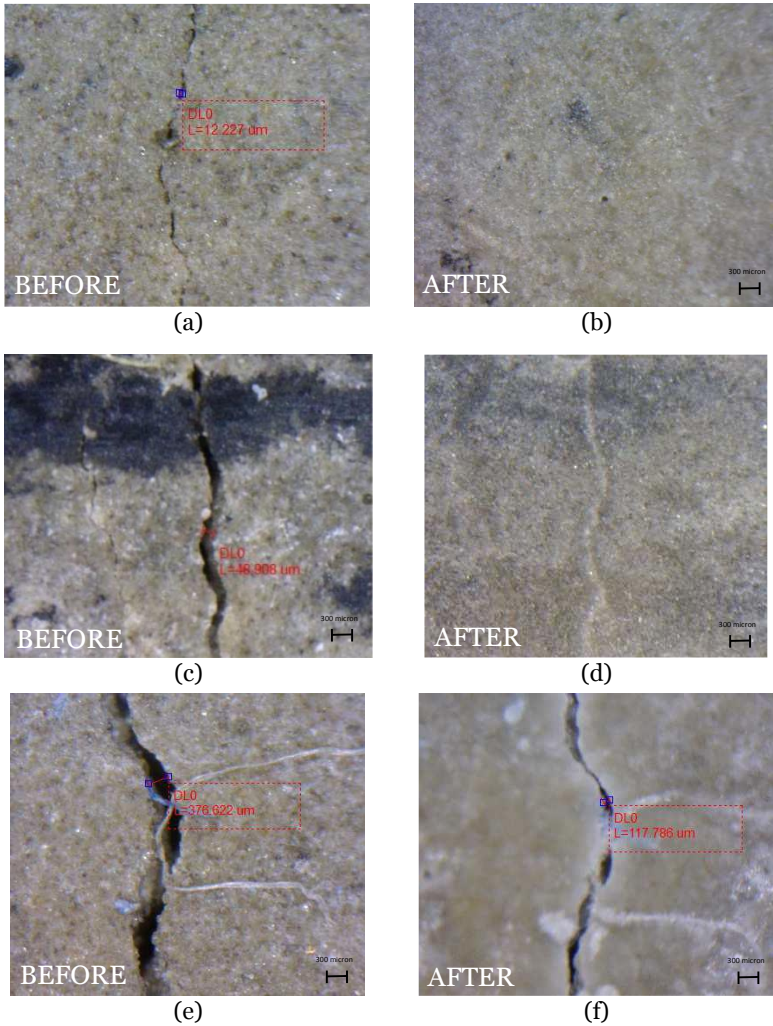


Figure 4.44. Healed cracks for specimens pre-cracked up to (a) $\text{cod}_{\text{tot}}=1\text{mm}$; (c) $\text{cod}_{\text{tot}}=2\text{mm}$ and (e) $\text{cod}_{\text{tot}}=0.5\text{mm}$ after the peak; (b,d,e) after one month of water immersion.

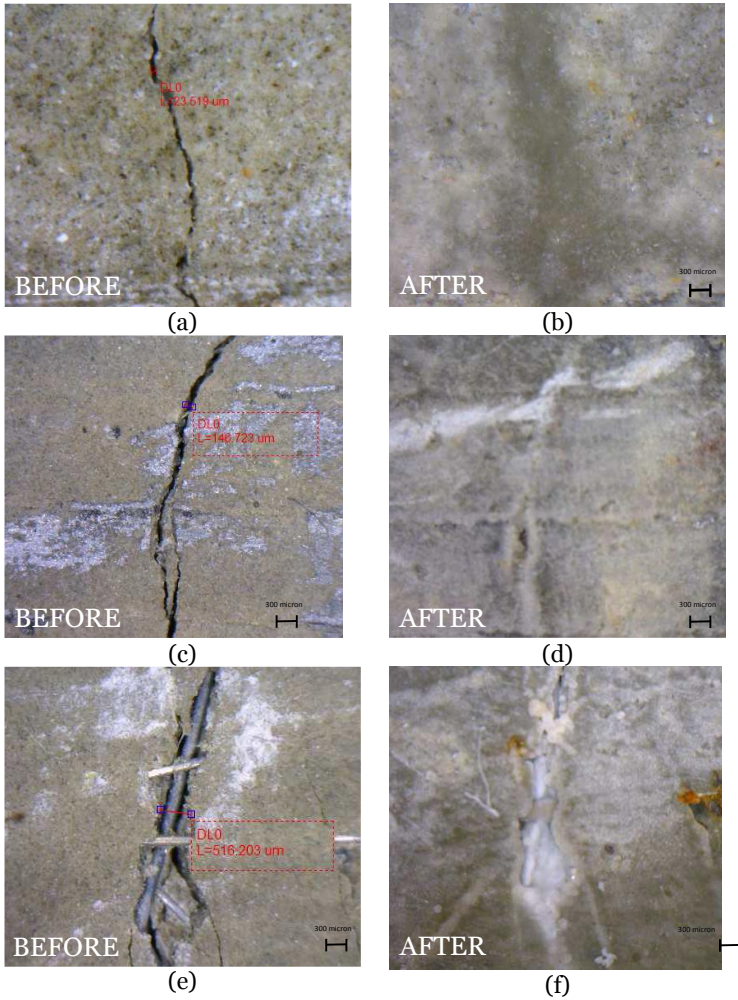


Figure 4.45. Healed cracks for specimens pre-cracked up to (a) $cod_{tot}=1\text{mm}$; (c) $cod_{tot}=2\text{mm}$ and (e) $cod_{tot}=0.5\text{mm}$ after the peak; (b,d,e) after six months of water immersion.

4.4.3.3.2. Index of Ductility Recovery

As it can be observed from typical stress crack-opening pre-crack and post-conditioning curves for deflection hardening specimens (Figure 4.41 to Figure 4.43), the self-healing reactions, besides a recovery of the load bearing capacity, assessed and evaluated as in the previous subsection, are likely to yield also a recovery of the ductility of the specimens.

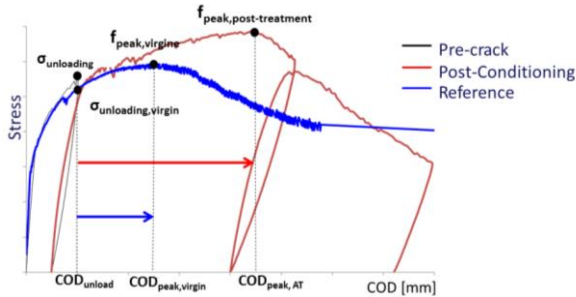


Figure 4.46 Schematic presentation for the Index of ductility recovery for the deflection hardening specimens

This can be clearly seen, in the case of specimens pre-cracked in the pre-peak stage, from the values of the Crack Opening Displacement measured at the peak load in the post-conditioning stage tests (e.g. Figure 4.46), which are higher than the ones measured for the un-cracked virgin specimens, even after same curing time and conditions as the ones underwent by the pre-cracked specimens.

Coherently with the engineering concept and significance of ductility, and Index of Ductility Recovery, IDuR, has been defined as follows, for specimens pre-cracked in the pre-peak stage:

$$IDuR = \frac{(COD_{peak, post-conditioning} - COD_{peak, virgin})}{(COD_{peak, virgin} - COD_{1stcrack, virgin})} \quad 4.13$$

As a matter of fact the index compares the gain in ductility that the specimens exhibits because of self-healing ($COD_{Peak, post-conditioning} - COD_{Peak, virgin}$), to the ductility that the virgin specimen would have anyway inherently exhibited.

For specimens pre-cracked beyond the peak, IDuR is simply defined as Index of Ductility Recovery:

$$IDuR = \frac{(COD_{peak,post-conditioning} - COD_{unloadingpre-crack})}{(COD_{peak,pre-crack} - COD_{unloading})} \quad 4.14$$

By observing the plot of IDuR vs. exposure/conditioning time (Figure 4.47 to Figure 4.49) for the different investigated cases, the following observations can be made:

- all the specimens pre-cracked up to 1 mm in the pre-peak regime exhibited (Figure 4.47), after conditioning, a better performance, in terms of ductility, than the specimens monotonically tested up to failure in their virgin state; anyway, a general worsening of the ductility recovery has been observed upon prolonged exposure times, with the only exceptions of specimens exposed to humid air and to wet-and-dry cycles. For specimens immersed in water, it can be reasonably hypothesized, similarly to what occurred for the strength recovery, that the initial improvement of the ductility could have been further affected by some leakage of the healing products; this is also likely to occur during the wet phase in specimens exposed to wet-and-dry cycles, but could have been counteracted by the precipitation of healing products which could occur undisturbed during the drying phase, also triggered by the humidity the specimen could have got when immersed. The worsening trends detected for specimens exposed to dry air is easily understandable; for specimens exposed to open air the worsening trend can be explained by the fact that the first six months of exposure encompassed the coldest and driest period of the year;
- for specimens pre-cracked in the pre-peak stage and up to 2 mm crack opening (Figure 4.48), except for the obvious and expectable case of specimens exposed to dry air, all other specimens exhibited a clear trend in improving the ductility recovery along with exposure time. Specimens immersed in water and pre-cracked at 2 months age showed an initial worsening (negative value of the index) with respect to the performance of the virgin specimen, once again most likely of some leakage of calcium hydroxide, which is likely to be higher because of the wider cracks. This leakage was also less likely to occur in specimens pre-cracked at an older age, because of the consumption of Ca(OH)₂ by the slag. Significantly, the wider crack openings, upon prolonged immersion times, promoted healing reactions at higher rates, which were able to effectively counteract the healing and yielding a recovery of the ductility;

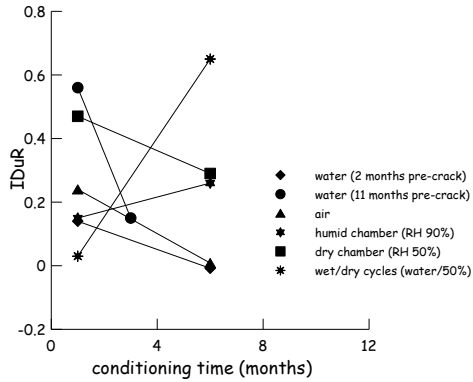


Figure 4.47. Index of Ductility Recovery vs. conditioning time for deflection hardening specimens pre-cracked up to 1 mm(hollow markers refer to values of single tests, solid markers represent average values of nominally identical tests).

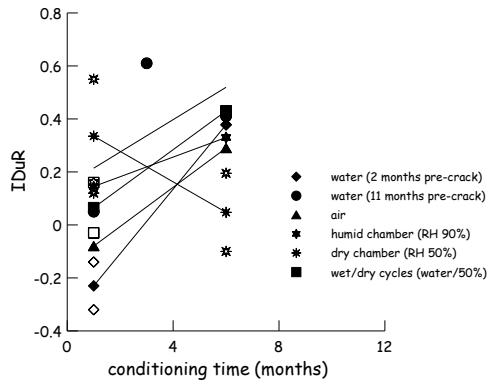


Figure 4.48. Index of Ductility Recovery vs. conditioning time for deflection hardening specimens pre-cracked up to 2 mm (hollow markers refer to values of single tests, solid markers represent average values of nominally identical tests).

- finally, for specimens pre-cracked beyond the peak, trends and values coherent with the expectable influence of exposure conditions have been measured.

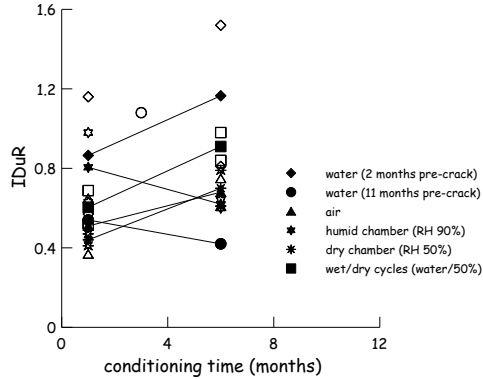


Figure 4.49. Index of Ductility Recovery vs. conditioning time for deflection hardening specimens pre-cracked up to 0.5 mm after the peak (hollow markers refer to values of single tests, solid markers represent average values of nominally identical tests).

4.4.3.3. Index of Damage Recovery

As described in the previous cases, for conventional concrete and deflection softening HPFRCCs, making a comparison between unloading-reloading cycles performed both during pre-cracking and post-conditioning tests, the values of secant unloading and tangent reloading stiffness ($K_{unl,j}$ and $K_{r,j}$), respectively denoted as $K_{unl,j}$ and $K_{r,j}$, at different levels “j” of crack opening were evaluated. From them, an index of damage recovery was calculated as (Equation 4.13):

Index of Damage Recovery = IDaR

$$IDaR = \frac{K_{reloading, post\ conditioning} - K_{unloading, pre-cracking}}{K_{loading, pre-cracking}} \quad 4.15$$

From Figure 4.51 to Figure 4.53 appear to be coherent with the previously discussed trends with reference to other indices.

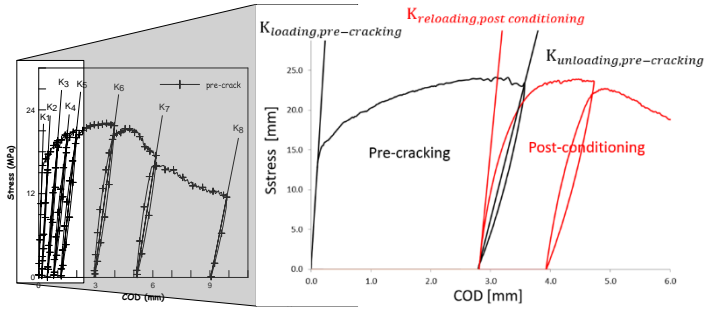


Figure 4.50. Schematic presentation for the used stiffnesses to calculate Index of Damage Recovery (Equation 4.16)

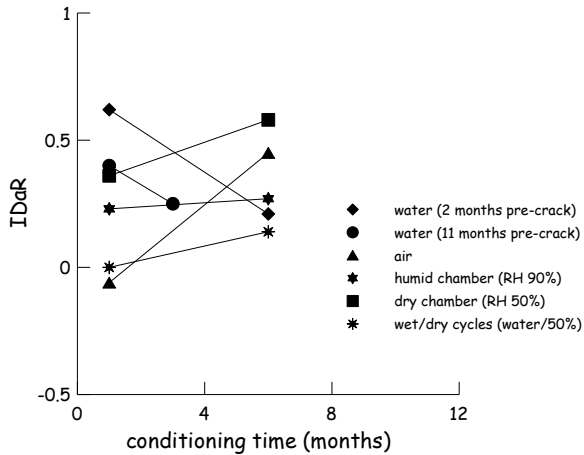


Figure 4.51. Index of Damage Recovery vs. conditioning time for deflection hardening specimens pre-cracked up to 1 mm.

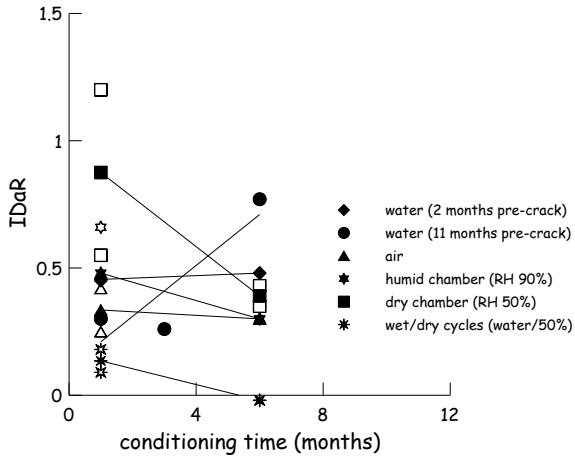


Figure 4.52. Index of Damage Recovery vs. conditioning time for deflection hardening specimens pre-cracked up to 2 mm (hollow markers refer to values of single tests, solid markers represent average values of nominally identical tests).

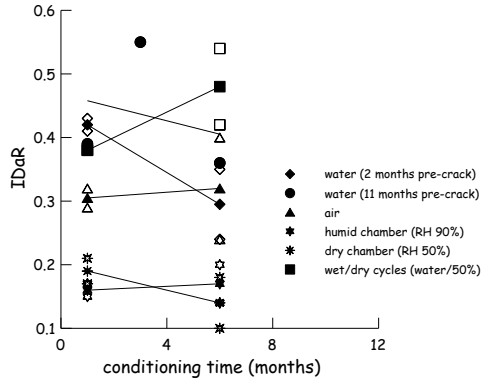


Figure 4.53. Index of Damage Recovery vs. conditioning time for deflection hardening specimens pre-cracked up to 0.5 mm after the peak (hollow markers refer to values of single tests, solid markers represent average values of nominally identical tests).

In particular:

- for deflection hardening specimens pre-cracked up to 1 mm in the pre-peak regime (Figure 4.51), prolonged immersion in water leads to a worsening in the stiffness recovery, the younger the pre-cracking age the higher this worsening; for all other exposure conditions a moderate improvement in the recovery was calculated;
- for specimens pre-cracked up to 2 mm in the pre-peak regime (Figure 4.52) and in the post-peak regime up to 0.5 mm after the peak (Figure 4.53), the recovery in the performance holds almost constant with conditioning time, with some expectable worsening in the case of exposure to dry environment. Availability of water generally yields to better results.

4.4.4. Damage evolution laws

Damage evolution laws has been calculated as well by comparing stiffness decay on both, pre-crack and the post-conditioning.

Moreover, from the definition of a continuum damage variable as an index of stiffness decay, damage vs. COD evolution curves were built (Figure 4.54).

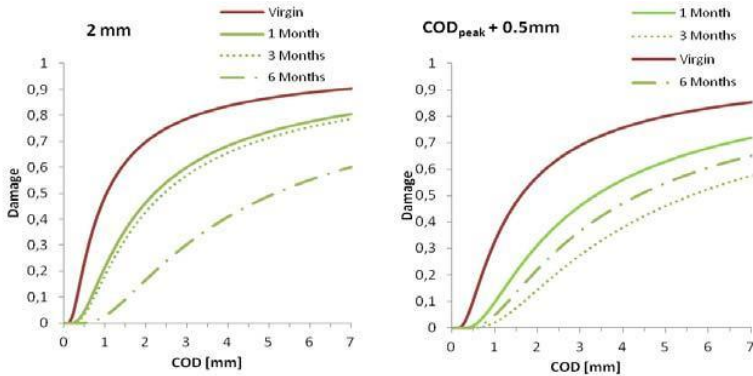


Figure 4.54. Fitted damage evolution laws for pre-cracked concrete specimens from water immersion (a, b) for specimen pre-cracked at 2 mm (a) and 0.5 mm after the peak (b).

Damage evolution laws have been built for all the conditioning type and the different crack opening. Here are presented just few typical examples

for specimens “conditioned” in the water immersion. The following statements based on showed results hold:

- specimens immersed in water (Figure 4.54) exhibited the largest effects in terms of “slowing” of the damage evolution law as a function of the exposure time;
- for the specimens with both initial damage level, lower one (COD=2mm) (Figure 4.54a) and higher level of damage (0.5mm AP) (Figure 4.54) the constant trend in the diminution of the damage evolution law has been observed as a result of the healing phenomena due to continued hydration; anyway it can clearly be observed how the evolution of the damage even after conditioning depends from the evolution of the damage law during the pre-crack stage.

4.4.4.1. Index of Crack Healing

From the evolution of stiffness all along the load path, measured as above, values of the scalar internal damage variable were calculated and damage evolution curves were built, for different exposure conditions, the effects of healing resulting, in a general “slowing” of the damage growth. From the comparison between the fitted trend in the pre-cracking and in the post-conditioning stages the crack closure due to self-healing could be estimated, as graphically explained in Figure 4.55 and an index of crack healing was defined as:

$$\text{Index of Crack Healing ICH} = 1 - \frac{\text{COD}_{\text{post-conditioning}}}{\text{COD}_{\text{pre-cracking}}} \quad 4.16$$

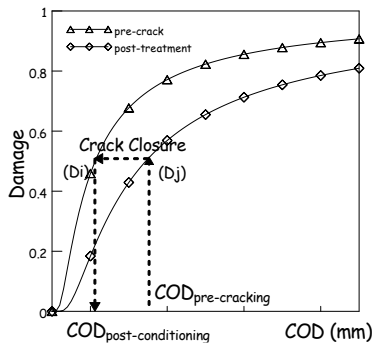


Figure 4.55. Graphical explanation of the procedure to estimate crack closure from damage evolution laws.

Results (Figure 4.56 to Figure 4.58) are – as far as the trends and the reference of pre-crack opening and exposure conditions - coherent with what already discussed with reference to the recovery of strength and stiffness.

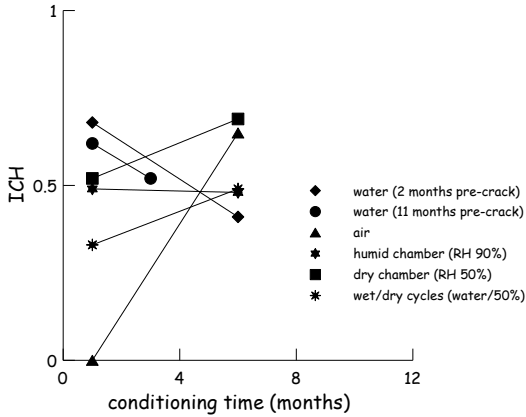


Figure 4.56. Index of Crack Healing vs. conditioning time for deflection hardening specimens pre-cracked up to 1 mm.

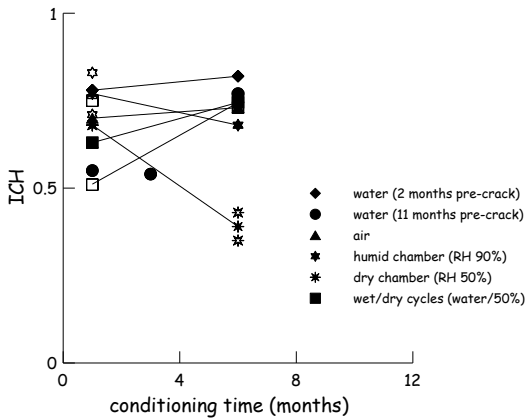


Figure 4.57. Index of Crack Healing vs. conditioning time for deflection hardening specimens pre-cracked up to 2 mm (hollow markers refer to values of single tests, solid markers represent average values of nominally identical tests).

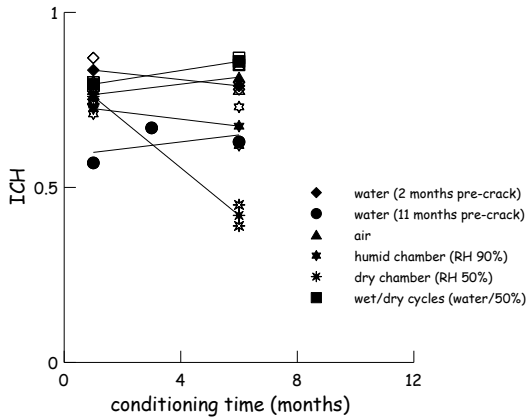


Figure 4.58. Index of Crack Healing vs. conditioning time for deflection hardening specimens pre-cracked up to 0.5 mm after the peak (hollow markers refer to values of single tests, solid markers represent average values of nominally identical tests).

4.4.5. Comparison Indices of Mechanical Properties Recovery and Index of Crack Healing

As done for deflection softening specimens the different Indexes related to the recovery of mechanical properties (strength, ductility, damage) have been plotted as function of the Index of Crack healing. Thus allows on the one hand to evaluate the coherence of the Indices definition, as proposed, and on the other provide a synopsis on the reference of the different exposure conditions for the whole set of investigated crack openings.

Despite the quite scattered results it can be in fact observed that the strength recovery capacity increases with the estimated crack healing, and the influence of the exposure conditions is confirmed. Similarly it happens for Index of Damage Recovery.

As far as the Index of Ductility Recovery is concerned the trend appear highly scattered and less clear, most likely because of the different definitions and significance of the indices for different pre-crack openings.

Anyways if plotted in the Index of the Stress Recovery (ISR) it appears that specimens getting stronger are also likely to become less ductile, which very make sense

This clearly adds new value and significance to the already well known high damage tolerance that High Performance Fiber Reinforced Cementitious Composites do inherently possess.

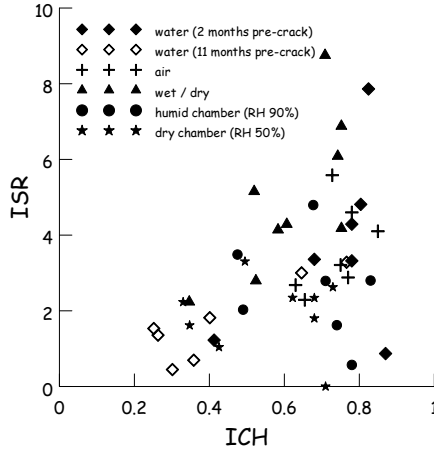


Figure 4.59. Correlation between Index of Stress Gain (ISR) and Index of Crack Healing (ICH) for the hardening specimens

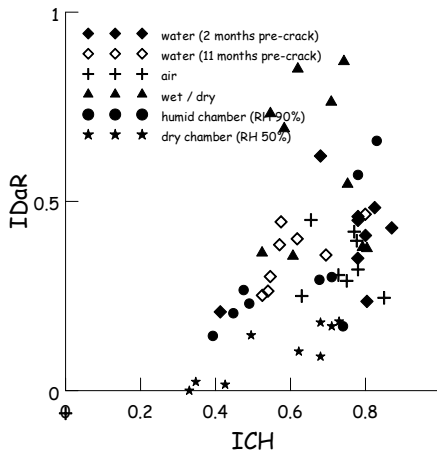


Figure 4.60. Correlation between Index of Damage Recovery (IDaR) and Index of Crack Healing (ICH) for the hardening specimens

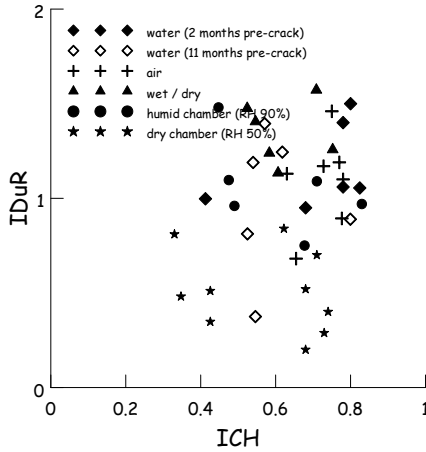


Figure 4.61. Correlation between Index of Damage Recovery (IDaR) and Index of Crack Healing (ICH) for the hardening specimens

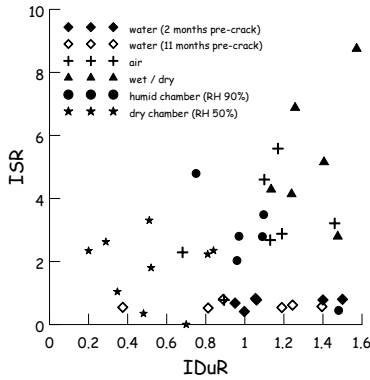


Figure 4.62. Correlation between Index of Ductility Recovery (IDuR) and Index of Stress Recovery (ISR) for the hardening specimens

4.4.6. SEM analyses

Due to the closure of the crack, showed in the Figure 4.63-Figure 4.65 shows the collected samples from a HPFRCCs specimen, which before the conditioning period was pre-cracked up to 100 μm and has been immersed in water for 6 months. The SEM observations were carried out at the end of conditioning period on the pre-cracked surface and on a fresh fracture surface.



Figure 4.63. Sample of HPFRCCs immersed in the water

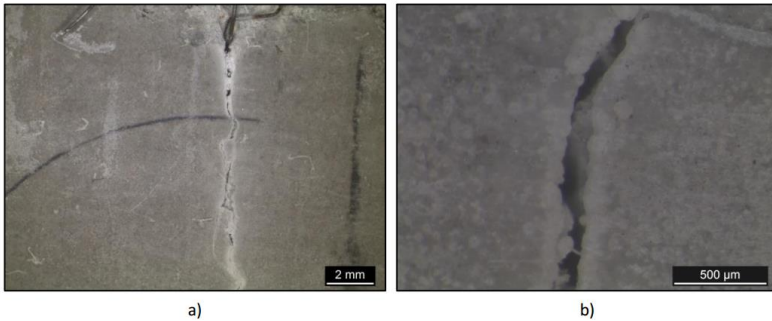


Figure 4.64. Microscopic images due to different magnification, a) 100 μm and b) 500 μm

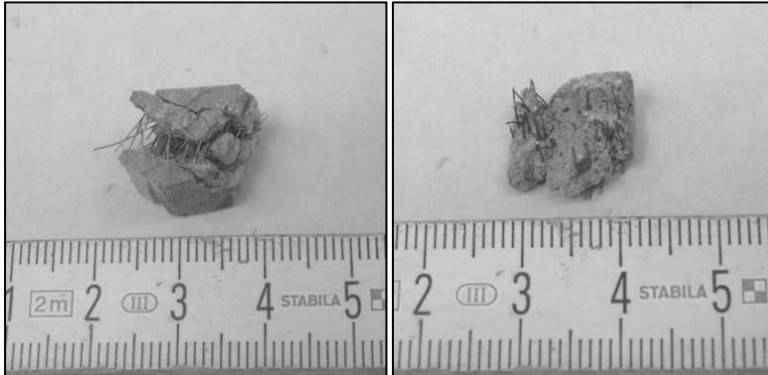


Figure 4.65. Macroscopic pictures of the extracted concrete in the cracked surface

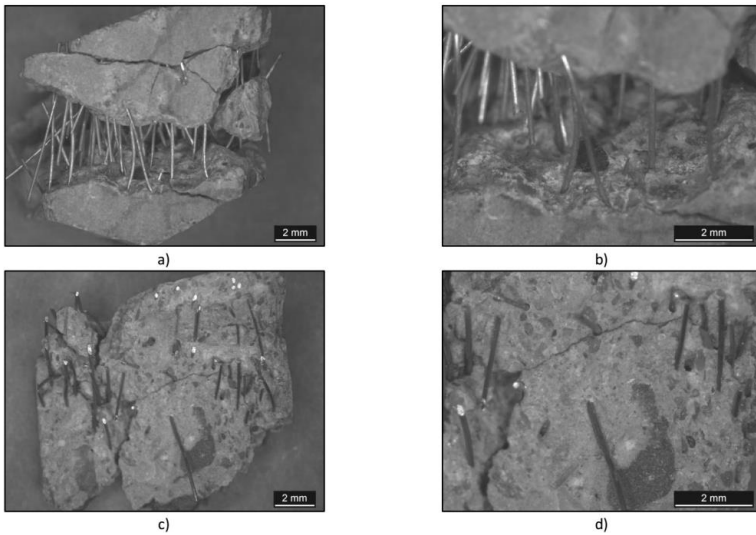


Figure 4.66. Magnified images of samples taken from the crack (a), (b) and fracture surface (c), (d) at different magnifications.

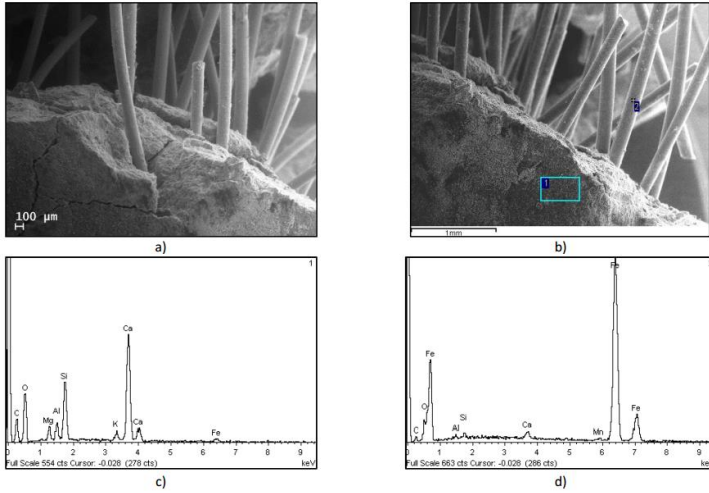


Figure 4.67. SEM images and EDS analysis of the sample taken from near the crack: detail of fibers and cement matrix (a) and (b), EDS of the cement paste to the edge of the crack and fiber (c), (d).

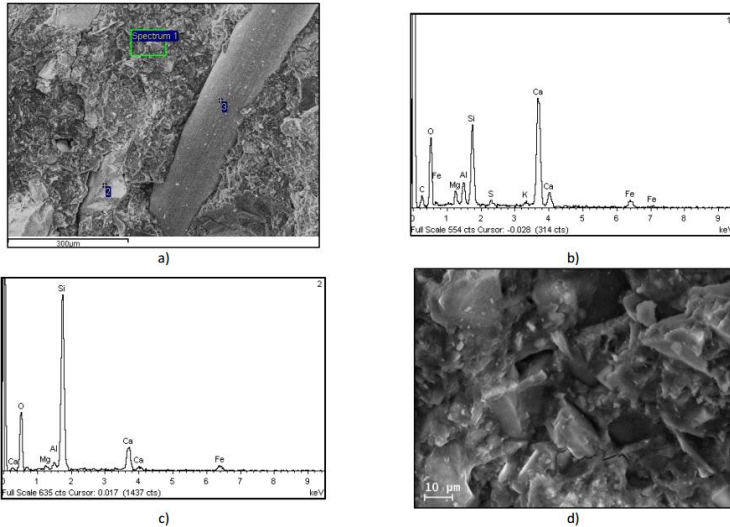


Figure 4.68. SEM images and EDS analysis of the cement paste on the cracked surface: detail of fibers and cement matrix (a) and (d), EDS of the cement paste on the cracked surface (b), and the self-healing product through the aggregate (c).

The sealed cracks that have shown a development of the of self-healing, have been analyzed and the presence of a crystalline structure can be seen in the Figure 4.64.

SEM observations, confirmed the presence of “healing” products on the cracked surface, due to the expected phenomenon of self-healing.

Analyzing the microstructure of the samples in the Figure 4.67a, it is possible, first of all to confirm the presence and the direction of steel fibers, while the Figure 4.67d shows the crystalline “coverage” of the aggregate by the healing products.

Furthermore, it is possible to observe the typical hydration morphology of the cement matrix by characteristic cement paste elements, which based on the EDS analysis (Figure 4.67,c), is represented mainly by calcium, silicon, aluminum, magnesium, etc. Another EDS analysis, carried out on the steel fiber (Figure 4.67,d), confirm the metallic composition of the fibers.

The observed cement paste of HPFRCCs is confirmed to be very compact, in fact, by analyzing the surface inside the crack (Figure 4.68.a), is observed an almost glassy structure (Figure 4.68,d), which makes it difficult to define different other structures inside the matrix. This, is believed to be due to the high amount of cement and slag, and to the very low water/binder ratio, which consequently produced a modest capillary porosity of the matrix.

The EDS analysis carried out in correspondence of the fracture of the sample, both on the cement paste (Figure 4.68,b) and on the aggregate (Figure 4.68,c). SEM pictures also confirmed that the healing products had the same typical composition of cement hydration products highlighted the nature of the siliceous sand used as the aggregate in this cementitious composite.

Thus is believed that the self-healing, is in this case mainly due to delayed hydration of the cement and slag. Because of cracking in fact, anhydrous binder particles – inside the specimens – are able to come in contact with water/air humidity and react with it.

This could not occur in un-hydrated specimens where the hard and impervious skin would prevent any significant penetration of water.

It hence seems that cracking is necessary to fully exploit the potential of delayed hydration of anhydrous binder particles inside the structure of the HPFRCC specimens.

4.4.7. Conclusion about HPFRCCs

An experimental study of autogenic self-healing ability of the HPFRCC has been presented, focusing the attention on the effects of crack healing on the recovery of mechanical properties, in terms of load bearing

and deformation capacity and stiffness. Different exposure conditions were investigated, ranging from immersion in water, exposure to humid (RH 95%) and dry atmosphere (50% RH), wet and dry cycles and exposure to open air (Northern Italy climate). Effects of exposure duration as well as of the crack opening were investigated. The results obtained and herein presented in a synoptic way confirmed the reliability of the proposed methodology to evaluate the self-healing ability of HPPFRCCs. Experimental results were analyzed in two different general groups, due to different alignment of fibers that resulted, as above said, in different deflection behavior, namely deflection hardening with multiple cracks and deflection softening with a single crack.

The following statements hold:

1. this category of advanced cement based composites possess an autogenic self-healing ability due to their inherent capacity to activate delayed hydration process of cement (and cement substitute) particles which are likely to remain un-hydrated because of the low water/binder ratios;
2. it is evident that the immersion in water and the exposure to high humidity was able to guarantee the highest levels of damage recovery. It is furthermore evident that when water immersion was extended, up to 6 months, the positive trend was maintained;
3. recovery of the residual strength can be observed, most likely due to delayed hydration of cement/binder un-hydrated particles, which, upon cracking, come in contact with water or environment moisture, depending on the exposure conditions;
4. the proposed indices provide reasonable estimation to quantify self-healing up to different crack openings; in one hand as far as the influence of the pre-crack opening is concerned it is evident that, whenever the pre-cracking was limited to 1 mm (within the pre-peak stable multi-cracking phase of the specimen behavior), the self-healing phenomena lead to the most significant recovery in terms of load bearing; on the other hand, for larger crack opening, but still within the pre-peak stable multi-cracking regime, ($COD_{pre-crack}=2\text{mm}$), the aforementioned effects start becoming visible only after prolonged immersion; it is also significantly worth remarking that, even in the case when a pre-cracking damage beyond the peak;
5. the effects of age of pre-cracking and immersion time on the entity of this residual strength recovery capacity can also be appreciated; specimens pre-cracked at 9 or 11 months exhibited a far lower self-healing capacity than those pre-cracked at 2 months, prolonged exposure time was anyway, even for older specimens, instrumental at achieving a significant healing of the quite large crack (0.5 mm). This is clearly witnessed by the new “cracking peak” detected in post-

immersion tests, followed by steep softening and then by a more gradual release of the stress, which can be evidently attributed to a quite strong re-establishment of “mechanical connections” between the two faces of the crack, due to the delayed hydration of anhydrous binder particles and the consequent formation of new hydration products which are likely to feature a high compatibility with the old material;

6. microscopic study, confirmed the closure of the crack after 3 and 6 months.

4.5. High Performance Reinforced Cementitious Composites with Hybrid Fibers

4.5.1. Introduction

In this part of the thesis the effect of natural fibres on the self-healing capacity of cementitious composites will be discussed and analysed. Natural fibres, through their porous micro-structure, can create a large number of moisture paths, through which moisture, absorbed by the same fibres, can be released “on demand” and activate delayed hydration processes which contribute to the healing of the cracks.

Reference has been herein made to a High Performance Cementitious Composite reinforced either with steel fibres only or with a hybrid mix of steel and sisal fibres. Influence of environmental conditions has also been studied and based on the expected effect of natural fibres the wet and dry cycles have been investigated, which is on likely to exalt and enhance the effects of self-healing on the recovery, if any, of mechanical performance.

Visual stereoscopically observation will be instrumental at visualizing the healed cracks and also assess the amount of crack closure to be correlated to the recovery of mechanical properties, evaluated as discussed in the previous section.

4.5.2. Four point bending test (4pbt)

The same set-up for the bending test performed on the HPFRRC with steel fibers has been employed in this case, where at the end of the scheduled conditioning period; specimens were tested up to failure.

From the nominal bending stress σ_N vs. COD curves, an evaluation of the effects of self-healing phenomena will be performed, following the same procedure as already developed for self-healing of ordinary concrete and HPRC with steel fibres.

In Figure 4.69 the σ_N vs. COD curves are shown for both deflection softening and hardening specimens and Reinforced with both steel and hybrid steel + sisal fibres.

Indices of Stress and Ductility Recovery have been computed as in the previous section for steel only HPRCCs and have been plotted in Figure 4.70 and Figure 4.71.

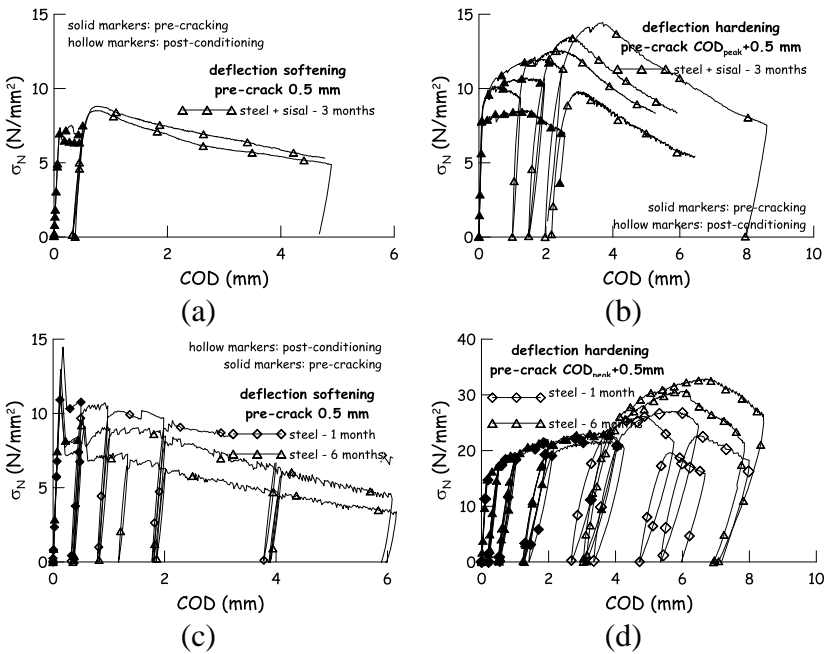


Figure 4.69. σ_N vs. COD curves for deflection softening (a,c) and deflection hardening (b,d) steel+sisal (a,b) and steel (c,d) specimens, for wet and dry cycles.

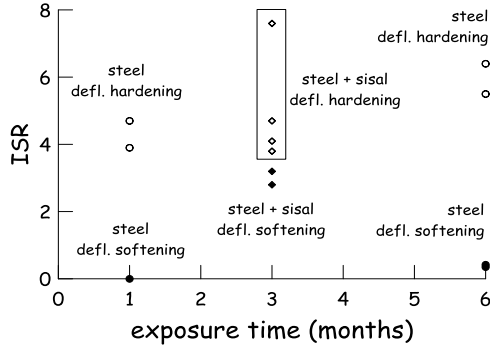


Figure 4.70. Index of stress recovery for different analyzed specimens

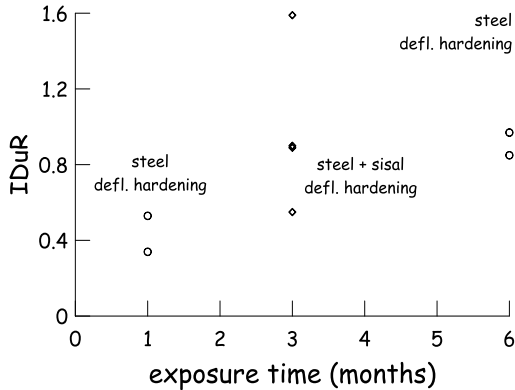


Figure 4.71. Index of of ductility recovery for different analyzed specimens.

It can be interestingly observed that:

- whereas deflection softening specimens reinforced with steel fibres only did exhibit negligible stress recovery capacity, either upon short or long term exposure, deflection softening specimens reinforced with a hybrid mix of steel and sisal fibres, even after three months of cycling, exhibited a significant capacity of recovery the stress bearing capacity lost upon pre-cracking softening stage (Figure 4.70);

- deflection hardening specimens, even when pre-cracked in the post-peak stage, exhibited a significant capacity of recovering both the stress (Figure 4.70) and the ductility (Figure 4.71); for steel specimens, for which evolution data along the exposure cycles were available, both the aforementioned properties positively evolved along the cycling time. It also significantly appear that, even after only three months cycling, specimens reinforced with steel and sisal fibres were able to provide a recovery, either in terms of stress or ductility, quantitatively comparable to the one exhibited by steel fibres upon a cycling time twice as much longer.

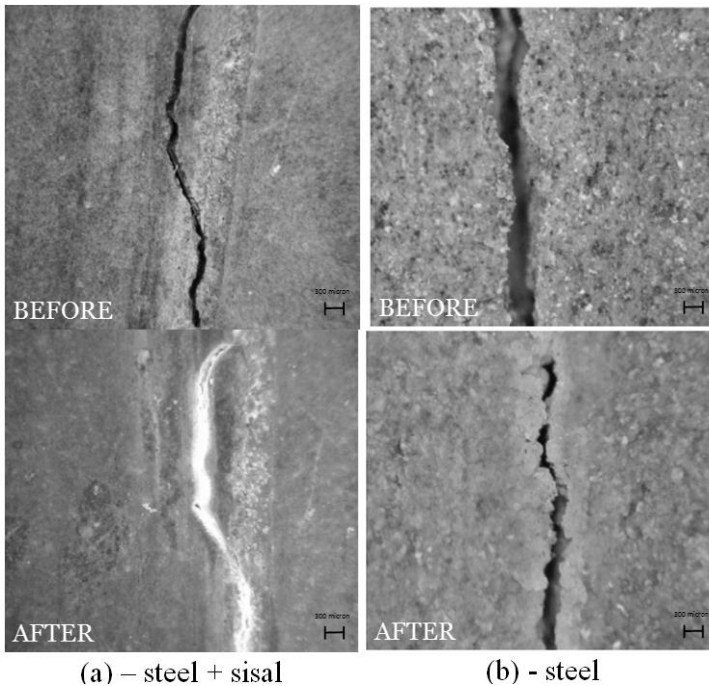


Figure 4.72. Completely healed cracks in steel+sisal (a) FRC deflection softening specimens after 3 months cycling and of partially healed cracks in steel (b) FRC deflection softening specimens after 6 months cycling (0.5 mm pre-crack; different scales of magnification).

This can be attributed to the effectiveness of natural fibres, when hybridized with other kind of fibre reinforcement, such as steel. As a matter of fact they are also promoters of self-healing reactions in cement based

materials, due to their hydrophilic nature, confirming the aforementioned assumption;

- a visual observation of the cracks in the pre-cracking stage and after the conditioning, shows the completely healed cracks just after 3 months with wet/dry cycles (Figure 4.72) in the case of composite reinforced with steel + sisal fibres whereas only partial closure is observed in the case with only steel fibres.
- In Figure 4.73 the healed crack is evident, but also it can be observed how the completely healed was so strong that because of the randomness of strength a new crack has been formed somewhere else

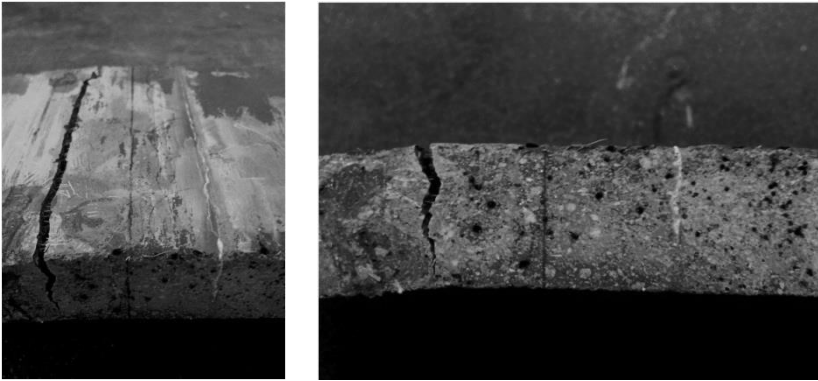


Figure 4.73. Completely healed cracks in steel + sisal and forming of new cracks after wet/dry cycles for about 3 months

4.5.3. Uniaxial Tensile Testing

Preliminary investigation on water and wet/dry cycles confirmed the potential of natural fibers as a vehicle of humidity inside the specimens and as facilitators of self-healing reactions.

From the experimental programme discussed in the previous chapter 3 direct tensile tests on double edge notched prismatic specimens have been also performed. As in the previous cases pre-cracked specimens and reference ones have been exposed to the same conditioning environment and for the same duration (i.e. 3 months under wet/dry cycles). Different mixes have been studied to quantify the effect of natural fibers:

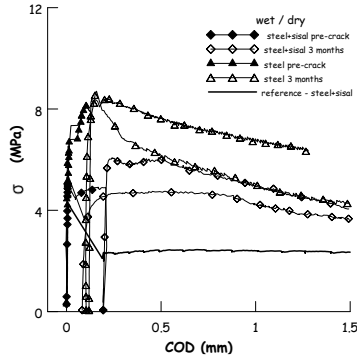


Figure 4.74. σ_N vs. COD response for uniaxial tensile test for double-edge-notched specimens for HPRCC with steel and steel + sisal after 3 months conditioning water immersion (a) and (b) wet/dry cycles

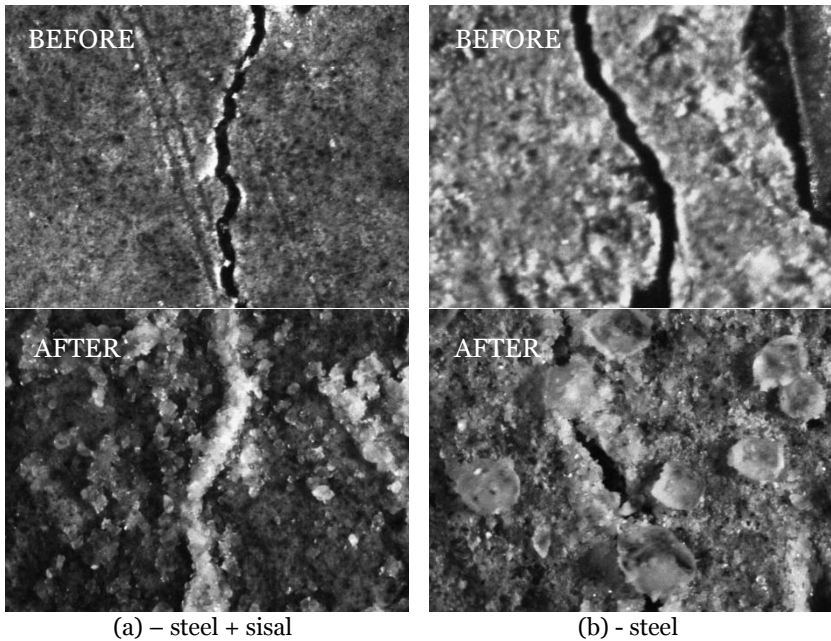


Figure 4.75. Healed cracks for; (a) steel + sisal HPRCC after 3 months wet/dry cycling and healed cracks in steel (b) HPRCC after 3 months wet/dry cycling.

A first mix, containing only Steel fibers $V_f=1.28\%$ (Reference HPFRCC); and another mix containing a hybrid fiber reinforcement consisting of steel fibers $V_f=0.64\%$ + Sisal fiber $V_f=0.64\%$.

It can be observed (Figure 4.74), as already inferred from results of bending tests that specimens reinforced with hybrid steel + sisal fibers exhibited in relative terms a recovery of the stress much more significant than for specimens with steel fibers only.

Visual observation of healed cracks confirmed the statements (Figure 4.75).

4.5.4. SEM and Thermo-gravimetric analysis

As a matter of facts cracks under different exposure conditioning, healed, as showed in Figure 4.72 and Figure 4.75 (in these cases under wet/dry cycling). In order to have a deeper insight and a better understanding of the healing mechanisms SEM and thermo-gravimetric investigations has been performed.

The analyses focused on understanding the nature of the healing products i.e. of the crystalline formation, which are responsible the sealing/healing of the cracks. In this case, the specimens were exposed 3 months to wet/dry cycles, and brought until failure, have been investigated.

Firstly, visual study has been performed on the cracked surface as it can be seen in the Figure 4.76.

SEM investigations have been performed on some of the “signed” zones, where it can be clearly seen the difference between the dark and the grey zone (Figure 4.77), the former mostly coinciding with the healed cracks surface and the later with the notched edges.

This “chromatic” difference was, at first moment attributed to some likely different “scales” of carbonation products.

In fact a SEM analyses of the cement paste in correspondence of the notches didn’t show any difference before/during/after the exposure in front of the healed crack (Figure 4.78).

On the other hand on the “healed” crack surface a high number of crystals has been observed(Figure 4.78).

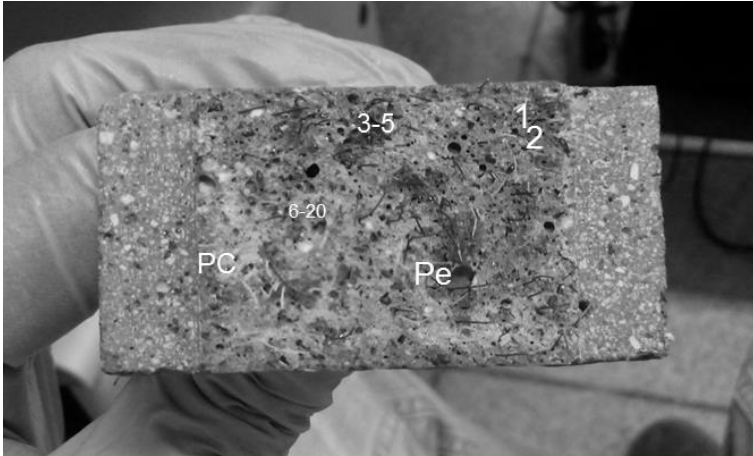


Figure 4.76. Macroscopic observation on the cracked surface after failure testing on uniaxial double-edge-notched prismatic specimens

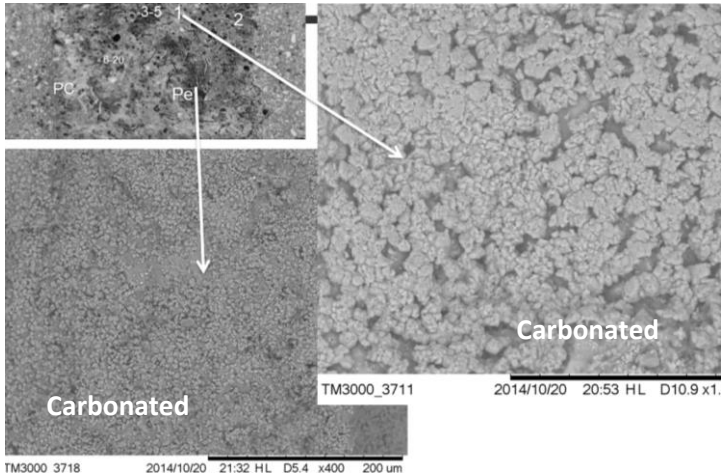


Figure 4.77. SEM investigations of the specimen showed in the Figure 4.76, for the dark and the grey zones.

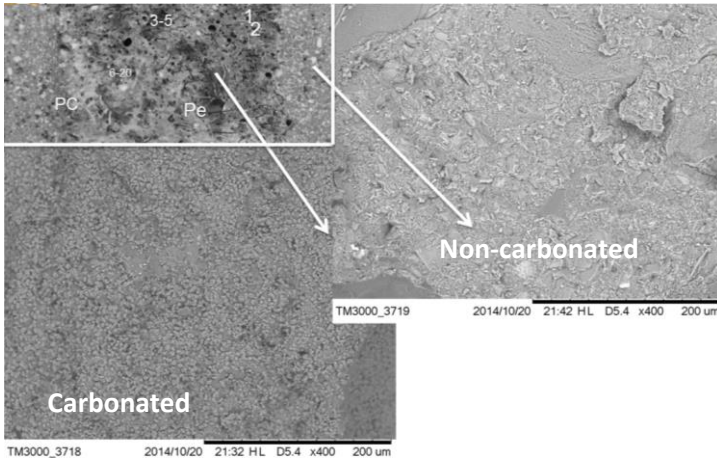


Figure 4.78. SEM investigations of the specimen showed in the Figure 4.76, for the dark and the notched zone

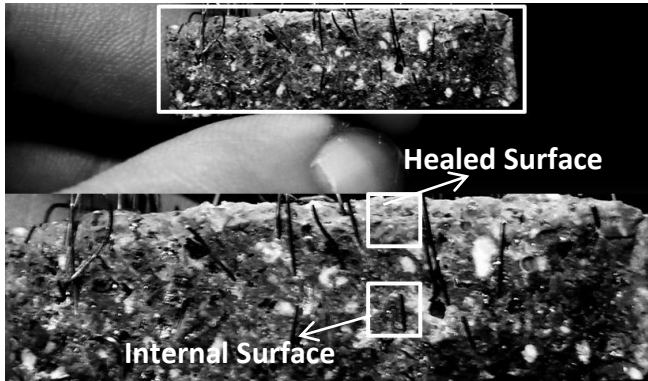


Figure 4.79. Investigated sample extracted from the healed specimen under wet/dry cycle for 3 months.

For a deeper investigation, a sample has been extracted from the healed crack surface, where it was possible to make a comparison between the internal – not-healed cement paste and the one that has been exposed and healed, as it can be seen in the Figure 4.79.

The presence of the crystals on the healed cracks is clear, but the processes that has been involved during the healing stage has been clarified by the thermography testing.

The thermo-gravimetric testing for the cement paste has been performed on four different samples;

- Reference cement paste matrix in the pre-cracking stage (named as matrix);
- Internal cement paste of the healed specimen (named as inside matrix);
- Cement paste on the cracked surface during the pre-cracking stage (crack surface) and
- The cracked surface after healing (named as Healed crack).

The thermo-gravimetric analysis of the matrix and its surface showed a mass loss that is related to cement hydration products: such as ettringite (76-84 °C), C-S-H (104-140 °C), C-H (460-465 °C) and CaCO₃ (620 - 645 °C).

Within the “matrix” a greater loss of water related to ettringite due to wet/dry cycles, was observed.

In other samples, such as “inside matrix” and the “crack surface”, similarities were found in the results of thermos-gravimetric tests which lead to hypotheses that delayed hydration reactions occurred.

The only difference that should be highlighted, is about the sample that has been extracted from the healed surface which, compared to other samples showed different peaks on mass loss which can be attributed to the “reactions” of crack closure, and can be referred to dihydroxylation, such as C-S-H (230-240 °C) while the second peak, can be referred to the decarbonation C-C (620-645 °C).

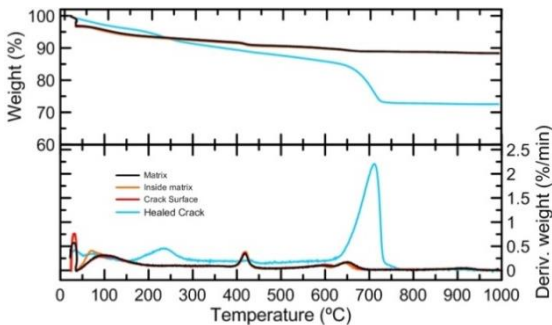


Figure 4.80. Thermo-gravimetric testing for different samples, for pre/post conditioning

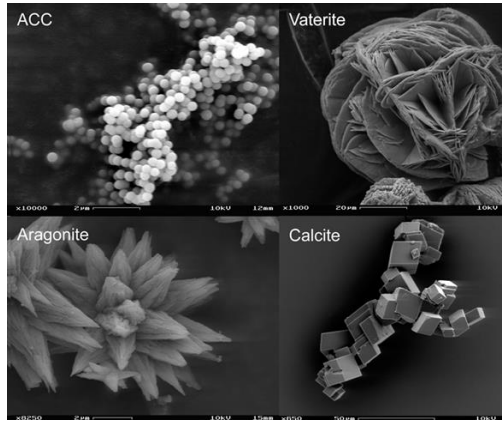


Figure 4.81. Polymorphic transformation of Calcium Carbonate (CaCO₃)

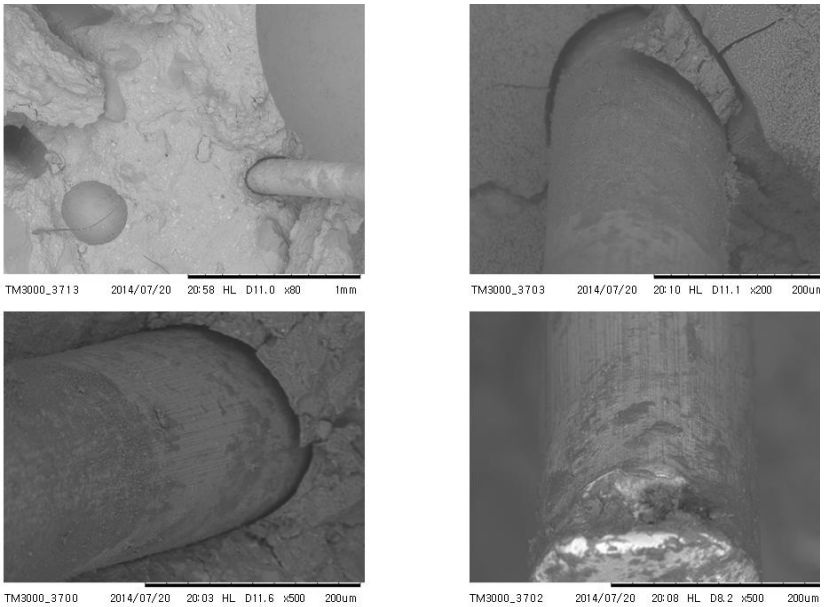


Figure 4.82. SEM images of the steel fibers at the pre-cracking stage

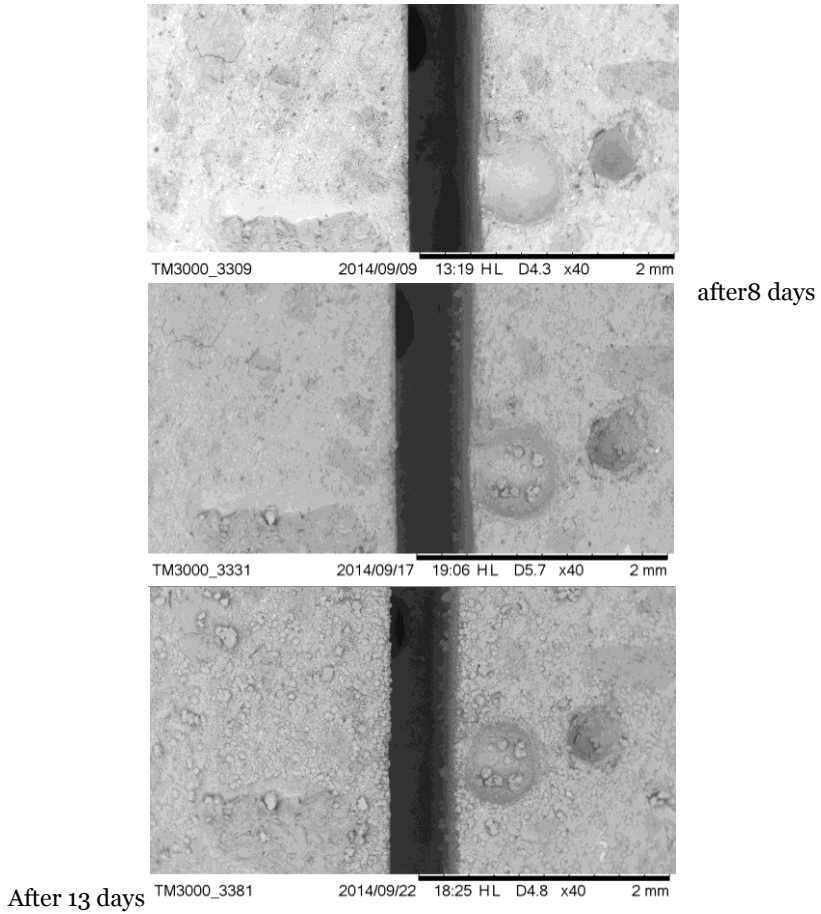


Figure 4.83. Crystal formation under wet/dry cycles

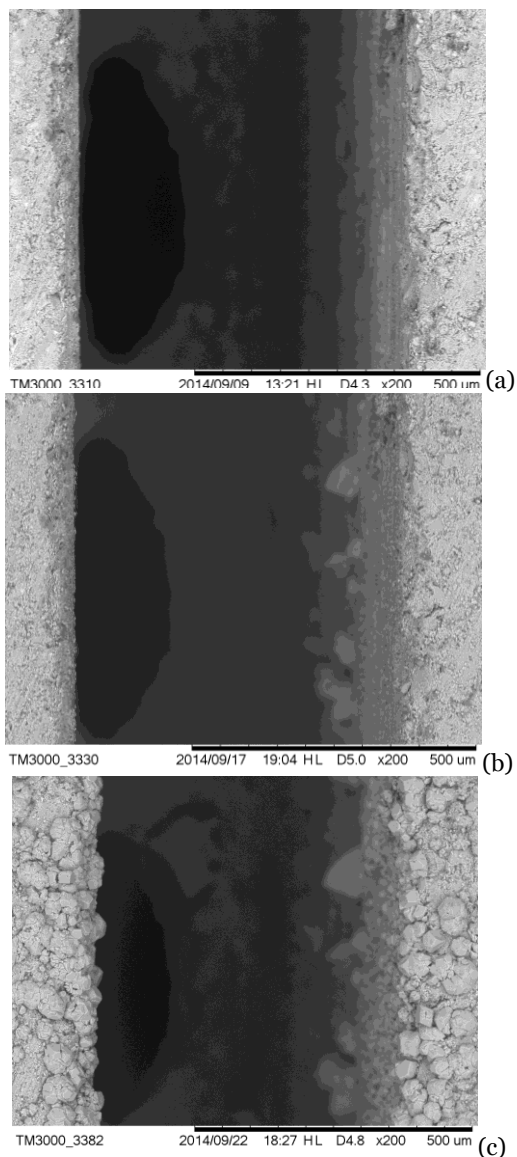


Figure 4.84. Crystal formation under wet/dry cycles

Through the SEM investigation, fiber bonding has been studied in different stages, such as at initial stage during pre-cracking (Figure 4.85) and at a later stage after the planned exposure (wet/dry cycles (Figure 4.86).

Observing the SEM images in Figure 4.82, it can be seen how the fibers well pulled out in a net way during the pre-cracking stage, performing the direct tensile testing.

Whereas after the wet/dry cycles, specimens that exhibited crack healing and stress recovery (Figure 4.74), the pull out was also accompanied by significant increasing of the fractured zone around the fiber, as it can be seen in the Figure 4.85.

This may be the result of an improved bond due to the self-healing reactions

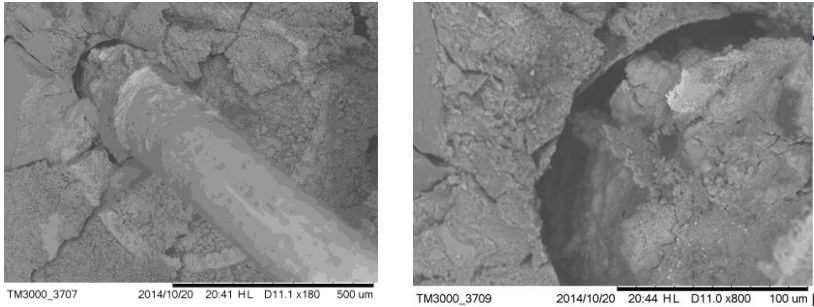


Figure 4.85. SEM observations for the steel fiber bonding with the cement matrix after the conditioning (3 months wet/dry cycles)

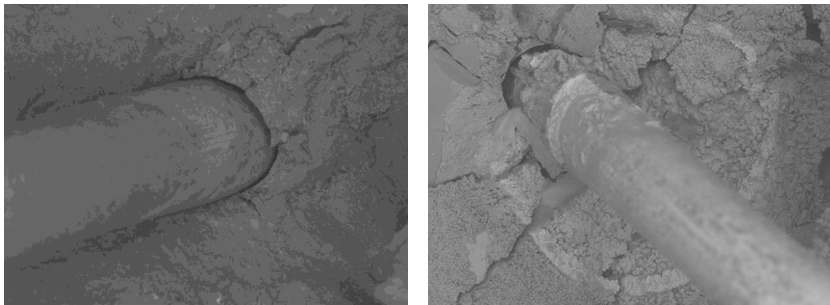


Figure 4.86. Comparison between SEM images obtained during the pre-cracking and after 3 months wet/dry cycles.

As a matter of fact, this could confirm the assumption that self-healing capacity of cementitious composites does not represent only the capacity to seal/heal the crack but as promotes the increasing of the bonding capacity of the fibers with the cement paste due to the increasing of the fracture energy to pull-out a single fiber (Figure 4.86).

Last but not the least, SEM investigation on the natural fiber (sisal), has been performed. It has been confirmed once again, as initially expected and confirmed through the mechanical performance, that natural fibers play the role of promoter on the self-healing capacity by absorbing/releasing the water inside the matrix (Figure 4.87,a), and after 3 months wet/dry cycle it can be clearly seen the concentration of the healing products around the fibers and its diffusion to the cementitious composite (Figure 4.87,a)

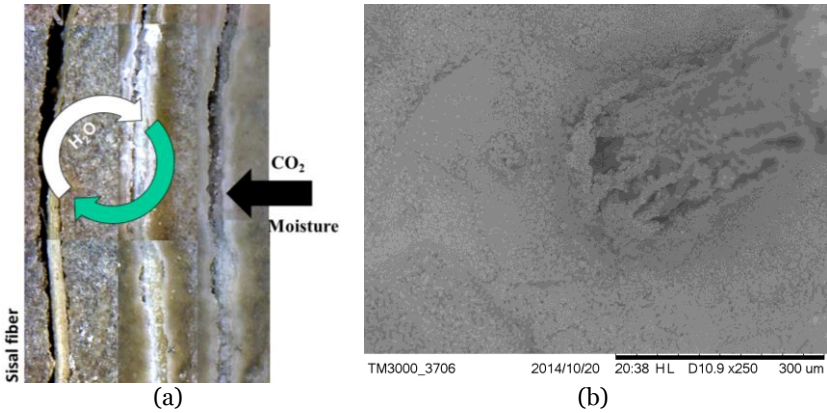


Figure 4.87. SEM observations for the sisal fibers; (a) the absorbing and releasing of the water inside the matrix and (b) the concentration of the healing product around the sisal fiber

The best way to predict the future

Is to invent it.

Alan Kay

5. Numerical Simulation of Self-Healing Capacity

5.1. Introduction

Despite the huge amount of experimental activity dedicated in the last less than fifteen years to formulate and validate different self-healing techniques and their effectiveness on the recovery of tightness and other engineering and mechanical performance, scant attention has been so far dedicated to the modelling of the same phenomena.

This gap highly needs to be filled in order to provide the scientific and engineering community valuable and reliable analyses and prediction tools which would allow to “design” the most suitable healing solution for the intended application in the sight of the expected performance.

In this thesis the issue of modelling will be tackled with reference to the case of normal strength concrete cured at 20°C and RH 90% up to 28 days and then pre-cracked and immersed in water. The experimental procedure discussed and analyzed in the previous chapters will be simulated making use of the Solidifaction Micrestress Microplane

(SMM) model (Di Luzio and Cusatis 2013) [161] for concrete, which making use the microplane model M4 and the solidification microprestress theory, is able to reproduce, as demonstrated, all the major effects of concrete behavior, such as creep, shrinkage, thermal deformation, aging, and cracking starting from the initial stages of its maturing up to the age of several years. The moisture and heat fields, as well as, the hydration degree are obtained from the solution of the hygro-thermal-chemical problem (Di Luzio and Cusatis 2009a, Di Luzio and Cusatis 2009b). This model is extended for incorporating the self-healing effects introducing an internal variable which characterize the self-healing process. Numerical examples are presented to validate the computational model developed and to show its robustness.

5.2. Solidification-Microprestress-Microplane (SMM) Model and Self-Healing Model

This model, entitled solidification-microprestress-microplane (SMM) model, amalgamates the micro-plane model and the solidification-microprestress theory and takes into account all the most significant aspects of concrete behavior, such as creep, shrinkage, thermal deformation, and cracking starting from the initial stages of curing up to several years of age. Age-dependent viscoelastic behavior under variable hygro-thermal conditions is described according to the solidification-microprestress theory.

Cracking/damage behavior is modeled through an age-dependent microplane model, in which the model parameters are assumed to be dependent on an aging variable evolving with the extent of early-age chemical reactions (hydration, silica-fume reaction, etc.) and temperature. Calibration and validation of the model is performed by the numerical simulations of the age-dependent response of sealed and unsealed specimens subject to a variety of loading conditions and/or drying. Comparison with experimental data shows that the SMM model can reproduce well the interplay of shrinkage, creep, and cracking phenomena during curing and drying.

The SMM formulation consists of a multi-physics framework that simulates, among others, the mechanical behavior of concrete, including viscoelasticity (creep/relaxation), cracking and damage, hygro-thermal deformations (shrinkage, swelling, thermal

expansion/contraction), heat transfer, moisture variation and moisture diffusion, and aging.

This model, as described into the introduction, has been extended to incorporate the self-healing effects, in particular, the delayed cement hydration, which is the main cause of the self-healing for young concrete, as well as the effects of cracking on the diffusivity and the opposite repairing effect of the self-healing on the microplane model constitutive laws.

Summarizing this model should be highlighted that how would be presented in the next sections, it overcomes most the limitations of models currently available in the literature and it is characterized by the following innovative aspects:

1. For the first time in the literature the considered microplane model, a general three-dimensional constitutive equation for concrete, is extended to account early age phenomena.
2. Aging effects are accounted for in a unified fashion through the concept of “reaction degree” which deals with the hygro-thermal aspects of early-age behavior (Di Luzio and Cusatis, 2009a,b) but never used in the contest of a comprehensive constitutive equation for concrete mechanical behavior.
3. A new aging law dependent on the more general reaction degree concept as opposed to the earlier adopted equivalent time is proposed for the solidification theory.
4. A new design concept has been introduced in this model due to the self-healing capacity of cementitious composites with and without crystalline admixture in particular by the delayed hydration process.
5. The model is calibrated and validated with reference of several sets of data.

5.3. Multi-Physics Formulation

The formulation proposed hereinafter consists of a multi-physics framework that simulates: (1) the mechanical behavior of concrete, including visco-elasticity (creep/relaxation), cracking and damage, hygro-thermal deformations (shrinkage, swelling, thermal expansion/contraction); (2) heat transfer due to environmental temperature variations (heating/cooling) and internal heat generation by exothermic chemical reactions; (3) moisture variation and moisture diffusion associated with environmental exposure (drying/wetting) and internal (chemical) water consumption; (4) the evolution of chemical reactions (cement hydration and delayed hydration,

silica-fume reaction, etc.) occurring at early-age in concrete and, more generally, in cementitious composites; and (5) aging, that is the evolution of the mechanical and hygro-thermal material properties from the time of casting to the completion of early-age chemical reactions and in case of occurring of cracks, the self-healing capacity depending on the environmental condition, crack opening and mix-constituents.

5.3.1. Mechanical Behavior

In this study, the classical assumption of Cauchy's continuum is adopted to describe the mechanical behavior of concrete at early age. The governing equations expressing the concepts of equilibrium and compatibility, can be then written as:

$$\nabla \sigma + \mathbf{b} = \mathbf{0} \quad \text{and} \quad \boldsymbol{\varepsilon} = \frac{1}{2}(\nabla \mathbf{u} + \nabla^T \mathbf{u}) \quad 5.1$$

where $\boldsymbol{\sigma}$; \mathbf{b} ; $\boldsymbol{\varepsilon}$; \mathbf{u} , are the stress tensor, the body force vector, the strain tensor, and the displacement vector, respectively. Note that thereafter bold Greek letters are used either to represent tensors or their vectorial contraction according to Kelvin notation: $\boldsymbol{\sigma} = [\sigma_{11} \sigma_{22} \sigma_{33} \sqrt{2\sigma_{23}} \sqrt{2\sigma_{13}} \sqrt{2\sigma_{12}}]^T$ and $\boldsymbol{\varepsilon} = [\varepsilon_{11} \varepsilon_{22} \varepsilon_{33} \sqrt{2\varepsilon_{23}} \sqrt{2\varepsilon_{13}} \sqrt{2\varepsilon_{12}}]^T$. Also, in Eq. (5.1) and hereinafter the direct dependence of all variable

The boundary value problem in Eq. (1) can be solved when appropriate (essential and/or natural) boundary conditions are prescribed and a constitutive equation is formulated. The constitutive equation formulated in this study is based on the assumption that the strain additivity holds and schematically is presented in Figure 5.1. One can write:

$$\dot{\boldsymbol{\varepsilon}} = \dot{\boldsymbol{\varepsilon}}^i + \dot{\boldsymbol{\varepsilon}}^v + \dot{\boldsymbol{\varepsilon}}^f + \dot{\boldsymbol{\varepsilon}}^d + \dot{\boldsymbol{\varepsilon}}^s + \dot{\boldsymbol{\varepsilon}}^t \quad 5.2$$

Where $\dot{\boldsymbol{\varepsilon}}$ is the total strain rate, $\dot{\boldsymbol{\varepsilon}}^i$ is the instantaneous strain rate; $\dot{\boldsymbol{\varepsilon}}^v$ is the viscoelastic strain rate; $\dot{\boldsymbol{\varepsilon}}^f$ is the purely viscous strain rate; $\dot{\boldsymbol{\varepsilon}}^d$ is the inelastic strain rate due to cracking and damage; and $\dot{\boldsymbol{\varepsilon}}^s$, $\dot{\boldsymbol{\varepsilon}}^t$ are hygral and thermal strains caused by variations of relative humidity and temperature, respectively. It is worth noting here that the strain additivity assumption, largely adopted in the concrete mechanics literature (Bazant & Planas 1997), is equivalent to the adoption of a rheological model, which, due to the series coupling, leads to a constant stress state in the different elements of the chain.

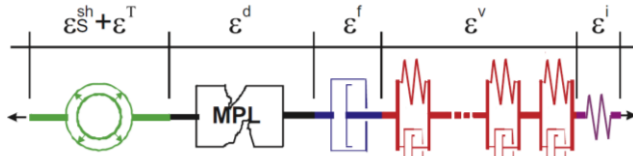


Figure 5.1. Schematic representation of the constitutive model. Courtesy by Di Lazio, Cusatis.

5.3.1.1. Microprestress - Solidification Theory

The instantaneous strain rate, $\dot{\epsilon}^i$ is the strain increment appearing immediately after the application of a stress increment, $\dot{\sigma}$ and can be expressed as $\dot{\epsilon} = q_1 G \dot{\sigma}$. At typical room temperatures and for saturation condition, parameter q_1 in (MPa⁻¹) is age independent as demonstrated by Bazant and Baweja (1995). In addition, if one assumes that material isotropy is preserved during the visco-elastic evolution of the material and that Poisson's ratio, $\nu=0,18$ is constant, then matrix G is the elastic compliance matrix with a unit Young modulus.

$$G = \begin{bmatrix} 1 & -\nu & -\nu & 0 & 0 & 0 \\ -\nu & 1 & -\nu & 0 & 0 & 0 \\ -\nu & -\nu & 1 & 0 & 0 & 0 \\ 0 & 0 & 0 & 2(1 + \nu) & 0 & 0 \\ 0 & 0 & 0 & 0 & 2(1 + \nu) & 0 \\ 0 & 0 & 0 & 0 & 0 & 2(1 + \nu) \end{bmatrix}$$

5.3

The viscoelastic strain rate, $\dot{\epsilon}^v$, is described according to the solidification theory (Bazant and Prasannan 1989a, Bazant and Prasannan 1989b), and it can be formulated as:

$$\dot{\epsilon}^v(t) = \frac{1}{v(\alpha)} \dot{\gamma} \text{ and } \gamma = \int_0^t \Phi(t - \tau) G \dot{\sigma} d\tau \quad 5.4$$

Where $\dot{\gamma}$ is the visco-elastic micro-strain rate of cement gel. The aging function, $v(\alpha)$, represents the volume fraction of cement gel

produced by early-age chemical reactions and it depends on the total reaction degree, α , which will be discussed later.

The non-aging micro-compliance function of cement gel is defined as $\Phi(t - t_0) = q_2 \ln [1 + (t - t_0)^{0.1}]$, in which $(t - t_0)$ is the loading time duration, q_2 (in MPa^{-1}), is a model parameter. It is worth noting that although the viscoelastic strain of the cement gel, $\gamma(t)$, is fully recoverable upon unloading, the macroscopic viscoelastic strain, ϵ^v , is only partially recoverable due to the effect of aging traduced by the function $v(\alpha)$.

The purely viscous strain rate, $\dot{\epsilon}^f$, represents the completely irrecoverable part of the creep strain, which it has been explained in the literature by slippage between adsorbed water layers hindered in cement nano-pores. Bazant and coworkers (Bazant et al. 1997, Bazant et al. 1997, Bazant et al. 2004) modeled purely viscous creep by introducing the concept of micro-prestress, S , which was assumed to represent an average measure of the stresses acting on the transverse nanopore bonds. Accordingly, under general temperature and relative humidity variations, viscous creep flow and evolution of micro-prestress can be formulated as:

$$\dot{\epsilon}^f = q_4 \kappa_0 S \psi \mathbf{G} \boldsymbol{\sigma} \quad \text{and} \quad \dot{S} + \omega \kappa_0 S^2 = \kappa_1 |\dot{T} \ln h + T \dot{h} / h| \quad 5.5$$

where ψ is the reduced time coefficient, $\psi = [0.1 + 0.9h^2] \exp [Q_s / (RT_0 - RT)] =, Q_s/R \sim 3000 \text{ }^\circ\text{K}$. Finally, k_0 (in $\text{MPa}^{-1} \text{ day}^{-1}$), k_1 (in MPa K^{-1}), and q_4 (in MPa^{-1}) are material parameters that need to be calibrated from experimental data. Note that while the general formulation depends separately on k_0 , k_1 , and q_4 , only parameter q_4 governs long-term basic creep behavior (Bazant et al. 2004).

5.3.1.2. Micro-plane Model for Cracking and Damage

Cracking and damage strain, $\dot{\epsilon}^d$, is described through a modified version of the Microplane Model M4 (Bazant et al. 2000, Di Luzio 2007). In order to amalgamate the microplane theory with the formulation presented earlier it is convenient to rewrite Eq. 5.1 as :

$$\dot{\epsilon} = \dot{\epsilon}^i + \dot{\epsilon}^v + \dot{\epsilon}^f + \dot{\epsilon}^m - \dot{\epsilon}^e + \dot{\epsilon}^s + \dot{\epsilon}^t \quad 5.6$$

where $\dot{\epsilon}^e = \bar{E}^{-1} \mathbf{G} \boldsymbol{\sigma}$ is an average elastic strain rate that needs to be subtracted from the strain rate calculated according to the microplane model in order to extract the cracking/damage strain: $\dot{\epsilon}^d = \dot{\epsilon}^m - \dot{\epsilon}^e$. Parameter \bar{E} , according to the original microplane formulation, has the

meaning of average elastic modulus and serves as dimensional parameter for the microplane boundaries, see Bazant et al. (2000). On the contrary, in the current formulation \bar{E} does not have physical meaning, since it is introduced only for numerical convenience, and it can be assigned prior to the model calibration and without loss of generality.

According to the kinematically constrained microplane model formulation, the strain vector on each microplane is the projection of the macroscopic strain tensor. By using the matrix notation introduced in Cusatis and Bazant (2008) one can write:

$$\epsilon_p = \mathbf{P}\epsilon^m \quad 5.7$$

where $\epsilon_p = \epsilon_N \ \epsilon_M \ \epsilon_L$ is the microplane strain vector, with $\epsilon_N =$ normal strain component, ϵ_M and $\epsilon_L =$ shear strain components.

$$\mathbf{P} = \begin{bmatrix} N_{11} & N_{22} & N_{33} & \sqrt{2}N_{23} & \sqrt{2}N_{13} & \sqrt{2}N_{12} \\ M_{11} & M_{22} & M_{33} & \sqrt{2}M_{23} & \sqrt{2}M_{13} & \sqrt{2}M_{12} \\ L_{11} & L_{22} & L_{33} & \sqrt{2}L_{23} & \sqrt{2}L_{13} & \sqrt{2}L_{12} \end{bmatrix} \quad 5.8$$

Matrix \mathbf{P} collects the components of the tensors $N_{ij} = n_i n_j$, $M_{ij} = (m_i n_j + m_j n_i)/2$ and $L_{ij} = (l_i n_j + l_j n_i)/2$; where n_i , m_i , and l_i are unit vectors defining a local Cartesian coordinate system on a generic microplane. The vector n_i is orthogonal to the microplane. If the microplane orientation is defined in a global spherical coordinate system characterized by the spherical angles ϑ and φ , then one can write: $n_1 = \sin \vartheta \cos \varphi$; $n_2 = \sin \vartheta \sin \varphi$; $n_3 = \cos \vartheta$; $m_1 = \cos \vartheta \cos \varphi$; $m_2 = \cos \vartheta \sin \varphi$; $m_3 = -\sin \vartheta$; and $l_1 = -\sin \varphi$; $l_2 = -\cos \varphi$; and $l_3 = 0$.

When appropriate microplane level constitutive equations are formulated, then the microplane stress vector, $\sigma_p = \sigma_N \ \sigma_M \ \sigma_L$, can be calculated and the macroscopic stress tensor can be computed from the principle of virtual work:

$$\sigma = \sigma_V \mathbf{I} + \frac{3}{2\pi} \int_{\Omega} D^T (\sigma_V - \sigma_V \mathbf{I}_p) d\Omega \quad 5.9$$

where Ω is the surface of a unit hemisphere; $\sigma_V = \sigma_{11}/3$ is the volumetric stress; $\mathbf{I} = [1 \ 1 \ 1 \ 0 \ 0 \ 0]^T$; $\mathbf{I}_p = [1 \ 0 \ 0]^T$; $D = P - V$; $V_{11} = V_{12} = V_{13} = 1/3$ and $V_{ij} = 0$ otherwise. The interested reader can find additional details of the adopted microplane constitutive equations in Bazant et al. (2000), Di Luzio (2007), Di Luzio (2009), Di Luzio and Biolzi (2010).

Since $\boldsymbol{\sigma}_P = \mathbf{F}_P (\boldsymbol{\epsilon}_P) = \mathbf{F}_P (\boldsymbol{\epsilon}^m)$, the macroscopic stress tensor can be expressed formally as $\boldsymbol{\sigma} = \mathbf{F}_P$ and, consequently, one can write:

$$\dot{\boldsymbol{\epsilon}}^m = \left(\frac{\partial \mathbf{F}}{\partial \boldsymbol{\epsilon}^m} \right)^{-1} \dot{\boldsymbol{\sigma}} \quad 5.10$$

However, it must be observed that, in general, the gradient of \mathbf{F} cannot be computed analytically and $\boldsymbol{\epsilon}^m$ must be computed numerically.

5.3.1.3. Hygral and Thermal Deformations

Humidity changes cause free hygrometric strain $\dot{\boldsymbol{\epsilon}}^s$ (swelling or shrinkage, for positive or negative relative humidity change, respectively) associated with changes in capillary tension, surface tension, and disjoining pressure. One can write $\dot{\boldsymbol{\epsilon}}^s = k_{sh} \dot{h} \mathbf{I}$ where the coefficient k_{sh} is assumed to be approximately constant although in the literature (Wittmann 1982). Such an approximation is motivated by the lack of an established formulation for such a dependence. Similarly, temperature changes cause thermal strain rates, which can be expressed as $\dot{\boldsymbol{\epsilon}}^t = k_t \dot{T} \mathbf{I}$ where again, the coefficient k_t is assumed to be a constant. This is approximately true at moderate temperatures although minor variations have been observed as function of temperature, relative humidity, and aging (Neville 1997).

5.4. Heat Transfer and Moisture Diffusion

The behavior of concrete, especially at early age, depends heavily on internal relative humidity, h , and temperature, T , whose distributions can be computed by imposing moisture mass balance and enthalpy balance equations in the volume of interest. For concrete mixes in which the binder is only Portland cement and for temperature not exceeding 90_C, one can write (Di Luzio and Cusatis 2009a)

$$\nabla \cdot (D_h \nabla h) - \frac{\partial \omega_e}{\partial h} \frac{\partial h}{\partial t} - \frac{\partial \omega_e}{\partial \alpha_c} \dot{\alpha}_c - \dot{\omega}_n = 0 \quad 5.11$$

$$\text{and} \quad \nabla \cdot (\lambda_t \nabla T) - \rho c_t \frac{\partial T}{\partial t} + \dot{\alpha}_c c \tilde{Q}_c^\infty = 0 \quad 5.12$$

where D_h is moisture permeability, ω_e is evaporable water-adsorption/desorption isotherm; $\dot{\alpha}_c = 0.253 \dot{\alpha}_c c$ is

rate of non-evaporable water; ρ = mass density of concrete; c_t = isobaric heat capacity (specific heat); λ_t = heat conductivity; c = cement content; \tilde{Q}_c^∞ = hydration enthalpy. It must be noted here that this theory does not account, as first approximation, for typically observed hysteresis during adsorption/desorption cycles (Feldman, 1968; Baroghel-Bouny et al., 1999), which has been recently explained by Bazant and Bazant (2012a,b) to be the consequence of two related mechanisms: snap-through instabilities during the filling or emptying of non-uniform nanopores or nanoscale asperities and the molecular coalescence, or capillary condensation, within a partially filled surface.

The water transport, described by the equation (5.11), is explicitly influenced by damage till now this effect was neglected in the hygro-thermal-chemical model of Di Luzio and Cusatis (2009a). The influence of damage in the framework of continuum mechanics and the governing mechanisms need to be smeared out and treated as an average solution of the problem. Therefore, in the first trial it is assumed that only permeability coefficient D_h depends on damage (crack width) of concrete. The crack width is calculated from the mechanical part of the model using a modified aging microplane model M4 for concrete (Di Luzio 2007, Di Luzio and Cusatis 2013). Currently there is few experimental data for permeability in cracked and fully saturated concrete (Wang et al. 1997, Aldea et al. 2000). Based on those experimental results, in the present model the effect of cracking on the increase of moisture permeability is taken such that D_h is multiplied by the normalized permeability coefficient, $f_D(\omega_c)$, which is obtained by dividing the permeability coefficient corresponding to cracked concrete by that of the un-cracked, which depends on the crack width w_c . A reasonable expression of $f_D(\omega_c)$ is given by

$$f_D(\omega_c) = 1 + \frac{999e^{n_c\xi}}{1-(1-e^{n_c})\xi} \quad 5.13$$

With

$$\xi = \min \left[\frac{\max(\omega_c - \omega_{c0}, 0)}{\omega_{c1} - \omega_{c0}}; 1 \right] \quad 5.14$$

This expression means that after the crack width w_c reaches a threshold value $\omega_{c0} \sim 0.05$ mm, water permeability of concrete increases up to its maximal value, which is about 1000 times the value for un-cracked concrete and, this value, it is reached for critical crack width, $\omega_{c0} \sim 0.2$ mm. For numerical and physical reasons a further increase of the crack width doesn't cause an increase of the permeability which remains hereafter constant. Since the transport of moisture in a crack is

described by the Fick's equation for continuous porous materials and we exploited it to include smeared (not discrete) cracks, it should be remarked that the permeability coefficient $D_{hf_D}(\omega_c)$ in a smeared crack approach has a different physical interpretation than in the un-cracked part of concrete, i.e., it does not represent the flow of water between two surfaces of a crack. Similar formulation has been proposed by Obolt et al. (2010) for the diffusivity coefficient in their model. It must be noticed that, for the sake of simplicity, the effect of the self-healing on the permeability is neglected for now. Nevertheless, this effect must be introduced in a further development of the proposed model.

5.5. Cement Hydration

For the concrete mixes of interest in this study, the main early-age reaction is the cement hydration – the reaction of free-water with unhydrated cement particles. This reaction mainly produces Calcium-Silicate- Hydrates (C-S-H) which is the main constituent providing stiffness and strength. Cement hydration can be characterized by the hydration degree (Ulm and Coussy 1995, Cervera et al. 1999, Gawin et al. 2006, Di Luzio and Cusatis 2009a), $\dot{\alpha}_c$, that represents the fraction of Portland clinker fully reacted with water. Its evolution law can be formulated as:

$$\dot{\alpha}_c = \frac{A_{c1} e^{-\frac{\eta_c \alpha_c}{\alpha_c^\infty}} e^{-\frac{E_{ac}}{RT}}}{1+(a-ah)^4} \left(\frac{A_{c2}}{\alpha_c^\infty} + \alpha_c \right) \cdot (\alpha_c^\infty - \alpha_c) \quad 5.15$$

where $a = 5.5$ (Di Luzio and Cusatis 2009b); E_{ac} is the hydration activation energy; R is the universal gas constant; η_c, A_{c1}, A_{c2} are material parameters; and α_c^∞ is the asymptotic value of the hydration reaction degree.

Following Pantazopoulo and Mills (1995), one can estimate the asymptotic degrees of cement hydration reaction as $\alpha_c^\infty = (1.032w/c)/(0.194+w=c)$, in which w/c is water to cement ratio. In this case, the overall degree of reaction (Di Luzio and Cusatis 2013), α , that represents an average measure of the total binder reacted (or, equivalently, a measure of the C-S-H produced) is $\alpha = \alpha_c$.

5.5.1. Self-healing

The self-healing is a water driven process and its kinetics is governed by the hydration of the un-hydrated cement or/and by the

reaction of additional materials, at least for the type of concrete mixture considered in this experimental campaign. The overall self-healing process can be as a first approximation described by a normalized overall reaction extent λ_{sh} , $\lambda_{sh} = 0$ for the end. The driving force of this overall reaction is the reaction affinity A_{sh} . To set up a reasonable and physically sound expression for A_{sh} one has to consider that it depends on the crack opening, the quantities of un-hydrated cement, the additives or other self-healing catalyst content, the moisture content in the pores of concrete near the crack, and the temperature. According to these facts, the self-healing rate may be expressed as:

$$\dot{\lambda}_{sh} = A_{sh}(1 - \lambda_{sh}) \quad 5.16$$

where:

$$A_{sh} = A_{sh0} \frac{e^{-\frac{E_{sh}}{RT}}}{1+(a-ah)^4} f_{\omega}(\omega_c) \quad 5.17$$

$$A_{sh0} = A_{sh1}(\alpha_c - \alpha_c^{\infty})c + A_{sh2}ad \quad 5.18$$

and

$$f_{\omega}(\omega_c) = \left\{ 1 + \left[\alpha_{\omega} - \alpha_{\omega} \left(1 - \frac{\max(\omega_c - \omega_{c0}, 0)}{\omega_{c1} - \omega_{c0}} \right) \right]^{b_{\omega}} \right\}^{-1} \quad 5.19$$

Where $a = 5.5$; E_{sh} is the self-healing activation energy; R is the universal gas constant; A_{sh1} and A_{sh2} are material parameters; c is the cement mass content; ad is the mass content healing admixture in mix design of concrete; and $f_{\omega}(\omega_c)$ is a function used here to relate the self-healing activity to the crack opening.

5.6. Aging Model

The phenomenon known as “aging” represents the change of the macroscopic behavior of concrete directly related to the modification of the internal material structure, which, in turn, is due to the evolution of nano- and micro-scale physical mechanisms and chemical reactions.

The main macroscopic observations relevant to aging are the following:

1. Stiffness increases whereas creep decreases with age. This is partly related to the increase of solidified material as a result of cement

hydration and other chemical reactions, such as silica- fume reaction. This type of aging-although continues for a long period of time - is predominant only in the first year or so of concrete life. However, reduction of creep is observed even for concretes much older than 1 year. This long-term aging was explained by physical modification in the nano-structures of C-S-H and, more specifically, by the relaxation of nano-scale self-equilibrated stress states developed during the hardening phase (Bazant et al., 2004).

2. Concrete strength, in both tension and compression, increases with age as a direct consequence of the produced C-S-H (Neville, 1997). Tensile and compressive strengths grow almost proportionally with the exception of the first few days (usually less than 3 days), during which the compressive-to-tensile strength ratio is lower than the final one (Oluokun, 1991; Oluokun et al., 1991; Kim et al., 2002, 2004). Evolution of strength with time is highly nonlinear and the strength build-up is much more significant at early-age even though it continues for several years. Experimental data show that, in most cases, up to roughly 90% of strength is typically gained in the first month after casting (Neville, 1997).

3. Concrete fracture energy also increases with age. However, the increase is not proportional to the increase in stiffness and strength and, thus, it leads to a reduction of the material characteristic length - which is proportional to stiffness and fracture energy and inversely proportional to the square of tensile strength (Hillerborg, 1985). This is mainly due to an intrinsic embrittlement of C-S-H and to the fact that fracture processes in concrete are not only dependent on the properties of cement gel but are significantly affected by the interaction between cement gel matrix and inclusions (aggregate particles as well as possible fiber reinforcing) (di Prisco et al., 2007). The reduction of material characteristic length is responsible for a more brittle behavior of old concretes, which are characterized by a steeper post-peak slope of typical load-displacement responses and a consequent faster loss of loading carrying capacity during failure (Petersson, 1980; Kim et al., 2004). See, for example, Table 2 which reports compressive strength, tensile strength, Young's modules, fracture energy, and the associated characteristic length for the experimental data of Kim et al. (2004).

4. Age also affects volume, size, and inter-connectivity of pores at different length scales. Generally speaking, old concretes tend to be denser and dryer materials than their early-age counterpart. This, in turn, changes the material properties and concrete behavior relevant to moisture diffusion and heat transfer.

In this model, the effect short term aging on both mechanical and hygro-thermal behavior is modeled in a unified manner through the concept of overall degree of reaction.

5.6.1. Stiffness and Creep

Age effect on stiffness and creep is modeled by the solidification theory (Bazant and Prasanna 1989a), which simulates directly the growth of solidified material at early age and it does so through the so called aging law previously introduced (see Eq. 5.20).

The adopted aging law is:

$$\frac{1}{v(\alpha)} = \left[\frac{\alpha_\infty}{\alpha} \right]^{n_\alpha} \quad 5.20$$

where n_α is a material parameter that can be calibrated by simulating experimental data on aging creep.

5.6.2. Strength and Fracture Energy

The degree of reaction is also the main internal variable used in this study to simulate the increase of strength and fracture energy at early age. The strength evolution is assumed to depend on the aging degree, α , defined as (Cervera et al. 1999)

$$\lambda = \left(\frac{T_{max}-T}{T_{max}-T_{ref}} \right)^{n_\lambda} (B_\lambda - 2A_\lambda \alpha) \alpha \quad 5.21$$

for $\alpha > \alpha_0$ and $\lambda = 0$ otherwise. The parameter α_0 defines the value of the reaction degree at the end of the setting phase, that is when concrete may begin to be considered a solid. Values of $\alpha_0 = 0.1-0.4$ have been proposed in the literature, depending on type of cement and water-to-cement ratio (de Schutter and Taerwe 1996). T_{max} represents the maximum temperature at which hardening of concrete is possible under standard conditions ($\sim 100^\circ\text{C}$). T_{ref} is the reference temperature for the experimental calibration of the aging model, thus for $T = T_{ref}$, it must result $\lambda = 0$ for $\alpha \leq \alpha_0$ and $\lambda = 1$ for $\alpha_\infty = \alpha_0$. By imposing these conditions one obtains $B_\lambda = [1 + A_\lambda (\alpha_\infty^2 - \alpha_0^2) / (\alpha_\infty^2 - \alpha_0^2)]$, in which n_λ , A_λ are model parameters that need to be identified from experimental data.

The concept of aging degree is used to account for early age phenomena within the modified microplane model M4 formulation. This is achieved by assuming that some material parameters k_1 , k_7 , governing

the microplane constitutive equations (stress-strain boundaries) are functions of λ , see for further details Di Luzio and Cusatis (2013).

Parameter k_1 scales all stress-strain boundaries in the radial direction; parameter k_2 governs the horizontal plateau of the shear (frictional) boundary which is activated under high shear deformation and high level of normal compression both typical of macroscopic compressive stress states under confinement. Parameters k_3 and k_4 define the volumetric stress boundary in compression, which is mainly activated under high compressive volumetric stresses. These first four parameters can be physically interpreted as parameters characterizing the behavior of C-S-H and its internal structure. If their ratio is held constant and for constant values of the other parameters (k_5 - k_7 discussed later) the macroscopic stress-strain curves scales proportionally one to each other. Based on these observations it is reasonable to assume the following relations:

$$\frac{k_1}{k_1^\infty} = \frac{k_2}{k_2^\infty} = \frac{k_3}{k_3^\infty} = \frac{k_4}{k_4^\infty} = \lambda$$

where $k_1^\infty, k_2^\infty, k_3^\infty$ and k_4^∞ are the asymptotic values of the same parameters.

Parameter k_5 governs the post-peak slopes of normal and deviatoric boundaries as well as the rate of shear behavior degradation due to tensile fracturing. This parameter modifies the slope of the softening branch of both macroscopic tension and compression stress-strain curves. From a physical point of view, k_5 can be interpreted as representative of mechanical interlocking and bridging effects occurring at the scale of aggregate particles. Such mechanical interaction is assumed in this study to be approximately age

independent, $k_5 - k_5^\infty = \text{constant}$, even though, arguably, age could have an effect on the behavior of the interface between aggregate and cement paste. As it will be shown later in this paper, this approximation does not limit the ability of the overall formulation to simulate relevant experimental data. Parameter k_6 scales vertically the normal stress boundary and the frictional cohesion. It affects also the so called “transition function” governing the behavior of the normal stress component as far as the volumetric-deviatoric coupling is concerned (see Appendix A and Di Luzio (2007) for a detailed discussion of the transition function). Macroscopically, an increase of k_6 leads to an increase of the tensile strength without significantly affecting the compressing strength. Consequently, it can be used to control the ratio between tensile strength and compression strength. As discussed earlier, experimental evidence

exists showing a decrease of such a ratio with age. This can be captured by setting:

$$k_6 = \begin{cases} k_6^0 - (k_6^0 - k_6^\infty)\lambda/\lambda_0 & \text{for } 0 \leq \lambda \leq \lambda_0 \\ k_6^\infty & \text{for } \lambda_0 \leq \lambda \leq 1 \end{cases} \quad 5.22$$

where k_6^0 and k_6^∞ are initial and asymptotic values, respectively, of the k_6 parameter.

modifies mainly the post-peak softening behavior under macroscopic compression: the smaller k_7 is, the steeper the macroscopic post-peak slope in compression results. This parameter can be then used to simulate embrittlement due to aging by setting k_7^0 and k_7^∞

In the microplane model M4 (Bazant et al. 2000), the constitutive relation in each microplane is defined by 1) incremental elastic relation and 2) stress-strain boundaries (softening yield limits) that cannot be exceeded. They may be regarded as strain dependent yield limits (Di Luzio and Bazant 2005). To account the effect of the self-healing on the material properties of concrete, the stress-strain boundary condition, F_N , on the normal component σ_N and ϵ_N , i.e. $\sigma_N \leq F_N(\epsilon_N)$ is modified. Since the self-healing induces a recovery of the strength, the expression of the boundary isn't modified but its current value is calculated as $F_N(\epsilon_N - \epsilon_N^{sh})$, where ϵ_N^{sh} is calculated as $\epsilon_N^{sh} = \lambda^{sh} \epsilon_N^*$ in which ϵ_N^* is the value of the maximum normal strain reached at the end of the cracking stage.

5.7. Numerical Results

The model, formulated as above, has been applied to simulate the case of normal strength concrete (NSC), pre-cracked at 1 months and immersed in water for 1 months.

Temperature, relative humidity, degree of reaction evolution and the degree of hydration, and self-healing recovery degree are obtained by solving the hygro-thermo-chemical problem imposing the environmental conditions described above. In Figure 5.2 the comparison between experimental and numerical results in terms of load crack opening response, highlights the reliability of the proposed model.

Figure 5.3 the evolution of the relative humidity for the specimen kept in water after the pre-cracking is presented.

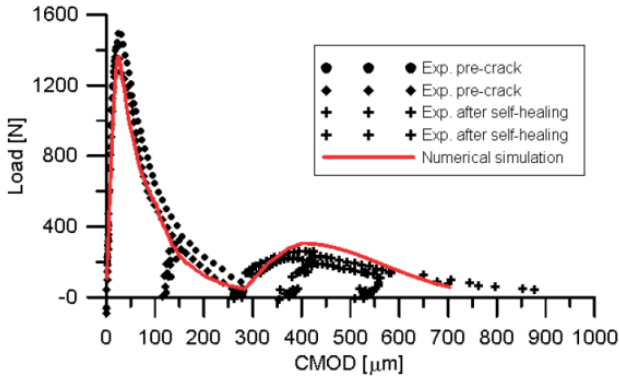


Figure 5.2. Load-COD curve obtained with 3pb tests from the same specimen before and after the 'self-healing'.

The comparison between the experimental and the numerical results in terms of the load vs. COD response is reported in Figure 5.2. A recovery of the load bearing capacity, with respect to the unloading value at which pre-cracking was performed in the first stage, is evident. A recovery of the flexural load equals to about 250 N is well reproduced by the numerical model, which corresponds to a recovery of about 17% of the maximum load capacity.

With reference to three-point-bending tests performed up to controlled crack opening and up to failure, respectively before and after exposure/conditioning recovery of stiffness and stress bearing capacity has been evaluated to assess the self-healing capacity.

The SMM model for concrete has been modified for incorporating the self-healing effects. The numerical example has shown that the proposed model properly describes the self-healing properties of a cementitious composite. Now, the numerical tool must be validated by simulating different hygro-thermal conditions and different concrete mixes.

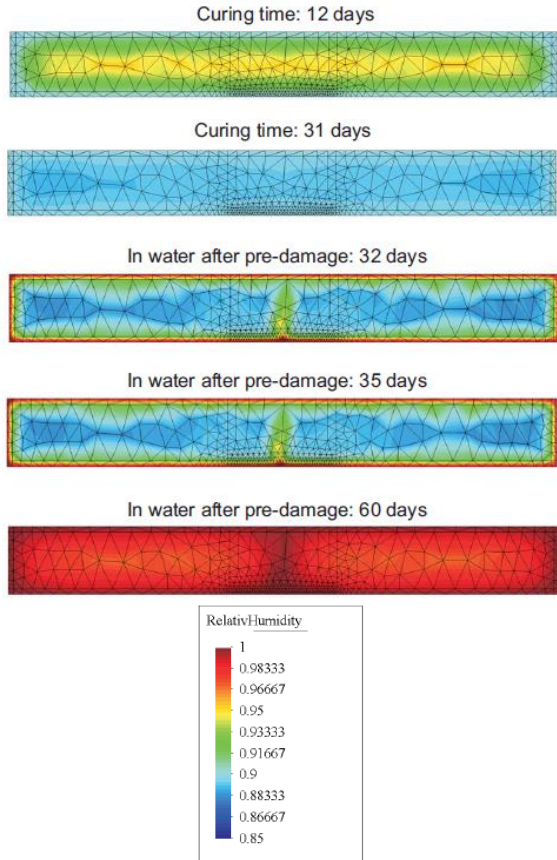


Figure 5.3. Relative humidity evolution in the longitudinal mid-plane of the specimen the curing (31 days) and the treatment in water (28 days).

5.8. Zero-Thickness Interface Formulation For Fracture Analysis For Self-Healing Concrete

5.8.1. Introduction

A discontinuous-based porosity-based model for concrete subjected to time-evolution self-healing phenomena is presented in this work. The model represents an extension of a fracture energy-based elasto-plastic interface formulation which now includes porosity evolution induced by self-healing mechanisms. The formulation accounts for the characterization of concrete failure behavior in mode I and II fracture types. The post-cracking response is considered by means of specific work softening rules in terms of work spent and porosity evolution. The self-healing in concrete specimens has also been investigated through an experimental program on normal strength concretes under different types of exposure such as air exposure and water immersion. The effects of the aforementioned phenomenon on the recovery of stiffness and load bearing capacities have been evaluated by means of three-point bending (3PB) tests performed up to controlled crack opening and up to failure, respectively, before and after conditioning. Such a tests are thus employed as benchmark to validate the proposed model formulation. Particularly, after outlining the mathematical formulation of the constitutive model for interface elements, numerical analysis are presented to validate its soundness and capability against these experimental data.

5.8.2. Zero-thickness interface model: general assumptions

This section summarizes the porosity dependent interface model formulated for analyzing the fracture behavior of quasi-brittle materials like concrete after self-healing processes. The model, based on a modification of the original proposal for interface elements [14], is characterized by the following constitutive equations written in rate format

$$\begin{aligned} \dot{\mathbf{u}} &= \dot{\mathbf{u}}^{el} + \dot{\mathbf{u}}^{cr} \\ \dot{\mathbf{u}}^{el} &= \mathbf{C}^{-1} \cdot \dot{\mathbf{t}} \\ \dot{\mathbf{t}} &= \mathbf{C} \cdot (\dot{\mathbf{u}} - \dot{\mathbf{u}}^{cr}) \end{aligned} \tag{5.23}$$

Where $\dot{\mathbf{u}} = [\dot{u}, \dot{v}]^t$ is the rate of the relative joint displacement vector decomposed into the elastic and plastic components, $\dot{\mathbf{u}}^{el}$ and $\dot{\mathbf{u}}^{cr}$, respectively. While, \mathbf{C} defines the normal/tangential elastic stiffness matrix,

$$\mathbf{C} = \begin{pmatrix} k_N & 0 \\ 0 & k_T \end{pmatrix} \tag{5.24}$$

The incremental stress vector is defined in the interface coordinates $\mathbf{t} = [\sigma_N, \sigma_T]^t$, being σ_N and σ_T the normal and shear components, respectively. In Eq. (5.3) the vector of the plastic displacement rate is defined according to the following non-associated flow rule

$$\dot{\mathbf{u}}^{cr} = \dot{\lambda} \mathbf{m} \tag{Equation 5.25}$$

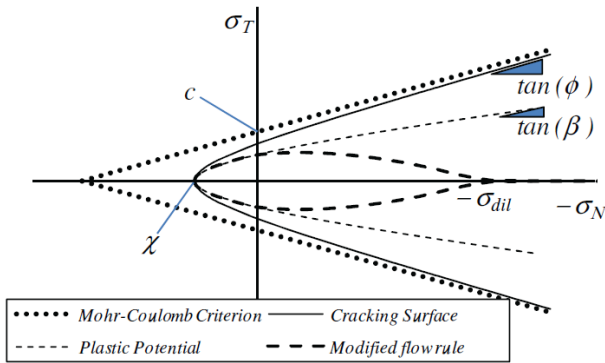


Figure 5.4. Failure hyperbola by Carol et al. [14], Mohr-Coulomb surface, plastic potential and modified flow rule.

where $\dot{\lambda}$ is the non-negative plastic multiplier derived from the classical Kuhn-Tucker loading/unloading and consistency conditions

$$\begin{aligned} \dot{\lambda} &\geq 0, & f &\leq 0, & \dot{\lambda}f &= 0 & \text{Kuhn - Tucker} \\ \dot{f} &= 0 & & & & & \text{Consistency.} \end{aligned} \tag{5.26}$$

In the above equations $f = f[\sigma_N, \sigma_T]$ outlines the yield condition of the model defined by means of the following three-parameter criterion (outlining the hyperbola represented in Figure 5.4)

$$f = \sigma_T^2 - (c - \sigma_N \tan \phi)^2 + (c - \chi \tan \phi)^2. \tag{5.27}$$

The tensile strength χ (vertex of the hyperbola), the cohesion c and the frictional angle Φ are material parameters needed for identifying the inelastic state of the interface model.

Eq. (5.21) describes the general non-associated flow rule which mainly controls the direction \mathbf{m} of interface fracture displacements. Particularly, the non-associated plastic direction is described by means of the transformation matrix operator \mathbf{A} as follows

$$\mathbf{m} = \mathbf{A} \cdot \mathbf{n} \tag{5.28}$$

where

$$\mathbf{n} = \frac{\partial f}{\partial \mathbf{t}} = \left[\frac{\partial f}{\partial \sigma_N}, \frac{\partial f}{\partial \sigma_T} \right]^t \tag{5.29}$$

the associated flow vector. Then, the transformation matrix \mathbf{A} in Eq. (5.24) has the following expression:

$$\mathbf{A} = \begin{cases} \begin{pmatrix} \frac{\tan \beta}{\tan \phi} & 0 \\ 0 & 1 \end{pmatrix} & \text{if } \sigma_N \geq 0 \\ \begin{pmatrix} \left[1 - \frac{|\sigma_N|}{\sigma_{dil}} \right] \frac{\tan \beta}{\tan \phi} & 0 \\ 0 & 1 \end{pmatrix} & \text{if } -\sigma_{dil} \leq \sigma_N < 0 \\ \begin{pmatrix} 0 & 0 \\ 0 & 1 \end{pmatrix} & \text{if } \sigma_N < -\sigma_{dil} \end{cases} \tag{5.30}$$

where β is the dilation angle of the plastic potential as highlighted in Figure 5.4 where $0 \leq \tan \beta \leq \tan \phi$. Thereby, the parameter σ_{dil} represents the normal stress at which the dilatancy vanishes

5.8.3. Fracture and Porosity-Based Softening Rules

The following unified function has been considered to account the softening rule of all internal parameters (controlling the evolution of the yield criterion in Eq. 5.23) under fracture processes which incorporates self-healing effects during the time

$$p_i = (1 - (1 - r_{pi}) S[\xi_{pi}]) SH[\psi] p_{0i} \quad 5.31$$

where p_i alternatively equals χ , c or $\tan \Phi$, being $p_i = p_{0i}$ their initial values and r_{pi} the residual parameters (Ferrara et. al).

5.8.3.1. Fracture-based scaling function

The proposed scaling function $S[\xi_{pi}]$ is expressed as follows

$$S[\xi_{pi}] = \frac{e^{-\alpha_{pi} \xi_{pi}}}{1 + (e^{-\alpha_{pi}} - 1) \xi_{pi}} \quad 5.32$$

based on the non-dimensional variable ξ_{pi} , which introduces the influence of the ratio between the current fracture work spent and the available fracture energies in mode I and II, G_f^I and G_f^{IIa} respectively,

$$\xi_\chi = \begin{cases} \frac{1}{2} \left[1 - \cos \left(\frac{\pi w_{cr}}{G_f^I} \right) \right] & \text{if } w_{cr} \leq G_f^I \\ 1 & \text{otherwise} \end{cases} \quad 5.33$$

$$\xi_c = \xi_{\tan \phi} = \begin{cases} \frac{1}{2} \left[1 - \cos \left(\frac{\pi w_{cr}}{G_f^{IIa}} \right) \right] & \text{if } w_{cr} \leq G_f^{IIa} \\ 1 & \text{otherwise} \end{cases} \quad 5.34$$

according to the C^1 continuity function proposed by Caballero et al., while the parameter α^2_{pi} , controls the decay form of such a scaling rule as shown in Figure 2.5

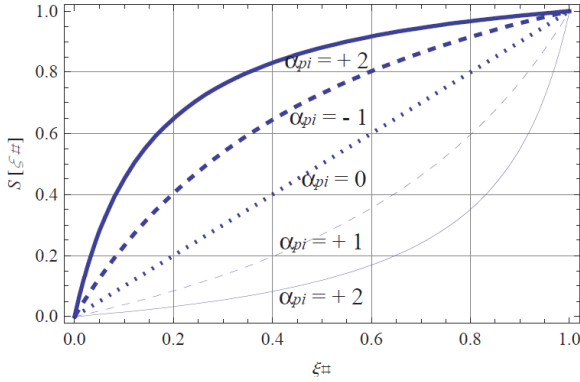


Figure 5.5. Scaling function $S[\xi_{\#}]$ (where $\# = p_i$) considering different values of $\alpha^2_{p_i}$

The fracture work spent ω_{cr} during the opening-sliding fracture process controls the actual evolutions of the material parameters χ , c and $\tan \Phi$, in softening regime of the interface constitutive law. The variable ω_{cr} , defining the necessary amount of released fracture work to open a single crack in tensile and/or shear fracture mode due to normal σ_N and/or tangential σ_T joint stresses, has been reported in (Etsé, Caggiano et al.)

5.8.3.2. Porosity-based scaling function

The proposed porosity-based rule for the self-healing description, namely $SH[\psi]$ in Eq.(5.27), is expressed as:

$$SH[\psi] = 1 + (1 - P_{p_i}[\psi])sh \quad 5.35$$

where sh (greater or equal than 0) is the self-healing scalar factor which interprets the recovery of the interface material properties due to the self-healing process. It is function of the porosity of the considered concrete through the following expression

$$P_{p_i}[\psi] = \frac{e^{-\theta_{p_i}\psi}}{1 + (e^{-\theta_{p_i}} - 1)\psi} \quad 5.36$$

where the ψ variable highlights the influence of the effective porosity as follows

$$\psi = \frac{1 - \cos\left(\pi \frac{\phi_c - \phi_0}{\phi_f - \phi_0}\right)}{2} \tag{5.37}$$

being Φ_c the effective porosity (Caballero et al.) in the interface plane, while Φ_o and Φ_f are two input parameters to be calibrated; Φ_o represents the maximum reachable value of the effective porosity in the concrete matrix: e.g., concrete, ideally without voids, can be represented with $\Phi_o=1$. Φ_f represents that value of the effective porosity at which the interface is totally softened: concrete with 100% of voids deals with $\Phi_f=0$. In Eq. (5.30) the parameter θ_{pi} accounts several possible shapes of the porosity description as highlighted in Figure 5.6

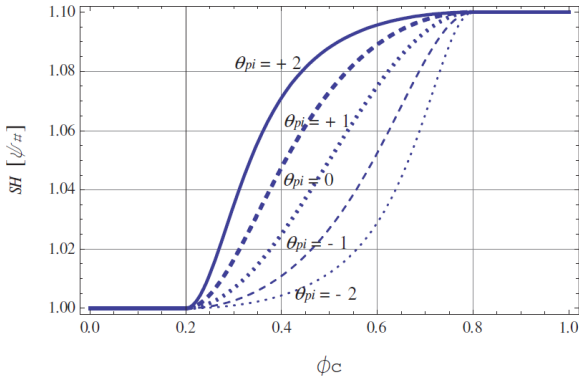


Figure 5.6. Porosity-based rule for the self-healing description $SH[\psi_{\#}]$ (with $\# = p_i$) against the effective porosity ϕ_c : as example the figure reports the case in which $\phi_0 = 0.8$ and $\phi_f = 0.2$.

5.8.4. Tangent Stiffness Operator

The interface elasto-plastic rate equations are obtained starting from the consistency condition of Eq. (5.22) which expands into

$$\frac{\partial f}{\partial \mathbf{t}} \dot{\mathbf{t}} + \frac{\partial f}{\partial \lambda} \dot{\lambda} + \frac{\partial f}{\partial \phi_c} \dot{\phi}_c = 0 \tag{5.38}$$

where the softening parameter $\bar{H} = -\frac{\partial f}{\partial \lambda}$ due to mechanical effects can be derived as

$$\bar{H} = -\frac{\partial f}{\partial \lambda} = -\frac{\partial f}{\partial p_i} \frac{\partial p_i}{\partial w_{cr}} \frac{\partial w_{cr}}{\partial \mathbf{u}^{cr}} \mathbf{m} \quad 5.39$$

while the porosity evolution is taken into account through the softening parameter I

$$I = -\frac{\partial f}{\partial \phi_c} = -\frac{\partial f}{\partial p_i} \frac{\partial p_i}{\partial \phi_c} \quad 5.40$$

The rate of the plastic multiplier follows from the combination between Equations (5.32), (5.19), (5.33) and (5.34)

$$\dot{\lambda} = \frac{\frac{\partial f}{\partial \epsilon} \cdot \mathbf{C} \cdot \dot{\mathbf{u}} - I \dot{\phi}_c}{\bar{H} + \frac{\partial f}{\partial \epsilon} \cdot \mathbf{C} \cdot \mathbf{m}} \quad 5.41$$

$$\dot{\mathbf{t}} = \mathbf{C}^{ep} \cdot \dot{\mathbf{u}} + \dot{\mathbf{t}}^\sigma[\dot{\phi}_c]. \quad 5.42$$

Then, the tangential interface stiffness for elastic degradation expands into

$$\mathbf{C}^{ep} = \left[\mathbf{C} - \frac{\mathbf{C} \cdot \mathbf{m} \otimes \mathbf{n} \cdot \mathbf{C}}{H + \mathbf{n} \cdot \mathbf{C} \cdot \mathbf{m}} \right] \quad 5.43$$

$$\dot{\mathbf{t}}^\sigma[\dot{\phi}_c] = \frac{I \dot{\phi}_c}{H + \mathbf{n} \cdot \mathbf{C} \cdot \mathbf{m}} \mathbf{C} \cdot \mathbf{m} \quad 5.44$$

5.8.5. Validation of the proposed interface model

This section aimed at demonstrating the validation of the proposed interface model. For the calibration purpose, experimental results on concrete specimens tested under three-point bending and presented in the work of for NSC are considered.

Figure 5.7 shows the geometry of the considered 100x50X450 mm³ concrete specimens while Figure 5.8 proposes the FE discretization

employed in the present analysis. Plane stress hypothesis and displacement-based control are assumed. Four-node iso-parametric elements, equipped with a linear elastic model, have been adopted in the FE mesh, while all non-linearities are concentrated within zero-thickness interfaces defined throughout the adjacent edges of the finite elements in the notched zone of the beam. Non-linear porosity and fracture-based laws were introduced in those interface elements according to the formulation outlined in Sections 5.7.2 and 5.7.3.

For the purpose of the numerical evaluations, a linear elastic material model was adopted for the concrete (describing the continuous elements), while the elasto-plastic interface model describes the non-linear response for the interface elements.

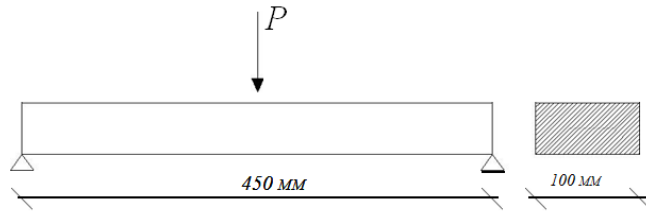


Figure 5.7. Specimen geometry according to experimental tests on 3PB

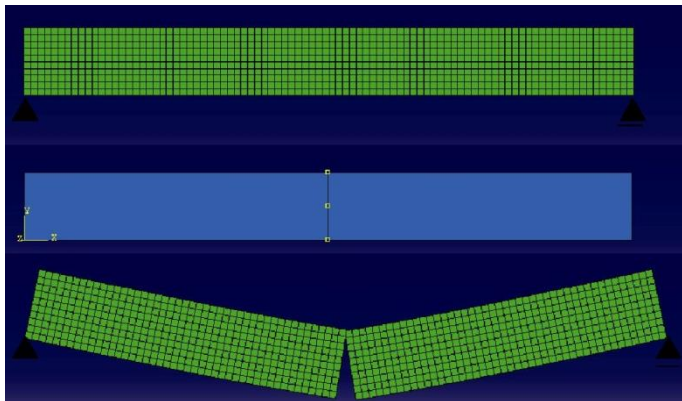


Figure 5.8. Finite element mesh, interfaces and possible crack path of the three-point bending.

The key geometric and material properties were chosen

according to the experimental evidences shown in the Capture 3. Based on the calibration procedure, the elastic modulus and Poisson's ratio of concrete was $E_c=21.7\text{GPa}$ and $\nu = 0.17$, respectively. Then, the mechanical parameters of the interface model are here listed: $k_N=500\text{ MPa/mm}$, $k_T = 200\text{ MPa/mm}$, $\tan \Phi_0=0.6$, $\tan \beta= 0.3$, $r_{\tan\Phi} = 0.67$, $\chi_o = 2.5\text{ MPa}$, $c_o = 5.0\text{ MPa}$, $G_I^I=0.065\text{N/mm}$, $G_{II}^{IIa}_f = 0.650\text{ N/mm}$, $\sigma_{dil}=10\text{ MPa}$, $\alpha = 0.5$, $\Phi_c = 0.46$, $\Phi_c=0.80$, $\Phi_f = 0.20$, $sh = 0.3$ and all remaining parameters were considered null.

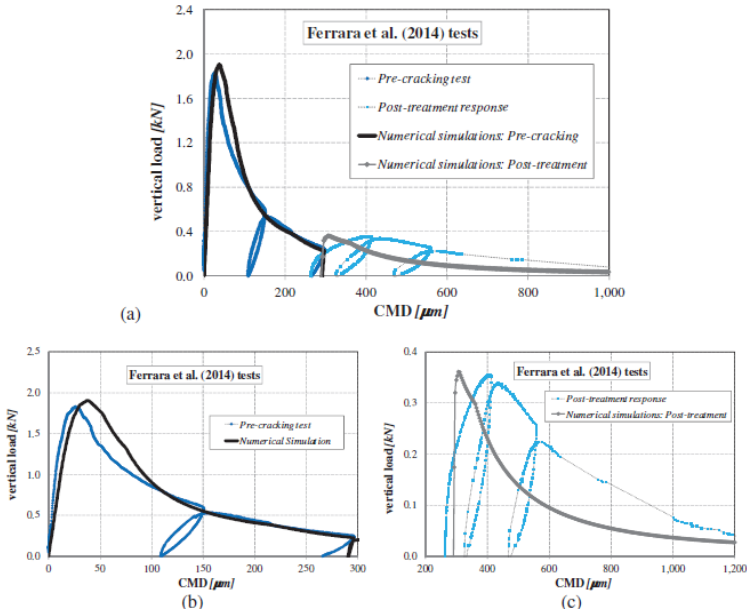


Figure 5.9. Load-deflection behavior on three-point beam: experimental results vs. numerical predictions

As example, Figure 5.9 shows the force-deflection curves against corresponding experimental results. It can be observed that the post-cracking response is well captured through the considered discontinuous approach based on non-linear interfaces. Furthermore, the comparison between the experimental and numerical results in terms of the load vs. crack opening displacement (COD) highlights as the model is able to predict the self-healing recovery of the load bearing capacity with respect to the unloading value at which the value decayed in the pre-cracking stage.

A recovery of the flexural load equals to about 250N is well reproduced by the numerical model, which corresponds to a recovery of about 17% of the maximum load capacity. However, and due to re-hydration self-healing phenomenon, a significant increase of the fracture energy takes place in the second-stage (post-treatment) of results of the analyzed three-point bending tests. This is introduced in the model throughout tabulated data which allows to give an opportune variation of the fracture energy against the porosity evolution. Particularly, based on the calibration data obtained from the numerical results, an increment of 12:07 % of fracture energy in mode I has to be considered for the proposed analyses presented in this section.

5.8.6. Concluding remarks

In this proposed model the formulation of a fracture and porosity-based interface for analyzing the self-healing capacity of cementitious composites has been simulated. Particularly, the proposed formulation explicitly modeled the porosity evolutions due to self-healing pore closures through functions which affect the strength parameters and softening rules of the proposed discontinuous model. Numerical analyses demonstrated the predictive capabilities of the constitutive model in terms of the most relevant aspects of the mechanical behavior of concrete after crack closure due to self-healing processes. The proposed interface model can be employed in mesoscopic analyses using mortar-mortar and mortar-aggregate interfaces aimed at simulating failure processes of concrete specimens under self-healing phenomenon. However, this aspect is beyond and will be addressed in future developments of the current research.

*It is not important the amount of your talent,
If you are not able to be part of a group or a community,
And if you give more importance to "I" than to "Us"*
Bernardo Rocha de Rezende

6. Conclusions and Future Perspectives

6.1. Conclusions

In this investigation a methodology has been proposed and validated to assess and quantify the effects of self-healing on the recovery of mechanical properties of different categories of cementitious composites, with and without crystalline admixtures, and under different exposure conditions. The proposed "three-step methodology" includes pre-cracking of specimens, natural or artificially accelerated environmental conditioning under different exposure conditions and, finally, fracture testing of the same specimens up to complete failure. The effects of self-healing is assessed and quantified by means of comparison between mechanical behavior parameters garnered through pre-cracking and failure tests on the same specimen. Tailored and thorough microstructural analyzes allowed to characterize the mechanism of the healing and thus provide sound justification to the observed microscopic

properties. Comparative data processing was performed also with the aim of defining self-healing indices, in terms of stiffness and load bearing capacity recovery, through which the ratio of crack closure, to the original crack opening, could be inferred.

All what has been herein discussed may open perspective for the use of these materials for the construction of new and the repair of existing structures.

The following conclusions can be described herein:

even normal strength concrete (NS) can exhibit an autogenous self-healing capacity, under favorable exposure conditions (high and continuous presence of water); this capacity is anyway high scattered;

- crystalline admixtures, are able, in NSC, to catalyze the aforementioned self-healing capacity recovery is more systematic and reliable due to their hydrophilic nature, they are also able to absorb moisture from the atmosphere thus results in a not negligible healing also in humid environment (not wet). This means there in effective and reliable engineered self-healing promoters;
- HPFRCCs possess an autogenous self-healing capacity as an outcome of the synergy between peculiar mix composition and crack control effect provided by the fibers. The performance of cracked and healed material can be even better there the one of an un-hydrated particles undergoing the same “curing” history, obviously as a function of crack opening, exposure conditions and duration. Cracking is in fact fundamental to expose to outdoor environment un-reacted cement/binder particles which can only in this way undergo delayed hydration and/or carbonation reactions responsible of self-healing.
- natural fibers, due to their hydrophilic nature, can absorb, even in not so favorable environmental conditions, water and/or humidity from outdoor environment and release it throughout the matrix. In this way they can effectively act as facilitator and enhancer of self-healing reactions;
- self-healing reactions can line to be a combination of delayed hydration and carbonation. The hydration products on the one hand deposit on the crack surfaces sealing and linking the cracked interfaces. On the other hand they enhance the quality of the fiber matrix-bond which also contributes to the recovery of the performance. The “facilitator” role of natural fibers has been demonstrated also in this case;
- a predictive model also to capture the essential of self-healing in NSC has been developed and effectively calibrated to be used also as a support for further investigation.

6.2. Future Perspectives

The experimental investigation presented in this dissertation is just a step in the framework of current and future investigations that are ongoing and planned to be performed. As described with the introduction nowadays code requests are not fulfilled mainly with reference to the structural stability but other issues such as sustainability, environmental integration (physical, social and historical), structural adequacy, economy, etc., need to be considered. Self-healing materials can offer a valuable solution to the solution to the aforementioned problems, contributing to increase the service life of engineering aspects and offer “greener” alternatives to civil engineering.

At the beginning of this work, the question was if self-healing is a concrete miracle, as called by Neville. As a matter of fact it has been shown through an extended experimental campaign that, self-healing if not a miracle, is a precious inherent capacity of cementitious composites, which can occur as a combined outcome of tailored mix design, controlled cracking and favorable exposure conditions the use of natural products of agricultural and food inherently which are widely available in poor and developing communities and countries. Their effectiveness as healing promoters would add a further significance to their inborn sustainable value as well as to the use of natural finer reinforced cementitious composites.

This surely deserves further investigation also in the sign of the several applications which could be foreseen for this category of materials.

Another interesting topic which deserves to be further investigated in view of its potential outcomes is the synergy between fiber reinforcement and crystalline/expansive self-healing admixtures because of the likely chemical pre-stressing effect of fibers which can be associated with the production of self-healing hydrates filling the crack and interacting with the fibers crossing.

It has also to be remembered that the knowledge of self-healing phenomena is now quite mature for the investigation to tackle coupled healing under sustained stress problems. This will provide valuable information more closely related to and representative of “true structural situations”

The development of sound, reliable and computationally effective predictive modelling tools has also to be continually pursued as it has been herein stated.

This will finally allow to “embed” as the self-healing into the design procedure, enabling the designer to “select” in a coherent

engineering framework the most suitable healing solution for the intended application in view of the required and expected performance.

References

- [1] Padea C., Guimaraes M., “The CO₂ uptake of concrete in a 100 year perspective”, Portland, Research and Development Center, Denmark, 2007
- [2] van Oss H.G., Padovani A.C.: “Cement Manufacture and the Environment, Part II: Environmental Challenges and Opportunities”, *Journal of Industrial Ecology* 7, 2003, Nop,1:pp.93-126
- [3] Fratzi K., Wagermaier R., Dunlop J.W.C., and Harrington, M.J.: “Bio-Inspiration From Naturally Healing Tissues”, Proceedings of Self-Healing Int. Conf. pp.406-4013
- [4] Model Code 2010, 1st complete draft, (2010), 1 vol., 2 vol.
- [5] Van Breugel K. “Is There a Market for Self-Healing Cement Based Materials?”, 1st International Concrete on Self-Healing Materials, Noordwijk, Holland (2007)
- [6] Van Breugel. K. “Self-healing material concepts as solution for aging infrastructure”, 37th Conference on our world in concrete & structures: 29 – Singapore (2012)
- [7] Li. M., Ranade R., Kan L., and Li V. C., “On Improving the Infrastructures Service Life Using ECC to Mitigate Rebar Corrosion”, 2nd International Symp. on Service Life Design for Infrastructure, 2010, no. 1.
- [8] Thompson, A.W., “On growth and Form” University of Cambridge, Dover Publications, edited (1992)
- [9] Weinkamer, R., Fratzi, P., “Mechanical Adaption of Biological Materials” Materials Science and Engineering, C31, 1164-1173 (2011).
- [10] Ghosh. S.K., “Self-healing Materials: Fundamentals, Design Strategies and applications”, 2009, Wiley-Vch Verlag GmbH&KgaA, 1-27
- [11] Qian, S., Zhou, J., De Rooij, M. R., Schlangen, E., Ye, G., & Van Breugel, K. (2009). Self-healing behavior of strain hardening cementitious composites incorporating local waste materials. *Cement and Concrete Composites*, 31(9), 613-621.
- [12] Abrams A. Autogenous Healing of Concrete [J]. *Concrete*, 1925: 10-50.
- [13] Gilkey H. J.–“Annual Survey of the American Chemistry”, Volume V, p.453, 1930
- [14] Whitehurs E. A. “Soniscope Tests Concrete Structures”, *ACI Journal*, February 191, 1951, Proc. V., pp. 433-444

References

- [15] Lauer, K.R. and Slate, F.O.: "Autogeneous healing of cement paste". *ACI Journal*, 1956. Vol.52, No. 6, pp.1083-1097.
- [16] Dhir, R. K., Sangha C. M. and Munday J. G. – "Strength and Deformation Properties of Autogenously Healed Mortars", *ACI J.* (1973); 70; 231-236.
- [17] Van Tittelboom K., Snoeck D., Wang J., and De Belie, N.: "Most recent advances in the field of self-healing cementitious materials", *Proceedings of Self-Healing Int.Conf.* pp.406-4013, 2013
- [18] Lepech M.D, Li V.C.: "Water Permeability of Engineered Cementitious Composites. *Cement & Concrete Journal Composites*", 31, 2009, pp.744-753
- [19] Edvardsen, C. "Water permeability and autogenous healing of cracks in concrete". *ACI Mater.J.* 1999, 96, 448–454
- [20] Lubelli, B., Nijland, T.G, Van Hees, R.P., "Self-Healing of Lime Based Mortars: Microscopy Observations on Case Studies" TU Delft Publ. March, (2011)
- [21] Neville, A., "Autogenous Healing-A Concrete Miracle?" *Concrete International*, 24, 2002, pp.76-82
- [22] M.R. Kessler, "Self-Healing: "A new paradigm in material design", *Journal of Aerospace Engineering*", V.221, Part G, 2007, pp.479-495
- [23] E. Schlangen, *Self-Healing Phenomena in Cement-Based Materials*. 2013.
- [24] Mihashi H, De Leite JPB. "State of the art report on control of cracking in early age concrete". *J. Adv. Concrete and Technology*, 2004; 2(2): 141-54
- [25] N. Ter Heide, "Crack healing in hydrating concrete," *Delft University of Technology*, 2005.
- [26] Hearn N., "Self-sealing , autogenous healing and continued hydration : What is the difference ?" *Mater. Struct.*, vol. 31, no. October, pp. 563–567, 1998.
- [27] De Rooij, M., Van Tittelboom, K., De Belie, N., Schlangen, E.: "State-of-the-Art Report of RILEM Technical Committee 221-SHC: Self-Healing Phenomena in Cement-Based Materials" , Vol. 11, 2013
- [28] Hearn N. and Morley C. T., "Self-sealing property of concrete Experimental evidence", *Mater. Struct.*, vol. 30, no. September, pp. 404–411, 1997.
- [29] Le Roy-Delage S., Guillot D., Dismuke K., Nelson E.,- "Self adaptive cement systems", U. S. Patent App. Publication, Pub. No.: US 2007/0137528 A, 2007
- [30] Yooa D.Y., Leec J.H., Yoona S.Y., "Shrinkage and Cracking of restrained ultra-high performance fiber-reinforced concrete slabs at early age" *Construction and Building Materials*,30, pp. 357-365 (2014)
- [31] Ahn T.H. & Kishi T., "The effect of geo-materials on the autogenous healing behavior of cracked concrete", *Conc. Repair, Reh. and Retr. II – 2009*
- [32] He H., Guo Zh., Stroeven P., Hu J. and Stroeven M., "Computer Simulation Study Of Concrete's Self-Healing Capacity Due To Un-hydrated Cement Nuclei In Interfacial Transition Zones", *Proceedings of the First International Conference on Self-Healing Materials*, 2007
- [33] Buchholz F. and A. Graham "Superabsorbent polymer technology" *J.M.*, 1998
- [34] Snoeck D., Van Tittelboom K., Steuperaert S, Dubrueel P., De Belie N., "Self-healig cementitious materials by the combination of microfibres and superabsorbent polymers" *Journal of Intelligent Material Systems and Structures* 25 (1), 13-24, (2014)

References

- [35] Kim J.S., Schlangen E., “*Super absorbent polymers to simulate self-healing in ECC*”, 2nd International Symposium on Service Life Design, 2010
- [36] Ferrara L., Krelani, V., P. Bamonte, G. B. E., “*An experimental methodology to assess the self-healing capacity of cementitious composites with “aero-crystallizing” additives*”, 2012
- [37] Ferrara, L. and Krelani, V. (2013). *A fracture testing based approach to assess the self-healing capacity of cementitious composites*, in Proceedings 8th Inte. Con. on Fracture Mechanics of Conc. and Conc. Str., FraMCoS-8, 10-14, pp. 331-340, 2013
- [38] Ferrara, L., Krelani, V., Geminiani, M. and Gorlezza, R.: “*Self-healing capacity of high performance fiber reinforced cementitious composites*”, in Proceedings fib2014 World fib Symposium, Mumbai, India, 10-14 February 2014.
- [39] Reinhardt H-W. and Jooss M., “Permeability And Self-Healing Of Cracked Concrete As A Function Of Temperature And Crack Width”, *Cement & Concrete Research*, 33: 981-985. (2003).
- [40] Powers T.C., Brownard T.L.: “Studies of the physical properties of hardened Portland cement paste”, *Am Concr Inst Proc*, 43 (1946), pp. 469–482
- [41] Fagerlund, M. Hassanzadeh G.; “Self-Healing Of Cracks In Concrete Exposed To Different Types Of Water - Effect On Chloride Penetration,” Lund, 2011
- [42] W. Ramm and M. Biscop, “Autogenous healing and reinforcement corrosion of water-penetrated separation cracks in reinforced concrete,” *Nucl. Eng. Des.*, vol. 179, no. 2, pp. 191–200, Feb. 1998
- [43] D’ambrosia M. D., “Early Age Creep And Shrinkage Of Emerging Concrete Materials”, Dissertation, University of Illinois at Urbana-Champaign, 2011
- [44] Mario C., - “*Scienza e tecnologia del calcestruzzo*”, Edizione Hoepli. (1987)
- [45] Ferrara L., Ferreira, S.R., Krelani, V. et al. “Effect of natural fibres on the self-healing capacity of high performance fibre reinforced cementitious composites”, *Proceeding SHCC3*, (2013)
- [46] P. Termkhajornkit, T. Nawa, Y. Yamashiro, and T. Saito, “Self-healing ability of fly ash–cement systems,” *Cem. Concr. Compos.*, vol. 31, no. 3, pp. 195–203, Mar. 2009.
- [47] S. Hee Kang, T. Ahn, D. Kim. “Effect of grain size on the mechanical properties and crack formation of HPRFRCC containing deformed steel fibers” *J Cement and Concrete Research*, 11(2011)
- [48] Y. Yang, M. D. Lepech, E.-H. Yang, and V. C. Li, “Autogenous healing of engineered cementitious composites under wet–dry cycles,” *Cem. Concr. Res.*, vol. 39, no. 5, pp. 382–390, May 2009
- [49] Gagne R., Argouges M., “A study of the natural self-healing of mortars using air-flow measurements”, *Materials and Structures* 45:1625–1638, (2012)

References

- [50] V. Mechterine. "Towards a durability framework for structural elements and structures made of", *Constr. and Building Materials*,31 (2012): 94-104 Rec 2011
- [51] C.M. Aldea, W.J. Song, J.S. Popovics,"Extent of healing of cracked normal strength concrete", *ASCE J Mater Civ Eng*, 2 (2000), pp. 92–96
- [52] Aldea. C.M., Song., W.J., Popovics, J.S., Shah. S.P., "Extent of Healing of cracked Normal Strength Concrete" *Journal of Materials in Civil Engineering*, February (2000).
- [53] Şahmaran, Mustafa, et al. "*Self-healing of mechanically-loaded self-consolidating concretes with high volumes of fly ash.*" *Cement and Concrete Composites*, 30.10 (2008): 872-879.
- [54] Ferrara L., Gettu R. and Albertini I., "Self-healing properties of steel fiber reinforced concrete with different additions" December, 2014
- [55] E. J. Jacobsen, S.; Sellevold, "*Self-Healing Of High Strength Concrete After Deterioration By Freeze/Thaw,*" *Cem. Concr. Res.*, vol. 26, no. 1, pp. 55–62, 1996
- [56] R. Abdel-Jawad, Y.; Haddad, "Effect Of Early Overloading Of Concrete On," *Cem. Concr. Res.*, vol. 22, no. 2, pp. 927–936, 1992.
- [57] Y. Yang, Yang E.H., and V. C. Li, "Autogenous healing of engineered cementitious composites at early ages," *Cem. Concr. Res.*, vol.41, pp.176–183, (2011)
- [58] S. Granger, a. Loukili, G. Pijaudier-Cabot, and G. Chanvillard, "Experimental characterization of the self-healing of cracks in an ultra high performance cementitious material: Mechanical tests and acoustic emission analysis," *Cem. Concr. Res.*, vol. 37, no. 4, pp. 519–527, Apr. 2007.
- [59] R. Tarun, et al., "Permeability of concrete containing large amounts of fly ash" *Cem Concr Aggregates*, 24 (5) (1994), pp. 913–922
- [60] Yu, Zhuqing, and Guang Ye. "The pore structure of cement paste blended with fly ash." *Construction and Building Materials* 45 (2013): 30-35.
- [61] Şahmaran M., Keskin S. B., Ozerkan G., and Yaman I. O., "Self-healing of mechanically-loaded self-consolidating concretes with high volumes of fly ash," *Cem. Concr. Compos.*, vol. 30, no. 10, pp. 872–879, Nov. 2008.
- [62] Qian, S. Z., J. Zhou, and E. Schlangen. "Influence of curing condition and precracking time on the self-healing behavior of Engineered Cementitious Composites." *Cement and concrete composites* 32.9 (2010): 686-693.
- [63] T. Kishi, T. Ahn, A. Hosoda, S. Suzuki, And H. Takaoka, "Self-Healing Behaviour By Cementitious Recrystallization Of Cracked Concrete," In *First International Conference On Self-Healing Materials*, 2007, No. April, Pp. 1–10.
- [64] S. Chaturvedi, R. Chandra, and V. Rai, "Isolation and characterization of *Phragmites australis* (L.) rhizosphere bacteria from contaminated site for bioremediation of colored distillery effluent," *Ecol. Eng.*, vol. 27, no. 3, pp. 202–207, Oct. 2006.
- [65] A. Gross, D. Kaplan, and K. Baker, "Removal of chemical and microbiological contaminants from domestic greywater using a recycled vertical flow bioreactor (RVFB)," *Ecol. Eng.*, vol. 31, no. 2, pp. 107–114, Oct. 2007.
- [66] M. R. Gollapudi, U.K.; Knutson, C.L.; Bang, S.S. and Islam, "A New Method For Controlling Leaching Through Permeable Channels," *Chemosphere*, vol. 30, no. 4, pp. 695–705, 1995

References

- [67] S. S. Ramachandran, S.K.; Ramakrishnan, V. and Bang, "Remediation of Concrete Using Micro-Organisms," *ACI Mater. J.*, p. 9, 2001.
- [68] K. Van Tittelboom, N. De Belie, W. De Muynck, and W. Verstraete, "Use of bacteria to repair cracks in concrete," *Cem. Concr. Res.*, vol. 40, no. 1, pp. 157–166, Jan. 2010.
- [69] J. Wang, K. Van Tittelboom, N. De Belie, and W. Verstraete, "Use of silica gel or polyurethane immobilized bacteria for self-healing concrete," *Constr. Build. Mater.*, vol. 26, no. 1, pp. 532–540, Jan. 2012.
- [70] R. Siddique and N. K. Chahal, "Effect of ureolytic bacteria on concrete properties," *Constr. Build. Mater.*, vol. 25, no. 10, pp. 3791–3801, Oct. 2011.
- [71] E. Schlangen, H. Jonkers, S. Qian, and A. Garcia, "Recent advances on self-healing of concrete," in *FRAMCOS7*, 2010.
- [72] H. M. Jonkers, A. Thijssen, G. Muyzer, O. Copuroglu, and E. Schlangen, "Application of bacteria as self-healing agent for the development of sustainable concrete," *Ecol. Eng.*, vol. 36, no. 2, pp. 230–235, Feb. 2010.
- [73] V. Wiktor and H. M. Jonkers, "Quantification of crack-healing in novel bacteria-based self-healing concrete," *Cem. Concr. Compos.*, vol. 33, no. 7, pp. 763–770, Aug. 2011.
- [74] Romualdi, J.P, Batson, G.B.; (1964). Tensile strength of concrete affected by uniformly distributed and closely spaced short lengths of wire reinforcement. *ACI Journal*, 61(6), pp 657–672.
- [75] Romualdi J.E., Shah. S.P.; (1979). Fracture and Multiple Cracking of Cementitious Composites. In S.W. Freiman, editor, *Fracture Mechanics applied to Brittle Materials*. Proceedings of the 11th National Symposium on Fracture Mechanics ASTM, pp 183–201.
- [76] ACI Committee 544 (1988a). Design Considerations for Steel Fiber Reinforced Concrete. *ACI Structural Journal*, 85(5), pp 563-580.
- [77] Naaman, A., Reinhardt, H.; (2006). "Proposed classification of hprc composites based on their tensile response". *Materials and Structures*, 39(5), pp 547–555.
- [78] Ozyurt, N., Woo, L.Y., Mason, T.O. and Shah, S.P.; (2006) Monitoring fiber dispersion in fiber reinforced cementitious materials: comparison of AC Impedance Spectroscopy and Image Analysis. *ACI Materials Journal*, 103 (5), pp 340-347
- [79] Ferrara, L., di Prisco, M.; (2001) Mode I Fracture behavior in concrete: Nonlocal damage modelling, *ASCE Journal of Engineering Mechanics*, pp 678-692.
- [80] L. Ferrara, Y.D. Park, S. Shah. A method for mix-design of fiber-reinforced self-compacting concrete. *CEM. AND Concr. Res.*, 37 (2007) 957-971
- [81] Ferrara, L., Park, Y.D. and Shah, S.P.; (2008). Correlation among fresh state behaviour, fiber dispersion and toughness properties of SFRCs. *ASCE Journal of Materials in Civil Engineering*, 20(7), pp 493-501
- [82] Ferrara, L., di Prisco, M., Lamperti, M.G.L.; , (2010). Identification of the stress–crack opening behavior of HPRCC: the role of flow-induced fiber orientation. In: Oh BH et al (eds) *Proceedings FramCoS 7*, Jiejiu, South Korea. pp 1541–1550.
- [83] Ferrara, L., di Prisco, M.; (2011). The role of fiber orientation on strain gardening/softening FRCCs: continuum damage modelling. RIO-SHCC2 RILEM international conference, Rio de Janeiro, Brasil.

References

- [84] L. Ferrara, M. Faifer, S. Toscani. A magnetic method for non destructive monitoring of fiber dispersion and orientation in steel fiber reinforced cementitious composites-part 1: method calibration, 2011, *Materials and Structures*, 45:575-589, 2012
- [85] Ferrara, L., Faifer, M., Muhaxheri, M., Toscani, S.; (2012). A magnetic method for non destructive monitoring of fiber dispersion and orientation in steel fiber reinforced cementitious composites: part 2: correlation to tensile fracture toughness. *Materials and Structures*, 45(4), pp 591-598.
- [86] Ferrara, L., Ozyurt, N., di Prisco, M.; (2011). High mechanical performance of fiber reinforced cementitious composites: the role of “casting-flow” induced fiber orientation. *Materials and Structures*, 44(1), pp 149–168.
- [87] Ferrara, L., Faifer, M., Muhaxheri, M., Toscani, S., Ottoboni, R.; (2011) “Sull’impiego di materiali cementizi fibrorinforzati ad alte prestazioni: dall’orientamento delle fibre all’ortotropia del comportamento meccanico” *Atti Giornate Aicap 2011*, Padova. pp 513-520
- [88] Ferrara, L., Faifer, M., Muhaxheri, M., Toscani, S.; (2012). Connecting Non-destructive Fiber Dispersion Measurements with Tensile HPRFCC Behavior High Performance Fiber Reinforced Cement Composites 6 RILEM State of the Art Reports 2, pp 43-50.
- [89] Ferrara L., Bottoni S., “Cacestruzzo fibrorinforzante autocompatante: analisi della disposizione delle fibre mediante l’uso di un fluido modello”, *Politecnico di Milano*, 2013
- [90] Yang Y, Yang E.H, and V. C. Li, “Autogenous healing of engineered cementitious composites at early age,” *Cement and Concrete Research*, 41, pp. 176–183, 2011
- [91] D. J. Hannant and J. G. Keer, “Autogenous healing of thin cement based sheets,” *Cem. Concr. Res.*, vol. 13, no. 3, pp. 357–365, 1983.
- [92] R. J. Gray and B. Shear, “Autogeneous Healing Of Fibre/Matrix Interfacial Bond In Fibre-Reinforced Mortar,” *Cem. Concr. Res.*, vol. 14, no. c, pp. 315–317, 1984.
- [93] D. Homma, H. Mihashi, and T. Nishiwaki, “Self-Healing Capability of Fibre Reinforced Cementitious Composites,” *J. Adv. Concr. Technol.*, vol. 7, no. 2, pp. 217–228, 2009.
- [94] Kan L.L., Shi H.S., Saulich A.R and V. C. Li, “Self-Healing of engineered cementitious composites materials,” *ACI Journal*, (6), 2010
- [95] E. Tziviloglou, “Self-healing in ECC materials with low content of different micro-fibers and micro-particles,” *Delft University of technology*, 2009.
- [96] S. Antonopoulou, “MSc-thesis Self-healing in ECC materials with high content of different micro-fibres and micro-particles,” *Delft University of Technology*, 2009.
- [97] M. R. De Rooij, S. Qian, H. Liu, W. F. Gard, and J. W. G. Van De Kuilen, “Using natural wood fibers to self-heal concrete,” *Concr. Repaiir, Rehabil. Retrofit. II*, pp. 229–234, 2009.
- [98] S. R. Ferreira, M. Della Torre, V. Krelani, L. Ferrara, F. de Andrade Silva, and R. D. T. Filho, “Effect of natural reinforcement on self-healing capacity of cement based composite Saulo Rocha Ferreira,” 2014.
- [99] Y. Ohama, “Recent Progress in Concrete-Polymer Composites,” *Adv. Cem. Based Mater.*, pp. 31–40, 1997.
- [100] M. Abd Elmoaty, “Self-healing of polymer modified concrete,” *Alexandria Eng. J.*, vol. 50, no. 2, pp. 171–178, Jun. 2011.

References

- [101]P. Łukowski and G. Adamczewski, "Self-repairing of polymer-cement concrete," *Bull. Polish Acad. Sci. Tech. Sci.*, vol. 61, no. 1, pp. 195–200, Jan. 2013.
- [102]J. S. Kim and E. Schlangen, "Self-Healing In Ecc Stimulated By Sap Under Flexural Cyclic Load," in 3rd International Conference on Self-Healing Materials, 2011, no. June.
- [103]K. Van Tittelboom and N. De Belie, "Self-Healing in Cementitious Materials—A Review," *Materials (Basel)*, vol. 6, pp. 2182–2217, May 2013.
- [104]S. R. White, N. R. Sottos, P. H. Geubelle, J. S. Moore, M. R. Kessler, S. R. Sriram, E. N. Brown, and S. Viswanathan, "Autonomic healing of polymer composites.," *Nature*, vol. 409, no. 6822, pp. 794–7, Feb. 2001.
- [105]Dry, C.M. Smart multiphase composite materials that repair themselves by a release of liquids that become solids. In Proceedings of Symposium on Smart Structures and Materials, Orlando, FL, USA, 10–12 October 1994.
- [106]H. Huang and G. Ye, "Application of sodium silicate solution as self-healing agent in cementitious materials," *Delft*, 2011.
- [107]A. Pelletier, M.M.; Brown, R.; Shukla, A. and Bose, "Self-healing concrete with a microencapsulated healing agent," Kingston.
- [108]C. Joseph, R. Lark, B. Isaacs, D. Gardner, and A. D. Jefferson, "Experimental investigation of adhesive-based self-healing of cementitious materials," *Mag. Concr. Res.*, vol. 62, no. 11, pp. 831–843, Nov. 2010.
- [109]S. V. Zemskov, H. M. Jonkers, and F. J. Vermolen, "Two analytical models for the probability characteristics of a crack hitting encapsulated particles: Application to self-healing materials," *Comput. Mater. Sci.*, vol. 50, no. 12, pp. 3323–3333, Jul. 2011.
- [110]S. Sangadji and E. Schlangen, "Self Healing of Concrete Structures - Novel Approach Using Porous Network Concrete," *J. Adv. Concr. Technol.*, vol. 10, no. 5, pp. 185–194, 2012.
- [111]S. Sangadji And E. Schlangen, "Porous Network Concrete: A New Approach To Make Concrete Structures Self-Healing Using Prefabricated Porous Layer," In 3rd International Conference On Self-Healing Materials, 2011, No. June.
- [112]Gardner, D., Jefferson, A., Hoffman, A., & Lark, R. (2014). Simulation of the capillary flow of an autonomic healing agent in discrete cracks in cementitious materials. *Cement and Concrete Research*, 58, 35-44.
- [113]Mihashi, H., KANEKO, Y., Nishiwaki, T., & Otsuka, K. (2001). Fundamental study on development of intelligent concrete characterized by self-healing capability for strength. *Transactions of the Japan Concrete Institute*, 22, 441-450.
- [114]Anderton G.L., "Evaluation Of Asphalt Rubber Binders In Porous Friction Courses", US Army corps of engineers, Interim Report CPAR-GL-92-1, 1992
- [115]Zwaag, S. (Ed.). (2008). *Self-healing materials: an alternative approach to 20 centuries of materials science*. Springer Science+ Business Media BV.
- [116]Rilem Self-Healing Report 2014 Road Materials and Pavement Design. ICAM 2009
- [117]Qiu, J., Van de Ven, M. F. C., Wu, S., Yu, J., & Molenaar, A. A. A. (2009). "Investigating the self-healing capability of bituminous binders". *Road Materials and Pavement Design*, 10(sup1), 81-94.
- [118]Bonnaure, F., A. Gravois, and J. Udron, "A New Method for Predicting The Fatigue Life of Bituminous Mixes," *Association of Asphalt Paving Technologists*, Vol. 49 Proc., Louisville, KY, Feb 1980.

References

- [119] Highway Agency Et Al, “Design Manual For Roads And Bridges. Pavements Design And Maintenance”, Pavement Design, Vol 7 HD, 2/01, 2001. The Stationery Office, London.
- [120] Van Dijk W., Moreaud H., Quedeville A., Uge P., “The fatigue of bitumen and bituminous mixes”, Proc. 3th int. Conference on the Structural Design of Pavements, London, September 11-15, 1972, p. 354-366.
- [121] Castro M, Sánchez JA (2006). Fatigue and healing of asphalt mixtures: discriminate analysis of fatigue curves. *Journal of Transportation Engineering* 132(2):168-174.
- [122] Carpenter SH, Shen S (2006). A dissipated energy approach to study HMA healing in fatigue. In *Transportation Research Record No:1970. Journal of the Transportation Research Board*:178-185.
- [123] Garcia, A., Schlangen, E., van de Ven, M., & Liu, Q. (2009). Electrical conductivity of asphalt mortar containing conductive fibers and fillers. *Construction and building materials*, 23(10), 3175-3181.
- [124] Grant TP (2001). Determination of asphalt mixture healing rate using the Superpave indirect tensile test. Master thesis, University of Florida, America.
- [125] Liu, Q., García, Á., Schlangen, E., & Ven, M. V. D. (2011). Induction healing of asphalt mastic and porous asphalt concrete. *Construction and Building Materials*, 25(9), 3746-3752.
- [126] Santagata, E., Baglieri, O., Tsantilis, L., & Dalmazzo, D. (2013). Evaluation of self-healing properties of bituminous binders taking into account steric hardening effects. *Construction and Building Materials*, 41, 60-67.
- [127] M.R. Kessler, “Self-Healing: A new paradigm in material design”, *Journal of Aerospace Engineering*, 2007
- [128] Van Tittelboom and De Belie, N.: “Self-healing in cementitious materials—A review. *Materials*, 6(6), 2182-2217.
- [129] Kan, L. L., Shi, H. S., Sakulich, A. R., & Li, V. C. (2010). Self-healing characterization of engineered cementitious composite materials. *ACI Materials Journal*, 107(6).
- [130] J. Y. Wang, N. De Belie, and W. Verstraete, “Diatomaceous earth as a protective vehicle for bacteria applied for self-healing concrete.,” *J. Ind. Microbiol. Biotechnol.*, vol. 39, no. 4, pp. 567–77, Apr. 2012.
- [131] R.P. Wool and K.M. O’Conner, “A theory of crack healing in polymers”, *J. Apl. Phys.* 1981
- [132] R.S. Trask, I.P. Bond, “Biomimetic self-healing of advanced composite structures using hollow glass fibers”, *Smart Mater. Struct.*, 2006, 15, 704-710
- [133] E.N. Brown, S.R. White, N.R. Sottos, “Retardation and repair of fatigue cracks in a microcapsule toughened epoxy composite, Part I: Manual infiltration, *Comp. Sci. Techno.*, 65, 2466-2473, 2005
- [134] de Rooij, M., Van Tittelboom, K., De Belie, N., & Schlangen, E. (2011). Self-healing phenomena in cement-based materials. Draft of State-of-the-Art report of RILEM Technical Committee.
- [135] Zhang, M., Han, N., Xing, F., & Schlangen, H. E. J. G. “Design of microcapsule system used for self-healing cementitious material”, *Proceedings of Fourth Int. Conf. on Self-Healing Mat.*, (2013) , p.12-15
- [136] Zemskov, S. V., Copuroglu, O., & Vermolen, F. J., “Interactive mathematical model of self-healing in carbonated cementitious materials”, *Proceedings of Fourth Int. Conf. on Self-Healing Mat.*, (2013), p. 134-137

- [137] Perelmuter, M. (2013). "Bridged crack approach to model materials self-healing", Proceedings of Fourth Int. Conf. on Self-Healing Mat., (2013), p. 138-141
- [138] Schlangen, E., & Joseph, C. "Modelling of Self-Healing Cementitious Materials", In *Self-Healing Phenomena in Cement-Based Materials*, Springer Netherlands. (2013), pp. 217-240
- [139] He, H., Guo, Z., Stroeven, P., Stroeven, M.: "Numerical assessment of concrete's self-healing potentials for promoting durability". *Int. J. Modelling, Identification and Control* 7(2), 142–147 (2009) S. Sangadji and E. Schlangen, "Self-healing of Concrete Structures - Novel Approach Using Porous Network Concrete," *J. Adv. Concr. Technol.*, vol. 10, no. 5, pp. 185–194, 2012.
- [140] Sugama, T. and Gawlik, K. (2003) *Materials Letters*, 57, 4282–90.
- [141] European Concrete Societies Network, *European Concrete Award 2014*, p.13
- [142] V. Wiktor, H. M. Jonkers, Boelens R., Goedhart J., Jagers S., Oldenkamp R., "A concrete solution for a concrete problem," Image Foundation
- [143] Loh G., "Microscopic Analysis On The Concrete Cores From Retaining Walls At Changhai Airport, Terminal 3", Reverton Engineering, Test Report, A6127/chf
- [144] Collepardi M. (2003) - "Il nuovo calcestruzzo", Edizioni Tintoretto.
- [145] UNI EN 12390-3 - "Hardened Concrete Testing– Part 3: Compression Strength Of The Specimen".
- [146] UNI EN 12390-5 - "Hardened Concrete Testing – Part 5: Compression Flexure Of The Specimen".
- [147] Pinto, R. C., Medeiros, A., Ivo, J. P., & Andrade, P. B. (2007). Use of ultrasound to estimate depth of surface opening cracks in concrete structures.
- [148] Maeda N. - "A method for reading and checking phase times in auto-processing system of seismic wave data", (1985).
- [149] Bungey J. H., Millard S.G. - "Testing of concrete in structures (3th edition)", Chapman & Hall, Wester Cleddens Road, Glasgow, 1996 (Capitolo 3).
- [150] Malhotra V. M., Carino N. J. - "Handbook on Nondestructive Testing of Concrete (2nd edition)", CRC Press, 2004 (Capitolo 8).
- [151] UNI EN 12504-4 - "Testing of Concrete Structures – Part 4: Calculation of the propagation velocity of".
- [152] Malhotra V. M., Carino N. J. - "Handbook on Nondestructive Testing of Concrete (2nd edition)", CRC Press (2004).
- [153] Farina, C. "Multilayer elements in fiber reinforced composites with high performance", Politecnico di Milano, (2011).
- [154] Caverzan, A. "High strain-rate uniaxial tensile constitutive behaviour in fibre-reinforced cementitious composites", (Doctoral dissertation, PhD thesis, Department of Structural Engineering, Politecnico di Milano, Milano). (2010).
- [155] CNR-DT 204 – "Instruction for Design, Execution and Monitoring of the Structures on Reinforced Concrete", Milan (2006).
- [156] UNI 11188 – "Steel Fiber Reinforced concrete structural elements"- Design, Execution and Monitoring", (2007).
- [157] Toledo Filho, R. D., Ghavami, K., Sanjuán, M. A., & England, G. L. (2005). Free, restrained and drying shrinkage of cement mortar composites reinforced with vegetable fibres. *Cement and Concrete Composites*, 27(5), 537-546.

References

- [158] Ghavami, K., Toledo Filho, R. D., & Barbosa, N. P. (1999). Behaviour of composite soil reinforced with natural fibres. *Cement and Concrete Composites*, 21(1), 39-48.
- [159] Silva, F. D. A., & Fairbairn, E. D. M. R. (2010). Physical and mechanical properties of durable sisal fiber-cement composites. *Construction and Building Materials*, 24(5), 777-785.
- [160] Ferrara L., Krelani V., Carsana M.,- “A *“Fracture Testing” Based Approach To Assess The Effect of Crack Healing on the recovery of mechanical properties of concrete with and without crystalline admixtures*”,. *Journal of Construction and Building Materials*, 68, (2014)
- [161] Di Luzio, G., & Cusatis, G. (2013). Solidification-microprestress-microplane (SMM) theory for concrete at early age: Theory, validation and application. *International Journal of Solids and Structures*, 50(6), 957-975
- [162] Aldea, C., M. Ghandehari, P. Shah, & A. Karr (2000). Estimation of water flow through cracked concrete under load. *ACI Matererials journal* 97, 567 – 575.
- [163] Bazant, Z. & J. Planas (1997). *Fracture and size effect in concrete and other quasibrittle materials* (W. F. CHEN ed.). New directions in civil engineering. CRC Press.
- [164] Bazant, Z. P. & S. Baweja (1995). Creep and shrinkage prediction model for analysis and design of concrete structures-Model B3. *Materials and Structures* 28, 357-365.
- [165] Bazant, Z. P., F. C. Caner, I. Carol, M. D. Adley, & S. A. Akers (2000). Microplane model M4 for concrete. I: Formulation with work-conjugate deviatoric stress. *Journal of Engineering Mechanics*, ASCE 126(9), 944-953.
- [166] Bazant, Z. P., G. Cusatis, & L. Cedolin (2004). Temperature effect on concrete creep modeled by microprestressolidification theory. *Journal of Engineering Mechanics* 130(6), 691-699.
- [167] Bazant, Z. P., A. B. Hauggaard, & S. Baweja (1997). Microprestress-Solidification Theory for Concrete Creep. II: Algorithm and Verification. *Journal of Engineering Mechanics*, ASCE 123, 1195-1201.
- [168] Bařant, Z. P., A. B. Hauggaard, S. Baweja, & F. J. Ulm (1997). Microprestress-Solidification Theory for Concrete Creep. I: Aging and Drying Effects. *Journal of Engineering Mechanics*, ASCE 123, 1188-1194.
- [169] Bazant, Z. P. & S. Prasannan (1989a). Solidification theory for concrete creep. I: Formulation. *Journal of Engineering Mechanics*, ASCE 115, 1691-1703. Bazant, Z. P. & S. Prasannan (1989b). Solification theory for concrete creep. II: Verification and application. *Journal of Engineering Mechanics*, ASCE 115, 1704-1725.
- [170] Cervera, M., J. Oliver, & T. Prato (1999). Thermo-chemomechanical model for concrete. I: Hydration and aging. *Journal of Engineering Mechanics*, ASCE 125(9), 1018-1027.
- [171] Cusatis, G., B. H. & Z. Bařant (2008). Spectral stiffness microplane model for quasi-brittle composite laminates: I. theory. *Journal of Applied Mechanics*, ASME 75(1), 021009-1021009-9.
- [172] de Schutter, G. & L. Taerwe (1996). Degree of hydration based description of mechanical properties of early age concrete. *Materials and Structures* 29, 335-344.

-
- [173] Di Luzio, G. (2007). A symmetric over-nonlocal microplane model m4 for fracture in concrete. *International Journal of Solids and Structures* 44(13), 4418 – 4441.
- [174] Di Luzio, G. (2009). Numerical model for time-dependent fracturing of concrete. *Journal of Engineering Mechanics*, ASCE 135(7), 632–640.
- [175] Di Luzio, G. & Z. P. Bazant (2005). Spectral analysis of localization in nonlocal and over-nonlocal materials with softening plasticity or damage. *International Journal of Solids and Structures* 42(23), 6071 – 6100.
- [176] Di Luzio, G. & G. Cusatis (2009a). Hygro-thermo-chemical modeling of high performance concrete. I: Theory. *Cement and Concrete Composites* 31(5), 301–308.
- [177] Di Luzio, G. & G. Cusatis (2009b). Hygro-thermo-chemical modeling of high performance concrete. II: Numerical implementation, calibration, and validation. *Cement and Concrete Composites* 31(5), 309–324.
- [178] Di Luzio, G. & G. Cusatis (2013). Solidification microstress microplane (smm) theory for concrete at early age: Theory, validation and application. *International Journal of Solids and Structures* 50(6), 957 – 975.
- [179] Di Luzio, G. Muciaccia, G. & L. Biolzi (2010). Size effect in thermally damaged concrete. *International Journal of Damage Mechanics* 19(5), 631–656.
- [180] K. Sakata and e. T.R. Najj (Eds.), *Proceedings of SCMT3 – Professor R. Gettu sessions, August 19-22, Kyoto, Japan*, pp. 103–112.
- [181] Gawin, D., F. Pesavento, & B. A. Schrefler (2006). Hygrothermo-chemo-mechanical modelling of concrete at early ages and beyond. part i: hydration and hygro-thermal phenomena. *International Journal for Numerical Methods in Engineering* 67(3), 299–331.
- [182] Neville, A. (1997). *Properties of concrete*. New York: John Wiley and Sons.
- Obolt, J., G. Balabanic, G. Perikic, & M. Kuter (2010). Modelling the effect of damage on transport processes in concrete. *Construction and Building Materials* 24(9), 1638 –1648.
- [183] Pantazopoulou, S. & R. Mills (1995). Microstructural aspects of the mechanical response of plain concrete. *ACI Matererials journal*. 92(6), 605–616.
- [184] Ulm, F. J. & O. Coussy (1995). Modeling of thermochemo mechanical couplings of concrete at early ages. *J. Engrg. Mech., ASCE* 121(7), 785–794.
- [185] Wang, K., D. J. DC, P. Shah, & A. Karr (1997). Permeability study of cracked concrete. *Cement and Concrete Research* 27(3), 381 – 393.
- [186] Wittmann, F. H. (1982). *Creep and Shrinkage Mechanics* (Z. P. Bazant and F. H. Wittmann ed.), *Creep and shrinkage of concrete structures* 6, pp. 129–161. John Wiley & Sons Ltd.
- [187] Kim, J.-K., Han, S.H., Song, Y.C., 2002. Effect of temperature and aging on the mechanical properties of concrete: Part I. Experimental results. *Cement and Concrete Research* 32 (7), 1087–1094.
- [188] Kim, J.-K., Lee, Y., Yi, S.-T., 2004. Fracture characteristics of concrete at early ages. *Cement and Concrete Research* 34 (3), 507–519.
- [189] Kim, J.-K., Moon, Y.-H., Eo, S.-H., 1998. Compressive strength development of concrete with different curing time and temperature. *Cement and Concrete Research* 28 (12), 1761–1773.
- [190] Oluokun, F., 1991. Prediction of concrete tensile strength from its compressive strength: an evaluation of existing relations for normal weight concrete. *Materials Journal – ACI* 88 (3), 302–309.
-

References

- [191] Oluokun, F.A., Burdette, E.G., Deatherage, J.H., 1991. Splitting tensile strength and compressive strength relationships at early ages. *Materials Journal – ACI* 88 (2), 115–121.
- [192] Hillerborg, A., 1985. The theoretical basis of a method to determine the fracture energy of concrete. *Materials and Structures* 18, 291–296.
- [193] di Prisco, M., Colombo, M., Ferrara, L., Bamonte, P., Bencardino, F., Dozio, D., Galeota, D., Galli, G., Gambarova, P., Gianmatteo, M.M., Gregori, A., Grimaldi, A., Marino, R., Rinaldi, R., Rizzuti, L., Spadea, G., 2007. *Fibre Reinforced Concrete for Strong, Durable and Cost-Saving Structures and Infrastructures*. Starrylink, Brescia, Italy, pp. 9–36 (FRC and HPFRC material properties).
- [194] Petersson, P.E., 1980. Fracture energy of concrete: practical performance and experimental results. *Cement and Concrete Research* 10, 91–101.

Curriculum Vitae

Name: Visar (Rexhep) Krelani
Date of Birth: December 17th, 1983
Place: Gjakova, Kosova
email: visar.krelani@polimi.it
vkrelani@hotmail.com

EDUCATION

1.

January 2011 – March 2015

PhD in Structural, Seismic and Geotechnical Engineering at Politecnico do Milano. Department of Environmental and Civil Engineering, DICA, Milan – Italy.

Doctoral Thesis Title: *Self-Healing Capacity of Cementitious Composites.*

Supervisor: Prof. Dr. Liberato Ferrara (Politecnico di Milano-Polimi)

Co-Supervisor: Prof. Dr. Romildo Dias Toledo Filho (Universidade do Rio de Janeiro-UFRJ)

2.

February 2008 – December 2010

Master of Science in Structural Engineering at University of Perugia, Italy

Master Thesis: *“Design of Pedestrian Bridge in the location San Martino in Colle (Perugia)”*

Supervisor: Prof. Dr. Annibale Luigi Materazzi,

Co-Supervisor: Dr. Ing. Marco Breccolotti.

3.

September 2006 - January 2008

Bachelor in Environmental and Civil Engineering at University of Perugia Italy

Bachelor Thesis: *“Preliminary Project and Construction of a Pedestrian Subway in Prishtina”*

Supervisor: Prof. Dr. Mariano Sartore.

4.

October 2002 – July 2006

Bachelor in Structural Engineering at Technical Faculty - University of Prishtina, Kosovo

Bachelor Thesis: *“Draft Proposal for the Circulation of Pedestrians and Vehicles in the Center of Prishtina”*

Supervisor: Prof. Ilir Rodiqi

